High Power Waveform Measurement System Enabling Characterisation of High Power Devices Including Memory Effects

A thesis submitted to the University of Wales, Cardiff
in candidature for the degree of

Doctor of Philosophy

By

Abdulrahman A Alghanim

Division of Electrical and Electronic Engineering
School of Engineering
Cardiff University
United Kingdom

January 2008

ProQuest LLC
789 East Eisenhower Parkway
P.O. Box 1346
Ann Arbor, MI 48106-1346

Summary

The increasing demand for higher data rates in wireless communication systems has led to the more effective and efficient use of all allocated frequency bands. In order to use the whole bandwidth at maximum efficiency, one needs to have RF power amplifiers with a higher linear level and memory-less performance. This is considered to be a major challenge to circuit designers. In this thesis the linearity and memory are studied and examined via the behaviour of the inter-modulation distortion (IMD). A major source of the in-band distortion can be shown to be influenced by the out-of-band impedances presented at either the input or the output of the device, especially those impedances terminated the low frequency (IF) components. Thus, in order to regulate the in-band distortion, the out of-band distortion must be controllable. This has necessitated the development of an upgraded measurement system, where, for the first time, the IF measurement system power is scaled up and extended from approximately 2W to approximately 100W. This was made possible by the design of high power IF bias tee and its integration with a high power IF test-set.

The investigation of the influence of out of-band distortion, particularly that at the low frequencies, generally referred to as base-band memory effects, on in-band distortion in high power LDMOS devices, has been made possible by the development of this pioneering, high-power modulated waveform measurement system since it allows for the observation and control of all relevant frequency components (RF, IF and DC). This measurement system is capable of handling IF and RF power levels in excess of 100W with bandwidths ranging from approximately 10 kHz to approximately 12GHz, which makes it particularly appropriate for the characterisation of devices used in base-station mobile communications system applications

These subsequent measurements demonstrate that the bandwidth, over which the base-band impedances must be controlled, should be extended beyond the generally accepted value of twice to at least four times the modulated bandwidth. Moreover, the measurement system permitted an intensive investigation of the base-band impedance terminations variations on inter-modulation distortion allowing an optimum to be found that minimise overall in-band distortion (circuit linearisation technique). Hence, indicating that it may be possible to meet the 3rd Generation Partnership Project (3GPP) standards for the maximum allowable adjacent channel leakage ratio (ACLR) in mobile terminals without using any extra linearisation techniques such as predistortion. These important observations have significant implications for modern PA linearisation techniques, as well as requiring careful consideration when designing PA bias networks.

Acknowledgements

I would like to thank my supervisor, Professor Paul Tasker, for his scientific guidance, encouragement and research support throughout my doctoral studies, as well as giving me many opportunities, to publish, travel and collaborate. I am also indebted to Dr. Johannes Benedikt who helped me to build on this excellent foundation.

I would also like to express my appreciation of my colleagues in the RF group. I am specifically grateful to Dr. Jonathen Lees.

I would like also to thank Freescale for supplying the LDMOS devices used in this thesis.

In addition to this I feel moved to thank my parents, for their incredible support, and unconditional love. This combined with the encouragement from my entire family who has helped me achieve my goal.

Finally, I would like to thank my best friend and lovely wife, Yousra, for her love, understanding, and sacrifices. Her presence, encouragement, and support over the years made this dissertation possible. I also must give special thanks to my daughter Aliah and son, Azzam, for making everyday fresh and new.

List of Publications

1. A. Alghanim, J. Benedikt, P. Tasker, A measurement test-set for characterisation of high power LDMOS transistors including memory effects, in: High Frequency Postgraduate Student Colloquium, Leeds, Uk, 5-6 Sept. 2005, pp. 29-32.

2. A. Alghanim, J. Lees, T. Williams, J. Benedikt, P. Tasker, Investigation of electrical base-band memory effects in high-power 20W LDMOS power amplifiers, in: European Microwave Conference, Munich, 9-12 Oct. 2007, pp. 48-51.

3. A. Alghanim, J. Lees, T. Williams, J. Benedikt, P. Tasker, Using activeIF load-pull to investigate electrical base-band induced memory effects in high-power LDMOS transistors, in Asia-Pacific Microwave Conference, Bangkok, 11-14 Dec. 2007.

4. A. Alghanim, J. Lees, T. Williams, J. Benedikt, P. Tasker, Investigation into the sensitivity of Electrical Base-Band Memory Effects to higher order IF components for High-Power LDMOS Power Amplifiers. Electronics Letters, Feb, 2008. 43(5): pp. 358-359.

5. A. Alghanim, J. Benedikt, P. Tasker, Investigation of electrical base-band memory effects in high-power 20W LDMOS transistors using IF passive load pull, in Information and Communication Technologies ""ICTTA '08"". 3rd. Damascus, Apr 7-11, 2008.

6. A. Alghanim, J. Benedikt, P. Tasker, Comparison of IF Active Versus IF Passive Load-Pull Using 20W LDMOS Device, in: META08, Marakkesh, May 7-11, 2008.

7. A. Alghanim, J. Lees, T. Williams, J. Benedikt, P. Tasker, Reduction of Electrical Baseband Memory Effect in High-Power LDMOS Devices using Optimum Termination for IMD3 and IMD5 using Active Load-Pull, in: International Microwave Symposium, Atlanta, June 15-20, 2008.

Table of contents

CHAPTER 1

Introduction

1.1. Introduction

The evolution of 3rd generation (3G) and 4th generation (4G) mobile communication services has generated more concerns about the development of the required power amplifiers of any communication system to date. 3G comes under the umbrella of the International Mobile Telecommunications programme (IMT-2000) which employs wideband code division multiple access (W-CDMA), achieving a transmission rate of 2 Mbit/s with a 5-MHz frequency bandwidth. The third generation of mobile communication systems is designed for applications such as Internet services, e-mail, database retrieval, video telephony, interactive video and sound (music and TV).

Despite the enhanced features of 3G systems, they are still severely constrained by bandwidth - particularly when handling full-motion video. New mobile communication services and applications require a higher

data bit rate that demands a larger bandwidth. The imperative to support these services and applications indicates the existing need for larger bandwidth. The 4th generation (4G) communication system will be capable of providing 100 Mbit/s and 1 Gbit/s speeds using channel bandwidths of 1.25 to 23 MHz and hence offering better quality (e.g. multimedia, video and sound).

The radio frequency (RF) power amplifier (PA) in base station systems is typically the most costly component. The increasing number of mobile users, combined with a growing demand for a higher data rate has driven RF designers to try and effectively utilise the entire allocated bandwidth to its maximum potential. This would require the designing of a linear power amplifier capable of producing a linear response over a wide bandwidth. Intensive research into the linearity of RF power amplifier of wireless communication has become a global focus.

The maximum allowable adjacent channel leakage ratio (ACLR) for mobile terminals are -33dBc and -43dBc for 5 MHz and 10 MHz respectively [1] [2]. Otherwise, distortion into adjacent channels and error in detection of the desired signal may occur. A typical value of carrier to inter-modulation (C/I) ratio for a linear power amplifier is 30 dB or more [3] [4]. The main technology for the implementation of 3rd generation (3G) cellular systems is wideband code division multiple access (W-CDMA). Its ACLR is illustrated in Figure 1. To minimise the interference between the channels, the slope of the window should be ideally as sharp as possible, and the inter-modulation distortion (IMD) ought to be kept to a minimum level.

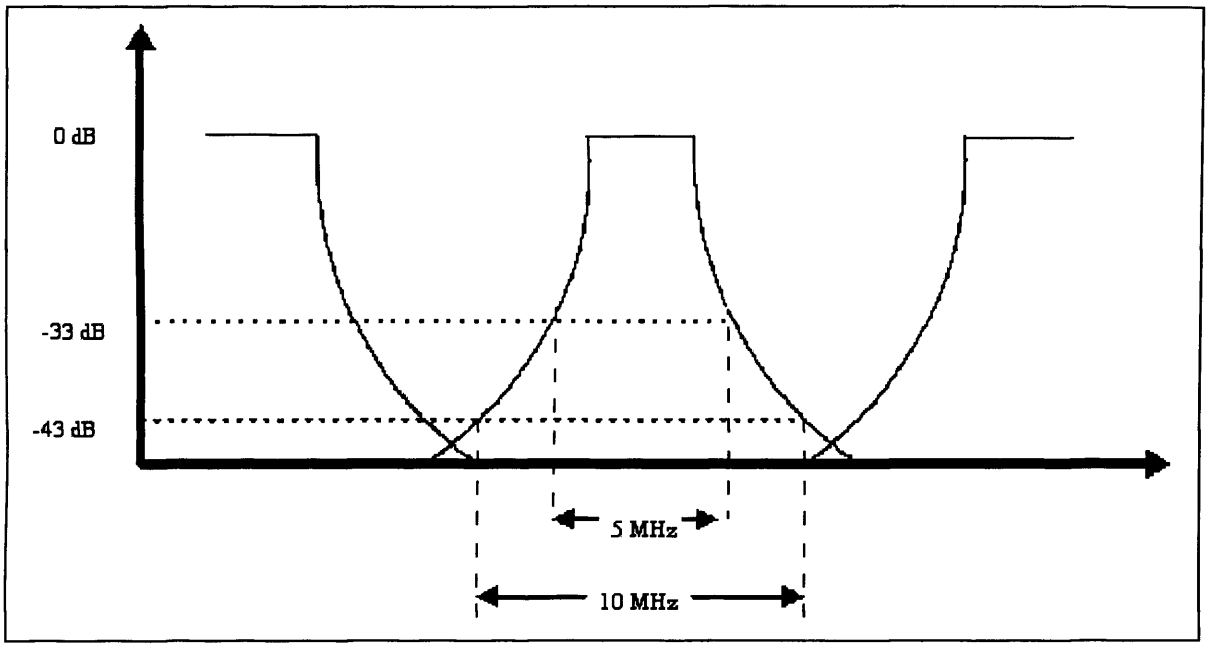

Figure 1.1 Illustration of the maximum ACLR vs. output power allowed by 3GPP.

To meet these challenging standards, RF power amplifier manufacturers and circuit designers must come up with a development approach allowing for high linear power amplifier behaviour, in order to use the whole available bandwidth in an efficient way.

Circuit designers have two main strategies for achieving a higher linear level: terminating the DUT to proper impedance through source and/or load pull or using one of the available linearisation techniques.

Linearisation techniques can be used to achieve a linear PA performance. However, PA memory effects, which can be defined in case of two-tone measurement as changes in the amplitude or phase of distortion components (IMD) caused by changes in modulation frequency ($\Delta\omega$), restricts the linearisation improvement capability and makes linearisation techniques more difficult to implement [5] [6].

Memory effects in microwave PAs are generally attributable to a number of physical processes that involve thermal [7], electrical [8] and surface effects [9]. Electrical memory, particularly the base-band electrical memory effect, is generally considered to be the major contributor. Therefore, one obvious way to develop a more complete understanding of memory and its origins is to attempt to eliminate the most likely contributing factor, base-band electrical memory, and then measure and analyse any residual effects which must be due to combination of the others.

Full investigation of electrical memory effect requires a thorough examination of all impedances presented across the complete frequency spectral (preferably from DC to some n^{th} RF harmonic). Unfortunately current commercial measurement systems do not accommodate low frequency impedance due to limitations in the technology utilised, i.e. high power couplers, at these frequencies [10] [11] [12].

The difficulty of investigating low frequency electrical memory is further compounded by the fact that ideally the biasing network should have zero impedance over the whole low frequency (IF) ranges. Otherwise, AC voltages may be generated and added to the power supply voltage, causing additional amplitude and/or phase modulation, which will then result in asymmetry in the IMD [3] [8]. In the case of 5 MHz W-CDMA signals, for example, such a bias network needs to be constant and ideally zero for at least eight decades of bandwidth. In contrast, designing a matching network with constant impedance for the RF frequency and its first 5 harmonics requires only one decade of bandwidth. This highlights the complexity of bias network design.

It is the significant impact of low frequency impedance on the performance of high power amplifiers that has motivated this thesis work towards developing and building a new measurement system suitable for characterising the performance of high power RF power amplifiers that is capable of both measuring and engineering the low frequency signal component.

The previously developed Cardiff waveform measurement system that incorporated an IF measurement capability could unfortunately only handle power levels of around 2W making it unsuitable for characterising high power devices.

The main objective of this thesis was to develop and scale up the existing Cardiff waveform measurement system that included the IF component from approximately 2W to about 100W with at least 8 decades of IF bandwidth. Thus making it suitable, for example, for W-CDMA systems. This development has led to realisation of a pioneering IF and RF waveform measurement system capable for the first time of handling power up to 100W. The new high power IF and RF measurement system is capable of fully controlling the input and output impedances at a frequency range of approximately 10KHz to 12GHz permitting an investigation of high power amplifier performance, not only appropriate for high frequency electrical memory effect but also for low frequency (base-band) electrical memory effect.

1.2. Organization of the Thesis

Basic background and theory of power amplifier linearity are discussed in chapter 2.

Chapter 3 gives an introduction to the modus operandi of the current measurement system (high RF power but low IF power). Chapter 3 provides also an overview of waveform engineering including source and load pull concepts. It includes a comparison between IF passive and active load pull using the new measurement system, followed by the proposed RF and IF high power measurement system.

Chapter 4 cover the development of the high power IF test-set which has required high power components. The main components in the IF measurement system are the directional coupler and the bias tee. The IF directional couplers were replaced with commercially available directional couplers providing the IF test set with a bandwidth of 100KHz-1GHz and a maximum power of 100W CW. Despite substantial efforts it was not possible to source a suitable IF bias tee capable of handling high DC and IF voltage and currents over a large bandwidth. Therefore, it was necessary to design suitable IF bias tees on site to complete the architecture of the IF set. The design, implementation and manufacturing process of the high power IF bias tee are explained in chapter 4, followed by testing and validation of the whole system. This has resulted in a new high power measurement system incorporating both RF and IF measurement and engineering functionality with a groundbreaking 100W power handing capability.

This measurement system is built for the purpose of characterising the linearity and memory effects observed in high power RF amplifiers at both low and high frequencies at power levels from 10 to 100W.

Chapter 5 provides an overview of testing, operation and validation of the whole system. It includes a comparison between IF passive and active load pull using the new measurement system, indicating the impossibility of using the IF passive load system to load pull very low frequency impedances anywhere around the smith chart. This highlights the dominance of the active over the passive IF load pull in the base-band region.

Detailed investigation of base-band memory effect is presented in chapter 6 using high power LDMOS devices. The results show that the bandwidth over which the base-band impedances are to be controlled must be extended to at least four times the modulated bandwidth. The results also highlight the existence of optimum IF impedance terminations that minimise overall in-band distortion.

The conclusion of the work is in chapter 7 with suggestions for future work.

1.3. References

1. A.Toskala, H.H.a., *WCDMA for UMTS: Radio Access For Third generation Mobile Communications*. 2nd ed. 2002, West Sussex: john Wiley & Sons, Ltd.

2. Leung, V.W., et al., *Analysis of envelope signal injection for improvement of RF amplifier intermodulation distortion.* Solid-State Circuits, IEEE Journal of, 2005. **40**(9): p. 1888.

3. Cripps, S.C., *RF Power Amplifiers for Wireless Communication.* 2006, Norwood,MA: Artech house.

4. Frederick H. Raab, P.A., Steve Cripps, Peter B. Kenington, and N.P. Zoya B. Popovich, John F. Sevic and Nathan O. Sokal, *"RF and Microwave Power Amplifier and Transmitter Technologies".* IEEE Transactions on Microwave Theory and Techniques, March 2003. **50**(1).

5. Carvalho, J.C.P.a.N.B., *Intermodulation Distortion in microwave and Wireless Circuits*. 2003, Norwood MA: Artech House.

6. Jeonghyeon, C., et al., *Optimum design of a predistortion RF power amplifier for multicarrier WCDMA applications.* IEEE Transactions on Microwave Theory and Techniques, 2004. **52**(2): p. 655.

7. Vuolevi, J.H.K., T. Rahkonen, and J.P.A. Manninen, *Measurement technique for characterizing memory effects in RF power amplifiers.* Microwave Theory and Techniques, IEEE Transactions on, 2001. **49**(8): p. 1383-1389.

8. Bosch, W. and G. Gatti, *Measurement and simulation of memory effects in predistortion linearizers.* Microwave Theory and Techniques, IEEE Transactions on, 1989. **37**(12): p. 1885-1890.

9. Parker, A.E. and J.G. Rathmell, *Bias and frequency dependence of FET characteristics.* Microwave Theory and Techniques, IEEE Transactions on, 2003. **51**(2): p. 588.

10. Alghanim, A., J. Benedikt, and P. Tasker. *A measurement test-set for characterisation of high power LDMOS transistors including memory effects.* in *High Frequency Postgraduate Student Colloquium, 2005.*

11. Spirito, M., et al., *Active harmonic load-pull for on-wafer out-of-band device linearity optimization.* IEEE Transactions on Microwave Theory and Techniques, 2006. **54**(12): p. 4225.

12. Focus Microwave. *Active Load Pull Systems: Strengths-Weaknesses-Alternatives [Online]*.[cited; Available from: http://www.focus-microwaves.com//template.php?unique=232.

CHAPTER 2

Background Theory of Power Amplifier

2.1. Linearity

Practically speaking active RF power amplifiers are not linear in their operation. If the active device is driven hard with input RF power, undesirable spurious signals collectively known as 'distortion' will be generated. The linearity of the device is dependant on how much distortion is generated. The two most widely used measures of linearity are 1dB Compression point and third order interception point.

2.1.1. 1dB Compression Point (P1dB)

An increase in input power causes the measured output power to roll off resulting in a drop in gain known as gain compression: a measure of the linearity of a device. The 1 dB compression point, which is defined as the point where the actual fundamental output power level is a 1dB less than the ideal one, determined from a slope of 1:1, due to device saturation. An

example of the 1dB compression point is shown in Figure 2.1, where at an input power of about 18 dBm, the actual output power is 1 dB less than the ideal characteristic. At this point, the correlation of 1:1 is no longer valid. An increase in the input power, however, will still increase the RF output power even at 7dBm above the one dB compression point, but at a much lower rate and with a much sharply clipped voltage or current waveforms.

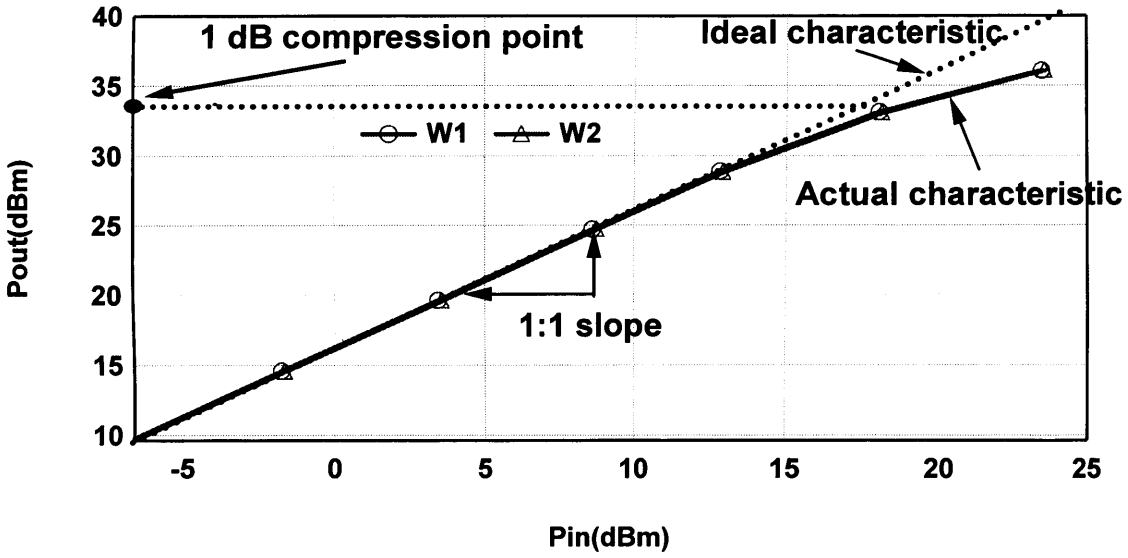

Figure 2.1Measured 1 dB compression point of 12W LDMOS amplifier

2.1.2. Third Order Interception Point (IP3)

Third order intercept point (IP3 or TOI) is another figure of merit that can be used to characterise the linearity of RF power amplifiers, particularly before compression [1] [2]. The higher the IP3, the lower the distortion, and therefore the more linear the power amplifier. The third order intercept point based on inter-modulation products can be defined in a similar manner to that of the 1 dB compression point: as the intercept point at which the fundamental

output, slope of 1:1, and the two-tone third order distortion product, slope of 3:1, intersect. This intercept point is purely a mathematical concept, and does not correspond to a physical power level. In many cases, the intercept point can not actually be reached in practice and lies beyond the damage threshold of the device.

For every dB increase in input power, the third order products will increase by 3 dB and therefore, this point is sometimes referred to as a 3:1 slope. The third order law says that the inter-modulation product grows to the power of three, in proportion to the input amplitude. However, this must be based on the assumption that the device is fully described by this particular power series. Figure 2.2 below shows that the third order intercept point is about 10 dB above the 1dB compression point, as can be expected [3].

It should be noted that neither the 1:1 nor 3:1 slope are valid for high input drive levels and therefore the device cannot be described by only three-order terms. Thus, as soon as the fundamental and the third order inter-modulation distortion signals compress, the extrapolated IP3 will be different [1, 4].

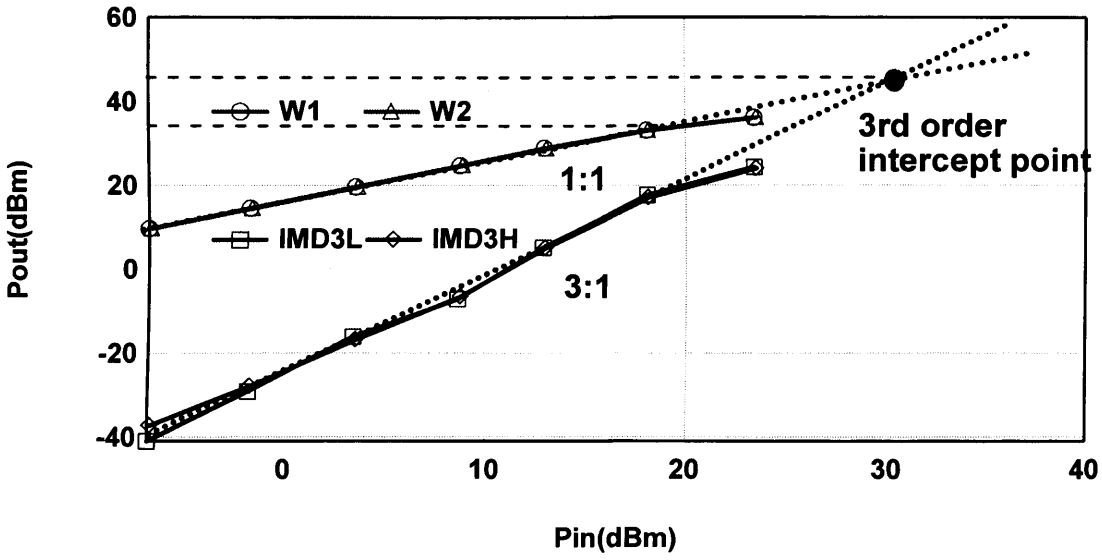

Figure 2.2 Illustration of measured third-order intercept for 12W LDMOS amplifier

2.2. Two-Tone Test

A convenient way to characterise the nonlinearity of RF power amplifiers is to use a two-tone test [1]. For a two-tone case with an input signal of the form:

$$v_{i1}(t) = A_1 \cos(2\pi f_1 t) \tag{2.1}$$

$$v_{i2}(t) = A_2 \cos(2\pi f_2 t) \tag{2.2}$$

$$v(t) = v_{i1} + v_{i2} = A_1 \cos(\omega_1 t) + A_2 \cos(\omega_2 t) \tag{2.3}$$

the output current would be:

$$i_o(t) = \sum_{n=0}^{n} a_n \bullet v^n(t) \tag{2.4}$$

$$= a_o + a_1 \bullet v(t) + a_2 \bullet v^2(t) + \ldots a_n \bullet v^n(t) \tag{2.5}$$

In (2.3) A_1 and A_2 are the amplitude of the input signal and ω_1 and ω_2 are the fundamental frequencies.

2.3. Linear Amplifier (First-Order Characteristic)

For a perfect linear amplifier, the input-output characteristic in (2.5) would have a linear response and can be modelled as:

$$i(t) = a_1 \bullet v(t) \tag{2.6}$$

where $a_0, a_2, \ldots a_n = 0$ and a_1 would be equal to the gain or attenuation of the system and the output would have the form $i(t) = a_1 \bullet v(t)$. Figure 2.3 illustrates the input output behaviour of the linear system in frequency domain.

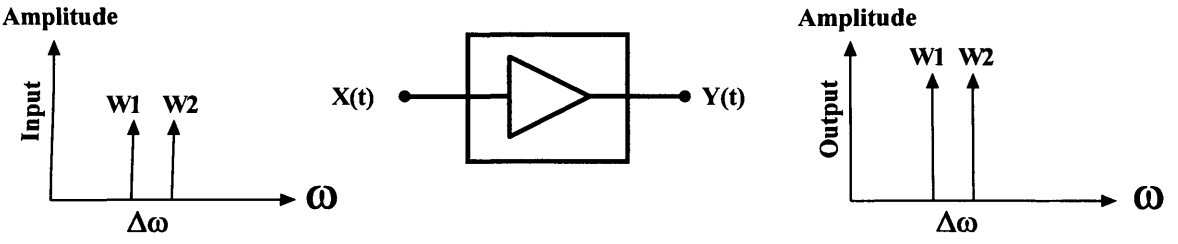

Figure 2.3 Frequency spectrum of Input and output signals of linear amplifier.

2.4. Non-linear Amplifier

Applying two signals or more of varying frequency to a non linear system will produce an output of the fundamental ω_1 and ω_2, which may be amplified or attenuated, as well as their harmonics with the unwanted sum and difference frequencies. The output frequency components of the two-tone input signal can be computed using:

$$m\omega_1 \pm n\omega_2 \text{ where m \& n are integers} \quad (2.7)$$

These unwanted signals are called inter-modulation distortion (IMD), although harmonics components are not usually included as part of the inter-modulation. The higher-order terms $a_2 \bullet v^2(t) + ... a_n \bullet v^n(t)$ in (2.5) generate inter-modulation products, which appear within the in-band (close to the fundamental tones) or out-of-band region (far from the fundamental tones).

2.4.1. Second-Order Characteristic

For a system that exhibits second-order nonlinearity, the transfer characteristic would be the one identified in (2.6) with the addition of a second term as follow:

$$i(t) = a_1 \bullet v(t) + a_2 \bullet v^2(t) \quad (2.8)$$

The transfer characteristic of this form is referred to second-order due to the squared term in (2.8). This equation (2.8) is presented graphically in Figure 2.4. Note that the second-order terms produce second order products at frequencies $2\omega_1$, $2\omega_2$ and $\omega_1 + \omega_2$ (all in the second harmonics band) in addition to $\omega_2 - \omega_1$ (in the DC & IF band). These components are out-off-band terms and not in-band (see Figure 2.4). In general, even-order terms generate out-of-band distortion.

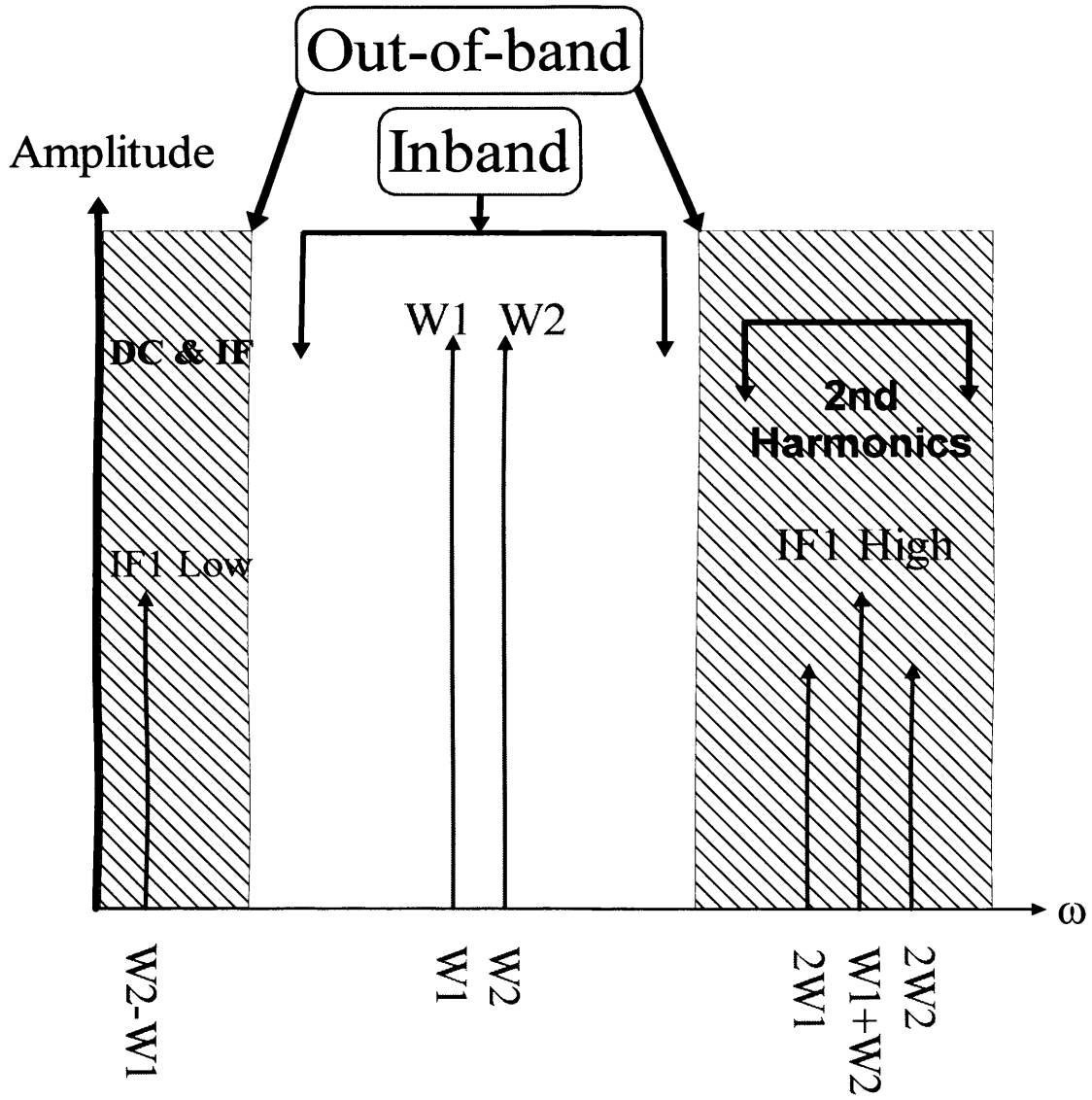

Figure 2.4 Two-tone spectrums up to second-order component polynomial transfer characteristic.

2.4.2. Third-Order Characteristic

The transfer characteristic with third-order terms is as follows:

$$i(t) = a_1 \bullet v(t) + a_2 \bullet v^2(t) + a_3 \bullet v^3(t) \qquad (2.9)$$

Third-order terms at frequency $2\omega_1-\omega_2$ and $2\omega_2-\omega_1$ are the most interesting inter-modulation products since they fall within the channel bandwidth. Generally speaking, odd-order terms generate in-band distortion.

Figure 2.5 shows the output signals ω_1 and ω_2, in addition to the unwanted distortion generated by the non-linear behaviour of the RF power amplifier up to the third-order.

Figure 2.6 and Figure 2.7 show the fourth-order and fifth-order nonlinearity respectively.

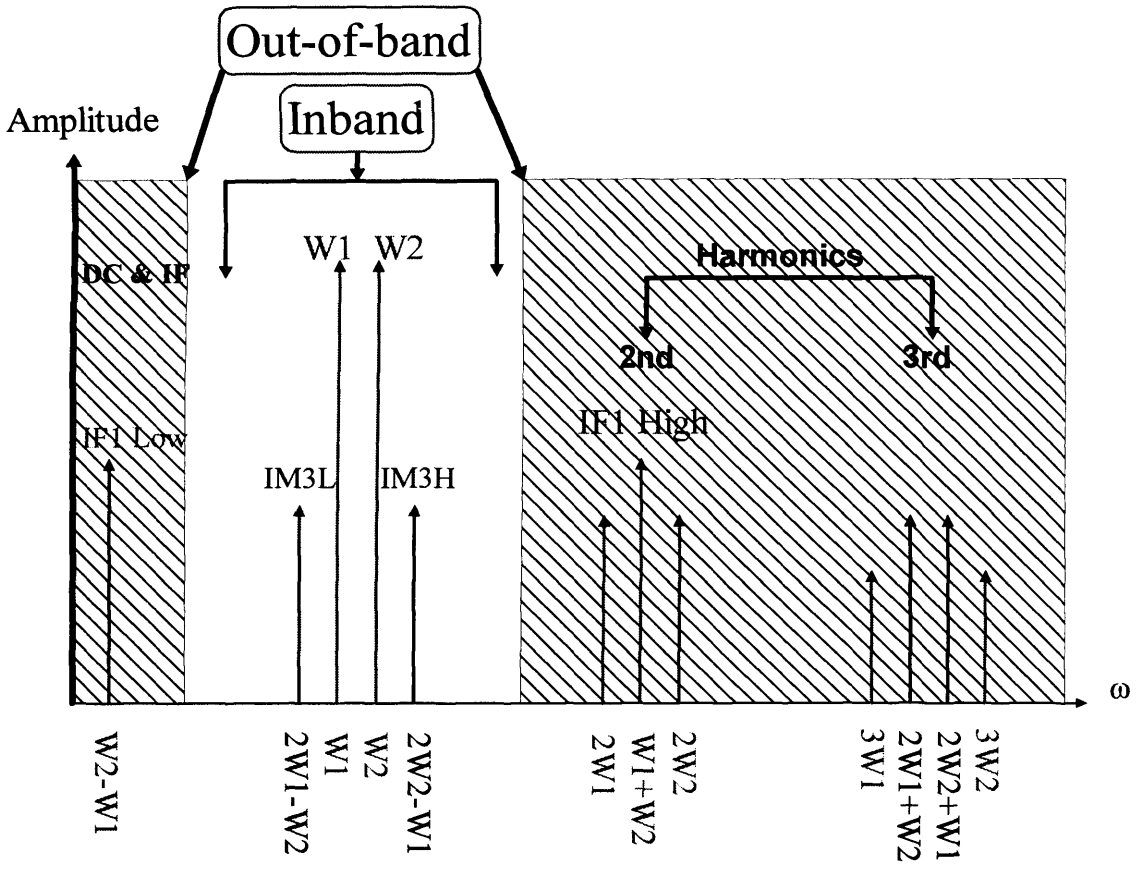

Figure 2.5 Two-tone spectrums up to third-order component polynomial transfer characteristic.

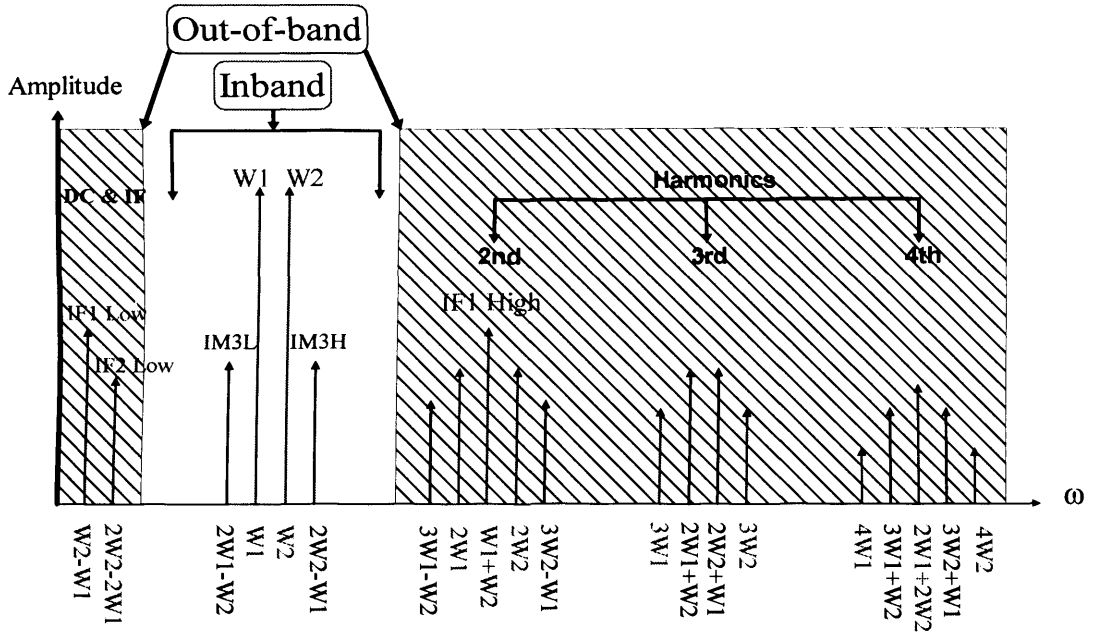

Figure 2.6 Two -tone spectrum up to fourth-order component polynomial transfer characteristic.

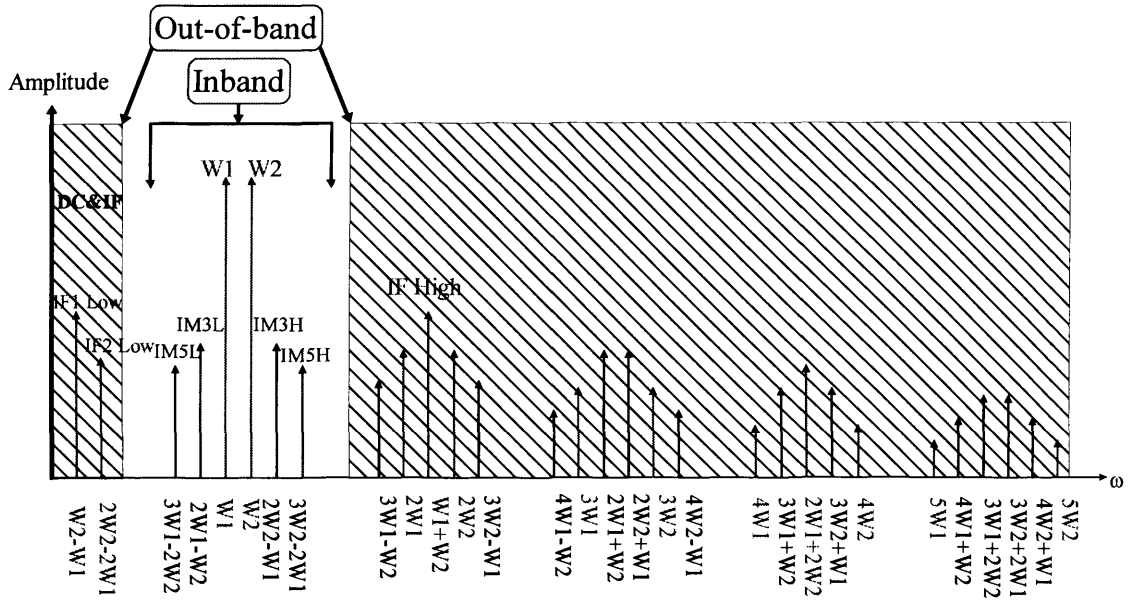

Figure 2.7 Two-tone spectrum up to fifth-order component polynomial transfer characteristic.

2.5. In-Band Distortion

In-band distortions are those inter-modulation products that fall within or close to the channel bandwidth, i.e. close to the fundamental frequencies ω_1 and ω_2, and therefore cannot be easily removed. Because of their impact on the performance of RF power amplifiers; these products are of most interest, especially the third-order components at frequency $2\omega_1-\omega_2$ (IM_{3L}) and $2\omega_2-\omega_1$ (IM_{3H}), which are located close to the required signal. They cannot therefore be easily filtered out, and are more important than the higher odd-number orders (such as IM_5, IM_7...etc) due to their lower amplitudes, particularly at low input level. In-band distortion frequencies are present when [1]:

$$m+n=1 \tag{2.10}$$

To find the in-band third order components of the two tone inputs, ω_1 and ω_2, $|m|\pm|n|$ and $m+n$ must equal to 3 and 1 respectively, which will result for example, in amplitude at frequencies of $2\omega_1-\omega_2$ and $2\omega_2-\omega_1$ of $\frac{3}{4}a_3A^3$. For the in-band fifth-order components $|m|\pm|n|=5$ and $m+n=1$ will produce frequencies $3\omega_1-2\omega_2$ and $3\omega_2-2\omega_1$ of amplitudes $\frac{5}{8}a_5A^5$, and so on for the higher in-band order components.

2.6. Out-of-Band Distortion

Unlike in-band products, out-of-band products are remote from the fundamental signals and therefore they can be easily filtered [1]. The fifth-order out-of-band spectra consists of five frequency bands, namely

the base-band (DC and IF band) as well as four harmonics bands (falling to the right of the in-band region) as can be seen in Figure 2.7. Because of their distance from the fundamental signals, out of-band components are usually utilised in the control of in-band distortion, which occurs in close proximity to the requisite fundamental signal and is consequently quite difficult to directly filter without compromising the desired signal. Therefore, out-of-band distortion components are considered to be a very important factor in terms of their effects on the behaviour of in-band distortion [5] [6] [7] [8].

Out of-band distortion frequencies are present when [1]:

$$m+n \neq 1 \tag{2.11}$$

The IF band (including DC) consists of the base-band components caused by those components of an even-number order such as second-order ω_2- ω_1 (IF_1); fourth-order $2\omega_2$-$2\omega_1$ (IF_2); sixth-order s $3\omega_2$-$3\omega_1$ (IF_3) and so forth, together with the harmonic bands generated by second-and higher-order components. Examples of this are the second-order products $2\omega_1$, $2\omega_2$ and $\omega_1+\omega_2$ in the second harmonic zone; the third order components $3\omega_1$, $3\omega_2$, $2\omega_1+\omega_2$ and $2\omega_2+\omega_1$ in the third harmonic zone and so on. Figure 2.7 illustrates a typical spectrum up to fifth-order nonlinearity.

To expand (2.5) to include all the distortion products up to the fifth order requires inserting equation (2.3) into (2.5) for $A_1=A_2$ to the fifth degree will yield an output signal:

$$\begin{aligned} i_o(t) &= a_o + a_1[A_1\cos(\omega_1 t) + A_2\cos(\omega_2 t)] \\ &+ a_2[A_1\cos(\omega_1 t) + A_2\cos(\omega_2 t)]^2 \\ &+ a_3[A_1\cos(\omega_1 t) + A_2\cos(\omega_2 t)]^3 \\ &+ a_4[A_1\cos(\omega_1 t) + A_2\cos(\omega_2 t)]^4 \\ &+ a_5[A_1\cos(\omega_1 t) + A_2\cos(\omega_2 t)]^5 \end{aligned} \tag{2.12}$$

Equation (2.12) could result in a negative frequency but only positive value are considered. Using the well-known trigonometric functions yields the following results:

$$y(t)=a_2A^2$$ DC Component

$$+\left(a_1A+\frac{9}{4}a_3A^3+\frac{25}{4}a_5A^5\right)\cos(\omega_1 t)+\left(a_1A+\frac{9}{4}a_3A^3+\frac{25}{4}a_5A^5\right)\cos(\omega_2 t)$$ Fundamental

$$+\left(\frac{1}{2}a_2A^2+2a_4A^4\right)\cos(2\omega_1 t)+\left(\frac{1}{2}a_2A^2+2a_4A^4\right)\cos(2\omega_2 t)$$ 2nd Harmonic

$$+\left(\frac{1}{4}a_3A^3+\frac{25}{16}a_5A^5\right)\cos(3\omega_1 t)+\left(\frac{1}{4}a_3A^3+\frac{25}{16}a_5A^5\right)\cos(3\omega_2 t)$$ 3rd Harmonic

$$+\left(\frac{1}{8}a_4A^4\right)\cos(4\omega_1 t)+\left(\frac{1}{8}a_4A^4\right)\cos(4\omega_2 t)$$ 4th Harmonic

$$+\left(\frac{1}{16}a_5A^5\right)\cos(5\omega_1)t+\left(\frac{1}{16}a_5A^5\right)\cos(5\omega_2)t$$ 5th Harmonic

$$+\left(a_2A^2+3a_4A^4\right)\cos(\omega_1+\omega_2)t+\left(a_2A^2+3a_4A^4\right)\cos(\omega_2-\omega_1)t$$ Envelope

$$+\left(\frac{3}{4}a_4A^4\right)\cos(2\omega_1+2\omega_2)t+\left(\frac{3}{4}a_4A^4\right)\cos(2\omega_2-2\omega_1)t$$ 4th Order (Envelope)

$$+\left(\frac{3}{4}a_3A^3+\frac{25}{8}a_5A^5\right)\cos(2\omega_1+\omega_2)t+\left(\frac{3}{4}a_3A^3+\frac{25}{8}a_5A^5\right)\cos(2\omega_1-\omega_2)t$$

$$+\left(\frac{3}{4}a_3A^3+\frac{25}{8}a_5A^5\right)\cos(2\omega_2+\omega_1)t+\left(\frac{3}{4}a_3A^3+\frac{25}{8}a_5A^5\right)\cos(2\omega_2-\omega_1)t$$ 3rd Order

$$+\left(\frac{1}{2}a_4A^4\right)\cos(3\omega_1+\omega_2)t+\left(\frac{3}{4}a_4A^4\right)\cos(3\omega_1-\omega_2)t$$

$$+\left(\frac{1}{2}a_4A^4\right)\cos(3\omega_2+\omega_1)t+\left(\frac{3}{4}a_4A^4\right)\cos(3\omega_2-\omega_1)t$$ 4th Order

$$+\left(\frac{5}{8}a_5A^5\right)\cos(3\omega_1+2\omega_2)t+\left(\frac{5}{8}a_5A^5\right)\cos(3\omega_1-2\omega_2)t$$

$$+\left(\frac{5}{8}a_4A^4\right)\cos(3\omega_2+2\omega_1)t+\left(\frac{5}{8}a_4A^4\right)\cos(3\omega_2-2\omega_1)t$$

$$+\left(\frac{5}{16}a_4A^4\right)\cos(4\omega_1+\omega_2)t+\left(\frac{5}{16}a_4A^4\right)\cos(4\omega_1-\omega_2)t$$ 5th order

$$+\left(\frac{5}{16}a_4A^4\right)\cos(4\omega_2+\omega_1)t+\left(\frac{5}{16}a_4A^4\right)\cos(4\omega_2-\omega_1)t$$ (2.12.a)

The advantage of the two-tone test is its ability to vary the envelope maximum of the input signal in order to test the device over its whole transfer characteristic range. It is therefore a suitable tool with which the effect of the base-band impedance on linearity and memory effect can be studied.

2.7. Memory Effects in RF Power Amplifier

RF power amplifier devices can be classified into two systems, namely memory-less systems and systems with memory. The nonlinearity input-output relation of memory-less systems can be described using Taylor expansion as:

$$i(t) = \sum_{n=0}^{n} a_n \bullet v^n(t) \tag{2.13}$$

$$= a_o + a_1 \bullet v(t) + a_2 \bullet v^2(t) + ...a_n \bullet v^n(t) \tag{2.14}$$

Where $a_o, a_1, a_2, ...a_n$ are real valued nonlinearity coefficients and n is the maximum order of nonlinearity. Coefficient a_o is the DC offset, a_1 is the linear component, a_2 *is* the nonlinearity second order, a_n is the nonlinearity nth order.

For a linear system, the input-output characteristic in (1.14) is modelled as $i(t) = a_1 \bullet v(t)$, where $a_o, a_2, ...a_n = 0$ and a_1 would be equal to the gain of the system. Interference in this case relates to only AM-AM behaviour.

For a non-linear system with memory the input-output relation can be described as:

$$i(t) = \sum_{n=0}^{n} a_n \bullet v^n(t) \tag{2.15}$$

$$= a_0 + a_1 \bullet v(t) + a_2 \bullet v^2(t) + ...a_n \bullet v^n(t) \tag{2.16}$$

Where $a_0, a_1, a_2, ...a_n$ can be complex valued nonlinearity coefficients [9].

For a linear system with memory, the input-output characteristic in (2.16) is modelled as $i(t) = a_1 \bullet v(t)$, where $a_0, a_2, ...a_n = 0$ and a_1 would be equal to the gain of the system.

Interference between signals may again cause distortion, which can pervade the bandwidth allocated for the information (desired) signal. However, in this case distortion relates to both AM-AM and AM-PM behaviour and the distortion will dependent of the tone separation frequency. Based on the behaviour of the distortion, devices can be classified into memory-less devices or devices with memory.

2.8. Memory-Less Devices

In a practical environment, devices in their natural state are not linear; therefore, they would produce some distortion at their output as a response to the applied input signal. It is noteworthy that distortion itself is not a memory effect. Nevertheless, a device would be described as memory-less provided that its distortion behaviour exhibits a constant phase and magnitude at different tone-spacing [10]. This could happen if the output signal was only a function of the instantaneous input signal. Figure 2.8 shows the IM_3 behaviour, and includes the two output tones (ω_1 and ω_2), which are clearly observed to be almost independent of the tone spacing frequency ranging between 2MHz and 10MHz at a single input drive level

and are, as required, symmetrical about the carrier frequency. This symmetry and a lack of any variation with tone separation frequency is a clear indication of the absence of memory effect in an environment where the fundamental and harmonic components were terminated to 10 Ω and IF components were terminated to 50 Ω.

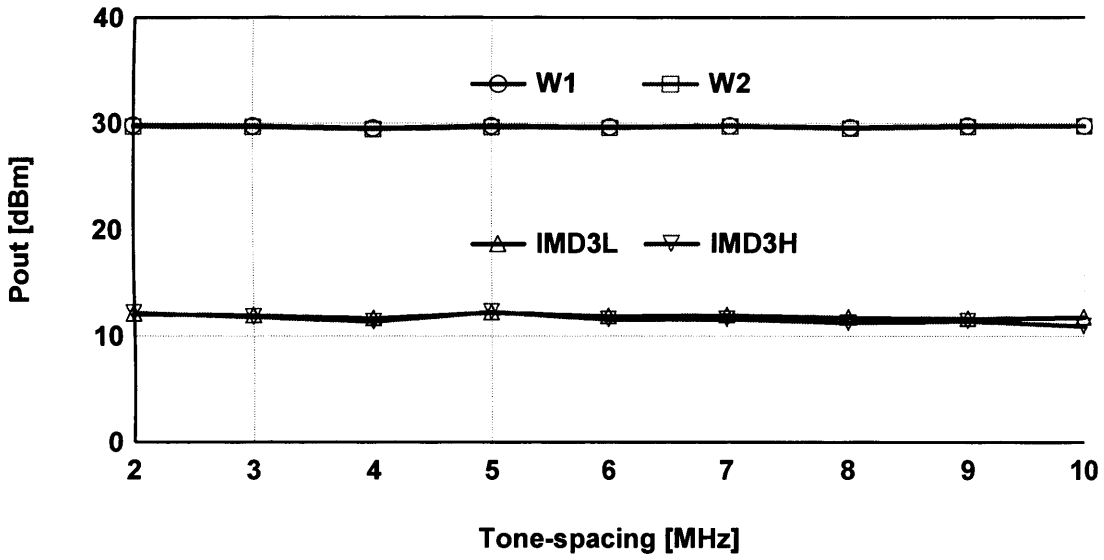

Figure 2.8 Measured output fundamental and IMD power for two-tone frequency separations for 20W LDMOS.

2.9. Device with Memory

A device with memory can be defined as if one where the output signal is a function of both instantaneous and previous input signals. However, a traditional definition for memory effects in the RF power amplifier community is: changes in the amplitude and/or phase of the inter-modulation distortion as a function of the modulation frequency [10] [11].

Figure 2.9 shows how a tone-spacing sweep ($\Delta\omega$) of a two-tone signal is employed as an indication of memory effect for a 3rd order polynomial modelled device. For example, a device would be said to exhibit magnitude memory effect, if a tone-spacing frequency sweep results in changes to the amplitude level of the inter-modulation distortion (IMD) as shown in Figure 2.9(b) or to asymmetry between IMD_{3L} and IMD_{3H} as shown in Figure 2.9(c).

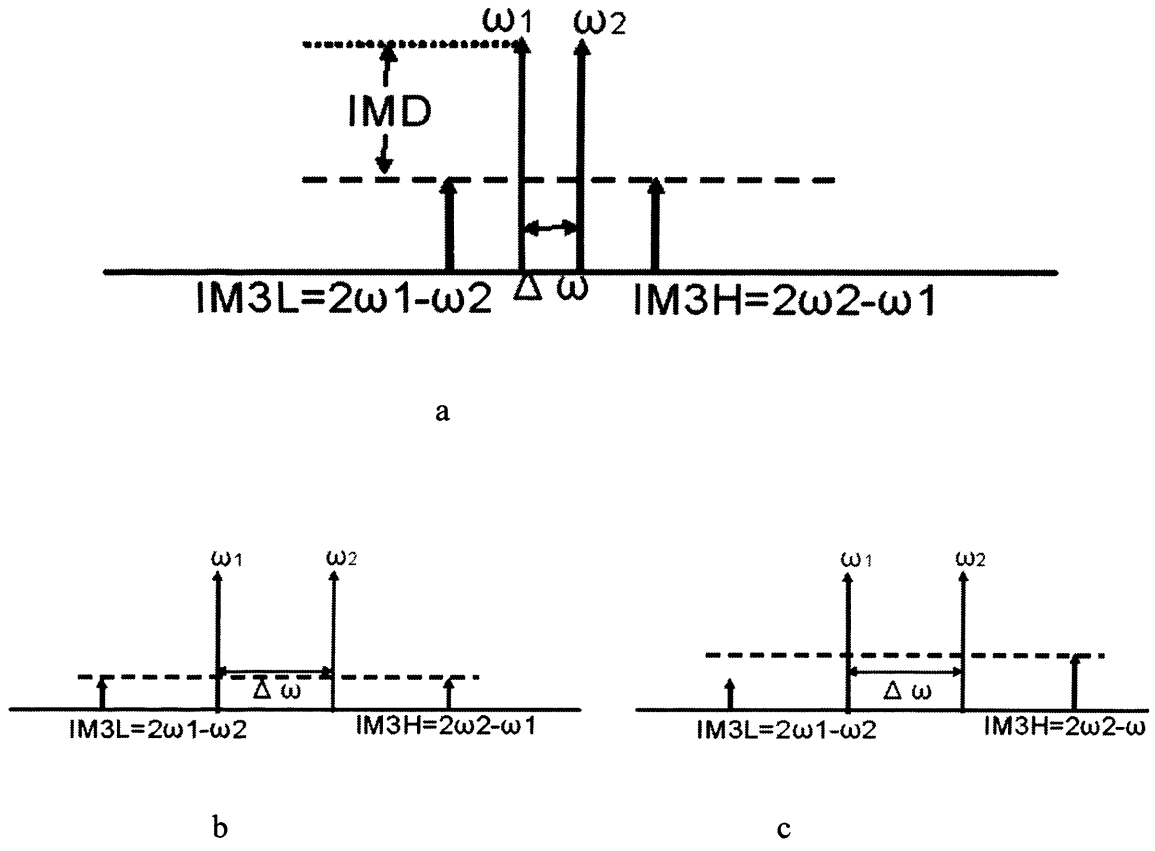

Figure 2.9 Definition of memory effect.

Another way of describing memory effects is a time lag, defined as an existence of a hysteresis, between AM-AM and AM-PM response, [11]

which creates uncertainty within the predictive model. In other words, for a nonlinear device with memory, the output signal of the device is not going to be only a function of its present input, but also appear as a function of the previous input.

Nevertheless, AM-AM and AM-PM are seldom used as precise characterisation technique for modelling devices with memory effect due to their inability to give comprehensive information on the device nonlinearity, such as in monitoring asymmetry in the IMD. [12] [13].

2.10. Source and Location of Memory Effects

Devices with memory effect can be classified into two categories: 'electrical' and 'thermal and trapping' memory effects [14] [10]. The most common contributors for causing memory effect can be summarised as:

- Device reactive components
- Input and output matching network
- Biasing network
- Coupling and de-coupling capacitor
- Thermal and trapping memory effect

Figure 2.10 illustrates the parts of the power amplifier structure attributed with the greatest responsibility for leading to the existence of memory effect.

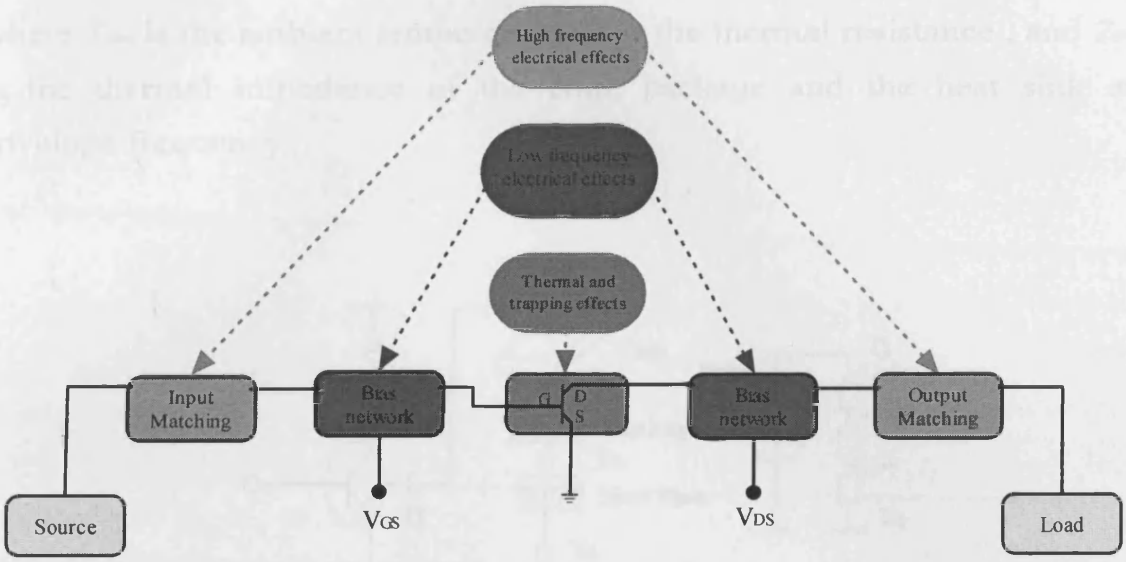

Figure 2.10 Typical sources of memory effect in power amplifier [After [15]].

2.10.1. Thermal and Trapping Memory Effects

High power devices can both produce and dissipated high power at low frequencies. This dissipated power varies according to time, which makes it frequency dependent and in turn may also lead to temperature variation in the transistor's junction. It is evident therefore that thermal effects diminish at high frequency because of the self-cooling which takes place when variation of the signal is too fast for the temperature to follow [13] but come into force strongly at lower frequencies.

The chip temperature can be modelled as shown in Figure 2.11 using this form [10]:

$$T = T_{amb} + R_{th} \bullet P_{diss}(dc) + Z_{th}(\omega_1 - \omega_2) \bullet P_{diss}(\omega_1 - \omega_2) \qquad (2.17)$$

where T_{amb} is the ambient temperature, R_{th} is the thermal resistance , and Z_{th} is the thermal impedance of the chip, package and the heat sink at envelope frequency.

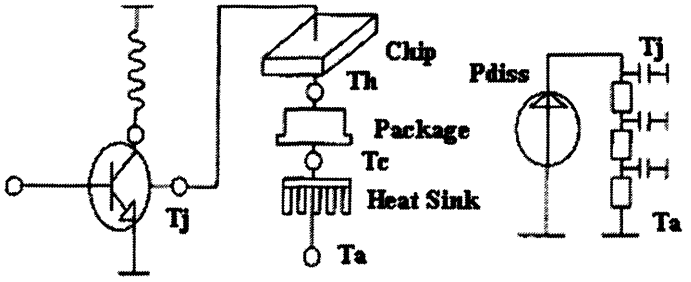

Figure 2.11 Physical and electrical model of the heat flow from active device (after [10])

For example the dissipated power in a Class A high power LDMOS device having VD=28V and ID=2 A, would be 56W. This amount of dissipation, when multiplied by thermal impedance at envelope frequency ($\omega_1 - \omega_2$) induces a high thermal variation in the device, as indicated in (2.17) which varies the thermal impedance, leading to a variation in the envelope voltage and resulting in a variation in IMD.

Trapping effects are inherent to the device itself and appear at low frequencies, potentially causing dispersion for the device conductance. This can cause variations in IMD with respect to modulation frequency (memory effect). In [16] trapping effects are shown to have appeared at low frequencies, when an electron and hole traps potential changes with envelope frequency and therefore have altered the intrinsic gain.

2.10.2. Electrical Memory Effects

Based on existing memory in the RF power amplifier, electrical memory effects can be subdivided into short-term memory effects and long-term memory effects

2.10.2.1. Short Term Electrical Memory Effects

Short-term memory effects (high frequency memory effects) are those signals which have a higher frequency (shorter time scale) than the information signal in a range close to the carrier signal. This kind of electrical memory effect is mainly caused by both the reactive components of the device in addition to input and output matching networks [11] [17]. It is caused by the variation of either or both the fundamental and the harmonics impedances at different frequencies. However, designing a matching network with approximately constant impedance for the RF fundamental signal, in addition to its harmonic frequencies may not be considered a difficult task, especially given that the RF fundamental signal and its harmonics would usually occupy a decade or less. Furthermore, the blocking capacitor at the input of the active device in combination with the parasites coil can cause memory effect [12]. Power amplifiers having short-term memory effects will usually have a static response for the information signal and may sometimes be treated as memory-less devices, since short-term memory effect has a time constant ($\approx$ns) much shorter than the time constant scale of the information signal ($\approx\mu$s). [17]

2.10.2.2. Long Term Electrical Memory Effects

Long-term memory effects (low frequency memory effects) have frequency of the order of the information signal itself (range from dc to a

few MHz) [18] [19]. This range of frequency is sometimes called 'intermediate frequency' (IF) or 'envelope frequency' when two-tone signal excitation is being used. Long-term electrical memory effects are typically due to the biasing network. In the case of a 5 MHz W-CDMA signal, for example, such a bias network needs to be constant and ideally, zero impedance at all low frequency (IF) ranges. Otherwise, AC voltages may be generated and added to the power supply voltage, causing amplitude and/or phase modulation, and resulting in asymmetry in the IMD [3] [14]. It is almost impossible to come up with a constant impedance for many frequency decades. This highlights the shortcomings of the simple bias network and the complexity of bias network design.

2.11. Waveform Engineering

Waveform engineering is very important especially when reduction of inter-modulation distortion is needed.

The voltage at the drain of LDMOS devices is the most significant factor in effecting the inter-modulation distortion components (IMD). As we have already discussed a two-tone test is often used to investigate the IMD performance through Taylor-series expansion. Taylor series expansion to the third order given by equation (2.18) can be used to describe the interaction with the device non-linearities which will cause a modification of all the frequency components in the resulting current waveforms.

$$i_o = a_1 v_i + a_2 v_i^2 + a_3 v_i^3 \qquad (2.18)$$

A simple description for the output current (IM_{3L} and IM_{3H}) containing the two-tone carrier stimulus with the injected IF difference component produced by the IF load-pull system combined with the second harmonic component ($2\omega_{1,2}$) is given by equations (2.19) and (2.20) [20]. This enables the variation of the magnitude and phase of the baseband as well as the second harmonic components to be used to vary the in-band distortion products.

$$IM_{3L} = D\cos\left[(2\omega_1)+\psi\right]+C\cos\left[(\omega_2-\omega_1)+\theta\right]+B+A(\cos\omega_1+\cos\omega_2) \quad (2.19)$$

$$IM_{3H} = D\cos\left[(2\omega_2)+\psi\right]+C\cos\left[(\omega_2-\omega_1)+\theta\right]+B+A(\cos\omega_1+\cos\omega_2) \quad (2.20)$$

where:

B is the DC bias voltage.

C and D are the magnitude of the base-band and the second harmonic signals, respectively.

θ and ψ are the phase of the base-band and the second harmonic signals, respectively.

It is clear that the optimisation of IM_3 terms is possible by controlling (engineering) either second harmonic or envelope (base-band) components. In this work however, only waveform engineering at the base-band will be considered.

The total third-order IMD_{3L}, for example, is a vector sum of third-order IMD_{3L} ($2\omega_1$-ω_2) caused by the third-order nonlinearity of the active device as a result of first mixing products and the mixing products of the signal at the second fundamental frequency ω_2 with the signal at $2\omega_1$ as a second mixing process in addition to the mixing products of the fundamental

frequency ω_1 with the signal of the envelope ω_2-ω_1 (IF_1) as a second mixing process. This is demonstrated in Figure 2.12. The total IM_3 as a function of only base-band impedance, and for fourth-order amplifier, can be modified by IF_1 and IF_2 ($2\omega_2$-$2\omega_1$) as:

$$IM_{3L} = E\cos\left[2(\omega_2-\omega_1)+\beta\right]+C\cos\left[(\omega_2-\omega_1)+\theta\right]+B+A(\cos\omega_1+\cos\omega_2) \qquad (2.21)$$

Where:

E and β are the magnitude and the phase of the base-band second harmonic signal (IF_2), respectively.

The vector diagram of this fourth-order amplifier is shown in Figure 2.13. In this arbitrary example, three boundaries are shown: the IF_1 boundary, the IF_2 boundary and the resultant IM_{3L} boundary, which is defined in this example by only the most two dominant base-band components (IF_1 and IF_2). It is possible according to this example to reduce IM_{3L} to zero. Higher IF components will theoretically effect inter-modulation distortion but their effect can be ignored, especially at low power, when compared to IF_1 or IF_2.

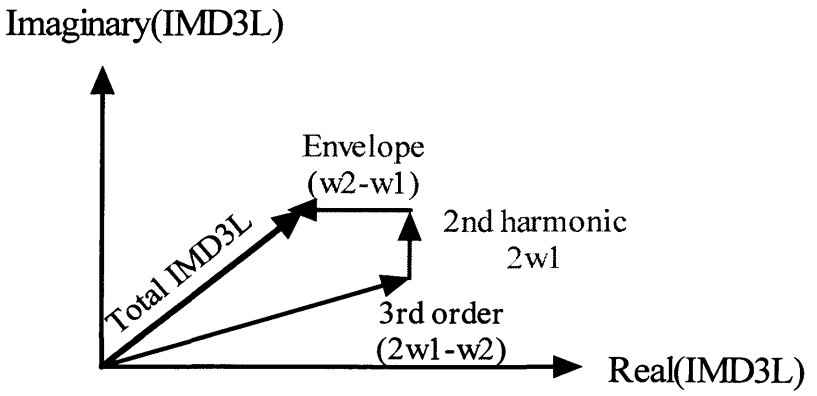

Figure 2.12 Composition of IM_{3L}.

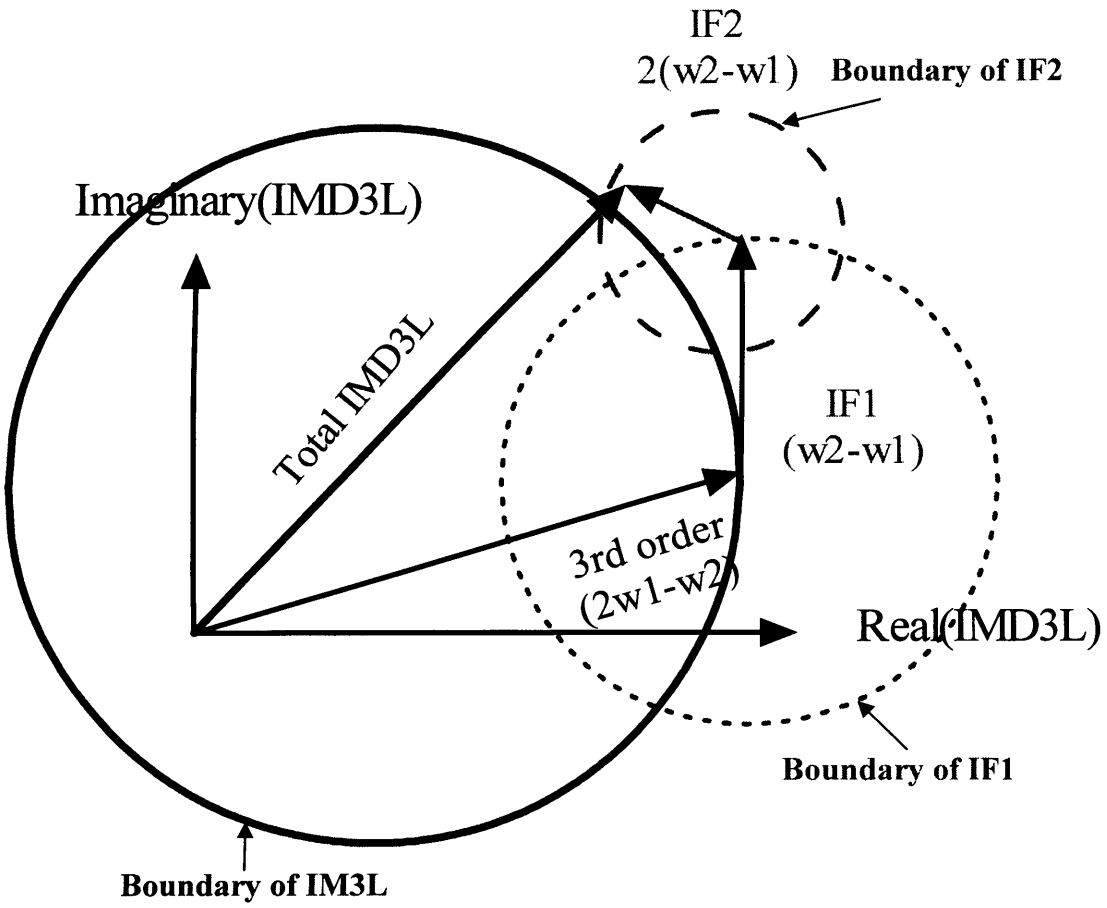

Figure 2.13 Boundary of IM_{3L} as a function of only base-band impedance (IF_1 and IF_2).

2.12. Classifications of Power Amplifiers

In modern communication systems RF power amplifiers are required to have efficiency and linearity over the range of power operation as well as adequate bandwidth. Efficiency is the ability to convert DC to RF energy with minimal wasted power and heat generation, while linearity is the ability to amplify the input signal without distortion.

Power amplifiers are divided into different Classes such as A, B, C...etc. The conduction angle of the drain (collector) current waveform is used to identify these Classes (see Figure 2.14). The main characteristic of these Classes is their trade-off between linearity and efficiency. Therefore, selection of a particular Class is determined by its application. High linearity and efficiency have become a figure of merit in CDMA base stations [21]. In a typical line-up of power amplifier chain, the power stage is often a Class B circuit for maximum efficiency; the driver stage a Class AB for a trade-off between linearity and efficiency, and pre-driver stage may be a Class A [6].

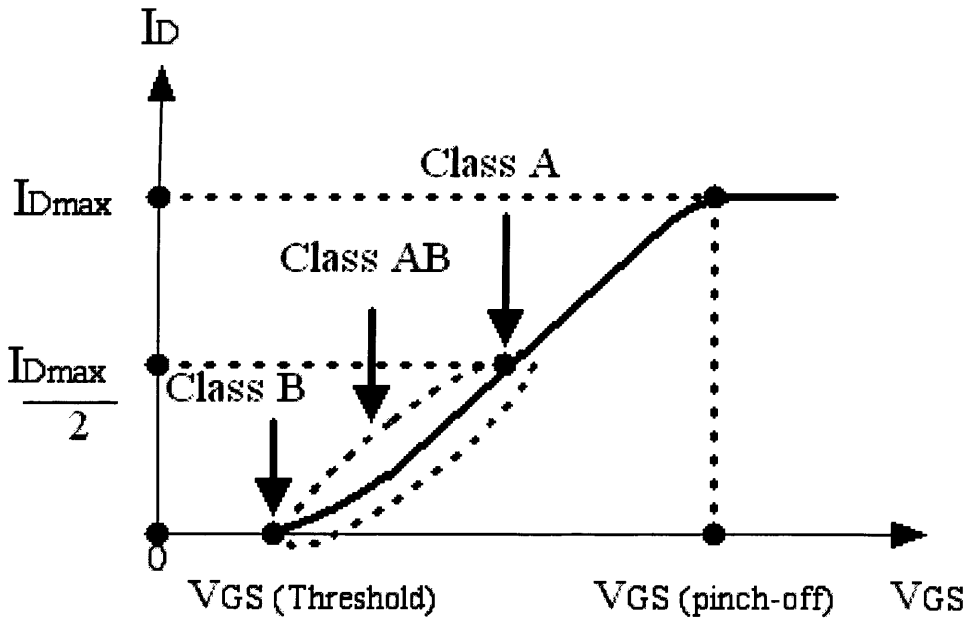

Figure 2.14 Classes of power amplifiers.

2.12.1. Class A Operation

In a Class A amplifier, the transistor is biased at a quiescent current Iq with the output current flow for the whole conduction angle at 360 degrees. Figure 2.15 shows the dc load line. The Q point is chosen to be in the middle of the load line so the signal will swing in either direction at the same intensity, and has the maximum probability not to compress. In this case, the transistor operates in the linear region between the saturation and cut-off of its transfer characteristic, and therefore maintains high linearity resulting in low distortion. Maximum efficiency of 50% can be achieved if V_{DS} minimum at I_{max} and I_{min} are set to zero, nevertheless, the practical efficiency is about 30% [22].

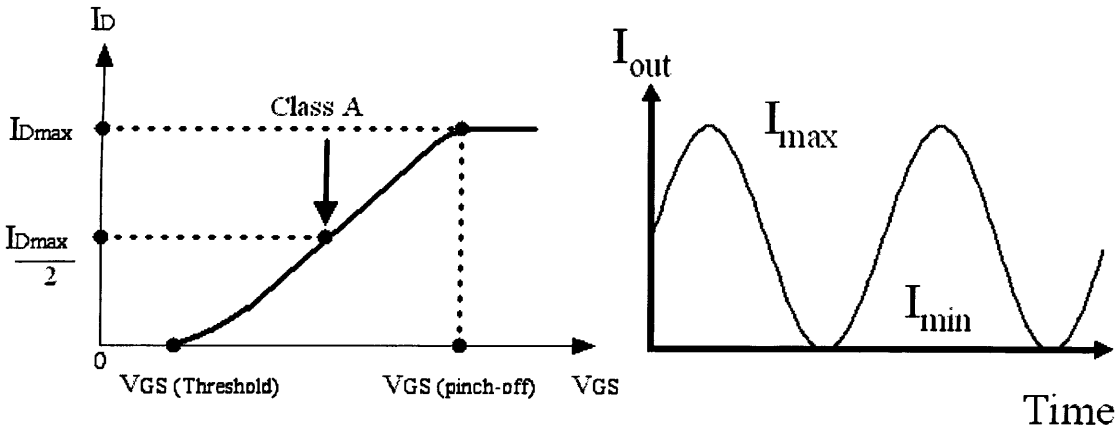

Figure 2.15 Transfer characteristic of Class A amplifier.

The efficiency is defined as the ratio of the output RF power divided by the DC supply power:

$$\eta = \frac{P_{out(RF)}}{P_{DC}} \qquad (2.22)$$

The maximum average power delivered to the load is given by:

$$P_{Lmax}=\frac{1}{2}\frac{Vrf^2}{R_L} \tag{2.23}$$

With Vrf equal to the DC drain voltage defined as V_{DD}, the output power is:

$$P_{Lmax}=\frac{1}{2}\frac{V_{DD}^2}{R_L} \tag{2.24}$$

The average power delivered by the DC supply is:

$$P_{DC}=\frac{V_{DD}^2}{R_L} \tag{2.25}$$

Hence the maximum efficiency is:

$$\eta=\frac{PRF}{PDC}=\frac{\frac{1}{2}\frac{V_{DD}^2}{R_L}}{\frac{V_{DD}^2}{R_L}}*100=50\% \tag{2.26}$$

Class A amplifiers are useful for applications where high linearity is required, but the drawback is the low efficiency leading to high power dissipation. To deliver, for example, 20W to the load, 40W needs to be supplied from the DC source. The extra 20W will be converted to heat in the power amplifier transistor, which requires a large cooling system such as a heat sink.

2.12.2. Class B Operation

Class B amplifiers are usually biased at dc quiescent current equal to zero (threshold), hence no output current will be drawn when no input signal is applied at the device input. The conduction angle of Class B amplifiers is

precisely 180 degrees, or just half the input cycle, thus the power dissipated is cut approximately to half.

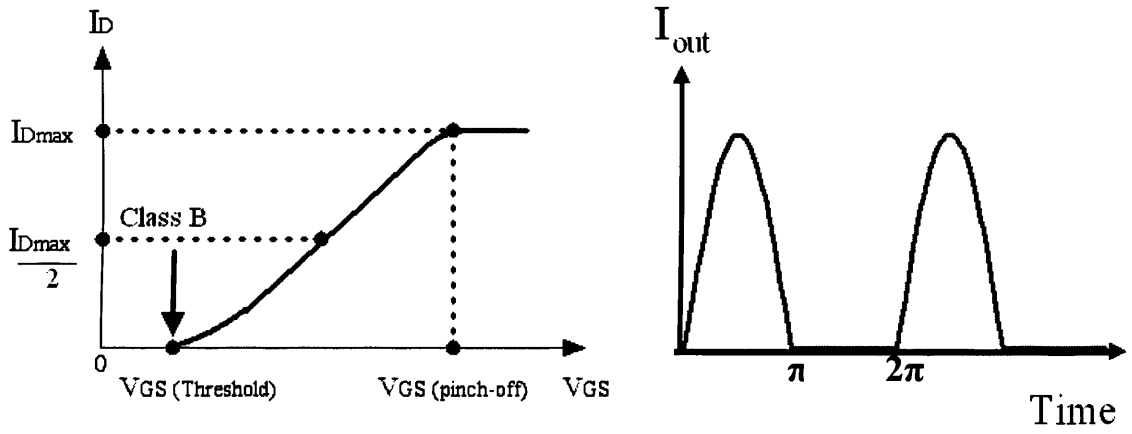

Figure 2.16 Transfer characteristic of Class B amplifier.

The output current waveform shows zero current for π <time< 2π as can be seen in Figure 2.16. Thus the average current will be:

$$I_{DC}=\frac{1}{T}\int_0^T I_{o(t)}dt$$
$$=\frac{Im}{\pi}=\frac{Vm}{\pi R_L}$$

The total power delivered by the two power supply is:

$$P_{DC}=2V_{DD}I_{DC}=2\frac{V_{DD}^2}{\pi R_L}$$

The output power is given by:

$$P_{RF}=\frac{1}{2}\frac{Vrf^2}{R_L}$$

With Vrf equal to the DC drain voltage defined as V_{DD}, the output power is:

$$\eta = \frac{\frac{1}{2}\frac{V_{DD}^2}{R_L}}{\frac{2V_{DD}^2}{\pi R_L}} * 100 = \frac{\pi}{4} 100 = 78.5\%$$

The efficiency in the case of Class B amplifiers is much higher than in Class A, bearing in mind that Class A are more linear than Class B. In compression with a Class A amplifier, only 25.5W is needed from the power supply to deliver 20W to the load. This example shows that the power dissipated in Class B is about 25% of that dissipated in Class A. It must therefore follow that a Class A amplifier has a higher power rating than a Class B amplifier.

2.12.3. Class AB Operation

In terms of linearity and efficiency, a Class AB amplifier is a compromise between Class A and Class B, as can be seen in Figure 2.17. Class AB is preferable when a trade-off between efficiency and linearity is involved [11].

The conduction angle will be between 360 and 180 degrees at a quiescent point above the cut-off and below the Class A bias point resulting in an efficiency level of between 50% and 78.5%.

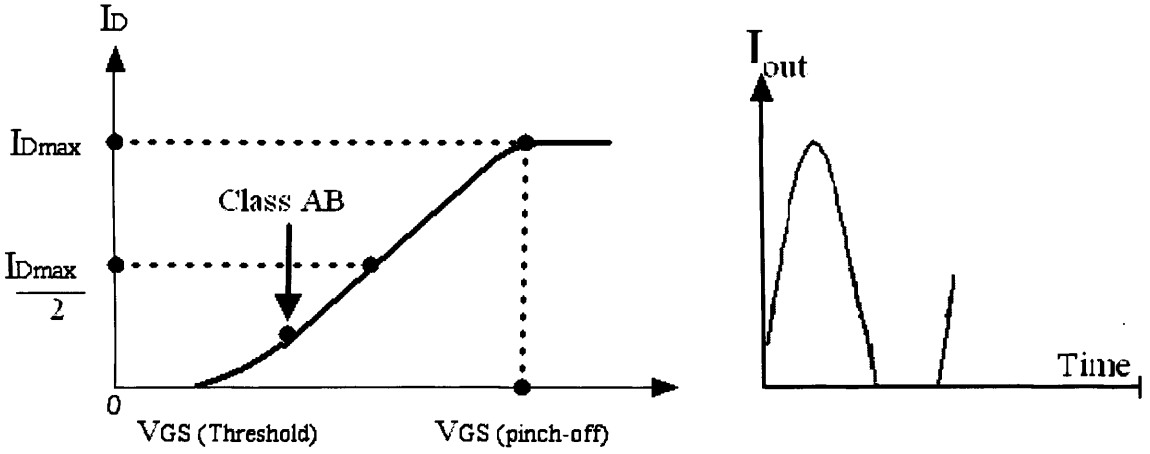

Figure 2.17 Transfer characteristic of Class AB amplifier.

2.12.4. Comparison between Class A, Class B and Class AB

An illustration of the effect of different Classes is made possible by using the non-linear high power measurement system with two-tone stimulus frequency of 2099 MHz and 2101 MHz, at different input powers, using a 20W LDMOS device at a constant drain voltage of 28V over a power sweep of approximately 8 dB. Figure 2.18 compares the lower fundamental output power (ω_1) and the lower inter-modulation distortion (IMD_{3L}) of the three different Classes. At a constant and low input power of 16 dBm, Class B has an output power magnitude greater in magnitude than Class A by 8 dBm, and about 3dBm greater than that of Class AB. The linearity of these Classes can be investigated by comparing their inter-modulation distortion level. It is clear that, out of the three devices, Class B produces the most distortion, but it is the behaviour of Class AB which is of greatest interest and importance in that it generates inter-modulation distortion equal in magnitude to that of Class A, especially at higher input

drive levels. This indicates that a Class AB amplifier is approximately equal in linearity to Class A, and can still provide sufficient output power when compared to a Class A amplifier. However, different linearisation techniques can be used to enable the use of more cost-effective and more power efficient amplifiers while maintaining an acceptable level of linearity.

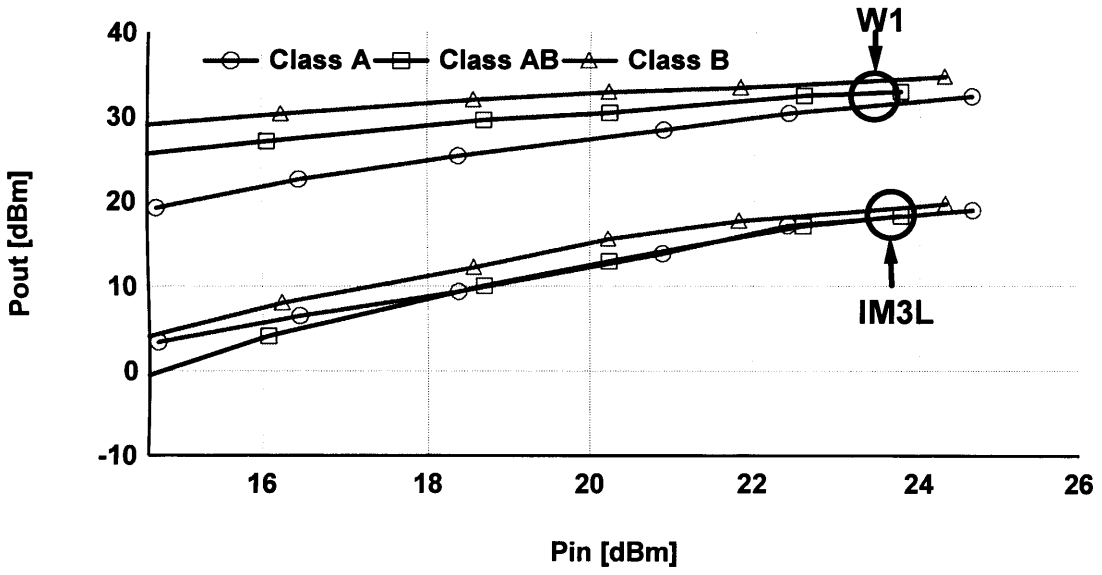

Figure 2.18 Comparison of Class A, Class B and Class AB amplifier.

2.13. Summary

This chapter has presented important background material for this thesis. Methods of identifying nonlinear amplifiers were reviewed by means of using two-tone test through Taylor-series expansion.

Memory effects are defined in this thesis as changes in the amplitude or phase of distortion components (IMD) caused by changes in modulation frequency ($\Delta\omega$) and will be used due to their ability to give comprehensive information on the device nonlinearity, such as in monitoring asymmetry in the IMD. Two kinds of memory effects do exist in RF power amplifiers: short-term memory effects and long-term memory effects. It is the long-term memory effect (low frequency signal), which is mainly caused by variation in the bias network impedance, which is going to be the main concern of the experimental investigations to follow. It is important therefore to find an access (port) to this signal. Hence, Chapter 3 shows how to measure and engineer this component.

2.14. References

1. Carvalho, J.C.P.a.N.B., *Intermodulation Distortion in Microwave and Wireless Circuits*. 2003, Norwood,MA: Artech House.

2. Choongeol, C., et al., *IIP3 estimation from the gain compression curve.* Microwave Theory and Techniques, IEEE Transactions on, 2005. **53**(4): p. 1197.

3. Cripps, S.C., *RF Power Amplifiers for Wireless Communication.* 2006, Norwood,MA: Artech house.

4. Cripps, S.C., *Microwave Bytes*, in *Microwave magazine.* 2007. p. 44-50.

5. Aparin, V. and C. Persico. *Effect of out-of-band terminations on intermodulation distortion in common-emitter circuits.* in *Microwave Symposium Digest, 1999 IEEE MTT-S International.* 1999.

6. Wang, N.L., et al. *28V High-Linearity and Rugged InGaP/GaAs Power HBT.* in *Microwave Symposium Digest, 2006. IEEE MTT-S International.* 2006.

7. Watanabe, S., et al. *Simulation and experimental results of source harmonic tuning on linearity of power GaAs FET under class AB operation.* in *Microwave Symposium Digest, 1996., IEEE MTT-S International.* 1996.

8. Cha, J.K., Ildu; Hong, Sungchul; Kim, Bumman; Lee, Jong Sung; Kim, Han Seok, *Memory effect minimization and wide instantaneous bandwidth operation of a base station power amplifier.* Microwave Journal, 2007. **v 50**(n 1): p. p 66-82.

9. J. Vuolevi, a.T.R., *Distortion in RF power amplifier*. 2003, Boston: Artrch House.

10. Vuolevi, J.H.K., T. Rahkonen, and J.P.A. Manninen, *Measurement technique for characterizing memory effects in RF power amplifiers.* Microwave Theory and Techniques, IEEE Transactions on, 2001. **49**(8): p. 1383-1389.

11. S. C. Cripps, *Advanced Techniqes in RF Power Amplifier*. 2002, Norwood,MA: ArtechHouse.
12. Bosch, W. and G. Gatti, *Measurement and simulation of memory effects in predistortion linearizers*. Microwave Theory and Techniques, IEEE Transactions on, 1989. **37**(12): p. 1885.
13. Draxler, P., et al. *Time domain characterization of power amplifiers with memory effects*. in *Microwave Symposium Digest, 2003 IEEE MTT-S International*. 2003.
14. Bosch, W. and G. Gatti, *Measurement and simulation of memory effects in predistortion linearizers*. Microwave Theory and Techniques, IEEE Transactions on, 1989. **37**(12): p. 1885-1890.
15. Ahmed, A., *Analysis, Modelling and Linearization of Nonlinearity and Memory Effects in Power Amplifiers Used for Microwave and Mobile Communications.PhD Thesis*. 2005, Kassel University.
16. Anthony, E.P. and G.R. James. *Relating Dynamics of FET Behavior to Operating Regions*. 2001.
17. Martins, J.P., N.B. Carvalho, and J.C. Pedro. *A Figure of Merit for the Evaluation of Long Term Memory Effects in RF Power Amplifiers*. in *Microwave Symposium Digest, 2006. IEEE MTT-S International*. 2006.
18. Vuolevi, J.H.K., T. Rahkonen, and J.P.A. Manninen, *Measurement technique for characterizing memory effects in RF power amplifiers*. Microwave Theory and Techniques, IEEE Transactions on, 2001. **49**(8): p. 1383.
19. Franco, M., et al. *Minimization of bias-induced memory effects in UHF radio frequency high power amplifiers with broadband signals*. 2007. Long Beach, CA, United States: Institute of Electrical and Electronics Engineers Computer Society, Piscataway, NJ 08855-1331, United States.
20. Brinkhoff, J. and A.E. Parker, *Effect of baseband impedance on FET intermodulation*. Microwave Theory and Techniques, IEEE Transactions on, 2003. **51**(3): p. 1045.

21. Yang, Y., et al., *Optimum design for linearity and efficiency of a microwave Doherty amplifier using a new load matching technique.* Microwave Journal, 2001. **44**(12): p. 20.

22. Pothecary, N., *Feedforward Linear power Amplifier.* 1999, Norwood, MA: Artech house.

CHAPTER 3

Measurement Infrastructure for Memory Investigation

3.1. Available Commercial Instruments

Traditionally, high-frequency measurement systems employ CW signals for the investigations of device characteristics. However, device characterisation at CW frequencies do not allow for the measurement and investigation of important device characteristics such as memory effects [1]. Unlike low frequency measurement it is rather difficult to measure, for instance, power using voltage and current directly by using conventional voltmeter or ammeter at RF frequencies [2], because they will interact and influence the accuracy of power measurement at RF/microwave frequencies. However, it is important to realise that power, unlike current or voltage, is one of the few fundamental quantities that can be directly measured.

With the revolution in wireless communications, microwave and RF frequencies usage is expanding; hence, developers of RF test equipments and measurement systems are driven to improve the performance of their systems.

3.1.1. Spectrum Analyzers

Spectrum analyzers are primarily a tool for the frequency domain. They are considered to be a very powerful instrument for measuring signals with frequencies ranging from approximately100 Hz to approximately 110 GHz. Common spectrum analyzers measurements are signal characteristics such as in-band signals (fundamental and distortion components), out-of-band signals (RF harmonic and IF components). Spectrum analyzer-based systems allow for the use of modulated signals. However, due to their limitations, they only permit the measurement of the spectrum magnitudes. Consequently, it is rather difficult to utilise such systems for the accurate and unambiguous analysis of non-linear circuits, since a limited set of magnitudes can generate an infinite number of current and voltage waveforms.

3.1.2. Vector Network Analyzers

Vector network analyzers are designed to measure both the magnitude and phase ratio of the voltage travelling waves. Their basic capability is to measure the s-parameters of an RF or microwave device and display the amplitude and phase ratio information in the frequency domain. They can measure transmission losses, return losses, gains, impedances, phases and group delay with a wide range from DC to 110 GHz for characterising components.

S-parameters can only accurately represent linear devices, such as filters, cables, connectors...etc, whose behaviour is determined solely by the linear equations. However, basic linear s-parameters cannot fully predict the behaviour of non-linear devices.

It would also be impossible to determine the voltages and currents at the device plane, since vector network analyzers only measure the ratio between the incident and the reflected voltage waveform but not their absolute values. Hence it would be difficult again from these measurements alone to develop a good understanding of the device non-linear behaviour.

3.1.3. Vector Signal Analyzers

The vector signal analyzers, a more recent advancement, can perform the same measurements as the spectrum analyzer while also providing information on the phase of the signal. Their bandwidth is not sufficient for fully non-linear characterisation. For example, a device under two-tone test with a tone-spacing of 20 MHz (the new high-bandwidth communications standards such as WiMax generate 20-MHz bandwidth signals) will generate in-band and out-of-band distortion. Therefore, in order to study the performance of the in-band distortion up to only 5^{th} order will require a minimum bandwidth of 200MHz. Also they do not allow for simultaneous measurement of base-band and harmonics signal components.

3.1.4. Large Signal Network Analyzers

Large signal network analyzers are similar to vector network analyzer. They have a wide bandwidth. For example, Maury Microwave's MT4463A Large-Signal Network Analyzer is operating from 600 MHz to

20 GHz with maximum power into test ports of 10 watts (+40 dBm) [3]. Further, they are capable of measuring the absolute values of the incident and the reflected travelling waves, which can be easily transformed to voltages and currents in the time-domain using an inverse Fourier transform. Despite having large bandwidth their lower frequency is relatively high (600 MHz). Therefore, they will not be suitable, for instance, to investigate low frequency memory effect for non-linear RF devices.

3.2. Non-Commercial Waveform Measurement System Architecture

To bridge the gap between all these instruments, measurement systems developed at Cardiff University have been focused towards building a novel fully functional RF waveform high-power time-domain measurement system. The basic CW approach is an extension of the measurement system demonstrated by Tasker, et al [4] and it is shown in Figure 3.1. This measurement system is sometimes referred to as Non-Linear Vector Network Analyzer (NLVNA), and consists of two directional couplers used to measure the incident and reflected waveforms with a bandwidth of 1GHz-12GHz and two bias tees [2] of the same bandwidth and a maximum current and voltage handling of 10A and 100V respectively. The RF couplers and bias tees are capable of handling up to 100W CW. The two triplexers are used to separate the fundamental, second, and third harmonic components to three ports, so that each frequency can be independently tuned using three ESGs to generate the desired terminating impedances (referred to as waveform engineering).

The 2-channel microwave transition analyzer is used to measure the incident waveforms a_n and the reflected waveform b_n at the device n^{th} port,

input and output, which are error corrected before being converted to voltages and currents, as follows:

$$V_n = \sqrt{z_o}(a_n + b_n) \tag{3.1}$$

$$I_n = \frac{(a_n + b_n)}{\sqrt{z_o}} \tag{3.2}$$

The key feature of this waveform measurement system is its ability to investigate the device performance in the time domain. This will provide a full insight into the non-linear behaviour of the device under test.

Unlike the large signal network analyzer, this waveform measurement system has a receiver and a test-set; therefore it is suitable for both waveform measurement and waveform engineering. This measurement system is capable of handling power up to 100W CW with a bandwidth of 1 GHz to 12 GHz, which makes it suitable for characterising devices at high frequencies. Nevertheless, the lower frequency that this measurement system can handle is 1 GHz, similar to the LSNA. This Cardiff high power CW measurement system is not capable of detecting modulated signals, which contain additional high and low frequency components generated by the non-linear device. For instance, the directional couplers and/or the bias tees exhibit large bandwidth yet have lower cut-off frequencies, in the range of several hundred megahertz, making them unsuitable for the detection of low-frequency IF signal components. Reference [5] [6] [7] [8] , has shown that the IF impedance, presented at the device plane can affect the in-band distortion. Because this measurement system cannot detect low frequency signals (<1 GHz) it was not suitable for investigating base-band memory effects.

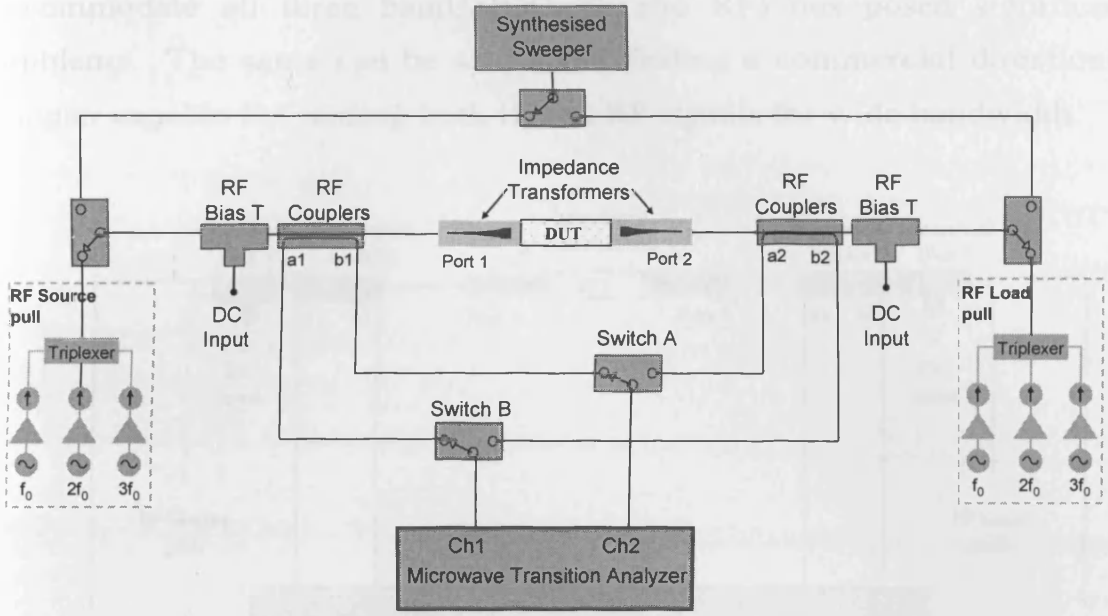

Figure3.1Schematic of the 100 W RF measurement system based on microwave transition analyzer (MTA) with a frequency range for the higher harmonics up to 12 GHz.

3.3. Ideal RF and IF Measurement System

The RF waveform measurement system on its own is not capable of, for example, measuring modulated low frequency IF components (ω_2- ω_1) because the RF bias tee is not capable of providing the device being tested with DC, IF and RF signals all at the same time. The problem is further compounded by the fact that the bandwidth of the RF directional coupler is 1 to 12 GHz making it impossible to detect the IF signals. In this case, the RF bias tee must be replaced by a triplexer in order to supply the DUT with the DC, IF and RF signals, and the RF directional coupler has to be replaced with a new broadband directional coupler capable of sensing both IF and RF signals. Figure 3.2 represents an ideal measurement system with optimum components. However, finding a commercial 4 port bias

tee (triplexer) with the required bandwidth and power handling to accommodate all three bands (DC, IF and RF) has posed significant problems. The same can be said about finding a commercial directional coupler capable for sensing both IF and RF signals for wide bandwidth.

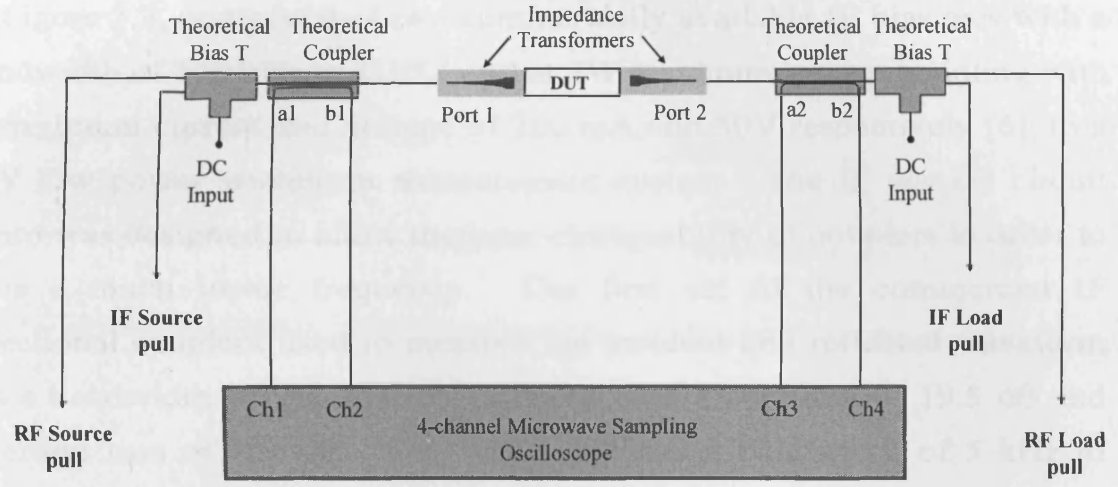

Figure3.2 Schematic of the theoretical high power time domain measurement system with IF and RF source and load pull capability.

3.4. Practical RF and IF Measurement System

To bring the ideal measurement system from the theoretical world to a practical environment, the CW high power measurement systems was further developed to detect the low frequency (IF) components and therefore study the effect of both IF and RF signals on device behaviour such as base-band memory effect. The aim being to have a system that could fully characterise and design RF power amplifiers at both high and low frequencies. The required four ports bias tee has been realised through means of two diplexers connected in series, and the required

directional coupler has been split to two couplers one for the RF frequencies and the other for the IF frequencies. This measurement system is shown in Figure 3.3.

This architecture was previously validated by adding an IF test-set, shown in Figure 3.3, composed of two commercially available IF bias tees with a bandwidth of 100 kHz to 1GHZ and at 2W maximum power handling with a maximum current and voltage of 200 mA and 30V respectively [6], to a CW low power waveform measurement system. The IF test-set circuit board was designed to allow the inter-changeability of couplers in order to have a much lower frequency. The first set of the commercial IF directional couplers used to measure the incident and reflected waveform has a bandwidth of 200 kHz to 250MHz with a coupling of 19.5 dB and insertion loss of 0.9 dB. The second set has a bandwidth of 5 kHz to 20MHz with a coupling of 11 dB and insertion loss of 0.9 dB. An Agilent 100MHz oscilloscope was used to sample and measure the low frequency IF signals allowing for the measurement of voltage and current waves between 100 kHz and 100 MHz.

The complete specifications of the IF test-set is mostly determined by the specification of both IF bias tee and the IF directional coupler, hence the maximum power of the test-set stands at only 2W with a low frequency of 100 kHz defined by the lower cut-off frequency of the IF bias tee, and the high frequency of either 250MHz or 20MHz depending on which directional coupler is used.

A possible integration of the high power RF and low power IF waveform measurement system is shown in Figure 3.3 and consists of two main entities: the RF test-set (upper level) with the components shown in green and the IF test-set (lower level) with the components shown in orange

which are identical in terms of both component architecture and principle of operation.

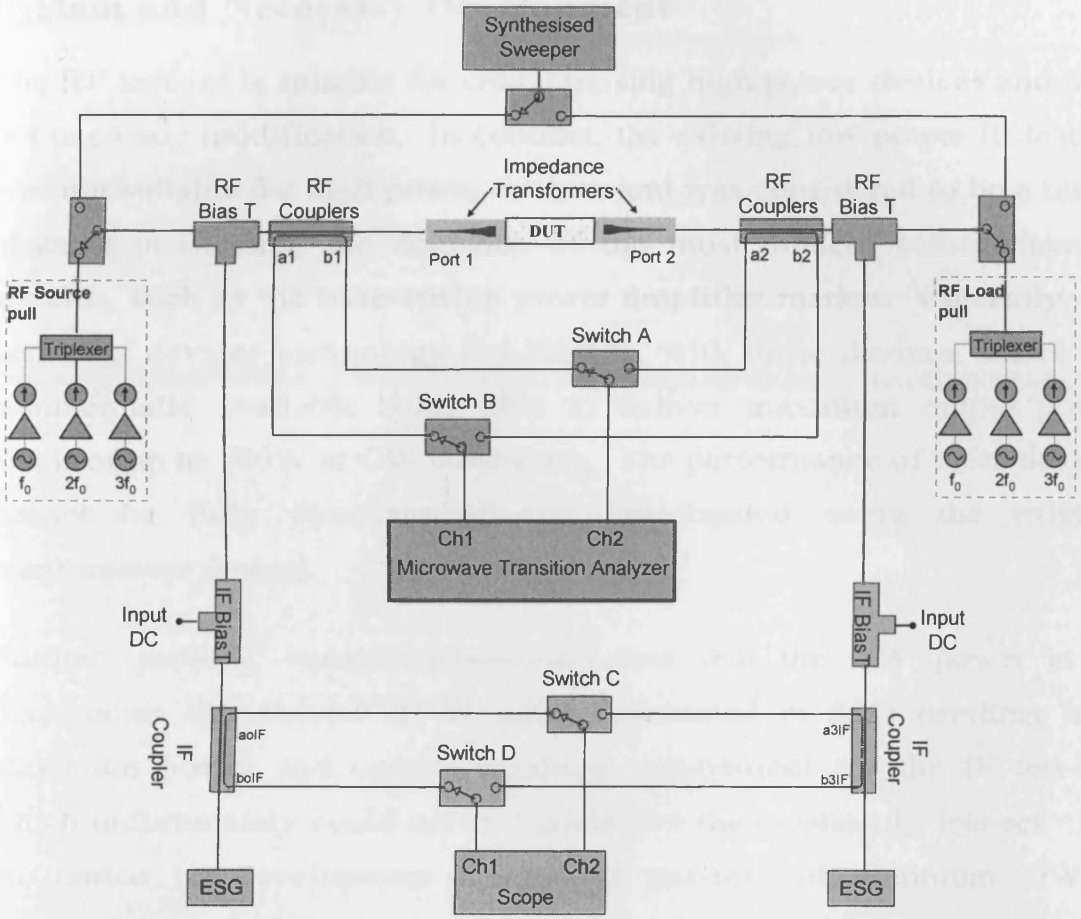

Figure3.3 Schematic of the high power RF and low power IF measurement system with active and source pull.

The architecture incorporates a combined IF and RF capabilities allowing for the collection of all four travelling waves at both IF and RF frequencies. The resulting measurement system has a bandwidth of

approximately 100 kHz to 12GHz allowing for waveform measurement at high and low frequencies.

3.5. Limitations of the Existing Waveform Measurement System and Necessary Development

The RF test-set is suitable for characterising high power devices and does not need any modification. In contrast, the existing low power IF test-set was not suitable for high power devices and was considered to be a major obstacle in meeting the demands of the most modern communication systems, such as the base-station power amplifier market. Currently, the dominant devices technology is LDMOS, with those devices, which are commercially available being able to deliver maximum output power levels of up to 180W at CW conditions. The performance of these devices cannot be fully characterised and investigated using the existing measurement system.

Further 'probing' measurements suggested that the CW power at IF frequencies can exceed 20 W when terminated in 50Ω resulting in a maximum power and current handling requirement for the IF test-set, which unfortunately could not be handled by the existing IF test-set. For this reason, the development of a new IF test-set with minimum 50W IF power and 10 A DC current was considered to be an immediate way of progressing to such high IF power.

Moreover, due to some limitations of the original MTA implementation, which will not be discussed in this work, the sampling of repetitive signals was limited to be between 10MHz and 40GHz, with the MTA was set to sample at its minimum sampling frequency of 10MHz. Therefore, this decreased the measurement system capability of sweeping the IF frequency from DC to 10 MHz. The minimum frequency of 10 MHz is

above the application space in terms of base-band memory effect. Sweeping the modulation frequency across the bandwidth of the modulated signal would provide a means of relating the performance of the device using a two-tone signal to the performance achieved with a modulated signal.

3.6. Proposed High Power IF and RF Waveform Measurement System

The existing measurement systems, which have been developed at Cardiff University, are not capable for detecting low-frequency signal components at high power levels. To overcome this problem, it was decided to design a suitable high power IF test-set to allow the observation and control of all relevant frequency components (RF, IF and DC)[6, 9].

The main objective of the proposed measurement system, therefore, was to upgrade the IF power handling capability from approximately 2 W and 0.2 mA range to approximately 50 W and 10 A range, making it suitable for characterising and investigating high power devices, such as base-station LDMOS transistors. These test-set specifications were considered to be a research challenge just two years ago [10] due to the complex requirements involved in implementing such a measurement system [9].

The proposed high power IF test-set is similar to the existing one (low power), but the components have high power, current and voltage specifications. The two major critical components in the IF test-set are the IF directional coupler and the IF bias tee. It was possible to find a suitable high power IF directional coupler (off-shelf) that met the proposed high power IF test-set specifications. The IF low power directional couplers would be replaced with the commercially available directional couplers,

manufactured by WERLATONE, to provide the IF test-set with a bandwidth of 10 kHz to 1GHz with a maximum power of 50W CW, combined with a coupling of 30 dB and a maximum insertion loss of 1.2 dB. However, despite substantial efforts, it proved impossible to source a suitable high power IF bias tee capable of handling high DC and RF voltages and currents over a large bandwidth. Therefore, it was decided to design suitable IF bias tees on site to complete the architecture of the IF test-set. The proposed IF bias tee design should have a bandwidth of 50 kHz to 50 MHz with the capacity to handle a current and voltage of 10A and 100V respectively, in addition to a typical insertion loss of 0.5 dB to the IF signal and a minimum isolation of 20 dB. Also another bias tee (mainly for the gate/base side which does not usually require high current) will be designed on site for a wide bandwidth of 50 kHz to approximately more than 300 MHz and a maximum current of 2A at 100V.

The proposed non-linear high power IF and RF measurement system, with a further modification to the previous measurement system architecture, is going to be as that shown in Figure 3.4. This measurement system consists of two main parts: the RF part (upper level) with the components shown in green and the IF part (lower level) with the components shown in orange which are identical in both component architecture and principle of operation. The two parts are separated by the RF bias tee which should have an IF bandwidth of at least an order of magnitude larger than the modulation frequencies used for device characterisation, in order to detect the fundamental and harmonic signal components of the IF signal.

The architecture incorporates a combined IF and RF capability allowing for the collection of all four travelling waves at both IF and RF frequencies. Diplexing the coupled RF and IF components of the signal prior to measurement is a key feature, and ensures phase coherence

between measured IF and RF components. Moreover, using the 4-channel microwave sampling oscilloscope is more compact and time-efficient than the previous system, where a microwave transition analyzer (MTA) was used for the RF frequency and an oscilloscope was used for the low frequency.

The RF test-set components will not be modified since it is already suitable for characterising high power RF amplifiers with a bandwidth of 1-12GHz and a maximum current and voltage handling of 10A and 100V respectively.

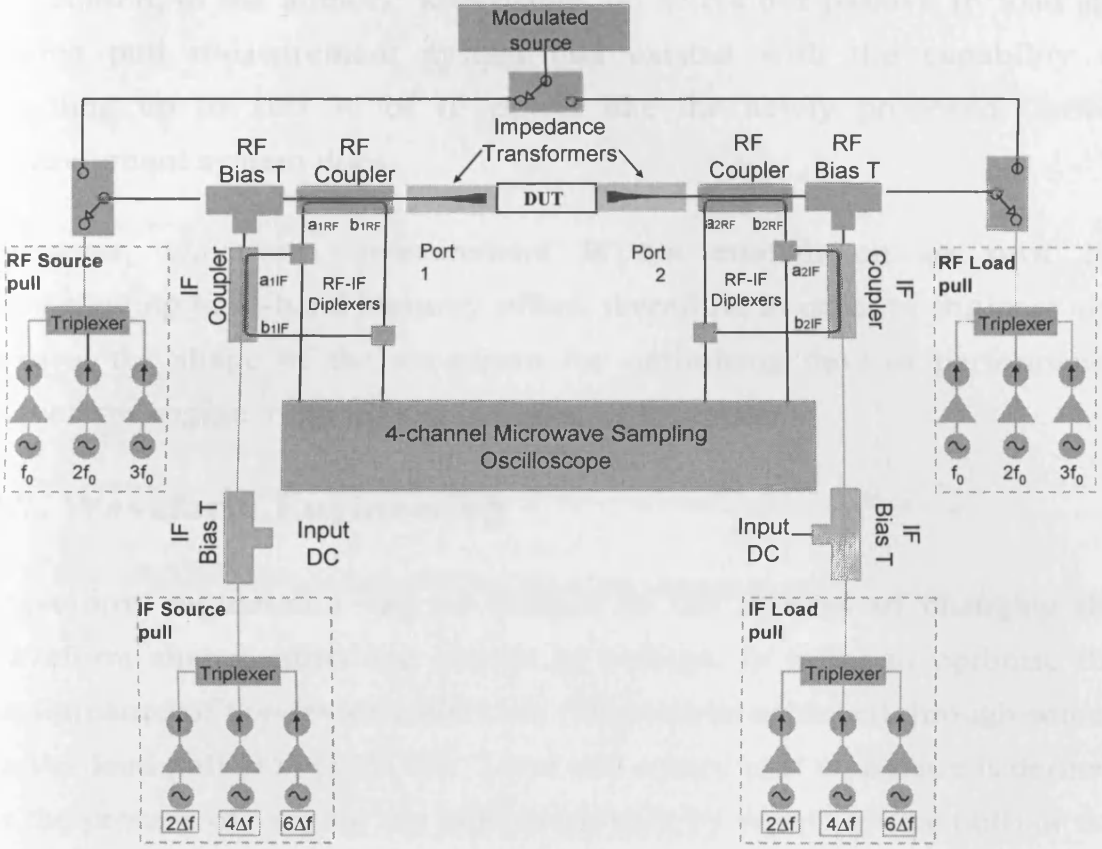

Figure 3.4 Schematic of the proposed high power RF and IF measurement system with active source and load pull.

The resulting measurement system will have the capability to handle RF power of more than 100W and IF power of more than 50W along with current and voltage of more than 10A and 100V respectively. The new measurement system can characterise devices for a bandwidth ranging from approximately 50 kHz to approximately 12 GHz. This measurement system is therefore suitable for investigating high and low frequencies memory effects.

In addition, to the authors' knowledge, no active nor passive IF load and source pull measurement system had existed with the capability of handling up to 100 W of IF power like the newly proposed Cardiff measurement system does.

However, waveform measurement is not enough on its own for investigating base-band memory effect, therefore, in order to engineer and control the shape of the waveform for optimising devices performance waveform engineering technique becomes essential.

3.7. Waveform Engineering

Waveform engineering can be defined as the process of changing the waveform shape, either the current or voltage, in order to optimise the performance of the device under test. This can be achieved through source and/or load pull [11] [12] [13]. Load and source pull technique is defined as the process of varying the impedance seen by input (source pull) or the output (load pull) of the device under test. The measurement system shown in Figure 3.4 has four ports, two ports for the RF test-set and two for the IF. This waveform measurement system is capable of maintaining both RF and IF load and/or source pulls for a bandwidth of approximately 50 kHz to 12 GHz.

3.7.1. RF Source and Load Pull

RF load and source pull is a technique based on the search for the optimum impedance seen by the device in order to investigate its performance e.g. efficiency, linearity, gain, and output power. This is important especially for the nonlinear device in which the performance with different load cannot be predicted using small signal s parameters. Source pull can be defined as the process of tuning (source pulling) the

input impedance seen by the input of the active device while the load pull is the process of tuning (load pulling) the output impedance seen by the active device.

Cardiff waveform measurement system is capable of characterising high power devices in excess of 100 W through RF load and/or source; however, in this measurement system it becomes crucial to load pull these devices at the same time. This is due to the fact that the optimum output impedance of high power LDMOS amplifiers is approximately less than 10 Ω while the measurement system impedance is 50 Ω. This large impedance difference between the device and the measurement system leads to insufficient power transfer. In order to maximise the power transfer and minimise the reflection coefficient, impedance transformer (matching impedance) is needed to match the DUT to the measurement system. Therefore, for this measurement system, input and output RF impedances were established at 10 Ohms using broad-band 5:1 impedance transformers [14] to match the device with the measurement system for maximum power transfer.

This approach becomes very important in the case of high power harmonic active RF load pull [15] [16]. For example, Figure 3.5 indicates that the load pull system has to deliver a power equal to ten times the power dissipated by the load at the device reference plane at reflection coefficient (Γ) of 0.95.

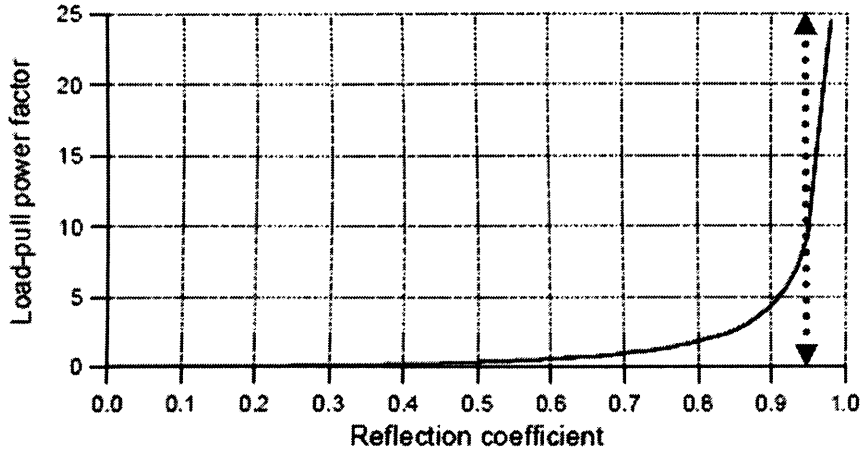

Figure3.5 Multiplication factor indicating the required maximum output power of the load-pull amplifier to generate a reflection coefficient of a given magnitude (after [16]).

3.7.2. IF Source and Load Pull

Load and source pull impedance is not restricted to RF fundamental or RF harmonics frequencies but can also include the source and/or load impedance at IF frequency. IF load and source pull measurement systems allow for controlling of the reflection coefficients seen by DUT from either its input or its output port at IF frequencies. This, for example, can be achieved by employing IF load pull to present any impedance desired to be visible to the output of the DUT, consequently reshaping the output of the voltage or current waveform for optimum performance. Figure 3.6(a) and 3.6(b) illustrates the output spectrum in the frequency domain and voltage waveform respectively of the output voltage for the 50Ω IF termination, while Figure 3.7(a) and 3.7(b) depicts the output for short IF impedance termination. Terminating the IF component with 50Ω or a short circuit dramatically changes the shape of the voltage envelope, as shown in Figure 3.6(b) and Figure 3.7(b). This example demonstrates

how important the IF load pull is in characterising the performance of the RF power amplifier.

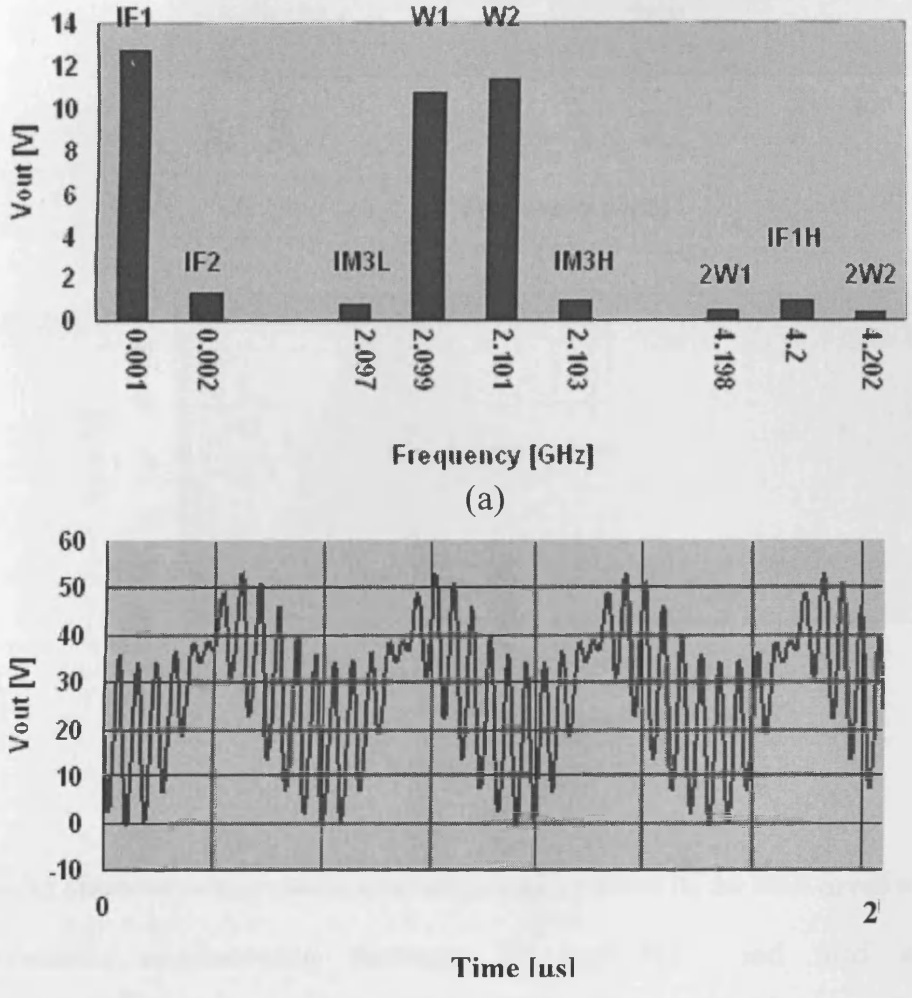

Figure3.6 Measured voltage spectrum (a) and voltage waveform (b) for 50Ω termination.

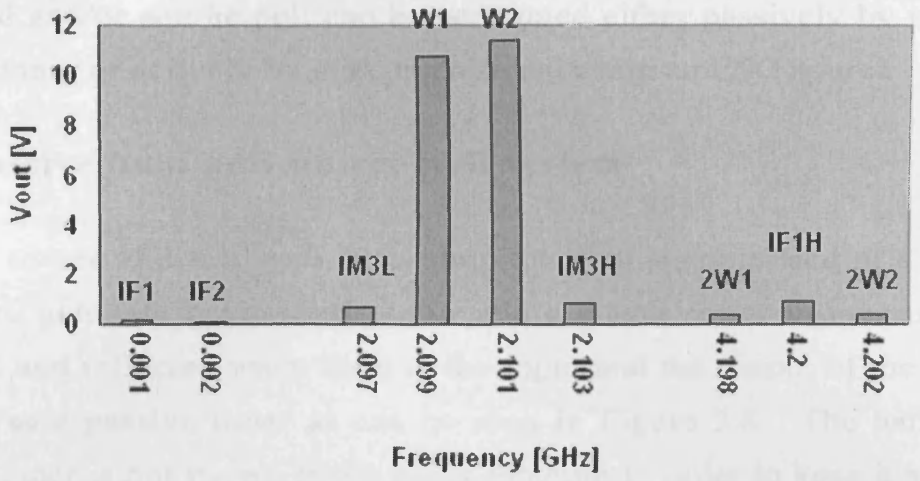

(a)

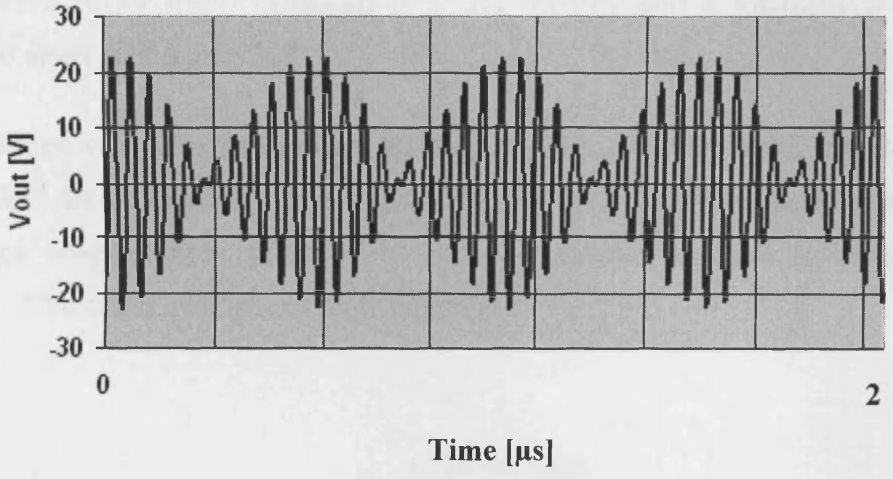

(b)

Figure3.7 Measured voltage spectrum (a) and voltage waveform (b) for short circuit termination.

Waveform engineering through IF and RF load and source pull demonstrate the importance of providing the suitable impedance to the device under test in order to achieve better performance. It will be shown later how effective this technique is for minimising inter-modulation distortion components [17].

The load and/or source pull can be performed either passively by using a manual tuner or actively by injecting a signal using an ESG source

3.8. Passive load and source pull system

Passive source and load pull in its simplest form is comprised of a signal source to generate the desired power and a power meter to measure the incident and reflected wave form at the input and the output of the DUT, as well as a passive tuner as can be seen in Figure 3.8. The harmonic passive tuner is not shown in the block diagram in order to keep it simple. The passive tuner itself contains a phase shifter and a variable attenuator as can be seen in Figure 3.8.

The incident wave b_2 generated by the device, for example, can be phase shifted and its magnitude can be varied by the variable phase shifter and attenuator respectively which will lead to modifying the reflected wave form a_2. The load generated is given by:

$$\Gamma = \frac{\text{reflected wave}}{\text{incident wave}} \tag{3.3}$$

$$\Gamma_L = \frac{a_2}{b_2} \tag{3.4}$$

It is now straightforward to use the load reflection coefficient to define the load impedance as:

$$Z_L = Z_o \frac{1+\Gamma_L}{1-\Gamma_L} \tag{3.5}$$

therefore presenting the impedance which is required to be visible to the DUT.

The same principle can be used to emulate the impedance, which is desired to be seen by the input of the DUT by using the source tuner.

The main advantage of the passive load pull is its capability of presenting an approximately constant reflection coefficient regardless of the input power generated by the signal generator (as expressed in Equation 3.5). Therefore, passive load pull is particularly pioneering and fast for the power sweep characteristic that requires constant impedance. For example, for a 20W LDMOS device, with a power sweep of some 11dB using the non-linear high power RF load pull measurement system, the maximum observed variation in Γ_L is less than 0.0003 in magnitude and less than 0.005 degrees in phase over the entire power sweep. In addition, the power handling capability is high due to the involvement of only passive components in the passive tuner system [18].

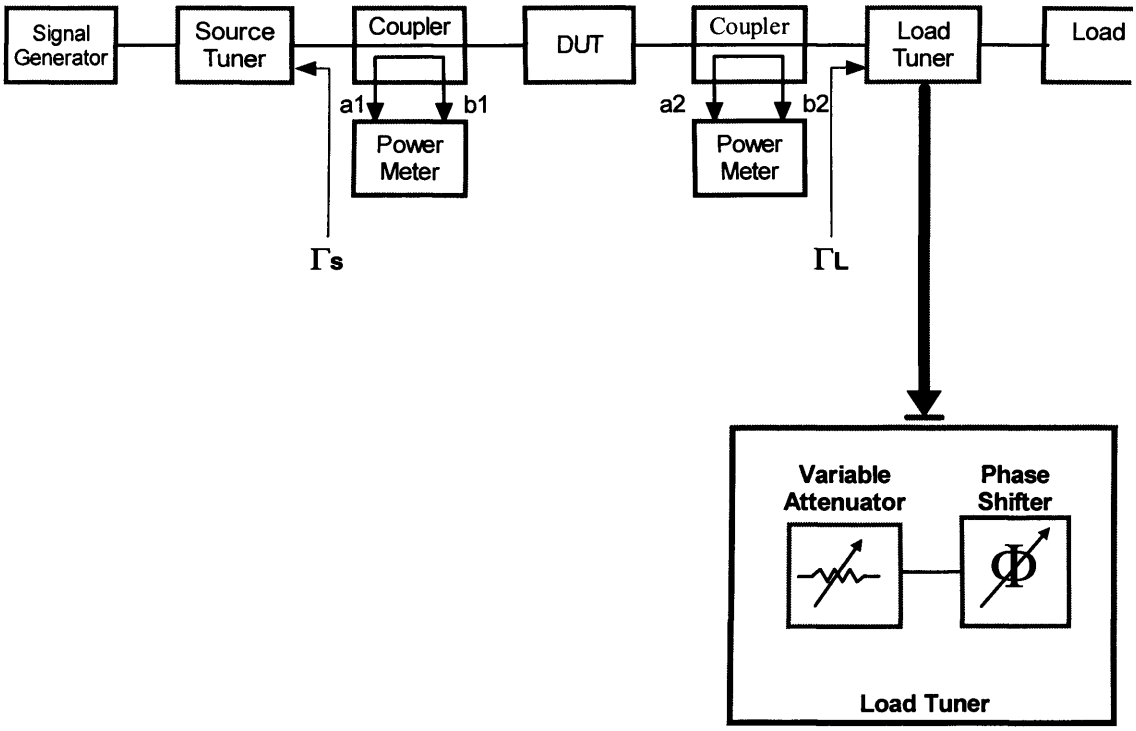

Figure3.8 Block Diagram of a simple passive load pull system

Passive fundamental load-pull is a relatively simple concept and is effective in allowing for the presentation of specific loads to specific frequency components generated by a device [19] [20]. However, in the case of passive harmonic load pull, presenting a high load reflection coefficient using a passive tuner is difficult, especially on the edge of Smith chart [21] [22]. Limited maximum reflection coefficient is considered to be the most important disadvantage of passive load pull.

Therefore, in order to adequately investigate devices and establish accurate optimisation, active load pull can be used instead.

3.9. Active source and Load Pull

Active source and load pull is similar to that of passive source and load pull. In the active source and load pull a signal is injected at the device input for source pull or at the output for the device load pull.

The previous section employed passive IF and RF load-pull in order to control the low and high-frequency impedances presented to the most significant IF and RF components generated by a device. This approach however, is restricted by the realisable reflection coefficients and the lack of controlling all IF and/or RF frequency components simultaneously without them affecting the magnitude of each other, making results difficult to interpret.

To overcome the limitations in achieving a maximum reflection coefficient, active load pull is substituted, allowing for full coverage of the Smith chart by compensating for any losses introduced between the device and the measurement system. The load reflection coefficient, for example, (Γ_L) can now easily be brought to unity (1) or even higher to compensate for losses introduced by the measurement system.

3.9.1. Open Loop Technique

A typical active open loop load pull technique, originally proposed by Takayama [23], is shown in Figure 3.9. This technique is sometimes referred to as the 'two-signal technique', as two independent signals are used. In its simplest architecture, open loop technique is composed of two signal generators combined with the DUT. The first signal generator is used to drive the input port of the device and the second independent

signal generator, which is connected to the device output port, is used to sweep the magnitude and the phase of the injected signal, hence obtaining the desired load reflection coefficient Γ_L. The main drawback of this technique is the variation of the load, as a result of changing the input power. This is due to the incident travelling wave into the device output a_2 from the load pull signal generator being independent from the device incident travelling wave b_2. Consequently, the open loop approach requires a complicated design in order to keep the load constant as proposed in [24].

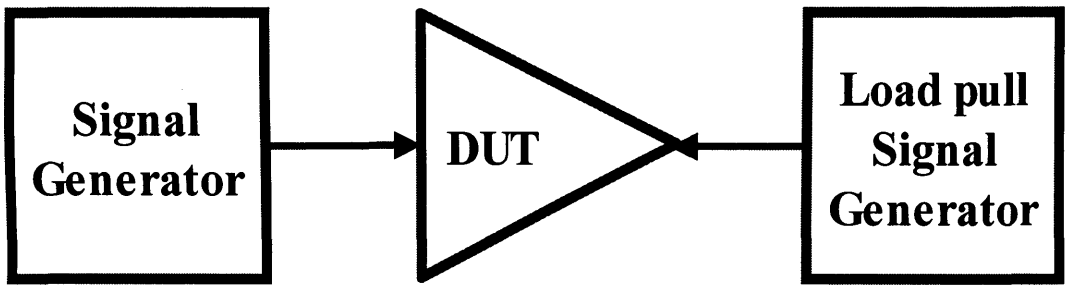

Figure3.9 Block diagram of typical active open loop

3.9.2. Closed Loop Technique

The configuration of the closed loop technique, as proposed by Bava [25] is shown in Figure 3.10. A directional coupler together with these necessary components are used to amplify and phase shift the coupled signal b_2 and then inject back the modified signal a_2 into the device output port. The load reflection coefficient therefore is now not a function of the input power since the device output signal adjusts the load reflection coefficient automatically. This method is also suitable when the output

frequency is different from the input frequency such as intermodulation distortion in the case of a two-tone test. The main disadvantage of this approach is the possibility of having oscillations due to the existence of the closed loop. Even in this simplified configuration it is clearly apparent that closed loop involves more components than open loop, consequently increasing the cost.

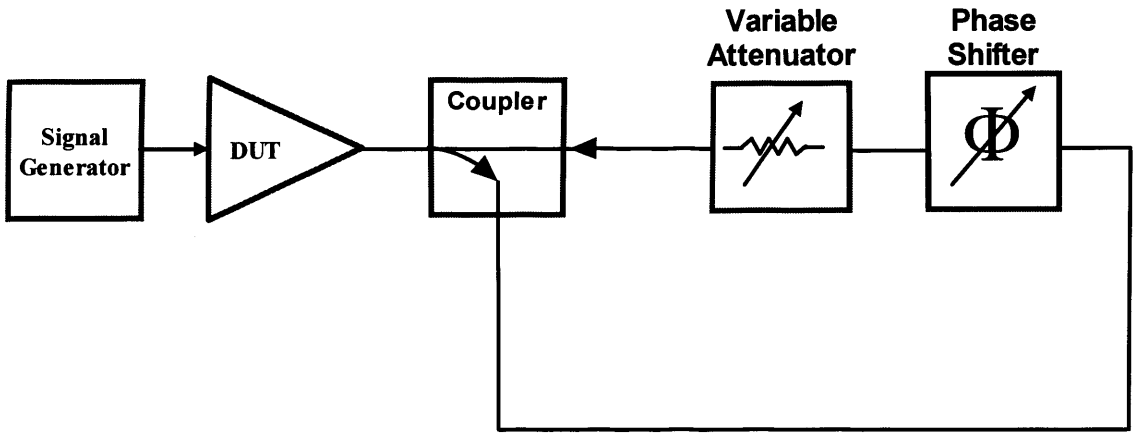

Figure3.10 Block diagram of active close loop.

The most important advantage of the active load pull in comparison to passive load pull is the ability and the precision of presenting any desired impedance inside or even outside the edge of the Smith chart.

3.10. Summary

This overview of RF test equipment and measurement systems provide overall guidance on what types of test instrumentation and measurement systems are needed to characterise the performance of RF devices. The existing measurement systems are not capable for detecting low-frequency

signal components at high power levels. The proposed high power IF and RF waveform measurement system has overcome this problem. It has the capability to handle RF power of more than 100W and will have the opportunity to handle IF power of more than 50W. The proposed measurement system can characterise devices for a bandwidth ranging from 50 kHz to 12 GHz. This measurement system with its capability of performing not only waveform measurement but also waveform engineering will be therefore suitable for investigating high and low frequencies memory effects through either passive or active load pull.

3.11. References

1. Vuolevi, J.H.K., T. Rahkonen, and J.P.A. Manninen, Measurement technique for characterising memory effects in RF power amplifiers. Microwave Theory and Techniques, IEEE Transactions on, 2001. 49(8): p. 1383-1389.

2. M. L. Sisodia, G.S.R., Basic Microwave Techniques and Laboratory Manual. 1987: Halsted Pr (August 1987).

3. LARGE-SIGNAL NETWORK ANALYZER TECHNOLOGY Preliminary Product Overview. 2003 [cited; Available from: www.maurymw.com.

4. Demmler, M., P.J. Tasker, and M. Schlechtweg. A Vector Corrected High Power On-Wafer Measurement System with a Frequency Range for the Higher Harmomcs up to 40 GHz. in European Microwave Conference, 1994. 24th. 1994.

5. Carvalho, J.C.P.a.N.B., Intermodulation Distortion in Microwave and Wireless Circuits. 2003, Norwood,MA: Artech House.

6. Williams, D.J., J. Leckey, and P.J. Tasker. A study of the effect of envelope impedance on intermodulation asymmetry using a two-tone time domain measurement system. 2002.

7. [1] Alghanim, A.L., J.; Williams, T.; Benedikt, J.; Tasker, P. Investigation of electrical base-band memory effects in high-power 20W LDMOS Power Amplifiers. in EUMC. 2007. Munich.

8. Alghanim, A.L., J.; Williams, T.; Benedikt, J.; Tasker, P. Using active IF load-pull to investigate electrical base-band induced memory effects in high-power LDMOS transistors. in APMC. 2007. Bangkok.

9. Alghanim, A., J. Benedikt, and P. Tasker. A measurement test-set for characterisation of high power LDMOS transistors including memory effects. 2005.

10. Teyssier, J.-P., et al., Large-signal characterization of microwave power devices. International Journal of RF and Microwave Computer-Aided Engineering, 2005. 15(5): p. 479.

11. Demmler, M., et al. A Vector Corrected High Power On-Wafer Measurement System with a Frequency Range for the Higher

Harmomcs up to 40 GHz in European Microwave Conference, 1994. 24th. 1994.

12. Benedikt, J., et al., High-power time-domain measurement system with active harmonic load-pull for high-efficiency base-station amplifier design. Microwave Theory and Techniques, IEEE Transactions on, 2000. 48(12): p. 2617.

13. Bensmida, S., et al., New time-domain voltage and current waveform measurement setup for power amplifier characterization and optimization. IEEE Transactions on Microwave Theory and Techniques, 2008. 56(1): p. 224-231.

14. Aboush, Z., et al. High power active harmonic load-pull system for characterization of high power 100-watt transistors. in Microwave Conference, 2005 European. 2005.

15. Aboush, Z., et al. High power harmonic active load-pull using broadband impedance transformers [power transistor measurement]

High power harmonic active load-pull using broadband impedance transformers [power transistor measurement]. in High Frequency Postgraduate Student Colloquium, 2004. 2004.

16. Benedikt, J., Novel high frequency power amplifier design system. 2002, Cardiff University.

17. Abdulrahman Alghanim, J.L., Tudor Williams, Johannes Benedikt, and Paul Tasker, Using active IF load-pull to investigate electrical base-band induced memory effects in high-power LDMOS transistors, in APMC. 2007, IEEE.

18. Muller, J.E. and B. Gyselinckx. Comparison of active versus passive on-wafer load-pull characterisation of microwave and mm-wave power devices. in Microwave Symposium Digest, 1994., IEEE MTT-S International. 1994.

19. Reveyrand, T., et al. A Smart Load-Pull Method to Safely Reach Optimal Matching Impedances of Power Transistors. in Microwave Symposium, 2007. IEEE/MTT-S International. 2007.

20. Benedikt, J., et al., High-power time-domain measurement system with active harmonic load-pull for high-efficiency base-station amplifier design. Microwave Theory and Techniques, IEEE Transactions on, 2000. 48(12): p. 2617.

21. DEVICE CHARACTERIZATION WITH HARMONIC SOURCE AND LOAD PULL. 2000 [cited; Available from: www.maurymw.com.

22. Schuberth, C., et al. Load Pull Characterization of GaN/AlGaN HEMTs. in Integrated Nonlinear Microwave and Millimeter-Wave Circuits, 2006 International Workshop on. 2006.

23. Takayama, Y. A New Load-Pull Characterization Method for Microwave Power Transistors. in Microwave Symposium Digest, MTT-S International. 1976.

24. Gaquiere, C., et al. A Novel 26-40 GHz Active Load Pull System. in European Microwave Conference, 1995. 25th. 1995.

25. Bava, G.P., U. Pisani, and V. Pozzolo, Active load technique for load-pull characterisation at microwave frequencies. Electronics Letters, 1982. 18(4): p. 178.

CHAPTER 4

High Power IF Bias Tee Design, Realisation and Validation

4.1. High Power IF Bias Tee Realisation

The greatest challenge to the development of the new high power IF test-set was presented by the IF high power bias tee, due to the required high power, large bandwidth and reasonable isolation between the DC and IF signal requirements.

The DC and IF requirements for the IF bias tee have been derived for the characterisation of LDMOS devices which represents, at the moment, the dominant device technology for the commercial base station market. Currently, the typical quiescent bias condition for LDMOS devices is V_{ds}=26-28V while the quiescent current can reach 10A, assuming a 40% drain efficiency at the maximum output power. The measurement systems, developed so far at Cardiff University, are capable of measuring LDMOS devices up to output power levels of 100W.

The IF power was chosen to be at around 50W and the IF bandwidth requirement, for the high power IF bias tee, was set to 50MHz which is an order of magnitude larger than the modulation bandwidth of W-CDMA systems, thus allowing for the measurement of the IF fundamental difference frequency and its first 5 harmonics at least. The resulting specification for the IF bias tee are summarised below:

- Maximum DC current handling: 10A
- Maximum DC voltage handling: 100V
- IF channel maximum power handling: 50W
- DC channel bandwidth: ≤50kHz
- IF bandwidth: ≤50MHz
- Isolation between DC port and IF port: ≥ 20 dB

4.2. Simplified Equivalent Circuit for Bias Tee

A bias tee provides two paths from a common node, designed for applications where DC and AC (IF) signals are applied to a device under test (DUT). The principle architecture of a bias tee is shown in Figure 4.1. It consists of just one capacitor to provide the DUT with the required IF signal (a short circuit for IF) and to block the DC signal from the measurement equipment connected to the IF port, and one inductor to supply the DUT with the required DC voltage and current, while blocking the IF signal from diverting to the DC supply (a high impedance for IF). The inductor represents a low pass filter while the capacitor represents a high pass filter.

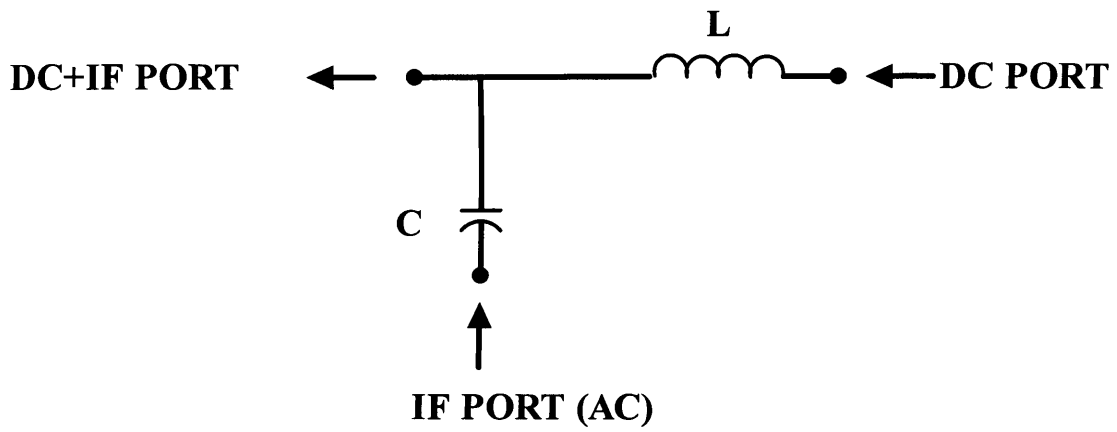

Figure 4.1 Simple bias tee

4.3. Bias Tee Construction

A relatively easy way to implement filters is to use microstrip or stripline structures [1]. However, microstrip or stripline structures are not practical at low frequencies due to their large geometries imposing space limitations. Instead, lumped element such as inductors and capacitors are usually used to implement such low frequency filters.

The utilised bias tee design process consisted of three phases: phase 1- investigation and design with ideal lumped components; phase 2- introduction of realistic components through the utilisation of complex models, and phase 3- investigation of higher order filters as shown in Figure 4.2. During the first phase, the optimum values of both inductor and capacitor were estimated for design centering; during the second phase, practical components and their models were utilised, but resulted only in a bias tee which did not meet the specification, while the third

phase was concluded with the creation of a viable IF bias tee, using a filter design approach.

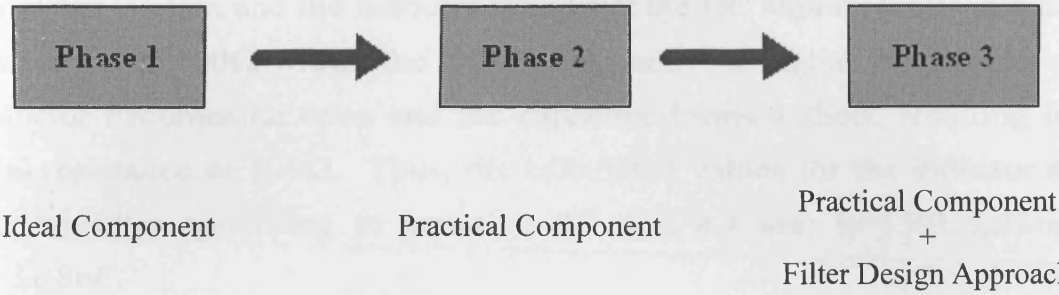

Figure 4.2 Three phases of bias tee design approach.

4.3.1. First Phase: Bias Tee Design using Ideal Components

The bias tee design process was initiated by a single ideal component for both filters, an inductor for the low pass filter and a capacitor for the high pass filter, as can be seen in Figure 4.3. The 3 dB cut-off frequency for each filter can be calculated using the following formulae:

$$F_c = \frac{1}{2\pi RC} \tag{4.1}$$

$$F_L = \frac{R}{2\pi L} \tag{4.2}$$

Through algebraic manipulations, we obtain

$$C = \frac{1}{2\pi F_c R} \tag{4.3}$$

and

$$L=\frac{R}{2\pi F_L} \tag{4.4}$$

In a matched two-port 50Ω system, termination impedances are 50Ω (Term1, Term2 and Term3) as seen in Figure 4.3. Assuming that the capacitor is open and the inductor is short at the DC signal results in a total resistance of 100Ω within the DC signal path. At higher frequencies the inductor becomes an open and the capacitor forms a short, resulting in a total resistance of 100Ω. Thus, the calculated values for the inductor and the capacitor according to equation 4.3 and 4.4 are: L=1591.5μH and C=31.8nF.

To ensure an appropriate cut-off frequency for both the DC IF ports, the inductor and the capacitor of the bias tee were calculated according to 'ideal' values and the bias tee itself was simulated using Agilent's Advanced Design System (ADS). The results of the simulated circuit are depicted in Figure 4.4. The 3dB cut-off frequency for the DC port is 10 kHz and the cut-off frequency for the IF port is 50 kHz (approximately as calculated). The IF insertion loss (in this work, the decrease in the transmitted signal will refer either to insertion loss or attenuation) is relatively good (approximately 0.1 dB) at frequencies equal or greater than 100 kHz. Furthermore, the minimum isolation achieved between the DC port and IF port is 22dB at 22 kHz.

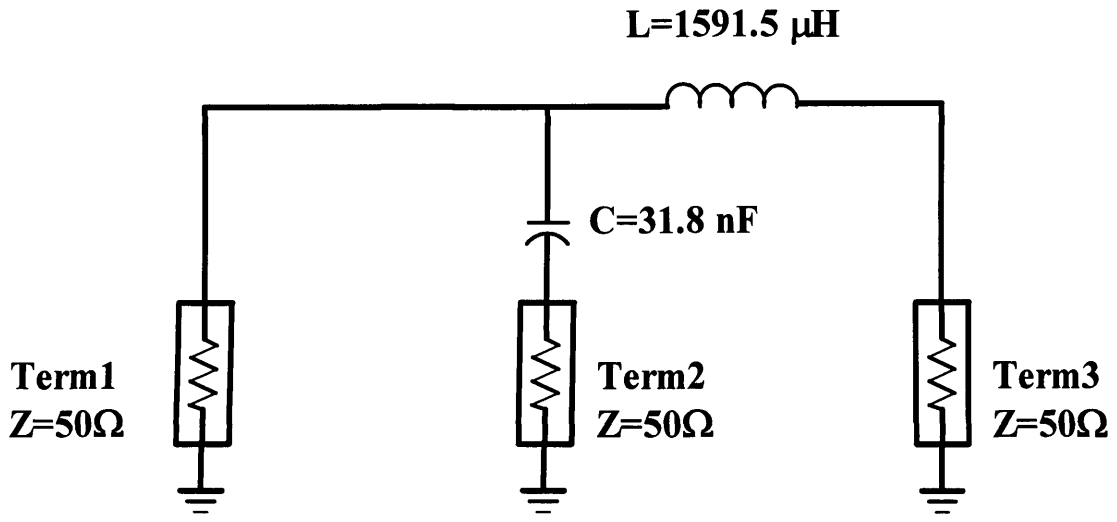

Figure 4.3 IF bias tee with ideal components.

This may indicate an adequate bias tee, but unfortunately, there are no off-the-shelf inductors with that large a value of inductance (1591.5 μH) while still being able to supply a current of 10A up to a sufficiently high self-resonant frequency.

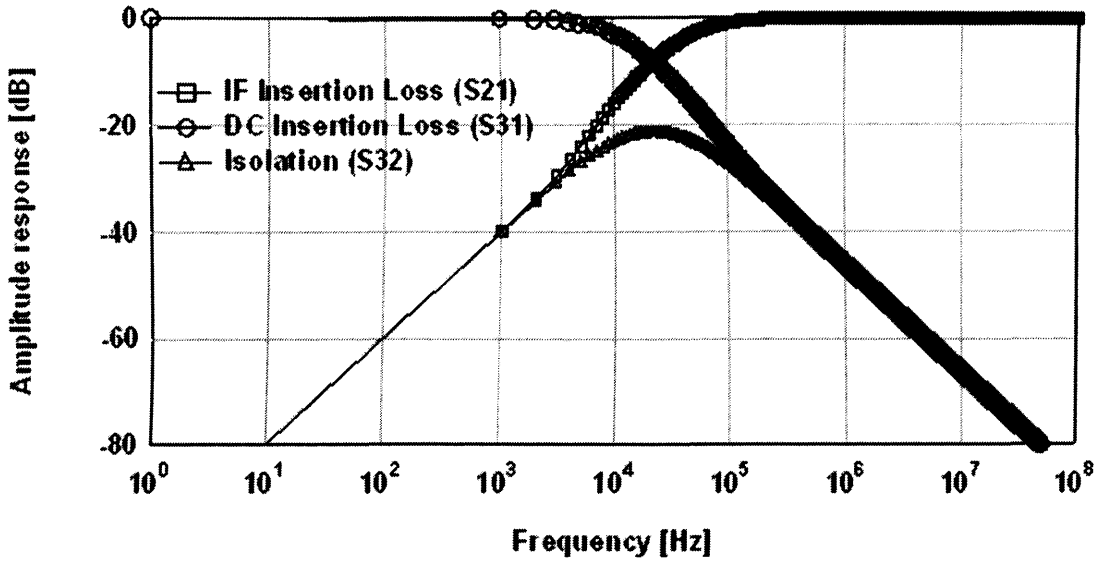

Figure 4.4 Simulated amplitude frequency response of the IF bias with ideal components.

4.3.2. Second Phase: Bias Tee Design using Practical Components

In order to implement a practical bias tee with the desired specifications, a practical passive inductor and capacitor must be used. Research into available inductors and capacitors indicates the trade-off between: self-resonant frequency, impedance, current and voltage. High current inductors with both high self-resonant frequency and high impedance have been more difficult to find. High self-resonant frequency ensures that the inductor will not resonate in the desired bandwidth and therefore will prevent the IF signal from entering the DC path while high impedance allows adequate attenuation at frequencies above DC and therefore increases the bandwidth. Therefore, a trade-off has to be made. So far, the inductor specifications found to be potentially the most compatible

with the design, are an inductor with inductance of 100 μH, effective series resistance (sometimes called ESR or R_s) of 0.1 Ω, self-resonant frequency of 3.1 MHZ and a DC current of 10 A. At first glance, this self-resonant frequency of 3.1 MHZ may not look sufficient to deliver a bandwidth of 50 MHz, but it cannot be ignored because the impedance of the inductor is still going to be high, even beyond the resonant frequency which validates its use. To investigate this, the simulations were performed using the equivalent circuit (model) for the off-the-shelf 100 μH inductor as shown in Figure 4.5. In this model, L represents the nominal inductance, C_p is the parasitic capacitance of the coil and R_s is the series resistance of the winding. Figure 4.6 displays the simulation results of this inductor model. The impedance plot shows that the impedance increases until the frequency reaches the self-resonant frequency, and then decreases due to the parasitic capacitance of the inductor. Also this plot indicates that the inductor has an impedance of magnitude greater than 600 Ω for frequencies ranging from 1 MHz to 45 MHz: enough to provide an attenuation of over 20 dB over that frequency range. This indicates the potential use of the inductor at levels even higher than the resonant frequency. However, the attenuation weakens as the frequency is increased beyond 45 MHz.

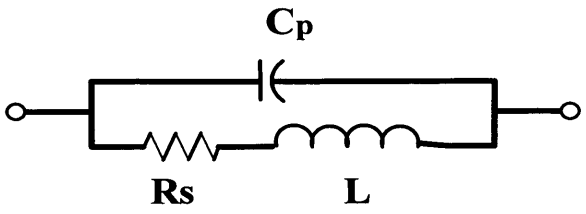

Figure 4.5 Inductor Equivalent circuit.

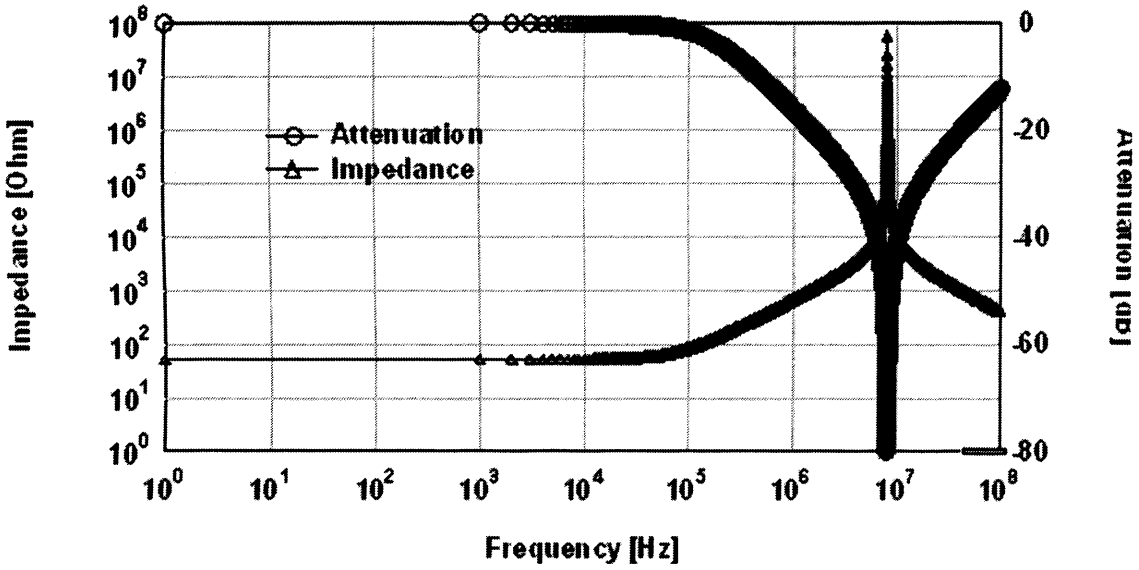

Figure 4.6 Simulated impedance and attenuation Frequency response of the 100 μH inductor.

What has been said about the inductor also applies to the capacitor with practical limitations to current and voltage. Based on an intensive search a capacitor was found with the most suitable characteristic that has a capacitance of 15 nF, self resonant frequency of 25.6 MHz and a maximum voltage of 1kV. The equivalent model for this capacitor is shown in Figure 4.7 with C as the nominal capacitance, L_s the self inductance of the leads and the plates, and R_s the dc capacitor resistance that represents loss due to heat.

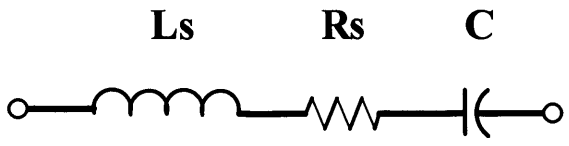

Figure 4.7 Capacitor Equivalent circuit

The next step was to construct the IF bias tee using the selected components (L=100 μH, C=15 nF) and to verify whether all the goals such as, bandwidth, power, isolation, etc are achieved. The high pass filter was built by connecting two of the off-the-shelf 15 nF capacitors in parallel, resulting in a total capacitance of 30 nF, which is close to the calculated ideal value. The low pass filter was built by connecting 16 inductors in series in order to meet the previously calculated ideal value of 1591.5 μH. The s parameters results in this configuration are shown in Figure 4.8. All responses are close to those previously achieved in Phase One, where just one, single inductor with an inductance of 1591.5 μH and a single capacitor of 31.8 nF were involved, hence meeting the design specifications. The slight change in the DC insertion loss and in the isolation, between the DC and the IF path, were mainly due to the resonant frequency of the inductor.

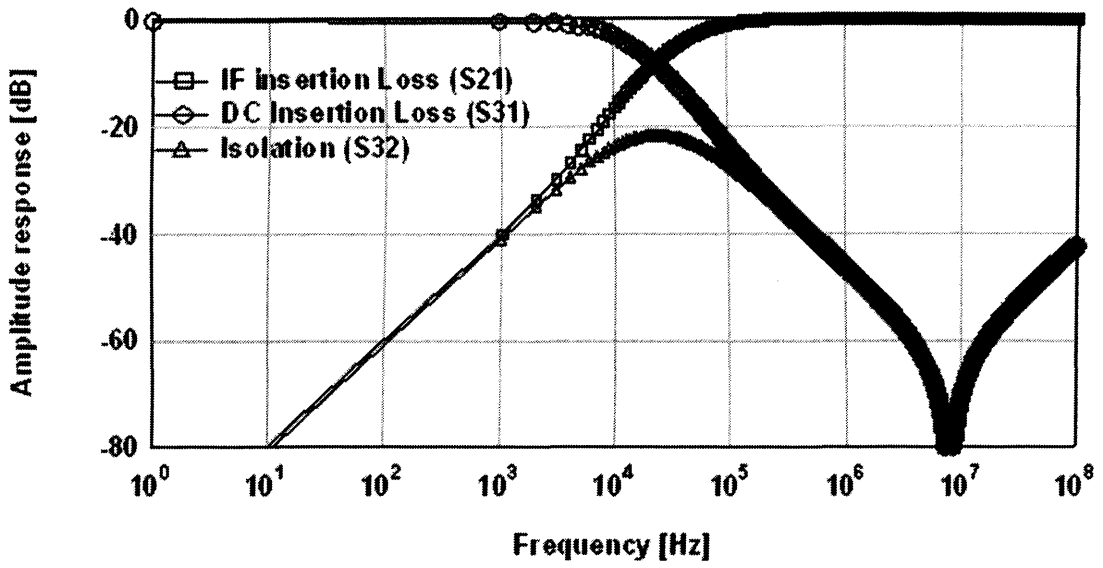

Figure 4.8 Simulated amplitude frequency response of the IF bias with practical components

However, the resulting design also introduces a problem due to an excessive DC loss. For example, the practical on-shelf inductor found has a series resistance of 0.1 Ω, so if the previous approach of having 16 inductors in series is adopted, then the total resistance of 1.6 Ω will be produced. This will generate a drop voltage of 16 V if 10 A (max drain current) was to be applied. Moreover, this approach of having 16 inductors makes up a great deal of space. To overcome this problem, higher order filters were proposed.

4.3.3. Third Phase: Bias Tee Design using a Filter Design Approach

Filters can be designed usually using the 'image parameter' or the 'insertion loss' methods. The image parameter method is simple; although its drawback is that its response in the passband and the stopband cannot be controlled. In contrast, the insertion loss method allows precise control

over the passband and the stopband of the frequency response across the entire operating range and also allows for improve filter performance using, for example, higher order filters in a straightforward way [2].

The insertion loss method of filter design is adopted in this bias tee design since it has been intensively used in modern filter design. The filter design is very far-reaching due to the large number of conceivable implementations [2]. The basic principle is addressed in this section. References [3] [5] give more detail about filter designs.

A prototype of a low-pass filter is shown in Figure 4.9(a) while its dual is shown in Figure 4.9(b). Either form 4.9(a) or 4.9(b) can be used as a low-pass filter since they are reciprocal and they will give the same response. A prototype of a high-pass filter is shown in Figure 9(c) while its dual is shown in 4.9(d). As in the low-pass filter, either form 4.9(c) or 4.9(d) can be used as a high-pass filter since they are reciprocal and they will give the same response.

To have a practical bias tee using filter design approach, the last element (at the output) of the low-pass filter must be an inductor and the last element (at the output) in the high-pass filter has to be a capacitor, otherwise, the DC signal or the AC signal will not go to the output port of the device under test but will go to ground instead. The circuit provided in Figure 4.10 illustrates this. In this example a bias tee was constructed through use of a low-pass filter and a high-pass filter with n=3 (3 sections). As already noted, this kind of filter construction is inappropriate for the bias tee design, since the presence of the capacitor C1 in the low-pass filter allows the IF signal to go to ground rather than going to the output port of the bias tee.

Figure 4.10 also demonstrates how easily the DC signal can be lost, proceeding from the DC port to ground via the inductor L1 on the high pass filter side. This calls for greater caution, when designing bias tees.

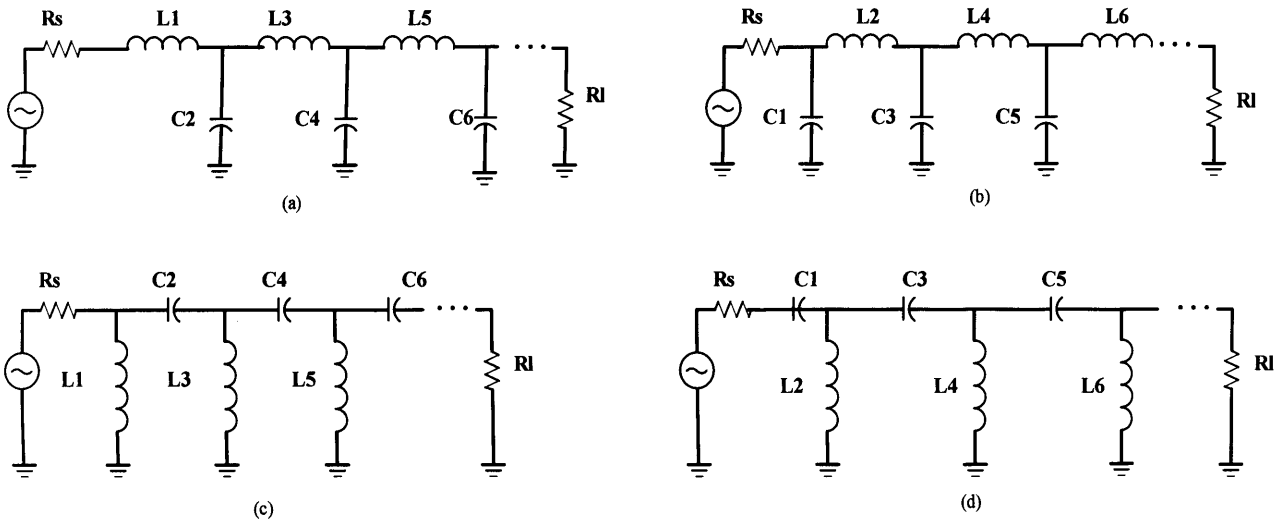

Figure 4.9 Ladder circuits for filters prototypes. (a) A low-pass filter prototype beginning with an inductor. (b) A low-pass filter prototype beginning with a capacitor. (c) A high-pass filter prototype beginning with an inductor. (d)) A high-pass filter prototype beginning with a capacitor.

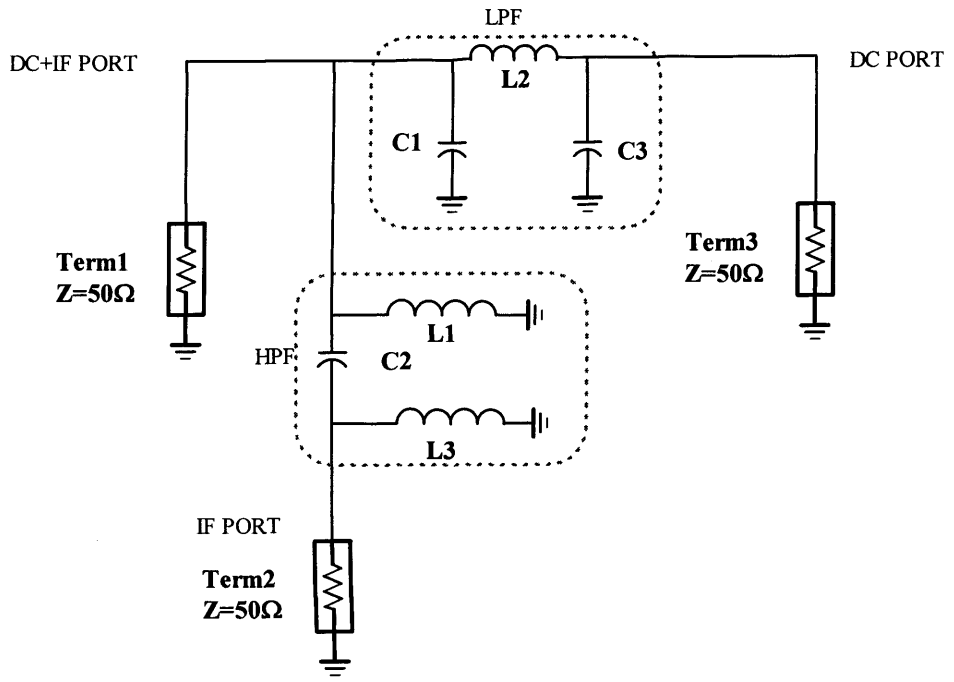

Figure 4.10 Schematic of prohibited bias tee

Table 1 below lists several of the original targets to be met in the provision of an appropriate bias tee:

Table 1 Bias tee specification

Filter Type	LPF	HPF
3 dB cut-off frequency	10 kHz	50 kHz
20 dB attenuation	100 kHz	20 kHz
Bandpass attenuation	$\leq$ 0.1 dB	$\leq$ 0.1 dB

The aim was to have the 3 dB cut-off frequency (F_c) at 10 kHz with an attenuation of ≥20 dB at 100 kHz for the low pass filter, together with a 3 dB cut-off frequency at 50 kHz and an attenuation of ≥20 dB at 10 kHz for the high pass filter. The reason behind choosing two different cut-off frequencies was to achieve adequate isolation between the DC and IF paths. Moreover, a lower cut-off frequency was selected for the DC path in order to prevent interaction with the IF path. The bias tee also required low insertion loss (attenuation) in the passband and wide rejection in the stopband as illustrated in Figure 4.11.

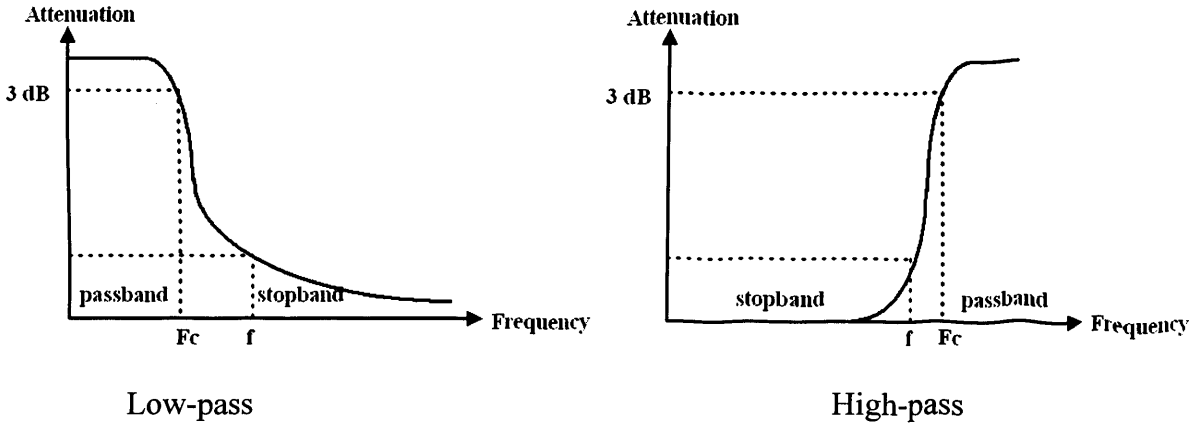

Figure 4.11 Characteristic response curves of filter.

The resulting bias tee uses a three-order filter type (n=3) of which three kinds were examined during the design process:

- Butterworth filter
- Chebyshev filter
- Bassel filter

For the purpose of achieving the required performance, several combinations of filters have been simulated using Agilent's Advanced Design System (ADS).

4.4. Bias Tee Simulation and Realisation

One example of a simulated circuit is depicted in Figure 4.12. The best results of all nine combinations of low-pass and high-pass filters were achieved with a Chebyshev filter with 0.01 dB ripple (low pass), and a Bessel filter (high pass). These results are depicted in Figures 4.13 and 4.14, which indicate very good isolation, with a worst case scenario of approximately 27dB at 23 kHz between DC and IF ports and an insertion loss of the IF path (s_{21}) at about 0.06 dB at 50 MHz, while the DC insertion loss (s_{31}) is always over 20 dB for all frequencies approximately greater than 50 kHz. The return loss in the bandwidth of interest is a minimum of 10 dB. The optimum circuit obtained has been realised using off-the-shelf inductors and capacitors.

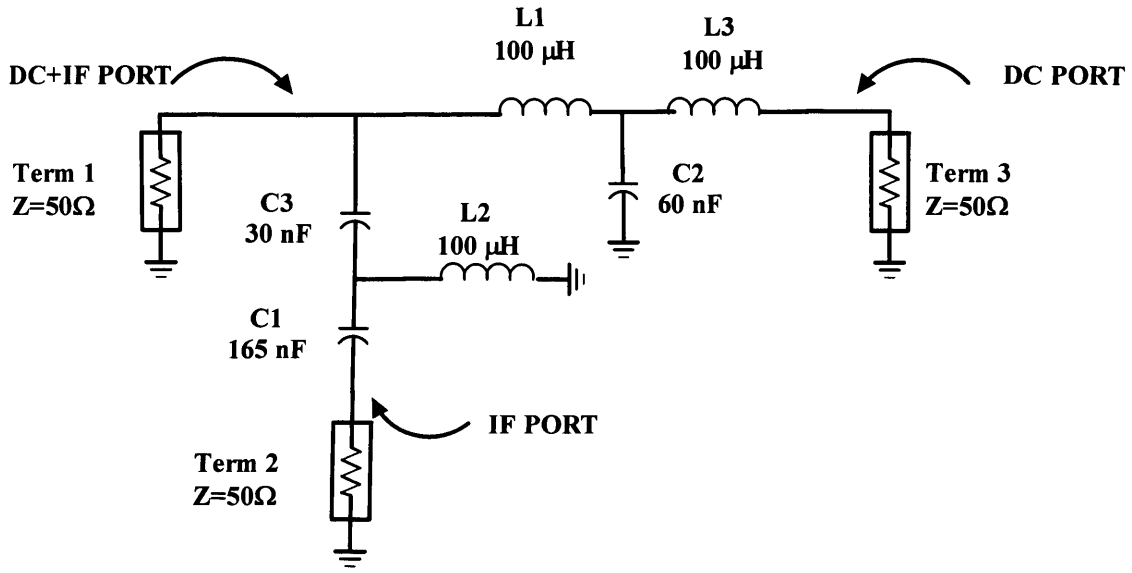

Figure 4.12 Final IF bias tee with practical component's values.

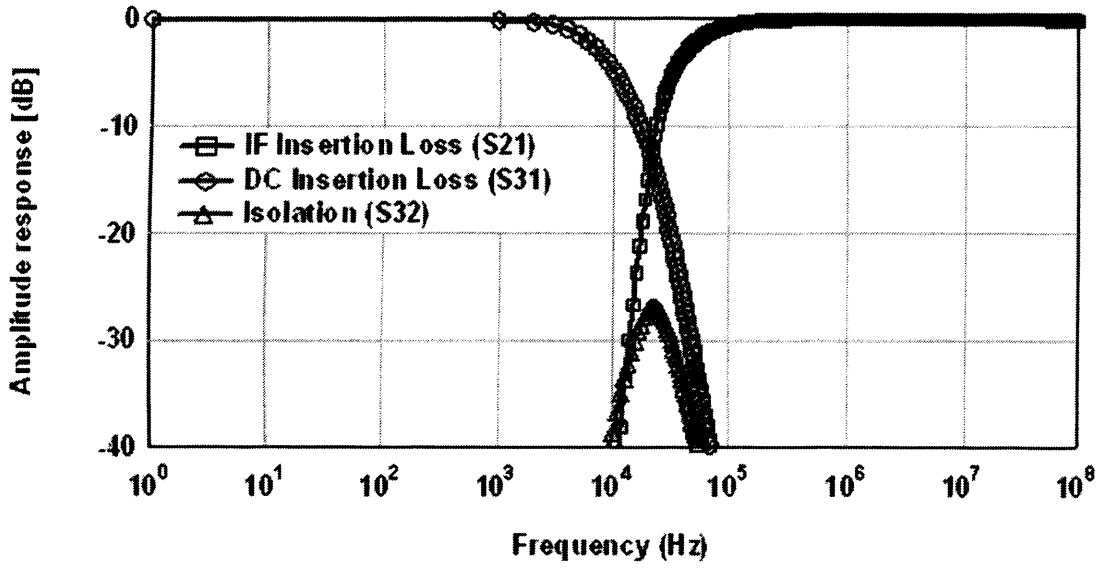

Figure 4.13 Simulated amplitude frequency response of the IF bias.

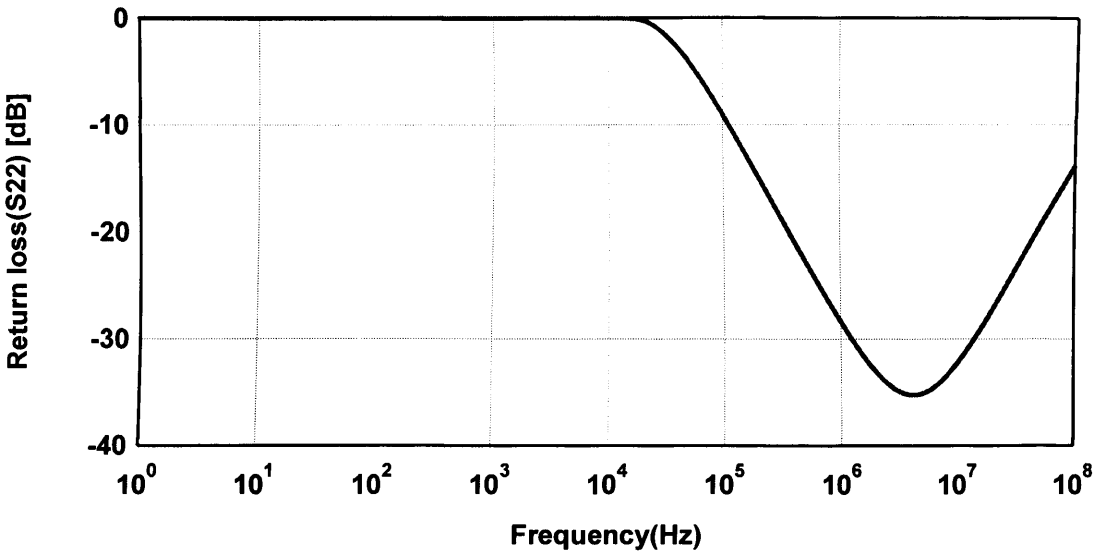

Figure 4.14 Simulated IF return loss of the IF bias tee

Figure 4.15 shows the photograph of the constructed high power bias tee containing its three ports. The DC signal can be applied or extracted from the bias tee through a BNC connector at the DC port, while the IF and the output signals can be applied or extracted from the bias tee via N connectors at the IF and the output port.

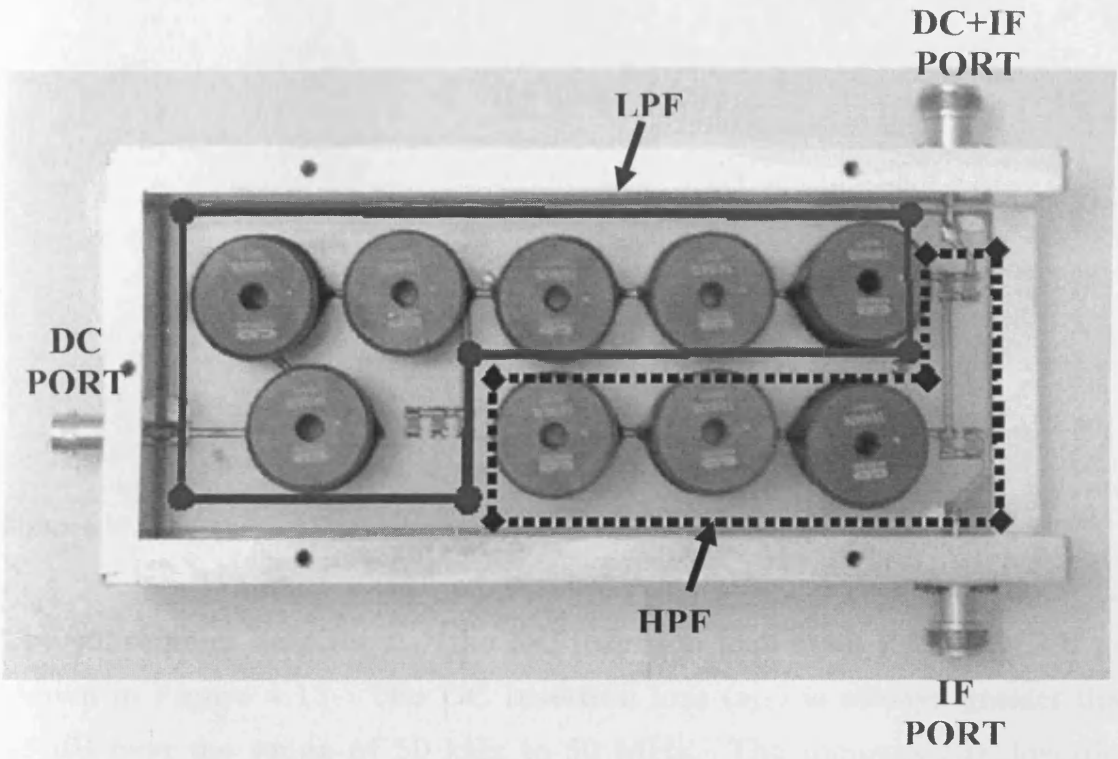

Figure 4. 15 photograph of the constructed high power bias tee

4.5. IF Bias Tee Measurements

Due to the fact that the available bandwidth of the VNA is only 30 kHz to 6 GHz, it was not possible to accurately measure the bandwidth between DC and 30 kHz of the IF bias tee. Therefore, it was decided that two different measurements would be carried out in which the 8753E VNA (vector network analyzer) was used for the first measurement for frequencies between 30 kHz to 100 MHz and the second measurement was undertaken using the set-up shown in Figure 4.16 for frequency ranges from DC to 30 kHz. In the second measurement, the insertion loss (IL) is defined as the ratio of two power levels: the available source (defined as Ps) and the available load power (Pr). It is expressed in decibels as:

$$IL=10\log\frac{Pr}{Ps}$$

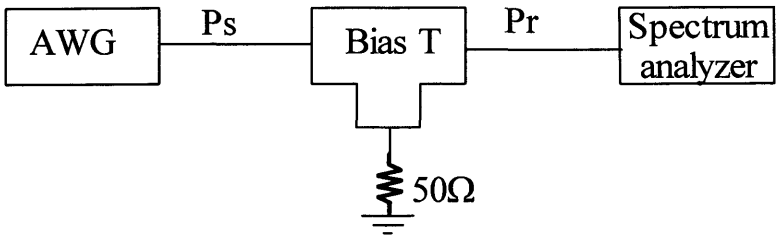

Figure 4.16 Low frequency Measurement set-up.

The subsequent data for s_{31} (the DC insertion loss from DC to DC+IF) is shown in Figure 4.17. The DC Insertion loss (s_{31}) is always greater than 35 dB over the range of 50 kHz to 50 MHz. The measured IF insertion loss of S_{21} (IF path) is about 0.1 dB at the cut-off frequency with the worst case being 1.2 dB at 50 MHz, as depicted in Figure 4.18.

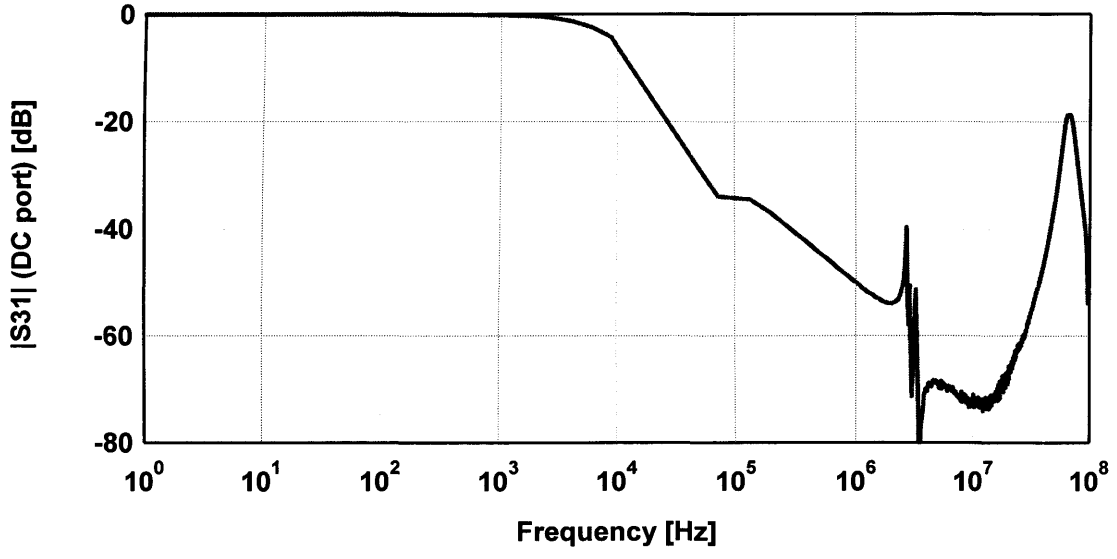

Figure 4.17 Measured insertion loss s_{31} (Dc port to DC+IF port)

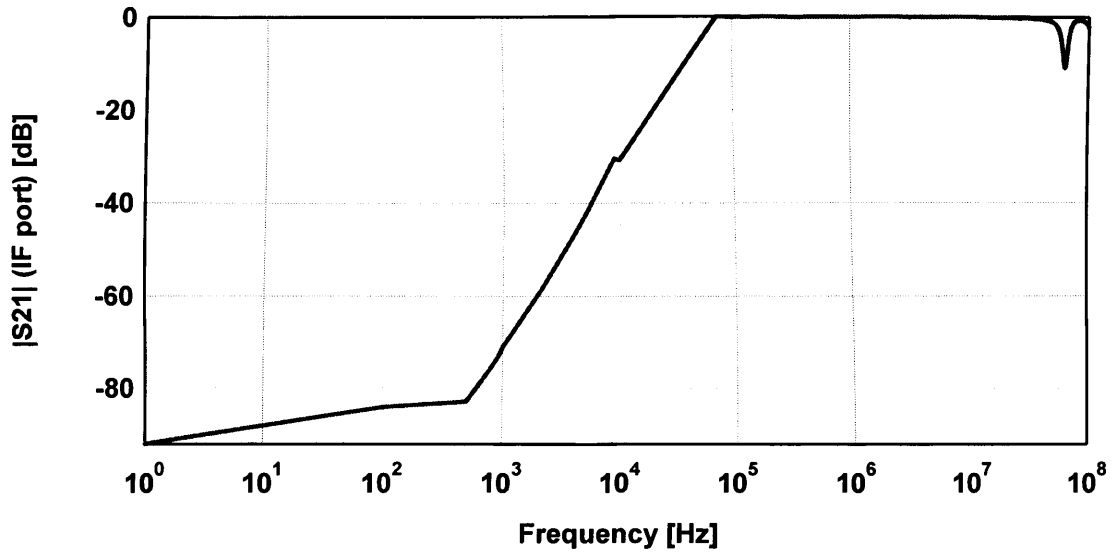

Figure 4.18 Measured transmission of IF port s_{21} (IF port to Dc+IF port)

Figure 4.19 shows a plot of s_{32}. The isolation between the DC port and the IF port (s_{32}) is 27 dB minimum for the whole bandwidth. The IF return loss is quite good for the frequency range 100 kHz to 45 MHz as is shown in Figure 4.20.

An additional DC test was applied to the IF bias tee, which showed a DC resistance of 0.8Ω and a DC current handling ability of 10A without causing any heating effects to the inductors.

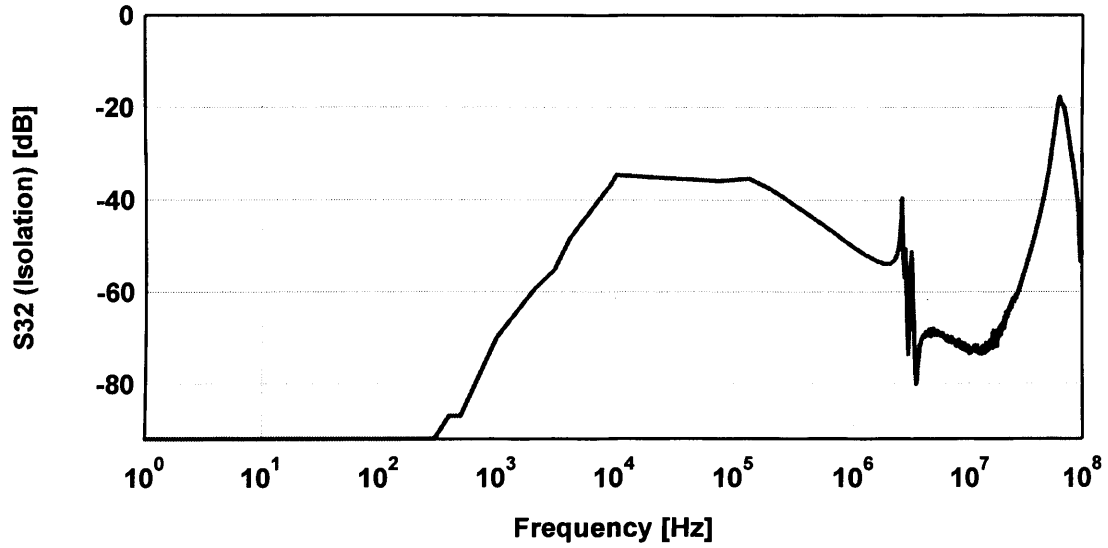

Figure 4.19 Measured Isolation s_{32} between DC port and IF port.

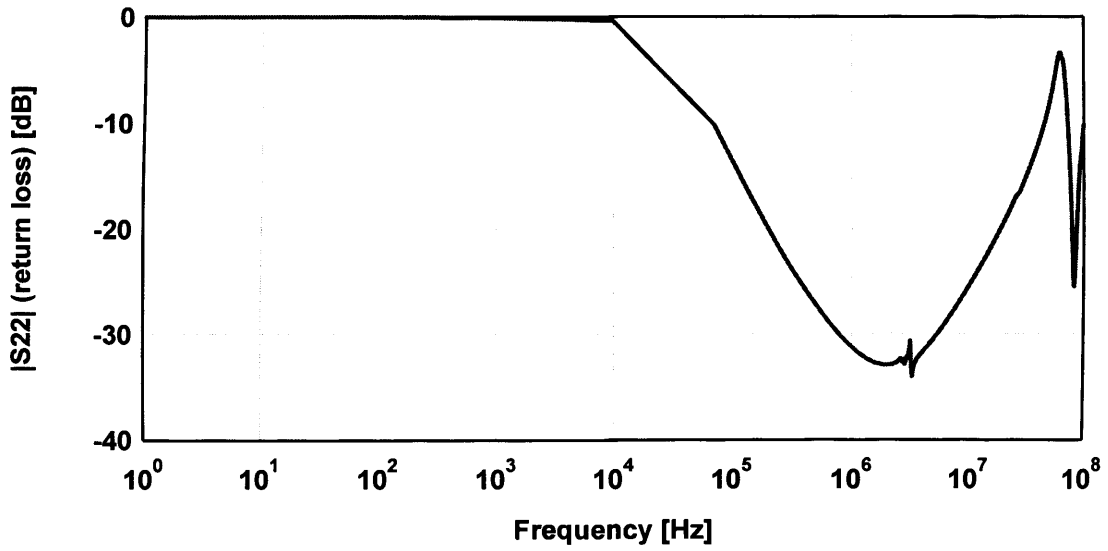

Figure 4.20 Measured IF return loss s_{22}.

The final test of the IF bias tee was to ensure that the IF bias tee would indicate the same performance for both low and high power. This has been achieved by terminating the output port (port 1) in a 20 Ω resistor, capable of handling a current up to 12A, while port 2 (IF port) was left open and port3 (DC port) was connected to a high current power supply, providing the DC port with the desired current of 10A for approximately 1 hour. The s-parameters ('hot' s-parameters) where then immediately measured and compared to the 'cold' s-parameters, recorded when the bias tee had been left unconnected for some time to cool down. The results of s_{31} hot and s_{31} cold are depicted in Figure 4.21. These shows identical results for both tests, demonstrating the excellent behaviour of the IF bias tee, while Table 2 shows the final IF bias tee measured performance, meeting the desired specifications.

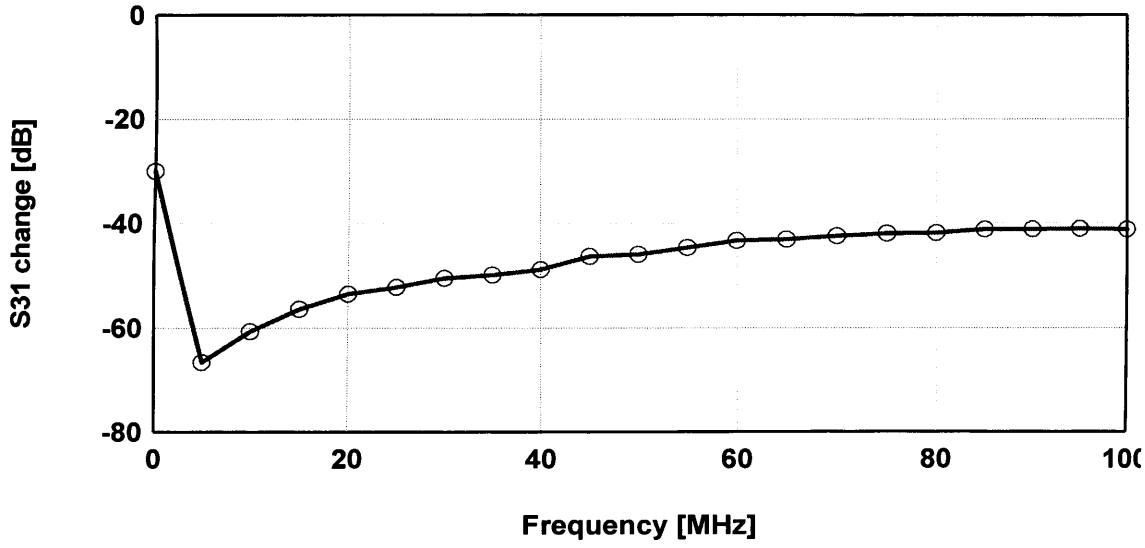

Figure 4.21 Measured changes in insertion loss s_{31} (DC port to DC+IF port)

Summary of Final High Power IF Bias Tee performance

Table 2 High power IF bias tee.

ELECTRICAL:	
frequency Range	**30 kHz – 50 MHz**
Bandwidth	**< 7kHz to > 50 MHz**
Insertion Loss **100 kHz – 15 MHz** **15 MHz – 45 MHz** **15 kHz – 50 MHz**	 **0.1 dB Typical** **< 0.5 dB** **1.2 dB Max**
Isolation (IF to DC port): **100 kHz – 50 MHz**	 **> 27 dB**
Return Loss	**>13 dB**
DC Voltage	**100 VDC Max**
DC Current	**7.8 A**
DC Path Resistance	**0.8 ohm**
Mechanical	
DC Port	**BNC Connector**
IF Port	**N Connector**
IF+DC port	**N Connector**
Overall Length	**18 cm**
Weight	**1.2 lb (0.5 Kg)**
Housing	**Aluminum**

4.6. Low Power IF Bias Tee

An extra bias tee was needed to supply the device input with the required DC voltage and current. Fortunately this bias tee does not need to handle high power since the device does not required high DC input current. The design process is similar to that of the high power bias tee. Therefore and in order not to be repetitive, only the final performance of the second bias tee is shown. For clarity Figure 4.22 below shows the final performance of the IF bias tee (in a linear scale for frequency up to 400 MHz) while Figure 4.23 shows the performance in a logarithmic scale for the same frequency range.

The final achieved specifications for this IF bias tee are summarised below:

- Maximum DC current handling: 2A.
- Maximum DC voltage handling: 100V.
- DC channel bandwidth: 50 kHz (>20dB).
- IF bandwidth (3 dB): 50 kHz to >400MHz.
- DC-AC isolation > 20dB for all frequencies.

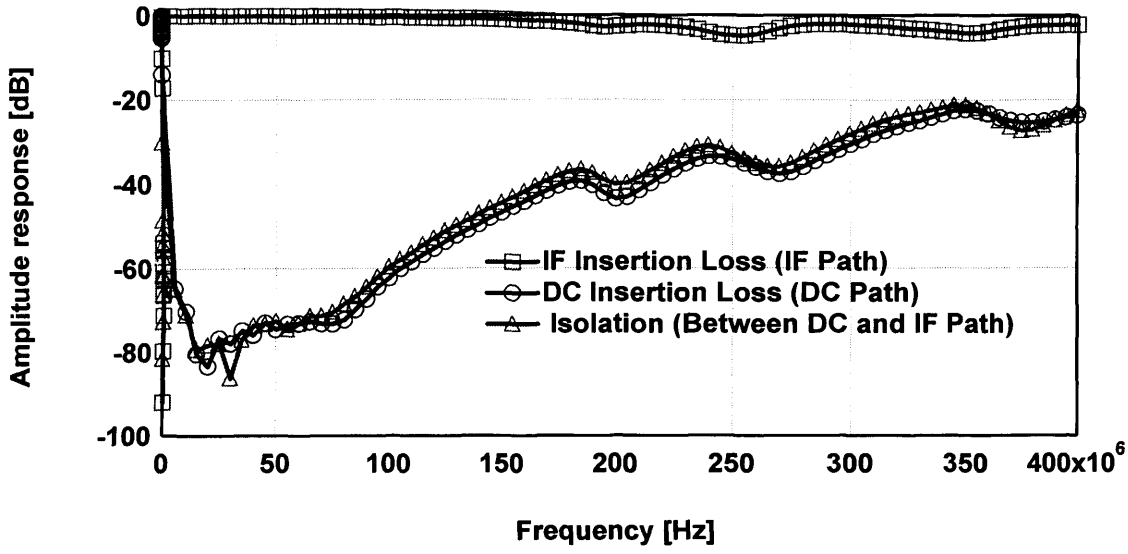

Figure 4.22 Measured amplitude frequency response of the IF bias using a linear scale for frequency up to 400 MHz.

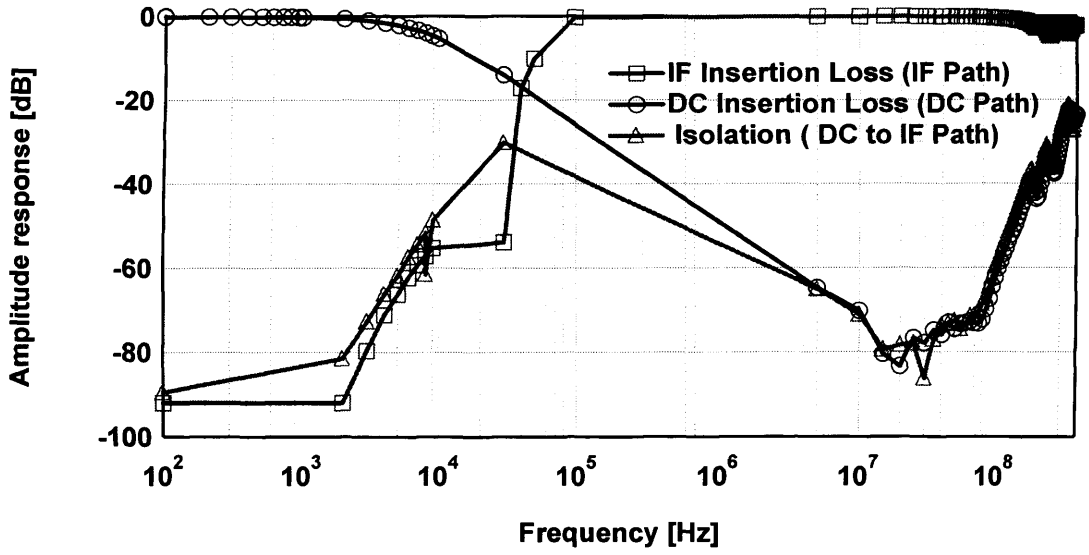

Figure 4.23 Measured amplitude frequency response of the IF bias using a logarithmic scale for frequency up to 400 MHz.

4.7. IF Diplexer

A diplexer in its simplest form is a network with three ports that combines two different frequencies from two sources into a single output or splits a signal into two paths. Based on how it is used, a diplexer can be either a splitter or a combiner. Similar to the bias tee, a simple diplexer consists of two filters, one for low frequency and the other for high frequency. It is also possible to design diplexers using two band-pass filters. Therefore, it could be said that a bias tee can be used as a diplexer but diplexers cannot be necessary used as a bias tee.

To complete the IF test-set and make it suitable for independently load pulling two IF components at one time, it was necessary to design and manufacture a suitable diplexer to separate these two IF harmonic components (IF_1 and IF_2) using a similar process to that adopted for the IF bias tee design.

The diplexer was designed according to the following specification: DC-1.1MHz (IF_1) and 1.8-10MHz (IF_2) with insertion loss of approximately 0.5 dB and 20dB of isolation. The achieved values for the insertion loss and isolation are shown in Figure 4.24. With this diplexer, it would be possible to independently load pull not only IF_1 but also IF_2 at Tone-spacing between ω_1 and ω_2 of 1 MHz when investigating base-band memory effect.

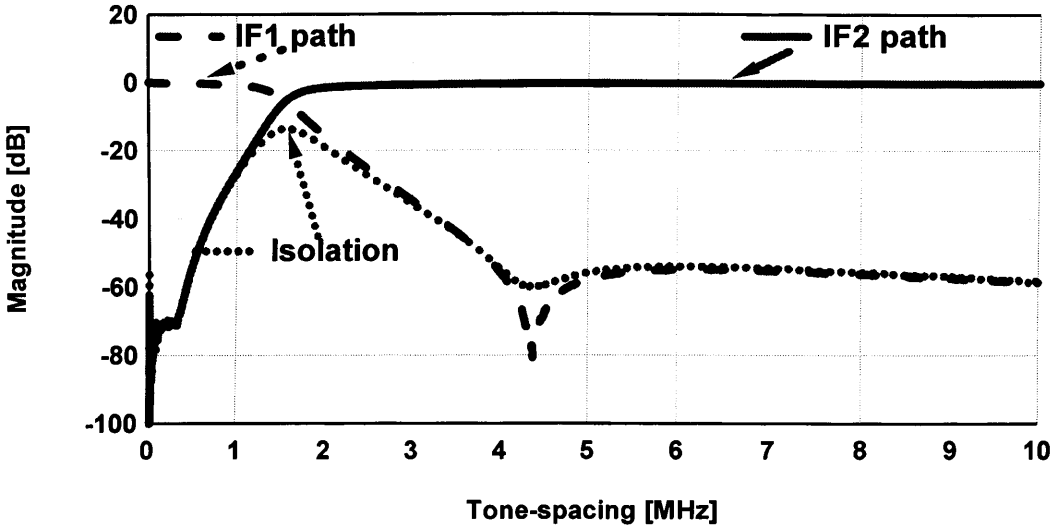

Figure 4.24 Measured frequency response for the IF diplexer.

4.8. High Power IF Test-Set Realisation

The final high power IF test-set realised is shown in Figure 4.25. It consists of two commercial IF directional couplers with a maximum power of 50 W and a bandwidth of 10 kHz to 1GHz. The two bias tees made on site: the high power version with a bandwidth of 50 kHz to 50 MHz and a maximum current handling of 10 A at 100 V and the low power version with a bandwidth of 50 kHz to 400 MHz and a maximum current handling of 2A at 100V. The IF test-set specifications has been driven from the components specification used to build it. Thus, the IF high power test-set bandwidth is 50 kHz to 50 MHz, defined by the lowest components bandwidth (high power IF bias tee) with a capability of handling current and voltage of 10A and 100V respectively. The IF test-set was designed with the flexibility of adding or replacing any of the present components in case it is needed. Therefore, it is possible for example to switch the high power IF bias tee which is designed to be

connected at the drain of the device (10A and 50 MHz of bandwidth) with the low power IF bias tee which is designed to be connected at the gate of the device (2A and 400 MHz) in order to expand the bandwidth from approximately 50 MHz to approximately 400 MHz.

This would improve frequency performance, especially for those applications when high drain current is not required but higher bandwidth is. This bias tee switching would extend the IF test-set bandwidth from approximately 50 MHz to 400 MHz. The IF load and source ports (see Figure 4.25) will allow for load and/or source pull and hence allow the investigation of the device performance such as base-band memory effects.

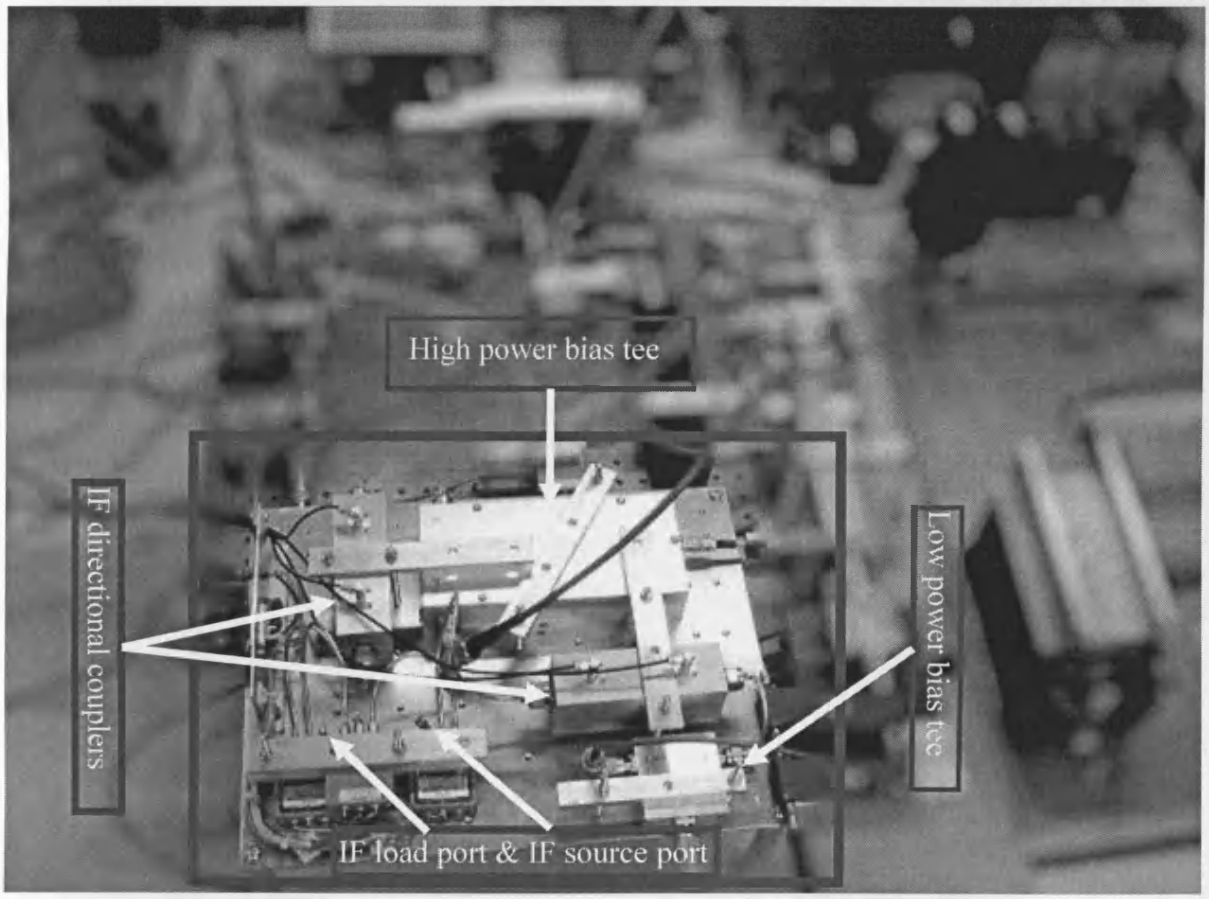

Figure 4.25 Realised high power IF test-set.

4.9. Summary

A new high power IF test-set has been developed, aimed at operating over the 50 kHz to 50 MHz frequency band for the measurement of IF frequency and capable of handling IF power of more than 50W. This was made possible by the design and realisation of IF bias tee which is capable of handling low-frequency IF signal components and its integration with a high power IF test-set. It is possible to consider the integration of this high power measurement capability with the established high power RF measurement capability, coupled with a sampling scope based receiver, that can delivered a measured solution for the characterising high-power devices under modulated signal conditions, which are relevant for the base-station market.

4.10. References

1. Hettak, K., et al. *A compact, high performance, semi-lumped, low-pass filter fabricated with a standard air bridge process.* in *Microwave Conference, 2005 European.* 2005.

2. Pozar, D.M., *microwave engineering.* 2nd ed. 1998, New York: Wiely.

3. Zverev, A.I., *Handbook of FILTER SYNTHESIS.* 1967, USA: John Wiley.

4. G. L. Matthaei, L.Y., and E. M. T. Jones, *Microwave Filters, Impedance-Matching Networks, and Coupling Structurs.* 1980, Dedham, Mass: Artech House.

5. Bowick, C., *RF Circuit Design.* 1982, Indianapolis: Newnes.

CHAPTER 5

Final Measurement System Architecture and Validation

5.1. New High Power Waveform IF and RF Measurement System Architecture

The new high power waveform IF and RF measurement system, with a further modification to the previous measurement system architecture, is shown in Figure 5.1.

The RF test-set components have not been modified, as mentioned in chapter 3, since it is already suitable for characterising high power RF amplifiers with a bandwidth of 1-12GHz and a maximum current and voltage handling of 10A and 100V respectively. With respect to the IF test-set, the low power bias tee used in the previous system (2W, 0.2A and 30V) has been replaced with the new high power IF bias tee which has a bandwidth of 50 kHz to 50 MHz with the capacity to handle a current and voltage of 10A and 1000V respectively, in addition to a typical insertion

loss of 0.5 dB to the IF signal and a minimum isolation of 22 dB. Also another bias tee has been designed on site for a wide bandwidth of 50 kHz to approximately more than 300 MHz and a maximum current of 2A at 100V. The IF low power directional couplers were replaced with commercially available directional couplers, manufactured by WERLATONE, to provide the IF test-set with a bandwidth of 10 kHz to 1GHz with a maximum power of 50W CW, combined with a coupling of 30 dB and a maximum insertion loss of 1.2 dB.

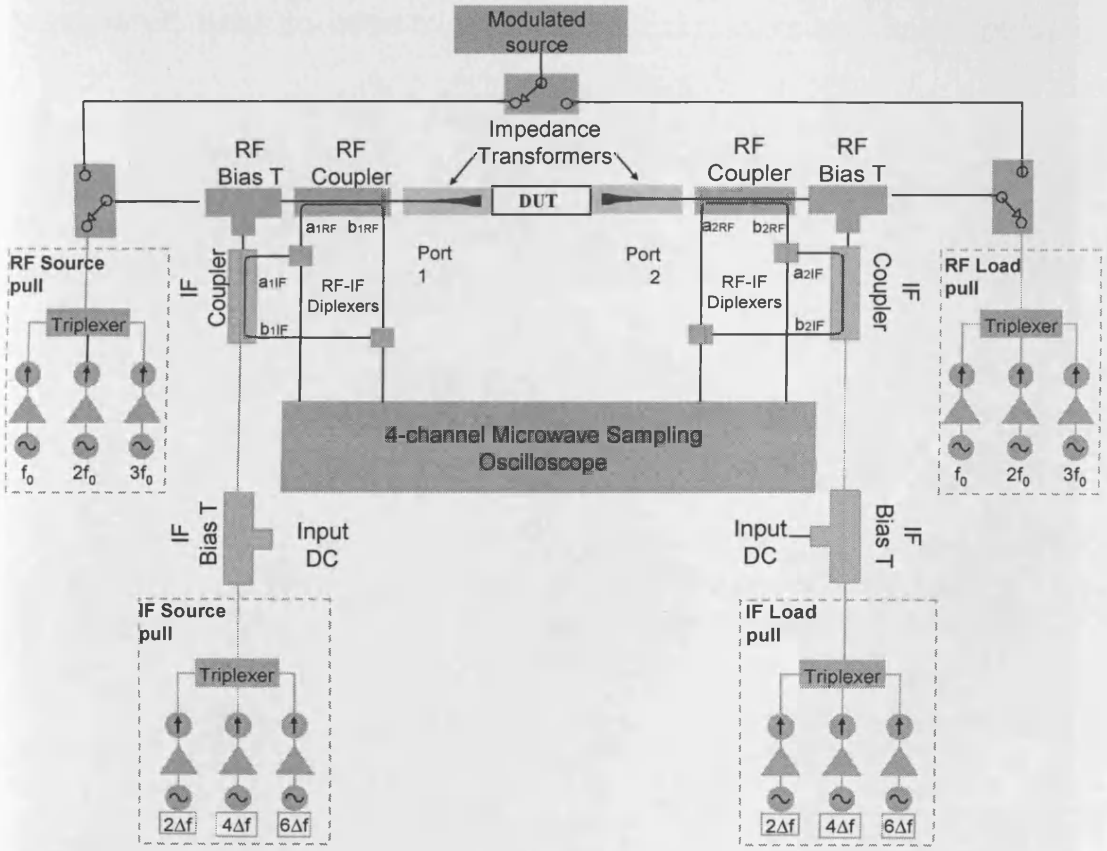

Figure 5.1 Schematic of the new high power RF and IF measurement system with active source and load pull.

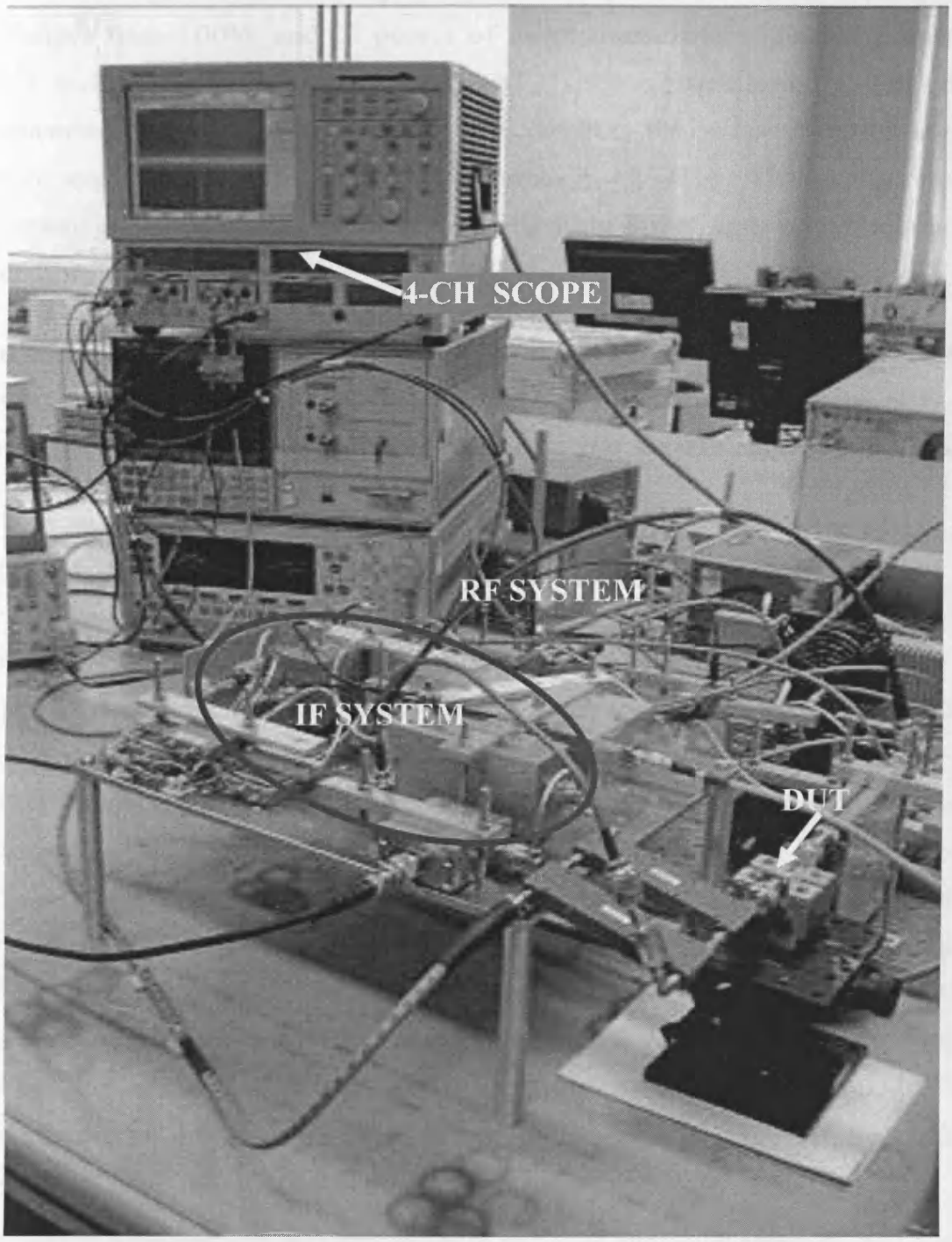

Figure 5.2 The new high power RF and IF measurement system

The resulting measurement system has the capability to handle RF power of more than 100W and IF power of more than 50W along with current and voltage of more than 10A and 100V respectively. The new measurement system can characterise devices for a bandwidth ranging from approximately 50 kHz to approximately 12 GHz. This measurement system is therefore suitable for investigating high and low frequencies memory effects.

In addition, to the authors' knowledge, no active nor passive IF load and source pull measurement system had existed with the capability of handling up to 100 W of IF power like the newly developed Cardiff measurement system does.

5.2. High Power IF Test-Set Test validation

In order to initially evaluate the performance of the new high power IF test-set it was decided to calibrate the IF measurement system and measure its s-parameters using the 8753E VNA in the presence of all IF components such as, IF bias tee, IF directional coupler, switches, diplexers etc, as can be seen in Figure 5.3. The measured insertion loss (s_{21}) from the input of the IF switch, through the IF directional coupler (J1), to either the output of the IF bias tee (DC+IF) or to the DC port presents a good indication of a useful IF measurement system in applications up to 50MHz as shown in Figure 5.4. The insertion loss for the whole IF system is only about 0.6 dB less than that achieved from the IF bias tee alone. This reduction in the insertion loss is mainly caused by the IF directional coupler.

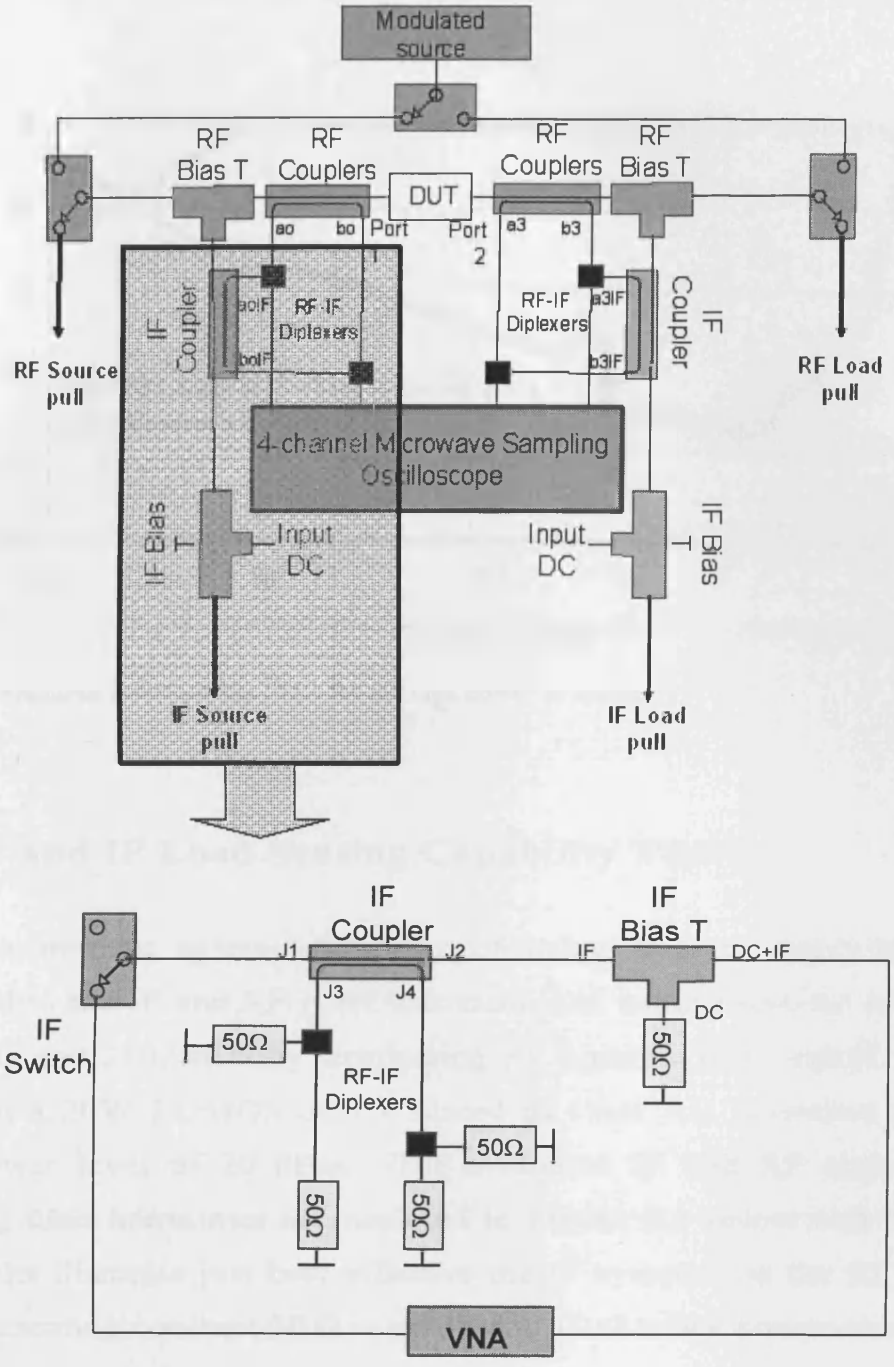

Figure 5.3 Schematic of high power RF and IF measurement system.

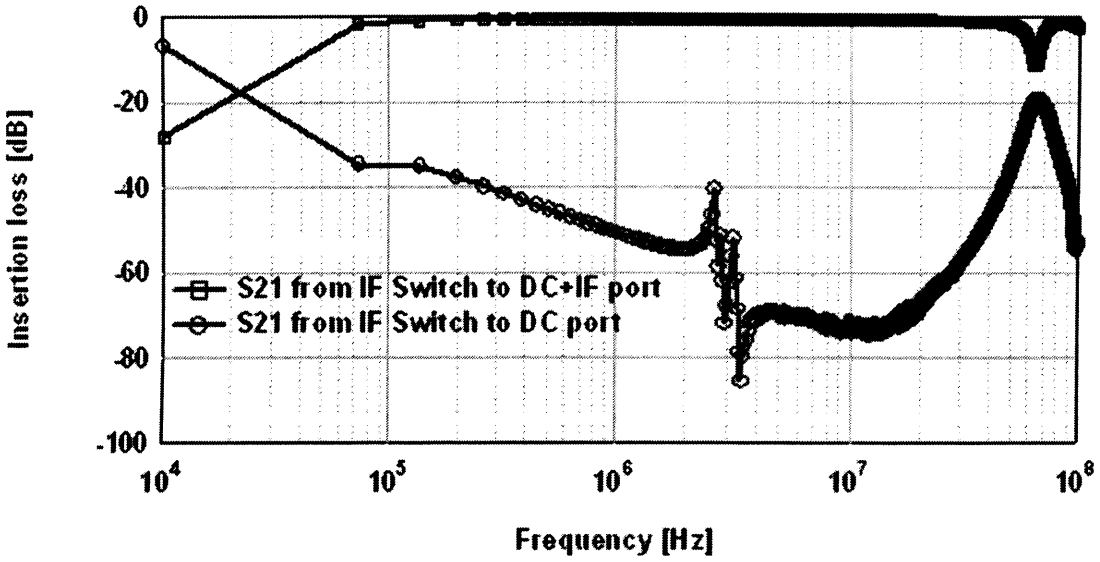

Figure 5.4 Measured insertion loss (S21) for the high power IF system.

5.3. RF and IF Load Sensing Capability Test

The measurement system capability of being able to sense the load presented to the IF and RF ports was examined using two-tone stimuli of 2098MHz and 2102MHz by terminating RF ports in 10 Ω and IF ports in 50 Ω, on a 20W LDMOS device biased as class AB operation at fixed input power level of 20 dBm. The evaluated IF and RF impedances, including their harmonics are depicted in Figure 5.5 below and Table 1. The results illustrate just how effective the IF system and the RF system are in presenting constant 50 Ω to the IF and 10 Ω to RF components.

Table 1 Measured real and imaginary impedances.

Impedance	IF_1	IF_2	IF_3	IF_4	W_1	W_2	$2W_1$	$2W_2$	$3W_1$	$3W_2$
Real	50.91	50.24	49.50	49.52	12.38	12.63	10.70	10.71	7.079	7.94
Imaginary	-3.01	-1.94	-1.82	-1.06	-0.14	-0.43	-1.17	-0.9	-3.73	-3.03

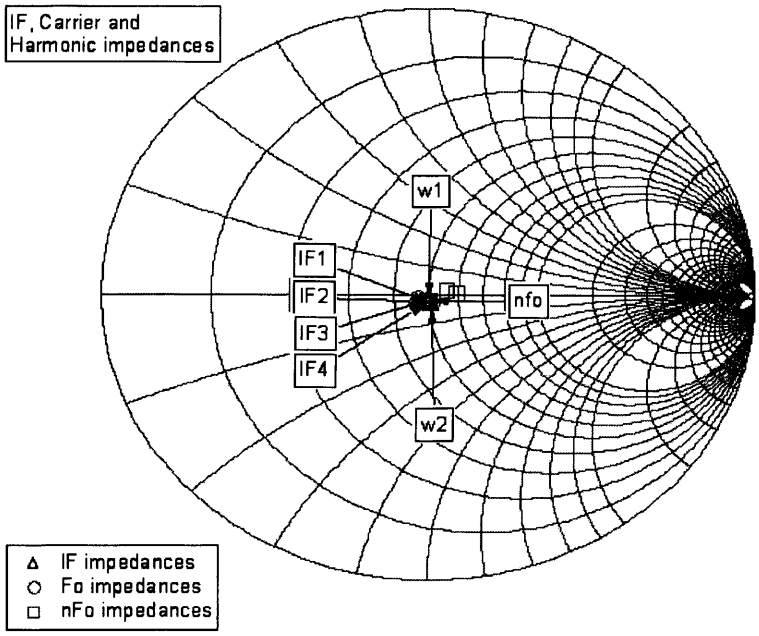

Figure 5.5 Measured baseband impedances at Zo=50Ω, as well as fundamental and harmonic impedances at Zo=10Ω.

The IF base-band impedance control is carried out, with the same device and tone-spacing as in the previous case, and the RF system terminated in 10Ω impedance, with an offset-short is used for the IF termination. It is important to note that when the offset-short termination is used, the load presented to the device can be engineered to be low (approximately zero), as reflected by the achieved results shown in Figure 5.6. The magnitude and phase of IF_1 are not exactly at zero and 180° respectively as one would expect for an ideal short circuit. This can be attributed to the losses introduced by the measurement system itself, has an impedance of a magnitude approximate equal to 6Ω and a phase of about 170° at a modulation frequency equivalent to 4MHz (ω_2-ω_1=2102-2098=4MHz). In a simple test of the systems performance an offset-short was replaced with

an offset-open. In this case, the IF_1 phase would be expected to move about 180°across the Smith chart from the previous value: 170° to approximately -10° corresponding to (170°-180°) and this is approximately what Figure 5.6 is showing, where the IF_1 impedance has been moved from near short to near open. The phase measurement accuracy will be verified in much greater detail in the following section.

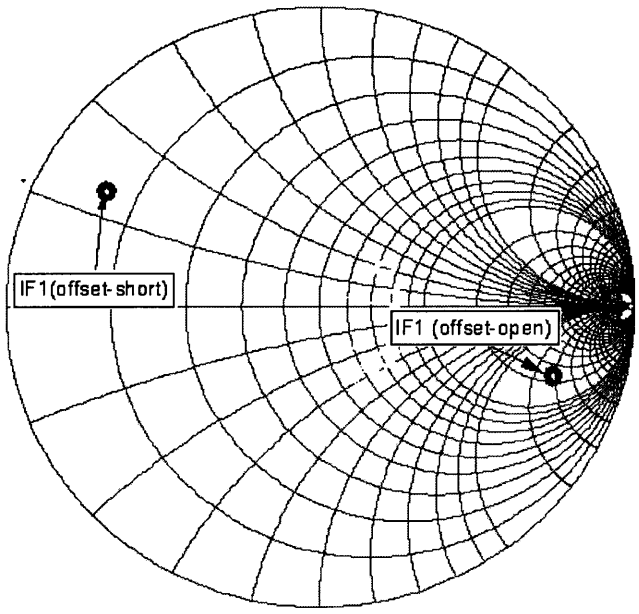

Figure 5.6 Measured IF impedances for offset-short and offset-open terminations

5.4. Demonstration of IF Phase Sweep using Passive Load Pull

The IF measurement system's ability to sweep the IF_1 phase around Smith chart will be examined using 'passive load pull', where coaxial cables of varying length will be connected to IF the port to sweep IF_1 impedance, as can be seen in Figure 5.7. The intention was to sweep the phase of IF_1 to

0°, 90°, 180°, 270° and back to 0° again. Figure 5.8 shows how effective the IF measurement system is in presenting the desired IF_1 phase.

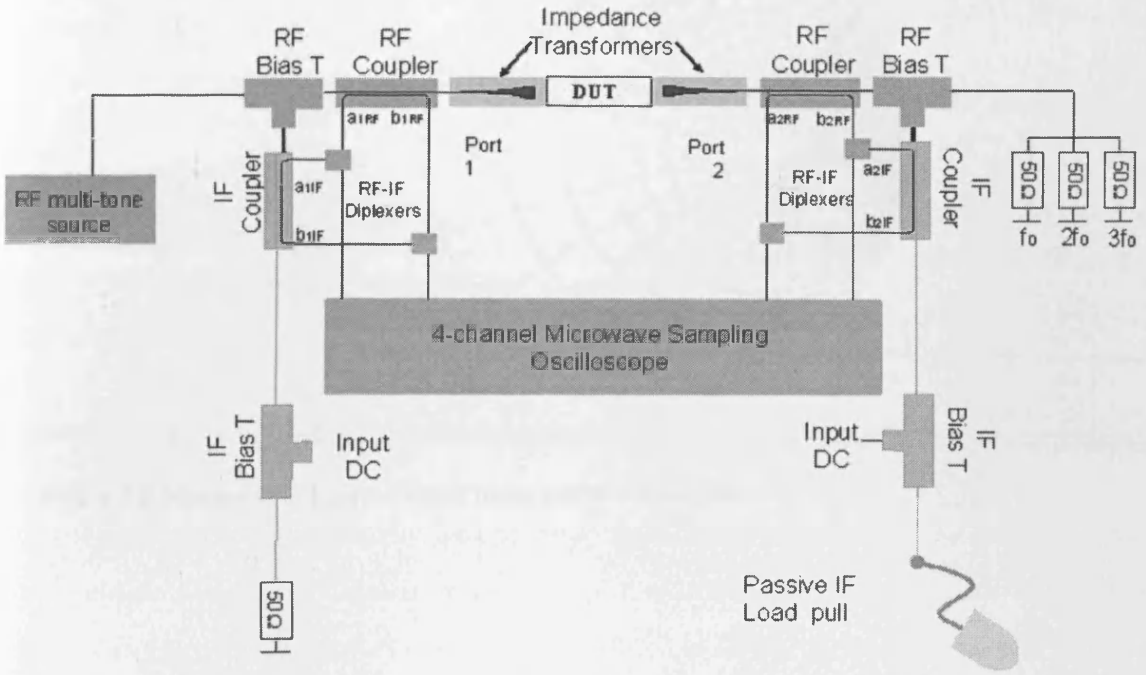

Figure 5.7 Schematic of the high power measurement system used to passively load pull the phase of IF1.

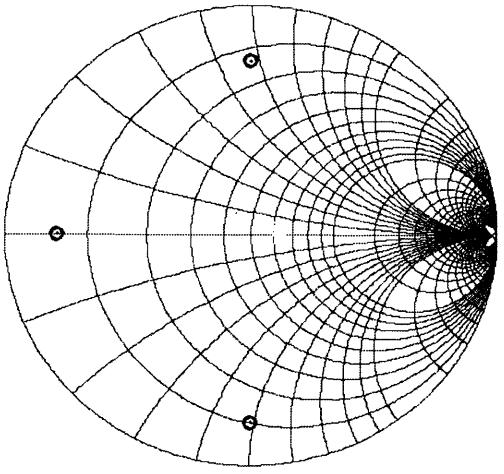

Figure 5.8 Measured IF1 impedances using passive load pull.

5.5. IF Load Pull Test using Passive Load Pull

Passive fundamental load-pull is a relatively simple concept and is effective in allowing for the presentation of specific loads to specific frequency components generated by a device [1] [2]. However, in the case of passive harmonic load pull, presenting a high load reflection coefficient using a passive tuner is difficult especially on the edge of the Smith chart [3] [4]. Limited maximum reflection coefficient is considered to be the most important disadvantage of passive load pull [5].

The problem is compounded at IF frequency (i.e., up to a few megahertz) when it comes to presenting a constant IF impedance passively across wide modulation bandwidths. Currently available commercial passive load pull measurement system such as, Maury or Focus system do not include base band frequencies [6]. To the author's knowledge there are no

commercially available IF passive or active load–pull system with the capability of handling up to 50 W of IF power and suitable for investigating baseband memory effect except for the one developed as a result of this research at Cardiff University [5].

It is important to mention at this stage that even for the Cardiff IF passive measurement system, it is almost impossible to load or source pull IF impedance at very low frequencies (into the range of some kHz) without severely limiting the magnitude of Γ. This will be demonstrated in the example below.

Examples of passive load pull are reported in Figure 5.9 to demonstrate and clarify the previous claim. The passive load pull ability to maintain constant IF impedance, observed by the output of the DUT, will be examined. The simplest method of synthesising an arbitrary impedance is to use a piece of coaxial cable as a classical tuner to load pull IF_1 impedance toward the optimum termination, which is defined as short [7]. Figure 5.9 shows the measured IF_1 impedances of a 20W LDMOS device at 2.1 GHz using two-tone excitation for two modulation frequencies of 0.37 MHz and 1 MHz. The magnitude of the reflection coefficient could not be brought to a perfect short circuit because of the expected losses and the delay introduced by the system itself. Nevertheless, it should be noticed that load pulling IF_1 to short (180 degree) at two different modulation frequencies of 0.37 MHz and 1 MHz, results in two different impedance magnitudes of 8.7 Ω and 5.9 Ω respectively. An increase in the impedance magnitude of about 2.8Ω is observed. This difference of 2.8Ω between the two modulation frequencies is a serious indication of how it would be difficult to sweep, for example, the phase of IF_1, at some kHz around the Smith chart without dramatically changing its magnitude. To emphasise this point, the length of the coaxial cable used in the

previous measurement to load pull IF_1 at Δf=0.370 MHz components can be calculated using this formula:

$$L=\frac{\varphi}{360^0}*\frac{C}{F}\frac{1}{\sqrt{\varepsilon}} \tag{6.1}$$

Where:

Φ = Phase of IF_1 in degree

C = Speed of propagation

F = Frequency of IF_1

ε = Dielectric constant of material (equal to 2.3 in the case of polyethylene material)

$1/\sqrt{\varepsilon}$ = Velocity factor

For simplicity, if we assume that the speed of the propagation is equal to the speed of light, the length of the coax cable would be approximately:

$$L=\frac{37.2}{360^0}*\frac{300000000}{370000}\frac{1}{\sqrt{2.3}}=55.25\ meters$$

For a consistent comparison, if for instance the location of the IF_1 impedance at Δf=1 kHz was found to be identical to that of IF_1 at Δf=370 kHz then the new length of the coax cable needed to load IF_1 at Δf=1kHz would be:

$$L=\frac{37.2}{360^0}*\frac{300000000}{1000}\frac{1}{\sqrt{2.3}}=20441\ meters$$

If 55.25 meter of a coax cable has an internal resistance of 2.8 Ω then it would be expected for a coaxial cable length of 20441 meter to have internal resistance of about:

$$R_{internal}=\frac{20441}{55.25}*2.8=1035.92\ \Omega$$

which shows how the magnitude of this impedance has been driven from the desired short towards an open circuit instead.

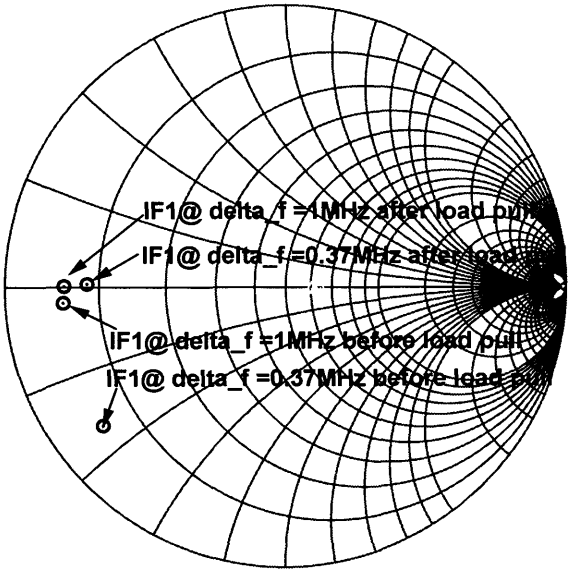

Figure 5.9 Measured IF_1 impedance for two modulation frequencies of 0.37 MHz and 1 MHz before and after load pull using passive load pull.

Even at higher IF frequencies, a passive approach cannot present a high load reflection coefficient for IF harmonic tuning since IF harmonic tuning also depends on the IF fundamental load pull tuning.

Figure 5.10 below is an example of base-band fundamental and second harmonic load pull. Load pulling both IF_1 and its second harmonic IF_2 through a diplexer, designed for this purpose (1 to 2 MHz), towards short circuit, requires more than one iteration around the Smith chart, which consequently leads to an increase in the magnitude of the IF impedances.

After all that has been said about IF passive load pull, it still provides a reasonable amount of information about the devices performance e.g. base-band memory effect, especially if the IF higher order components (IF_2, IF_3 ...etc) are negligible.

The first experiment shows how easy, simple and cheap the passive load pull is, and in addition, it maintains a constant load for different power levels. Obvious disadvantages of this approach related to the limitations of the passive IF load and source pull are illustrated and reported in Figure 5.9 and Figure 5.10. Firstly Figure 5.10 indicates that the maximum achievable load reflection coefficient (Γ_{Lmax}) is only about 0.82, and secondly, it shows the difficulty of sweeping the phase of Γ without severely degrading its magnitude at low IF frequencies. This highlights the complexity of the IF load pull in comparison to RF harmonic load pull.

Figure 5.10 shows the unsatisfactory consequences of IF fundamental (tone spacing) and IF second harmonic (two times tone spacing) impedances being load pulled simultaneously. It is therefore important, in the case of passive load-pull, to recognise the need for a family of diplexers due to the large IF bandwidth involved. This is difficult and

costly to design and hence considered to be a major problem in practise. To avoid this, a physical diplexer is needed to fulfil this role. It could be via the IF power amplifier, which can be used as a diplexer, if two signals from the arbitrary wave generator (AWG) are combined by a combiner and then fed to the input of the IF power amplifier, (see Figure 5.11). In order to adequately investigate devices and establish accurate optimisation, active load pull can therefore be used instead. Accurate load pull measurement data are required to create the accurate behavioural model needed in the designing of power amplifiers.

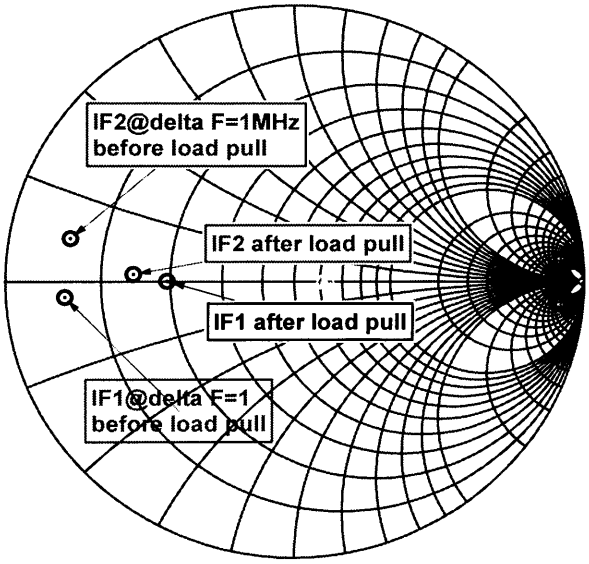

Figure 5.10 Measured IF_1 and IF_2 impedance for tone-spacing of 1MHz before and after load pull using passive load pull.

5.6. Demonstration of IF Phase Sweep using Active Load Pull

Passive load pull is easy and inexpensive to maintain, but the drawback is its limited maximum reflection coefficient, as the previous section has illustrated. To overcome the limitation of achieving the maximum reflection coefficient, active load pull is substituted to allow full coverage of the Smith chart, by compensating for any losses incurred between the device and the measurement system. The load reflection coefficient (Γ_L) can now easily be augmented to 1 or even larger.

The measurement system illustrated in Figure 5.11 was used for this investigation. The coaxial cable connected to the IF port in the previous section is replaced with an arbitrary waveform generator (AWG), followed by an IF power amplifier to inject a signal capable of sweeping the phase of the IF components.

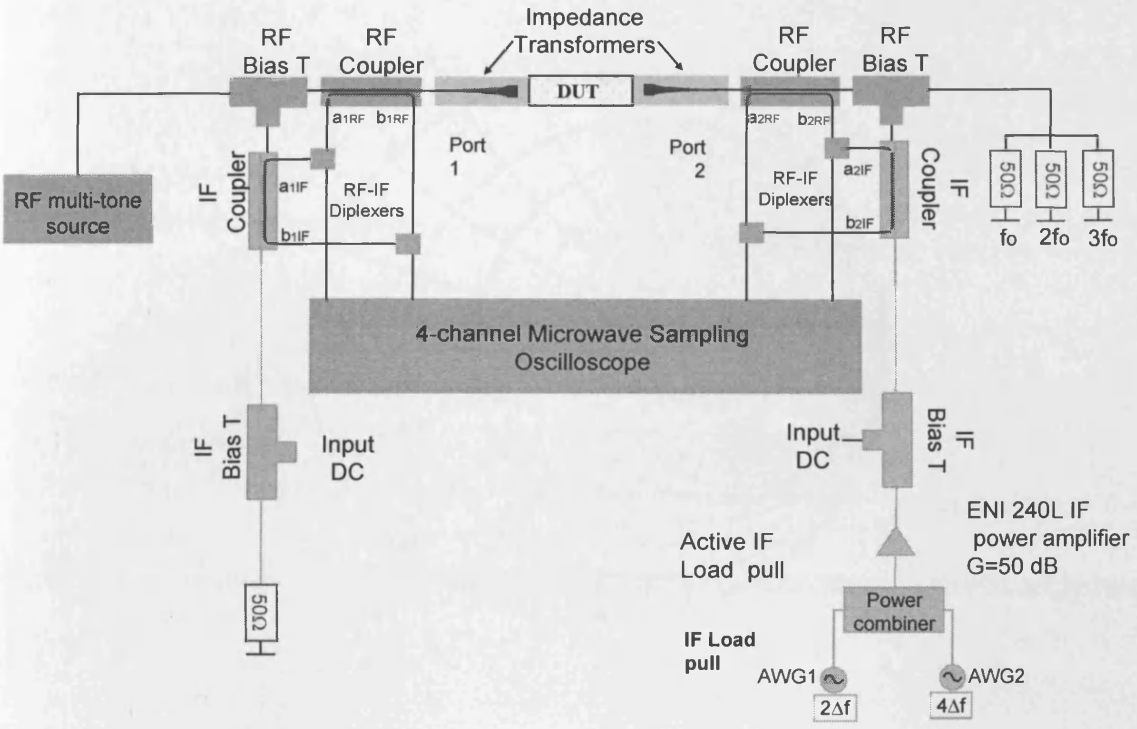

Figure 5.11 Schematic of the high power measurement system used to actively load pull the phase of IF_1.

Figure 5.12 indicates the advantage of the active load pull over passive load pull, showing full coverage of the Smith chart. The active IF load pull measurement has been successfully undertaken at different reflection coefficient, to determine the effects of the low frequency IF load impedance on the linear behaviour of the DUT, such as its effect on distortion components. IF load pull can also be used to find the optimum IF load which might minimise the inter-modulation distortion terms.

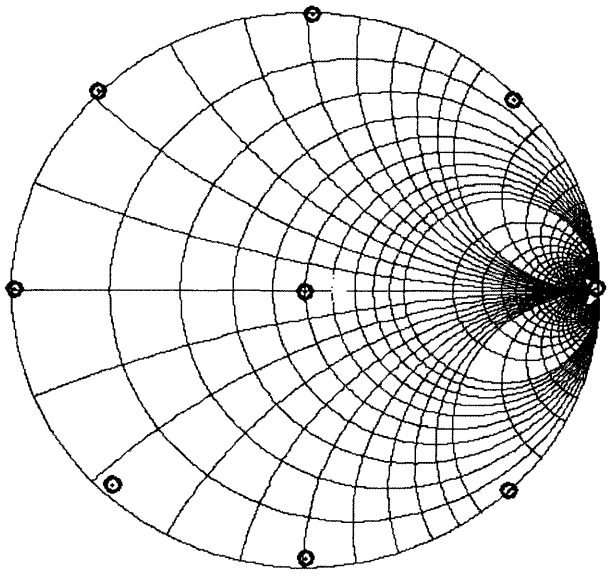

Figure 5.12 Measured IF1 with phase sweep for 5MHz frequency separation using active load pull.

5.7. Non-Linear High Power Measurement System Test

Validation of the performance of the non-linear high power measurement system required satisfactory calibration. The system was fully vector-error corrected, and could therefore account for any errors introduced due to losses, mismatches and imperfect directivities in the system. This allowed for the measurement of the complete modulated voltage and current waveforms and impedances, which exist at the DUT plane. This performance was achieved through the characterisation of a 20W LDMOS device at 2.1 GHz using two-tone excitation.

5.8. Power Transfer Characteristic using Single-Tone Measurement Test

Single tone (CW) measurement provides a basic method of evaluating the linearity characterisation of RF devices. The CW power sweep, for example, is a helpful tool in showing the most common parameter describes the linearity performance extracted under single tone conditions, AM-AM and AM-PM distortion along with quantifying the device 1 dB compression point.

Demonstration of single tone test has been achieved using the non-linear high power measurement system to characterise the 20W LDMOS device performance including its harmonics behaviour under single tone test. Figure 5.13 below shows the output power spectrum of the fundamental and harmonics obtained from increasing the input power at frequency stimulus of 2.1 GHz.

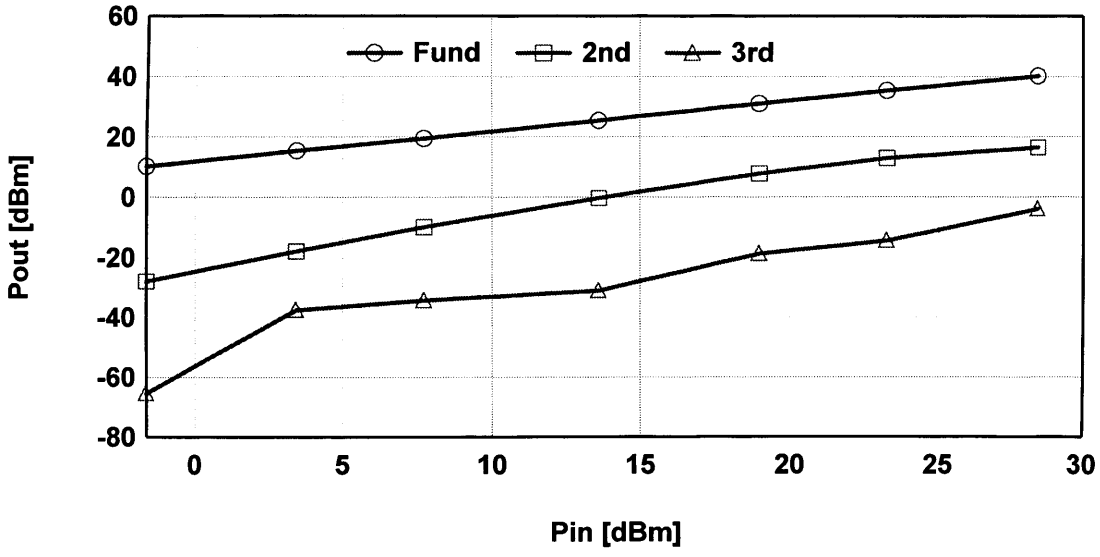

Figure 5.13 Measured single tone power sweeps at 2.1 GHz.

5.9. Power Transfer Characteristic using Two-Tone Measurement Test

The measurement system was again put in a calibrated state to examine the relationship between input and output power. In this case, the device was biased as class AB and stimulated by a two-tone stimulus frequency of 2098 MHz and 2102 MHz while terminating all ports to 50Ω. The input power was swept from -5dBm (linear region) to 25 dBm (compression) in steps of 5 dBm. The output power of a power amplifier can not increase indefinitely, so there will be a point at which the input power increase will not produce a corresponding rise in output power.

Figure 5.14 shows the classical power transfer characteristics of a 20W LDMOS device as a result of increasing the input power. As can be seen the output fundamental tone power increased linearly to an input power of approximately 20 dBm before the device started to saturate. The output power sweeps revealed a 1 dB compression point of about 33 dBm. The measurement system also recorded the non-linear behaviour IM_3 components $(2\omega_1-\omega_2)$ and $(2\omega_2-\omega_1)$ generated by the device. A constant increase was observed in the magnitude of IM_3 below a saturation level of 33 dBm at which point the device reached its optimum limit, and therefore the output power of IM_3 began to compress as was expected. The compression point can also be identified by the gain plot as a function of the input power as seen in Figure 5.14, where the gain started to compress at an input power equal to 20 dBm. The results indicated the measurement system's ability to measure behaviour in the device under two-tone excitation.

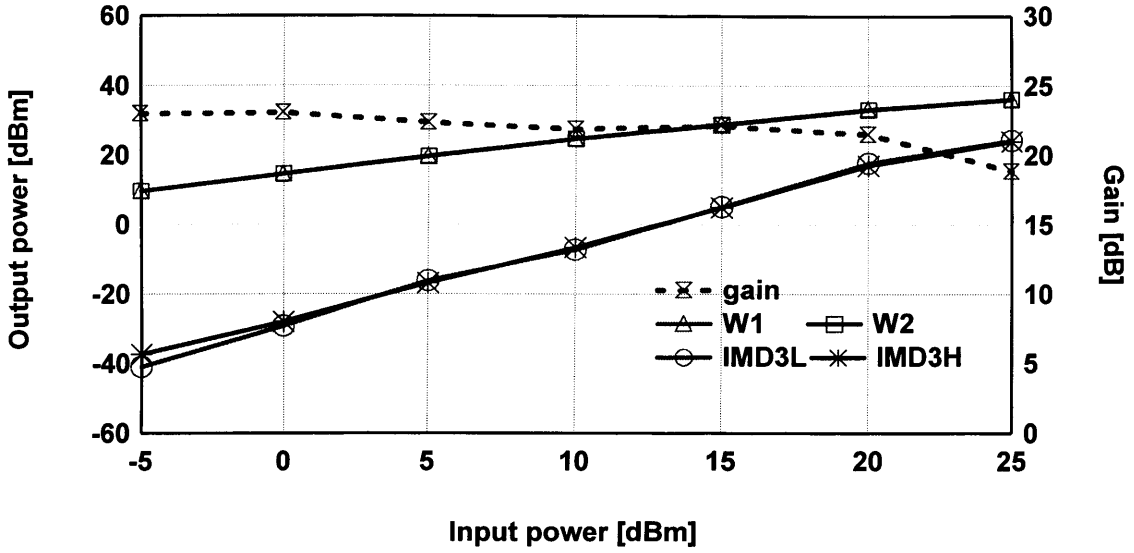

Figure 5.14 Measured two-tone power sweeps for 4MHz frequency separation.

5.10. Repeatability Test

The measurement system's repeatability and accuracy were tested and demonstrated using a-20W LDMOS device characterised at 2.1 GHz for tone- spacing of 1MHz and biased as class AB using the two-tone technique. In the first test, the input power was swept from approximately 17 dBm to approximately 37 dBm in 11 steps with averaging equal to 64 (Case 1). In the second test, the same measurement was repeated but this time, the power sweep's steps were increased from 11 steps to 41 steps with averaging of 256 (Case 2). This increase in number of steps and averaging increased the accuracy and hence indicates whether the measurement is repeatable or not, in addition, it gives an indication of the optimum number of steps required for characterising such a high power device.

Figure 5.15 shows the lower output fundamental power ω_1 and the third order inter-modulation distortion lower output power IMD_{3L} for both Cases 1 and 2 of a two-tone technique. For plot clarity and the fact that they are very similar to ω_1 and IMD_{3L}, ω_2 and IMD_{3H} were not included.

It appears from Figure 5.15 that the device performance is well defined whether using Case 1 or Case 2. However the difference, in dB, between ω_1 (Case 1) and ω_1 (Case 2) is defined as Delta ω_1 while the difference between IMD_{3L} (Case 1) and IMD_{3L} (Case 2) is defined as Delta IMD_{3L} and shown in Figure 5.16. As can be seen, Delta ω_1 is better than -12dB at and below the 1 dB compression point and better then -34 dB for Delta IMD_{3L}. These results validate the measurement system repeatability. It is instructive to determine the required tolerance for input power steps and averaging to maintain time efficient measurements. Experimental experience showed that the time required for a power sweep with 11 steps and 64 averaging (Case 1) was approximately 1 hour while for a power sweep with 41 steps and 256 averaging (Case 2) was approximately 6 hours. For efficient time management therefore, it seems that it is too time consuming to perform such a measurement with such a high number of steps and averages. Furthermore, this time issue will be further compounded when measurements involve a frequency sweep.

Moreover, it is interesting to realise that the 4^{th} generation 20W LDMOS devices biased as class AB, with IF port terminated to short and the other ports to 50 Ω, do not have IMD sweet spots (minimum IMD values). Unless those sweet spots appear below the dynamic range of the measurement system (approximately 50 dB).

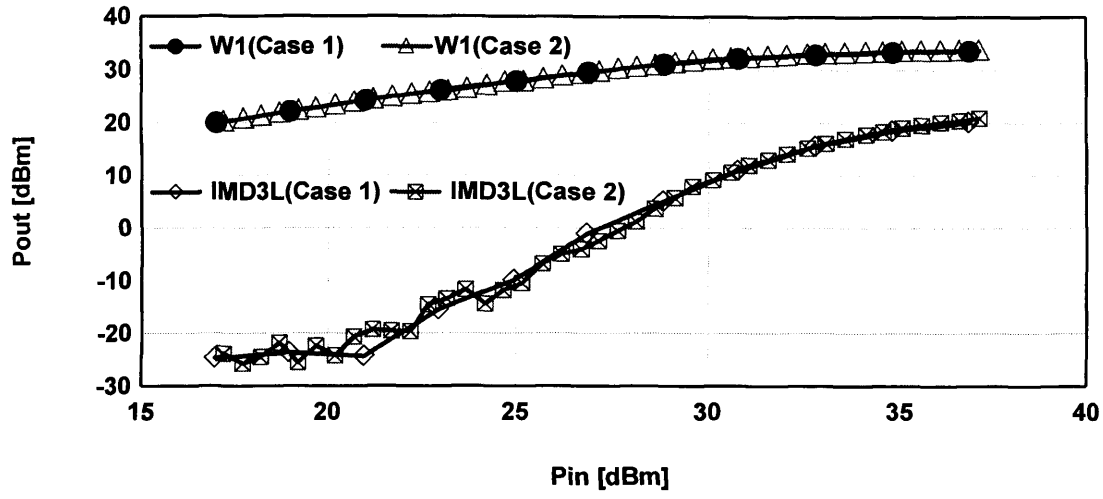

Figure 5.15 Measured output power difference for Case 1 and Case 2.

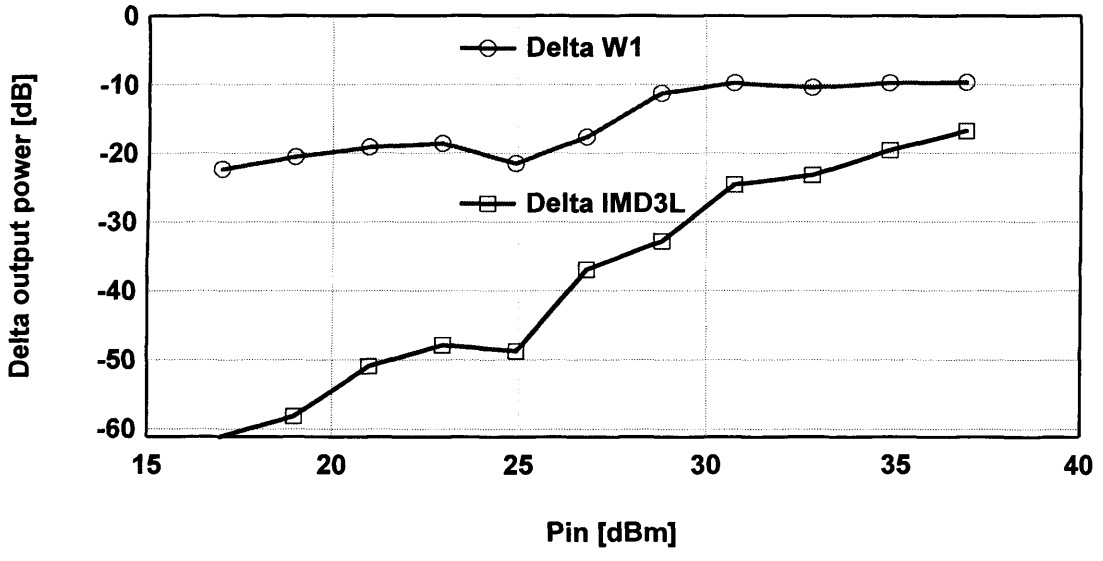

Figure 5.16 Difference in output power between Case 1 and Case 2.

In conclusion, an accurate and repeatable measurement system under two-tone technique has been demonstrated. The input power increment of 1dB with averaging of 64 (Case 1) is appropriate since it describes device performance very well as explained.

5.11. Base-Band Memory Effect Test using Passive Load Pull

Examination of the measurement system's ability to predict the electrical base-band memory effect is tested through passive IF load-pull using the non-linear load pull measurement system shown in Figure 5.17. The passive IF load-pull system, consisting of coaxial cables, was used to present a short circuit impedance to the output IF_1 component, common practice for envelope termination [8] [7], in order to achieve the predicted symmetrical IMD terms. In this measurement the RF fundamental and RF harmonics of the measurement system were terminated with the nominal impedance of 10Ω, while load pulling the fundamental of the IF load component to a short circuit. This validation is performed on a 20W LDMOS device characterised at 2.1 GHz for two-tone spacing, 1 MHz and 5 MHz. The values for the IF load reflection coefficient (Γ_L), at the reference planes of the DUT relating to the two modulation frequencies at fixed short load, prove to be interesting. In this measurement, therefore, the IF load port of the measurement system was terminated in the offset-short, without load-pull, while sweeping input power for the two different modulation frequencies of 1 MHz and 5 MHz.

Figure 5.17 shows the variation in the IF load impedance and hence the IF load reflection coefficient (Γ_L) as a function of the modulation frequency.

The magnitude of the reflection coefficient could not be brought to a complete short circuit because of the losses and the delay introduced by the system itself. Figure 5.18 shows the measured RF two-tone power as well as the output inter-modulation IMD performance as a function of both the input drive level and the base-band impedance, presented to the drain of the device for the two modulation frequencies. The measured system was able to detect and measure output tones ω_1, ω_2 and IMD components. The magnitude of the inter-modulation products IM_{3L} and IM_{3H} at tone-spacing of 1 MHz is different to that one at 5 MHz. it is difficult to determine whether the change in the IMD magnitude, at constant input drive level, is a result of the modulation frequency sweep or due to the variation of the base-band impedance. Hence, the need to keep one variable constant, while sweeping the other.

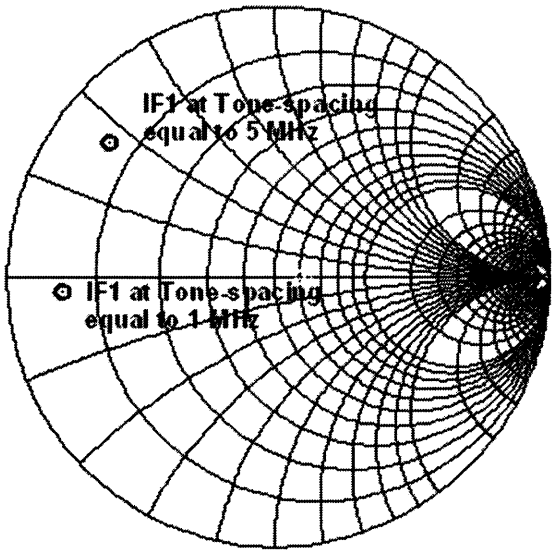

Figure 5.17 Measured IF_1 impedance vs. tone-spacing before load pull.

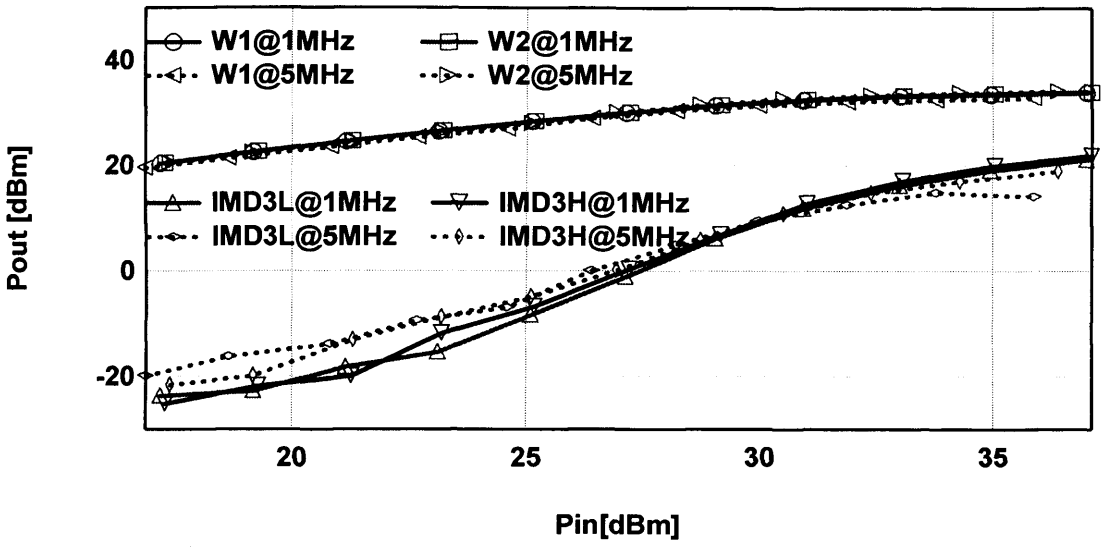

Figure 5.18 Measured two-tone power sweeps (ω_1 and ω_2) and IMD3 for two two-tone frequency separations before load pull.

The system's ability to maintain a constant IF impedance, demonstrated at the output of the DUT, will be examined through passively load pulling the IF_1 impedances almost to a short-circuit, while sweeping input drive levels at two-tone spacing of 1 MHz and 5 MHz. In this experiment, multiple and varying lengths of coaxial cables were used to load pull all the IF_1 impedances depicted in Figure 5.19 as close to short (180°) as possible.

Figure 5.20 illustrates just how effective the IF measurement system is in maintaining almost constant base-band impedance, regardless of frequency variations. The impedance magnitude of IF_1 at 1MHZ was found to be about 5.5 Ω while the impedance magnitude of IF_1 at 5 MHz is approximately 10 Ω.

It is important to realise that the passive load-pull limits the maximum achievable magnitude of Γ_L due to inherent losses introduced by the system and by the coaxial cable used to load-pull the IF_1 impedances.

Figure.5.20 plots the measured value of the output RF two-tone power performance (ω_1 and ω_2) and of inter-modulation distortion IMD_3 as a function of input power level at two different modulation frequencies of 1 and 5 MHz. As can be seen from this graph, the behaviour of the two output tones (ω_1 and ω_2) and $IMD_{3L\&H}$ is observed to be approximately independent of the tone spacing frequency however, describing this plot in detail is beyond the scope of this section and covered in chapter 6. These plots highlight how useful the measurement system is in measuring and engineering base-band impedance presented at the device plane and therefore allow the investigation of memory effect.

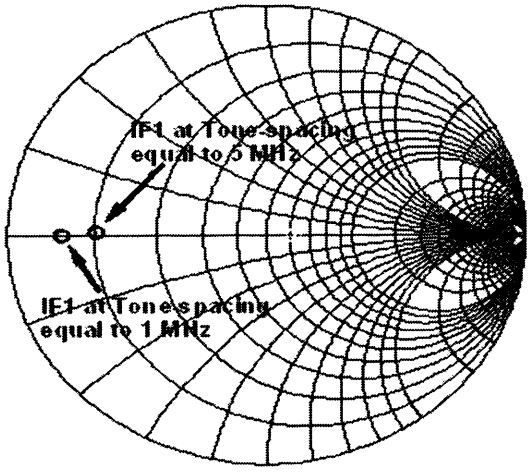

Figure 5.19 Measured IF_1 impedance vs. tone-spacing after load pull.

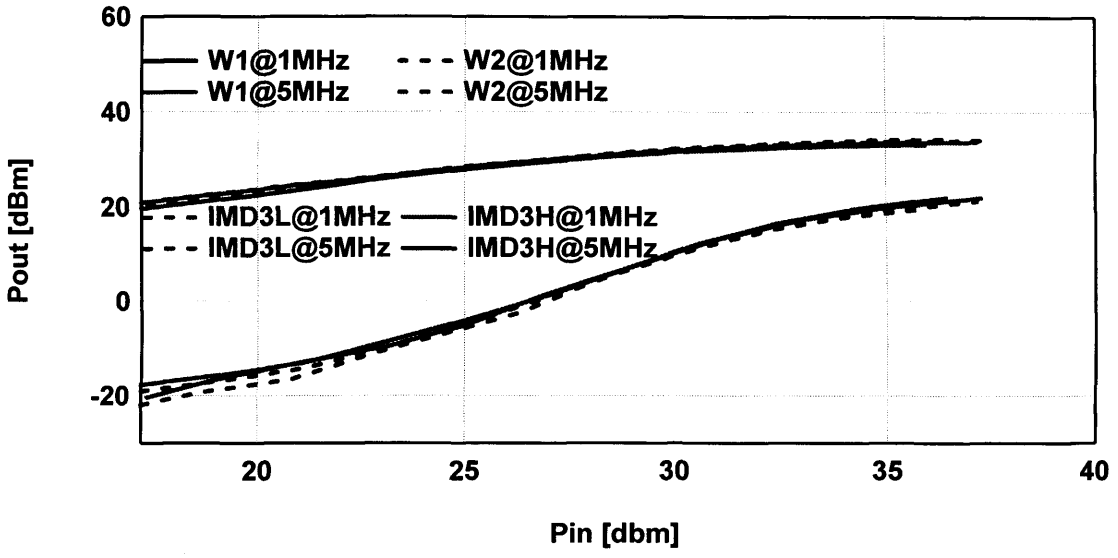

Figure 5.20 Measured two-tone power sweeps (ω_1 and ω_2) and IMD_3 for all two-tone frequency separations after load pull.

5.12. Spectrum of Interest for High Power LDMOS Devices

All harmonics with order greater than 3 and all mixing products with order greater than 10 are found to be very close to the lower dynamic range of the measurement system, resulting in noisy measurements at low drive levels. Therefore, the system calibration will be performed for 3 harmonics and mixing terms up to the 10^{th} order. This is shown in Figure 5.21. The measured output power was taken with IF_1 and IF_2 terminated to a short. It is clear that the level of IMD_{9L} defined as 9^{th} in Figure 5.21 and 3^{rd} harmonic components are very small; hence it was not necessary, for all measurements performed in this thesis, to calibrate for higher harmonics and mixing orders.

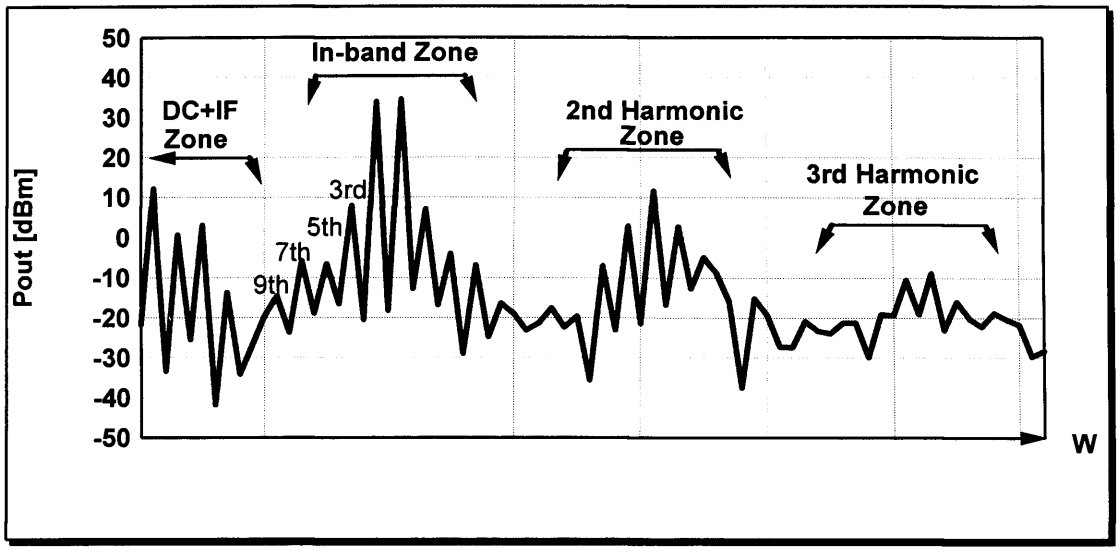

Figure 5.21 Measured spectrum output power for three harmonics with mixing terms of ten.

5.13. Summary

A new high power IF measurement system has been developed aimed at operating over the frequency range 50 kHz to 50 MHz defined by the bandwidth of the IF bias tee. This bandwidth is an order of magnitude greater than the modulation bandwidth of W-CDMA systems.

The IF bandwidth of the measurement system can be extended to approximately 350 MHz by replacing the previous bias tee (50 MHz bandwidth and 10A) with another bias tee designed on site, to operate at 2A and an IF bandwidth of 350 MHz. The developed IF measurement system provides for both measurement and engineering, via passive and active sources and load pull, of the IF signals. The realised IF measurement system is capable of handling IF power of more than 50W. The integration of the developed high power IF test-set with the high power RF measurement system (100W) has enabled the investigation of

the effects of the low frequency IF terminations and high frequency RF terminations on the output RF performance to be initiated. Complete verification of the measurement system's ability to handle all frequency bands, especially and most importantly IF base-band, has been achieved for the first time at these high power levels.

5.14. References

1. Reveyrand, T., et al. *A Smart Load-Pull Method to Safely Reach Optimal Matching Impedances of Power Transistors.* in *Microwave Symposium, 2007. IEEE/MTT-S International.* 2007.

2. Benedikt, J., et al., *High-power time-domain measurement system with active harmonic load-pull for high-efficiency base-station amplifier design.* Microwave Theory and Techniques, IEEE Transactions on, 2000. **48**(12): p. 2617.

3. *DEVICE CHARACTERISATION WITH HARMONIC SOURCE AND LOAD PULL.* 2000 [cited; Available from: www.maurymw.com.

4. Schuberth, C., et al. *Load Pull Characterisation of GaN/AlGaN HEMTs.* in *Integrated Nonlinear Microwave and Millimeter-Wave Circuits, 2006 International Workshop on.* 2006.

5. Alghanim, A.L., J.; Williams, T.; Benedikt, J.; Tasker, P. *Investigation of electrical base-band memory effects in high-power 20W LDMOS Power Amplifiers.* in *EUMC.* 2007. Munich.

6. Spirito, M., et al., *Active harmonic load-pull for on-wafer out-of-band device linearity optimisation.* IEEE Transactions on Microwave Theory and Techniques, 2006. **54**(12): p. 4225.

7. Williams, D.J., J. Leckey, and P.J. Tasker. *A study of the effect of envelope impedance on inter-modulation asymmetry using a two-tone time domain measurement system.* 2002.

8. Carvalho, N.B. and J.C. Pedro. *Two-tone IMD asymmetry in microwave power amplifiers.* in *Microwave Symposium Digest., 2000 IEEE MTT-S International.* 2000.

CHAPTER 6

Base-Band Memory Effects in High-Power LDMOS Power Amplifiers

All measurements in this thesis work are performed on:

I. Fourth Generation (HV4) 20W LDMOS.

II. Seventh Generation (HV7) 20W LDMOD.

III. Seventh Generation (HV7) 12W LDMOD.

Due to external and unforeseen factors relating to the deterioration of devices used during the research process it was not possible to restrict the work to one particular device. Table 1 below summarises the measurements reported in Chapter 6.

Table 6.1 Work summary.

Experiment #	Device	Test type	IF1 impedance	IF2 impedance	Drain voltage	Tone-spacing
Experiment # 1 Section 5.1	HV4 20W	Passive	5.9 – 10.3Ω	Not controlled	28V	370 kHz to10 MHz
Experiment # 2 Section 5.2	HV7 20W	Passive	4.6 -6.8Ω	Not controlled	20V	370 kHz to 10 MHz
Experiment # 3 Section 5.3	HV7 20W	Active	short 50 Ω	50 Ω 50 Ω	28V	1 to 6MHz *
Experiment # 4 Section 5.4	HV7 12W	Active	short short 50 Ω	short 50 Ω 50 Ω	28V	370kHz to 7MHz**

Memory effects are complex phenomena that present major problems in modern high-power linear microwave PA design. Specifically, these effects have a large influence on spectral symmetry and modulation frequency sensitivity, which in turn impacts an overall linearity and importantly the suitability of a power amplifier (PA) to linearisation through pre-distortion.

Memory effects in microwave PAs are generally attributable to a number of physical processes that involve thermal [1] [2] [3], electrical [2] [4] and surface trap effects [5]. Although electrical memory is generally considered as the major contributor, the relative significance of the different effects however is still not clearly understood. One obvious way to develop a more complete understanding is to attempt to remove the most likely contributing factor, and to measure and analyse any residual effects due to the others [6] [7] [4].

* See reference [7] in the publication list for baseband memory effect investigating for tone-spacing ranging from 1 MHz to 10 MHz

** See reference [3] in the publication list for baseband memory effect investigating for tone-spacing ranging from 1 MHz to 10 MHz

6.1. Base-Band Memory Effect Investigation using passive Load Pull (First Approach)

This measurement is performed on a Freescale forth generation (HV4) 20W LDMOS device characterised at 2.1 GHz for tone-spacing ranging between 0.37MHz and 10MHz. The two-tone measurement was performed with the device biased in class AB at a drain voltage of 28V and a gate voltage of 3.6V resulting in a quiescent current of 161 mA.

In this work, simple two-tone modulation and inter-modulation product symmetry, as a function of varying excitation tone-spacing, is used as a reliable indicator of the presence of memory effects [8] [9].

The fundamental and harmonics of the measurement system were terminated with the nominal impedance of 10Ω while the IF measurement system was used to emulate a simple practical resonant bias network as shown in Figure 6.1. To achieve this, the IF measurement system was used to present a short impedance, a common practice for envelope termination [8] [10] in order to achieve symmetrical IMD terms, to the output IF_1 component over the frequency range from 1 and 2 MHz (default optimum). The termination at the other frequencies was allowed to vary in a manner similar to the case of a practical bias network.

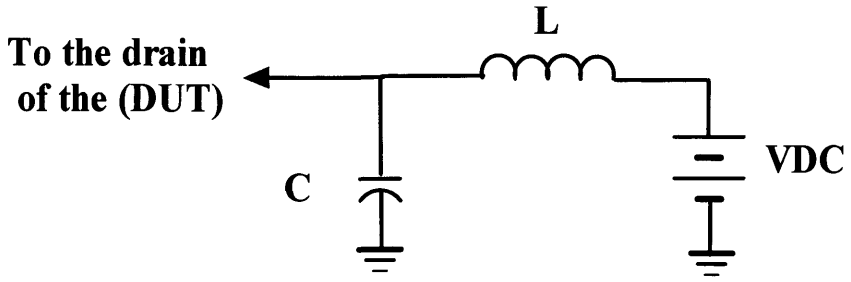

Figure 6.1 Simple bias network.

Figure 6.2 shows the variations in the IF_1 load impedance, in the case of a practical bias network, and hence the IF load reflection coefficient (Γ_L) as a function of the modulation frequency. The magnitude of the reflection coefficient could not be brought precisely to short because of the losses and the delay introduced by the system itself.

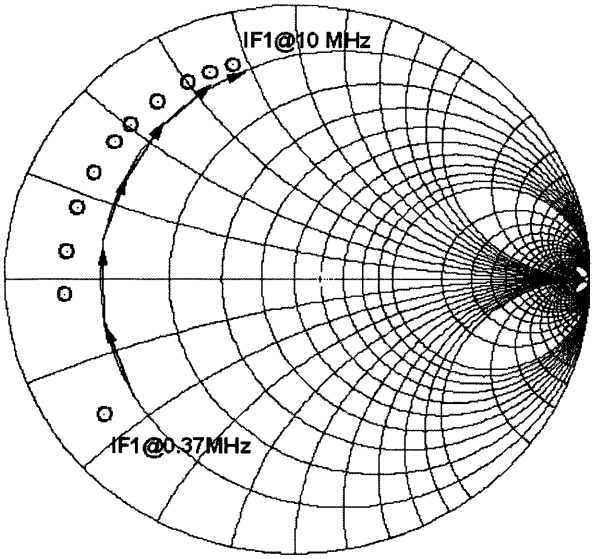

Figure 6.2 Measured IF_1 impedance vs. tone spacing without load pull.

Figure 6.3 shows the measured RF two-tone power performance as a function of both the input drive level and the base-band impedance presented to the drain of the device for all tone spacing from 0.37MHz to 10MHz. The measured output inter-modulation products, IM_{3L} and IM_{3H}, are frequency dependent and demonstrate all the characteristics of memory. The variation in the inter-modulation distortion IM_{3L} and IM_{3H}, for example, is greater than 10 dB at an input drive level of 29 dBm at which the device starts to compress.

This is clearly summarised in Figure 6.4 which plots the measured values of both fundamental output power and inter-modulation distortion IMD_3 as a function of tone-spacing, at a fixed input power level of 29 dBm. The fundamental of the output ω_1 and ω_2 remains constant and independent of the modulation frequency. With regard to the inter-modulation distortion IM_{3L} and IM_{3H}, it is clear that the linearisation level (magnitude) of IMD_3 is degraded at a higher tone-spacing frequency. For example, the magnitude of $IMD3_{L\&H}$ at tone-spacing of 1 MHz is approximately 0 dBm while it is about 10 dBm at tone-spacing of 10 MHz. This highlights the complexity of bias network design.

With regard to the fundamental output power, ω_1 and ω_2, a maximum symmetry was observed at low tone-spacing frequencies while a difference of approximately 2 dBm is observed at a tone-spacing of 10 MHz. It is important to mention that the difference between the fundamental output power, ω_1 and ω_2 as can be seen in Figure 6.4 is correlated and found to be proportional to the variation observed in the input power (ω_{1in} and ω_{2in}) as can be seen in Figure 6.5. Since these two signals are applied at the input of a power amplifier, it would be expected that the power amplifier would in amplifying these two signals and would amplify the difference between them as well. Therefore, the asymmetry in the output signals, ω_1 and ω_2, is attributed to the asymmetry in the input signals [11].

However, it is still difficult to distinguish whether the change in the IMD magnitude, at constant input drive level, is a result of the variation of the base-band impedance or associated with other sources of memory effect such as thermal or trapping memory.

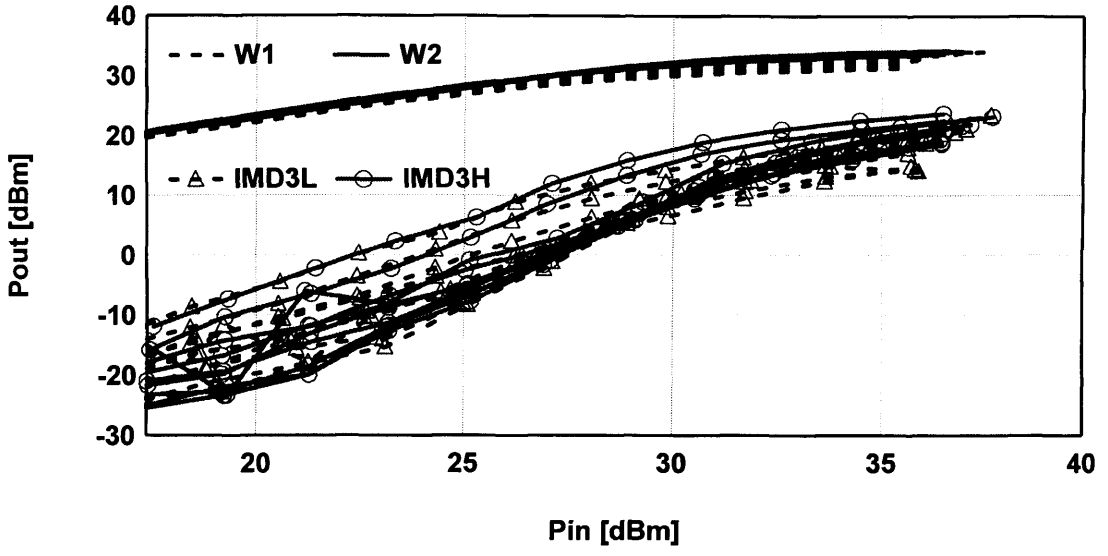

Figure 6.3 Measured two-tone power sweeps (w_1 and w_2) for all two-tone frequency separation ranging from 0.37 to 10 MHz.

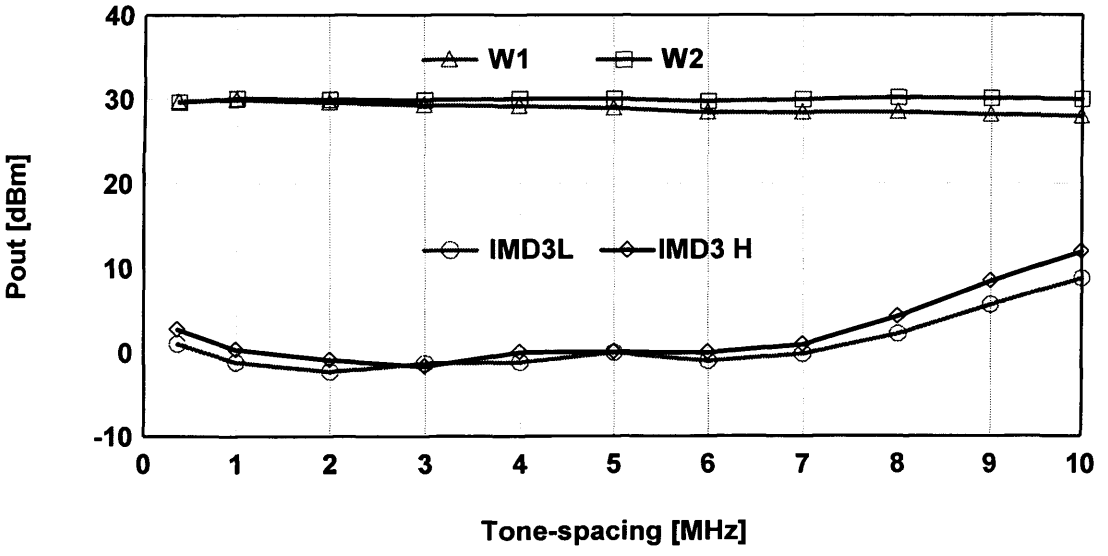

Figure 6.4 Measured fundamental and IMD power vs. Tone-spacing at 30dBm input drive level.

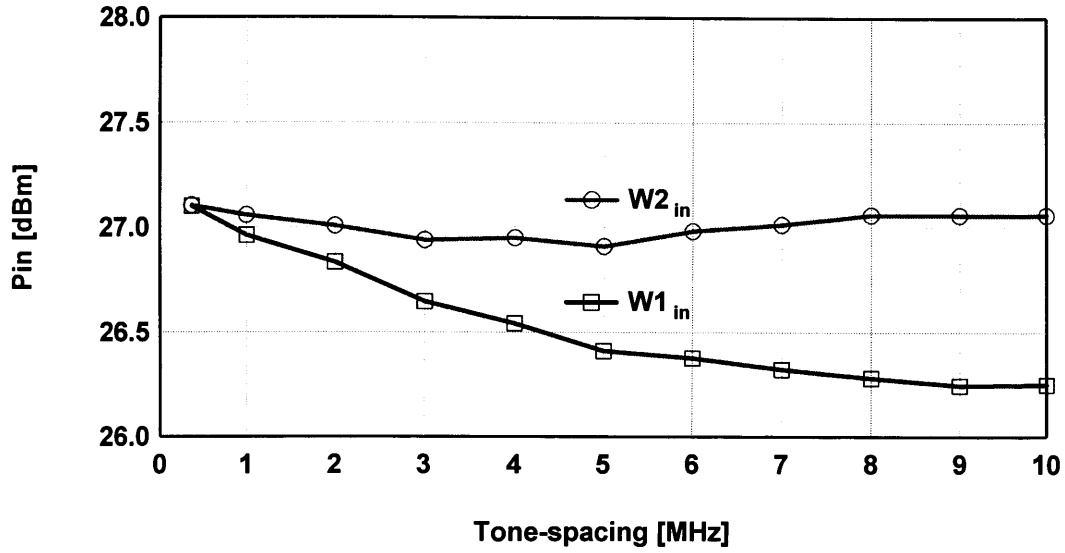

Figure 6.5 Measured fundamental input power (ω_1 and ω_2) vs. Tone-spacing.

In the second experiment, the passive IF load pull system was used to emulate an ideal bias network, which would have short circuit impedance for all tone-spacing ranging between 0.37MHz and 10MHz.

In this passive load pull experiment multiple pieces of coaxial cables with different lengths were used to load pull all the IF_1 impedances depicted in Figure 6.6 as close to short (180°) as possible. It is clear that the impedance IF_1 at 1MHz is very close to 180° and therefore, it would be easy to load this point to short with the minimum of coaxial cable. In contrast, the situation was quite different when dealing with the impedance IF_1 at 2 MHz located just above the 180° axis. It therefore needed to be rotated about 355° around the Smith chart in order to bring it to short. Load pulling this point required a very long coaxial cable of approximately 50 meters, which resulted in maximum loss.

Figure 6.6 illustrates just how effective the IF measurement system is in maintaining an almost constant and almost short impedance, regardless of frequency variations.

Using a two-tone signal with different tone spacing from 0.37MHz to 10MHz and an input drive level sweeping from 17dBm to 37dBm, the two-tone output fundamentals (ω_1 and ω_2) as well as the output inter-modulation IMD are shown in Figure 6.7. The maximum asymmetry between IM_{3L} and IM_{3H} at input power of 29 dBm, corresponding to 1 dB compression point, is less than 3 dB as opposed to an asymmetry of 10dB before employing load pull to emulate ideal bias network. It was immediately evident, through the lack of output fundamentals (ω_1 and ω_2) and IMD variations with respect to tone-spacing frequency, that electrical memory can be suppressed by designing an ideal bias network [8] [12] [13]. This is clearly summarised again in Figure 6.8, which plots the measured values of both RF fundamental output power and inter-modulation distortion IMD_3 as a function of tone-spacing, at a fixed input power level of 29 dBm. The fundamental of the output ω_1 and ω_2 as well as the inter-modulation distortion IM_{3L} and IM_{3H} remain constant and independent of the modulation frequency. Figure 6.8 also indicates the improvement achieved when designing ideal bias network with constant impedance at all modulation frequencies. For example, $IMD_{3L\&H}$ in the case of ideal bias network have been improved by approximately 10 dBm at 10 MHz in contrast with the simple practical bias network.

It must be taken into account that the passive load-pull limits the maximum achievable magnitude of Γ_L due to inherent losses introduced by the system and by the coaxial cable used to load pull the IF_1 impedances (as mentioned in Chapter 5).

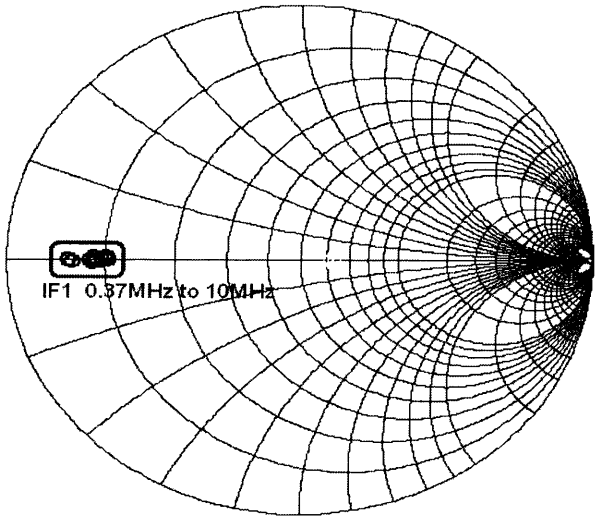

Figure 6.6 Measured IF_1 impedance vs. tone spacing using ideal bias network.

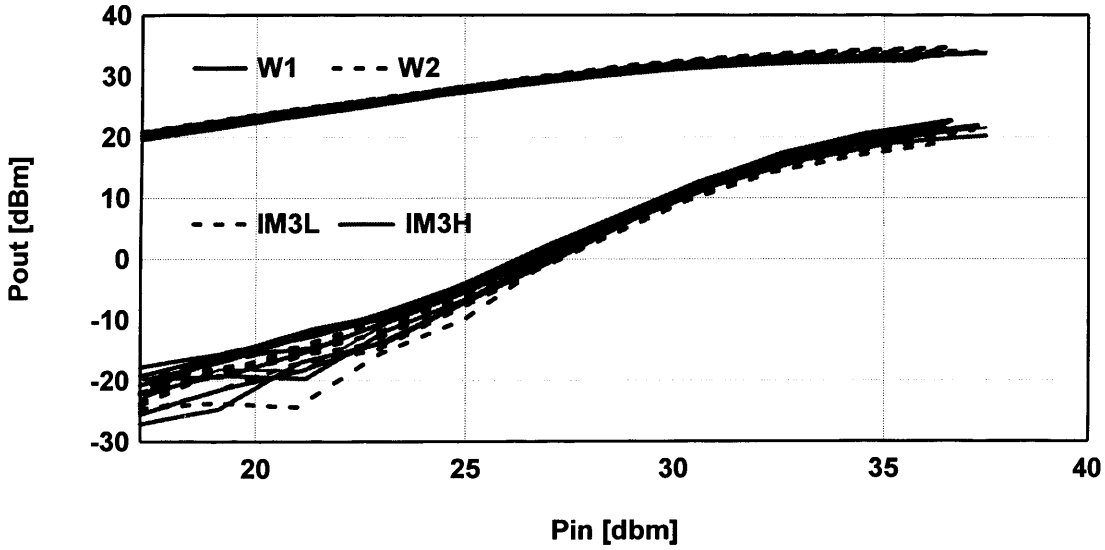

Figure 6.7 Measured two-tone power sweeps (w_1 and w_2) for all two-tone frequency separations.

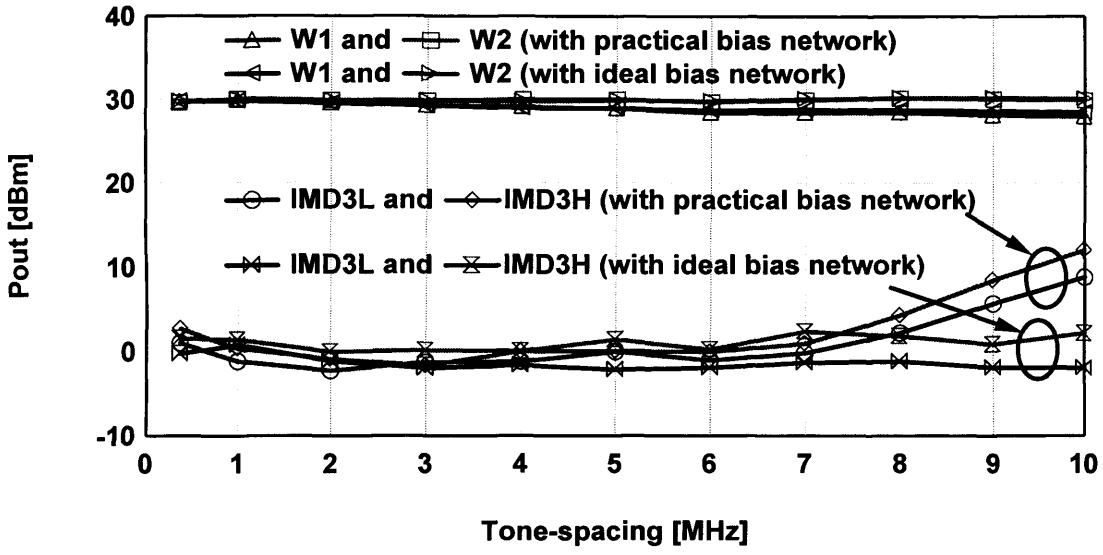

Figure 6.8 Measured fundamental and IMD power vs. Tone-spacing at 30dBm drive level for both practical and ideal bias networks.

It should be mentioned at this stage that the base-band impedance was not quite constant for all two-tone spacing (as seen in Figure 6.6). The impedance magnitude of IF_1 at 2MHZ is found to be about 10.3 Ω (worst case) while the impedance magnitude of IF_1 at 1MHz is around 5.9 Ω (best case).

It is as yet unclear whether the IMD asymmetry of 3 dB at the 1 dB compression point was a result of the IF_1 impedance magnitude variations from 5.9 Ω to 10.3 Ω, which were introduced by the long coaxial cable involved in the previous measurement, or from other sources of memory. Therefore it was decided to carry out an extra passive load pull measurement in which the aim was very consistent base-band impedance (ideally 5.9 Ω in this passive case) for the whole modulation frequency.

6.2. Base-Band Memory Effect Investigation using Passive Load Pull (Second Approach)

This measurement is performed on a Freescale seventh generation (HV7) 20W LDMOS device characterised at 2.1 GHz for tone-spacing ranging between 0.37MHz to 10MHz. The two-tone measurement was used with the device biased in class AB at a drain voltage of 20V and a gate voltage of 2.8 V, resulting in a quiescent current of 151 mA.

In order to minimise the physical length of the passive delay elements required at IF_1, and achieve approximately constant IF_1 impedance, passive load pull is used, with a different procedure to the one used in the previous section. An offset-short termination was used for values of two-tone spacing between 0.37MHz and 3MHz (range-1), whereas an offset-open termination was used for values of tone-spacing between 4MHz and 10MHz (range-2) as can be seen in Figure 6.9.

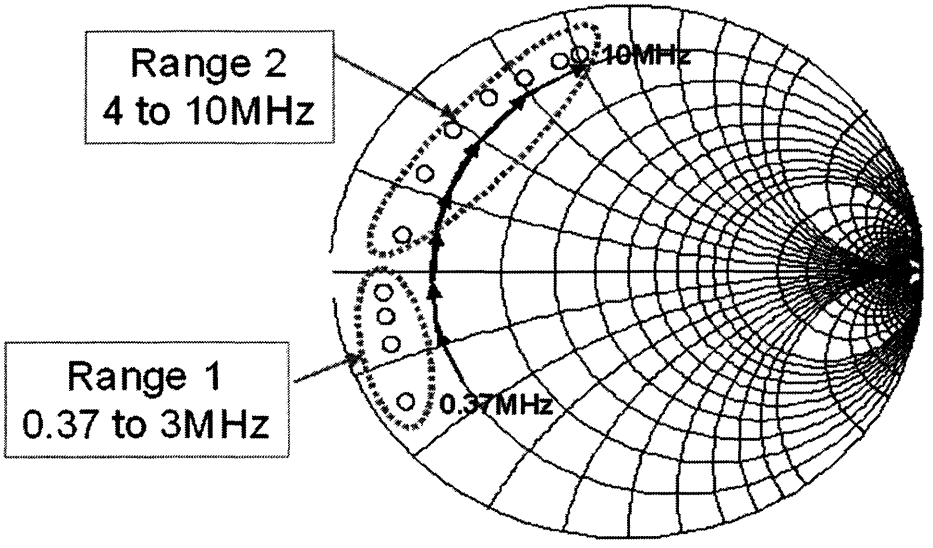

Figure 6.9 Measured IF_1 impedance vs. tone spacing without load pull.

The length of the coaxial cable that needed to be used in this measurement to load pull all the IF_1 components can be calculated using this formula:

$$L=\frac{\varphi}{360^0}*\frac{C}{F}\frac{1}{\sqrt{\varepsilon}}$$

Where:

Φ = Phase of IF_1 in degree

C = Speed of propagation

F = Frequency of IF_1

ε = Dielectric constant of material (equal to 2.3 in the case of polyethylene material)

$1/\sqrt{\varepsilon}$ = Velocity factor

In order to minimise the physical length of the passive delay elements required at IF_1, an offset-short termination was used for values of two-tone spacing between 0.37MHz and 3MHz (range-1), whereas an offset-open termination was used for values of two-tone spacing between 4MHz and 10MHz (range-2). For example, in order to load pull IF_1 at 4 MHz using offset short, the length of the coaxial cable would be approximately:

$$L=\frac{356}{360^0}*\frac{300000000}{4000000}\frac{1}{\sqrt{2.3}}=50meters$$

When using the offset-open instead, the IF_1 impedance at 4MHz shown in Figure 6.9 would rotate by about 180° degree, and therefore, the new required length of the coax cable would be:

$$L=\frac{176}{360^0}*\frac{300000000}{4000000}\frac{1}{\sqrt{2.3}}=25meters$$

Reducing the coaxial cable length to almost half decreases the loss and the magnitude of the base-band impedance as well as reducing the expense. Figure 6.10 shows the variation in the base-band impedance magnitude is between 4.3-6.8 Ω and much less than in the previous experiment (5.9-10.3Ω).

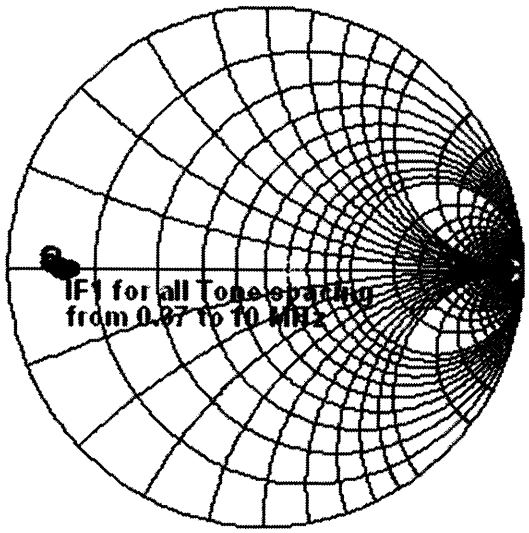

Figure 6.10 Measured impedance vs. tone-spacing after load pull.

The base-band impedance variation in this case is less than the variation in the previous approach where offset-short termination was used for the whole tone-spacing frequency.

Figure 6.11 shows the measured RF two-tone power performance as a function of input drive level for all tone spacing. The behaviour of the two output tones (ω_1 and ω_2) is clearly almost independent of the tone spacing frequency.

With regards to the inter-modulation products, $IM3_L$ and $IM3_H$, two distinct responses are observed. This is clearly summarised in Figure 6.12, which plots the measured value of inter-modulation distortion IMD_3 as a function of

two-tone spacing, at a fixed input power level of about 23.2 dBm. This is 5dB below the 1 dB compression point and identified as Pref (see Figure 6.11).

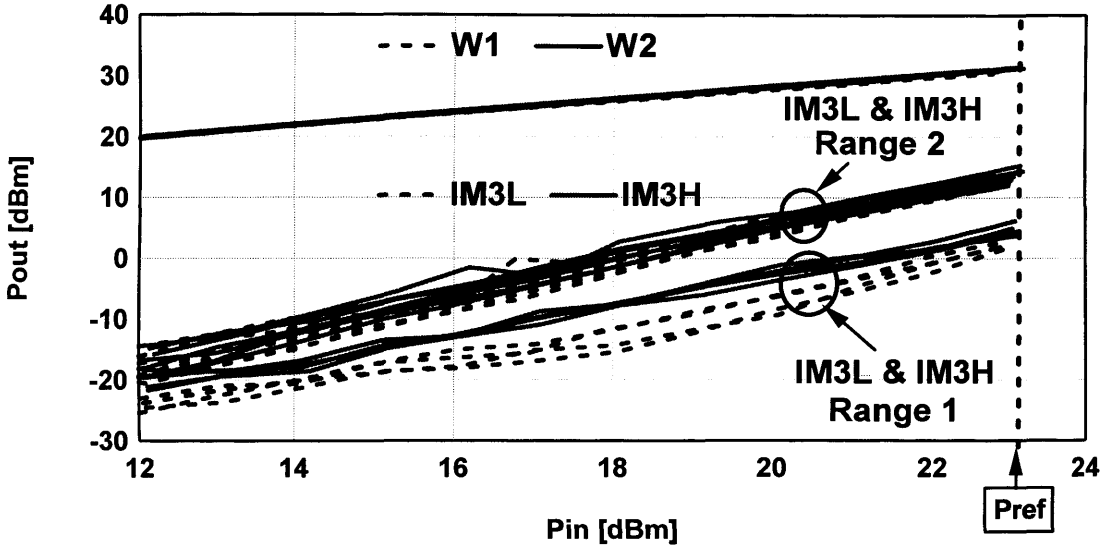

Figure 6.11 Measured two-tone power sweeps (w_1 and w_2) for all two-tone frequency separations.

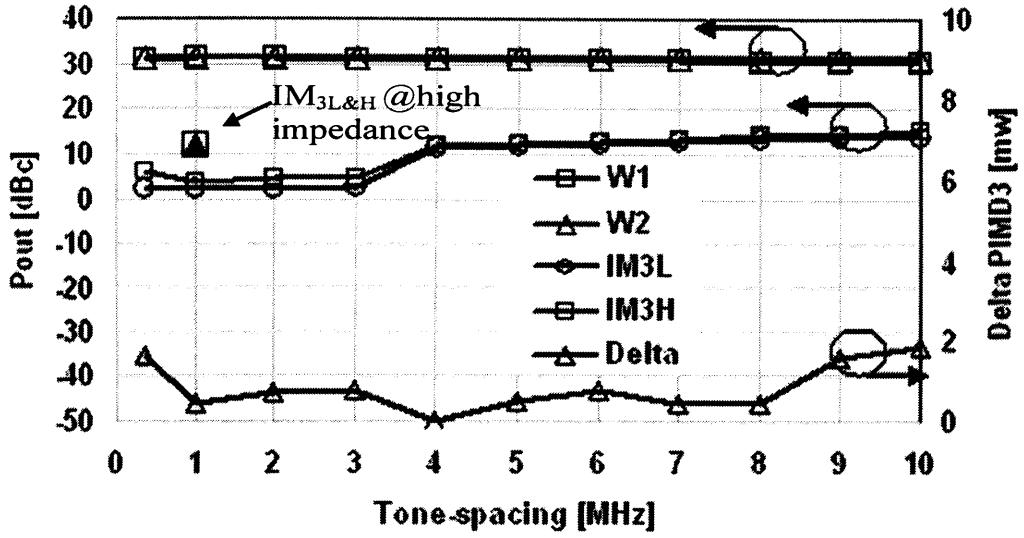

Figure 6.12 Measured IMD power and delta (the difference between IM_{3H} and IM_{3L}) for two impedance regions, at different two-tone frequency separations and at a constant drive level.

The results in Figure 6.11 and Figure 6.12 are completely unexpected and differ from those predicted. Even though the base-band impedance (IF_1) is less frequency dependent when compared with the first approach, a transition of more than 7 dBm in the output $IMD_{3L\&H}$ is presented (see figure 6.12). The only difference between the first approach and the second approach is the procedure of presenting short circuits to IF_1 components. This transition is in direct correlation to the two different passive load-pull regions (offset-short termination and offset-open termination). It should be noted that the other higher IF components (IF_2, IF_3...etc) are generally ignored during memory investigations and discussions.

To help understand what causes the variation in results between the first and second approaches it was decided to plot the base-band impedance IF_2 for both cases.

Figure 6.13 illustrates the measured IF_2 components in both approaches. It is important to note however that in the first approach, the offset-short termination is used for all frequencies ranging from 0.37-10 MHz and the IF_2 load presented to the device is low impedance (as seen in Figure 613(a)). In the second approach, however, when the offset-short termination is used (range-1), the IF_2 load presented to the device is low impedance. On the other hand, when the offset-open termination is used (range-2), the IF_2 load presented to the device is relatively high impedance. For example, figure 13(b) shows how the impedance presented to IF_2 varies significantly, moving around the Smith chart for the two termination cases and values of two-tone spacing. Interestingly, the second approach, although very effective in presenting near constant impedances to IF_1, is ineffective in stabilising the impedance presented to IF_2 and other higher IF components.

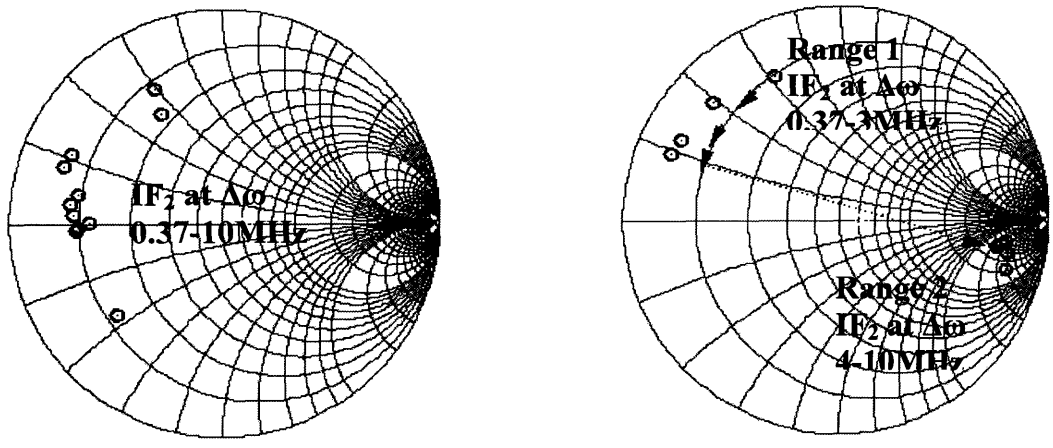

(a) (b)

Figure 6.13 Measured IF_2 impedance for (a) first approach and (b) second approach with two Ranges.

Figure 6.12 shows that IMD3 is approximately 26 dBc over range-1 and approximately 17 dBc over range-2. The transition from region-1 to region-2 in Figure 6.12 is a result of changing the procedure from offset-short to offset-open, as explained earlier. This procedure, which led to the presentation of low IF_2 impedance in range 1 and high IF_2 impedance in range 2, caused the transition between these two ranges. This variation in IF_2 impedance is considered to be the primary cause of the observed variation in IMD_3 response where a difference of 7 dB is observed between range 1 and range 2, highlighting just how important the second base-band component IF_2 is [14].

To clarify this, figures 6.14 and 6.15 show the corresponding measured IF current components generated by the non-linear behaviour of the transistor along with the resulting IF voltage components developed by the IF load impedances. Clearly it can be seen that the dominant current component is IF_1, again seen to be highly constant across frequencies due to the control of the corresponding IF_1 impedance component. However, there is also a significant IF_2 current component, which when presented with a high enough impedance is capable of generating a dominant IF_2 voltage component. Consequently, IF_2 voltage changes rapidly from 0.73V to approximately 5.5V between range 1 and range 2, resulting in a different IM_3 distortion in the two regions.

To confirm this interpretation, it was necessary to design and manufacture a suitable diplexer to separate the two IF harmonic components. The achieved isolation between IF_1 and IF_2 was 20dB. Using this approach, the magnitude of the IF_2 reflection coefficient at 1MHz tone-separation shown in Figure 6.13(b) was now independently load-pulled towards an open circuit (region-2), whilst maintaining a constant IF_1 load. The achieved variation in IF_2 impedance at 1 MHz results in a shift in the $IM_{3L\&H}$ value, identified in Figure 6.12 as $IM_{3L\&H}$ @high impedance, to that consistent with the region 2 values

achieved at higher tone-separation. This highly controlled elimination of the IMD_3 variation with tone-separation used is solid evidence of the preceding interpretation.

The dB scale initially gives the impression of having IMD_3 asymmetry in range 1, which is investigated further by calculating the difference (delta IM_3) between IM_{3L} and IM_{3H} in milliwatts (mW). In absolute terms, the measured asymmetry remains largely constant for all values of two-tone spacing, regardless of the existence of the two impedance regions, (as seen in Figure 6.12).

This result suggests that all significant IF impedance components must be controlled and correctly terminated in order to remove the electrical memory.

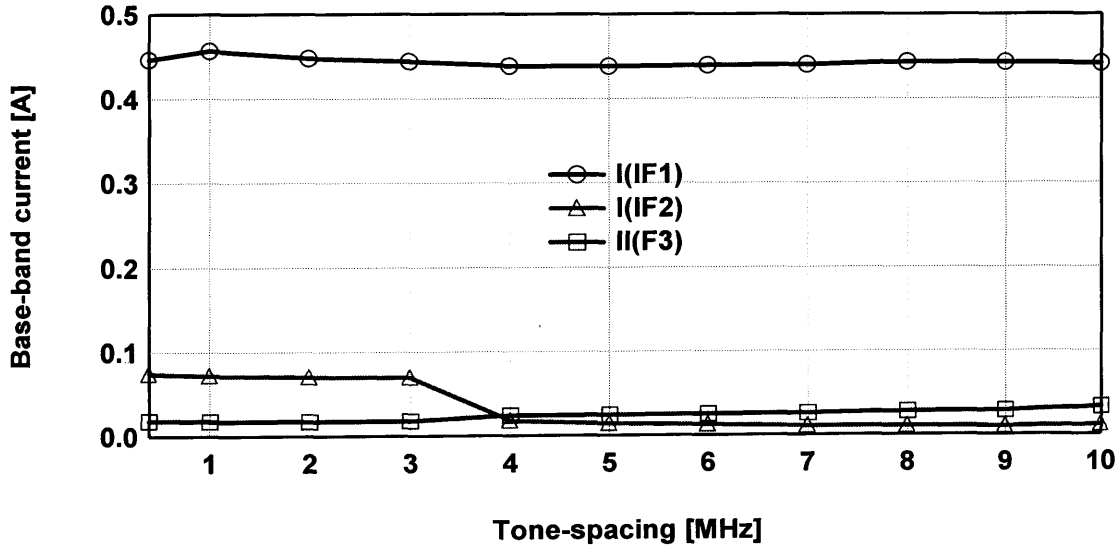

Figure 6.14 Measured output base-band current vs. Tone-spacing.

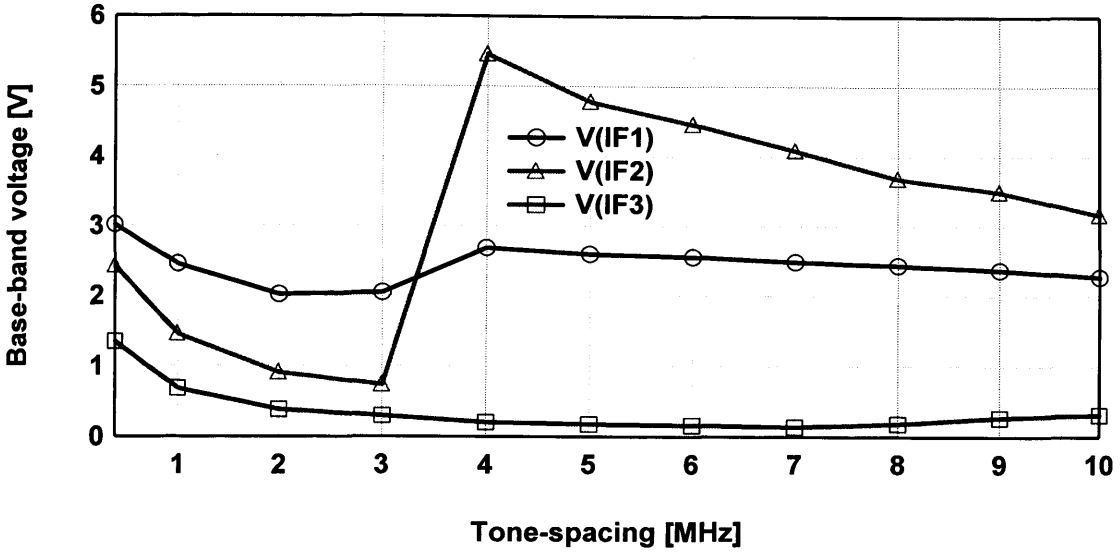

Figure 6.15 Measured IF voltage vs. Tone-spacing.

These measurements demonstrate how electrical memory introduced by non-ideal, low frequency base-band impedances represents the most significant contributor to overall observed memory effects in high-power LDMOS PA design. Suppression of electrical memory has been achieved to a certain degree through the use of passive IF load-pull, and the synthesis and presentation of frequency invariant IF impedances. Using this approach, a more or less constant spectral symmetry has been demonstrated over a wide modulation bandwidth.

Measurements show that third order inter-modulation behaviour is not only dependent on the most significant IF component (IF_1), but is also very sensitive to higher order IF components. This important observation has major implications for modern PA linearisation techniques, as well as requiring careful consideration when designing PA bias networks. The results show that the bandwidth over which the base-band impedances must be controlled must be extended to at least four times the modulated bandwidth.

Passive load-pull is simple, cost-effective, has high power-handling capability and constant load while sweeping power. Despite these advantages, passive load pull has a limited maximum IF load reflection coefficient (Γ_{Lmax}). To overcome this drawback, the need for better measurement accuracy pushed towards IF active load pull which does not have any IF load reflection coefficient limitations. Also it would be important to ensure that the variation in the $IMD3_{L\&H,}$ which was observed in the second approach, is fully correlated to the variation in the IF_2. This could be achieved by keeping IF_1 constant while sweeping IF_2. Moreover, it would be necessary to use the active load pull in order to investigate the cause of asymmetry between $IMD_{3L\&H,}$ which was found to be approximately 3 dB in the frequency range of 0.37-3 MHz, when the second approach was applied regardless of whether it was related to the variation in IF_2 or to another factor (other impedance such as harmonic impedances).

6.3. Base-Band Memory Effect Investigation using Active Load Pull

In this section, base-band or IF active load-pull is used to provide an effective way to engineer all the significant IF components generated as a result of multi-tone excitation, independent of modulation frequency. In this approach specific IF impedance environments are presented to a device in order to probe the sensitivity to IF impedance variations. These investigations are performed on a 20W HV7 LDMOS device characterised at 2.1 GHz. In the previous section passive IF load-pull was employed in order to control the low-frequency impedances presented to the most significant IF components generated by a device. This approach however is restricted by a number of factors: firstly the realisable reflection coefficients are limited by the presence of significant losses associated with both the IF test-set and the physically long delay-lines necessary to realise the required offset short terminations. As a

consequence, the minimum IF impedance realisable using this system was approximately 4.3-10.3Ω, which is some way from the targeted short circuit. This is especially significant considering the relatively low optimum output impedance of the high-power LDMOS device employed. Secondly, only one IF frequency component could be controlled at any one time. As a consequence, while controlling of the most significant IF frequency component, the other IF components are terminated in arbitrary impedances, making results difficult to interpret.

In this investigation, active IF load-pull has been used to offer fully independent control of the impedance presented to all the significant IF components generated by a 20W LDMOS device, overcoming all of the problems associated with the previously described passive approach. Using two-tone modulation, the IM_3 inter-modulation products are measured as a function of varying excitation two-tone spacing and IF impedance. By using active IF load-pull to control IF drain impedance, it can be shown that the measured IM_3 terms are a strong function of the IF impedance over bandwidths that are at least four times that of the modulation frequency.

For a high power device, such as the 20W LDMOS used in this measurement, the IF components generated are large. This is especially true of IF_1 (twice the modulation frequency) and IF_2 (four times the modulation frequency), the most dominant base-band components. The measured output spectrum for a two-tone stimulus of 2098.5 MHz and 2101.5 MHz when RF ports were terminated to 10 Ω, IF source port to 50 Ω and IF load port in approximately 7 Ω is shown in Figure 6.16. It should be noted that the magnitude of the output power of IF_1 is approximately 31 dBm and is comparable to the magnitude of ω_1 and ω_2 hence, this signal (IF_1) can not be load pulled directly using only an arbitrary waveform generator (AWG).

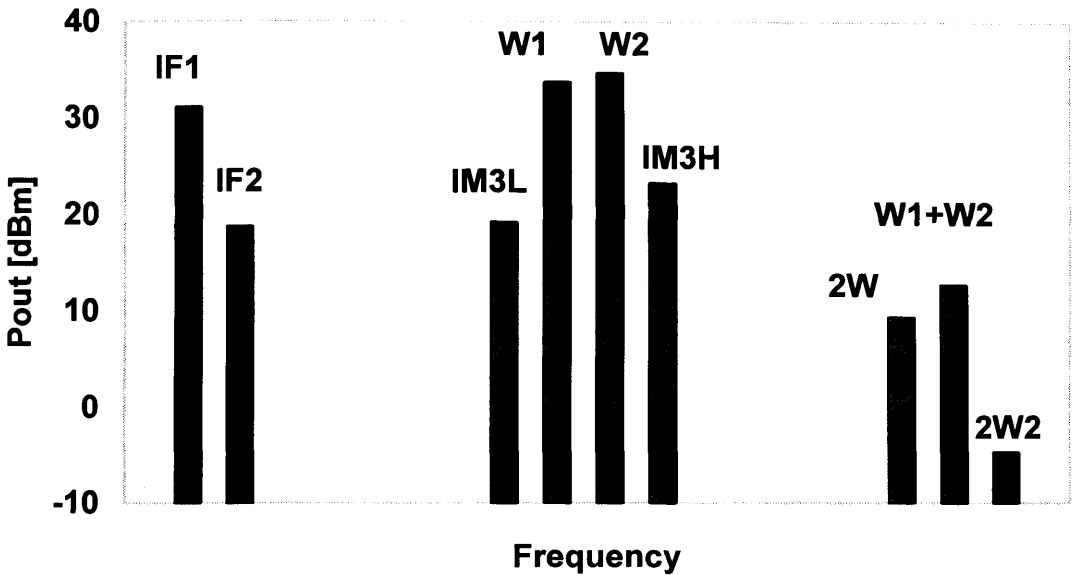

Figure 6.16 Measured simplified two-tone spectrum for 20W LDMOS device when RF ports of the measurement system were terminated with the nominal impedance of 10Ω, IF source port in 50 Ω and IF load port in 7 Ω.

In order to actively load-pull these components; an ENI 240L 20 kHz to 10 MHz, 40W linear power amplifier was used to amplify the signal from the arbitrary wave generators (AWG) as seen in Figure 6.17. This integrated measurement architecture provides the ability to present, independently, specific impedances to the two significant IF frequency components, allowing for instance a constant IF impedance environment to be maintained across a wide IF bandwidth (50 kHz to 50 MHz) during two-tone excitation.

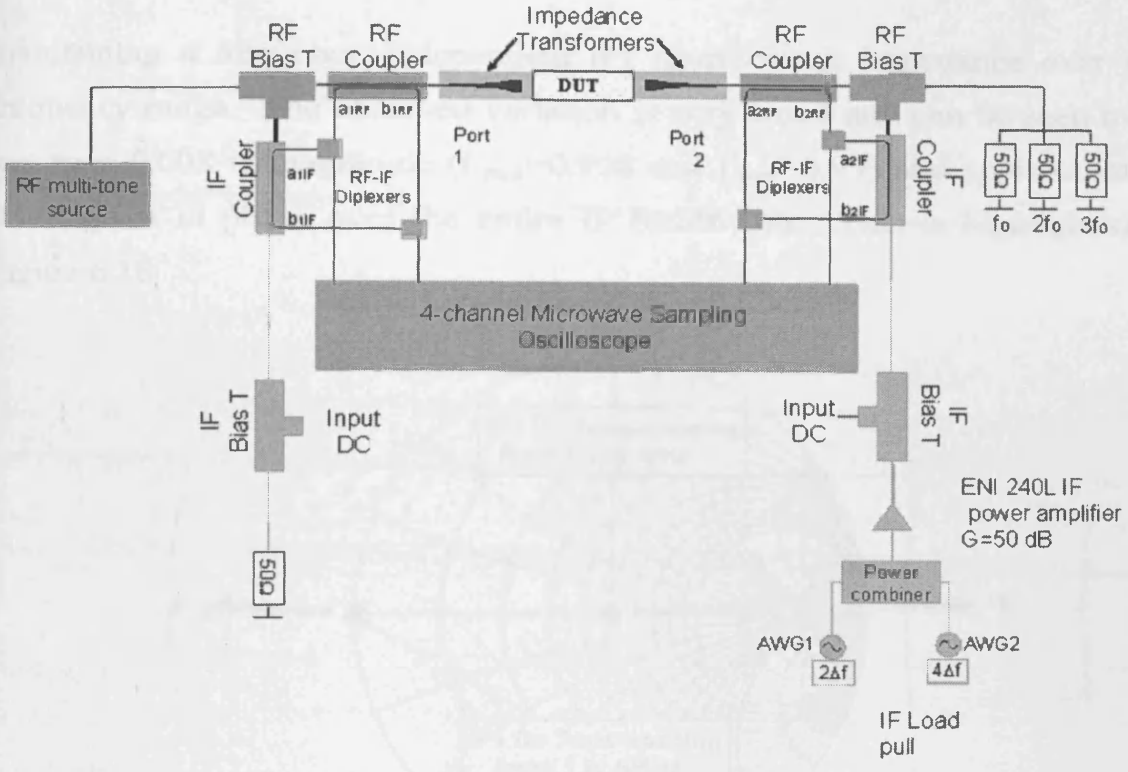

Figure 6.17 Schematic of the high power measurement system

To achieve the desired IF impedances active IF load-pull was employed to independently engineer different, frequency independent, impedance environments at the two significant IF components; IF_1 and IF_2, defined in Figure 6.17. It is important to note that IF_2 is not successfully load-pulled for modulation frequencies greater than 12 MHz due to bandwidth limitations of the IF PA. The advantage of using active load pull is the ability to keep IF_2 constant for all tone-spacing frequency while observing the device performance as a function of only IF_1, unlike passive load pull when IF_2 was varying as tone-spacing frequency vary (section 5.1 and 5.2). Therefore, termination of IF_1 frequency components into a short circuit while fixing IF_2 to 50 Ω would be possible for all tone-spacing ranging between 1 MHz and 6 MHz. Figure 6.18 illustrates just how effective the IF load-pull is in

maintaining a frequency independent IF_1 short circuit impedance over this frequency range. The observed variation is very small and can be seen to be less than 0.008 in magnitude (Γ_{max}=0.998 and Γ_{min}=0.99) and approximately 0.1 degrees in phase over the entire IF bandwidth. This is highlighted in Figure 6.18.

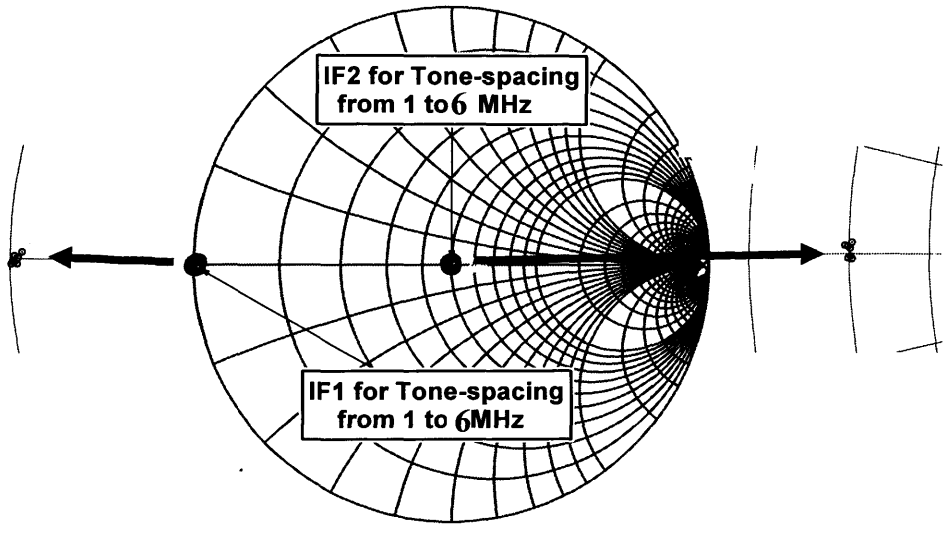

Figure 6.18 Measured $IF_1$and IF_2 vs. two-tone frequency spacing.

Figure 6.19 presents the measured two-tone RF spectral power performance for the case where a short circuit is presented to IF_1 and 50 Ω presented to IF_2. In this case the two-tone frequency spacing is 2MHz. This plot shows typical behaviour: a 1:1 slope for the two fundamental tones and an approximately 1:2.5 slope for IM_3 inter-modulation components over a power sweep of some 30 dB. It should be noted that the slope of IMD_3 indicates that the system cannot be completely described by the 3rd order polynomials but should consider higher order polynomials such as the 5th order (see equation 2.12.a).

Thus, the fifth-degree term at frequencies $3\omega_2$-$2\omega_1$ and $3\omega_1$-$2\omega_2$ (IMD_5) are plotted as well.

Figure 6.20 summarises the IM_3 and IM_5 behaviour for different values of tone-separation ranging between 1 and 6 MHz, at a single drive level (Pref). This power level corresponds to a point approximately 1dB below the 1dB compression point.

The behaviour of the two output tones (ω_1 and ω_2) is clearly observed to be almost independent of the tone-separation frequency. The observed IMD_3 and IMD_5 responses are found to be modulation frequency independent only between 4 and 6 MHz.

It is important to note that the observed variation in IM_3 and IM_5 component magnitude observed below 3 MHz is not related to variation in base-band impedance.

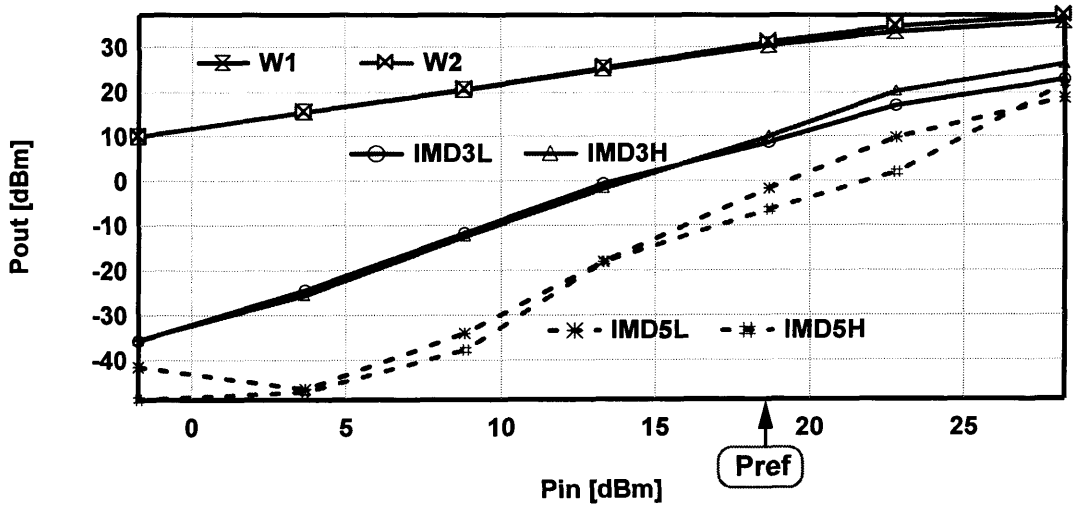

Figure 6.19 Measured two-tone power sweeps for 2MHz Tone-spacing where short circuit is presented to IF1 and 50Ω to IF2.

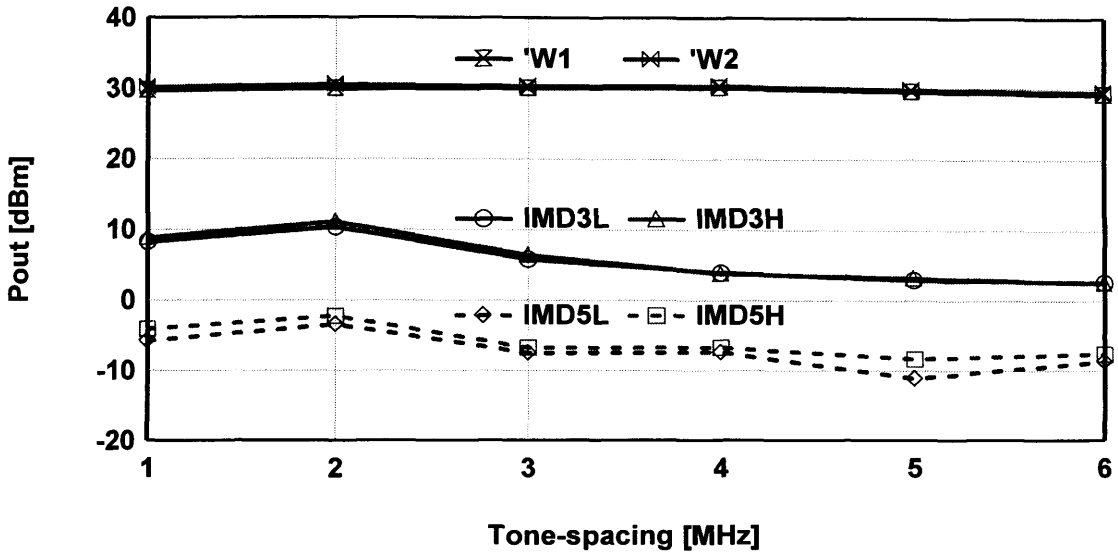

Figure 6.20 Measured fundamental and IMD power at different Tone-spacing at a constant drive level of 1dB below the 1dB compression point (see Pref in Figure6.19) where short circuit is presented to IF1 and 50Ω to IF2.

To help understand this behaviour, figures 6.21 and 6.22 show the corresponding measured IF current components generated by the non-linear behaviour of the transistor along with the resulting IF voltage components developed by the IF load impedances. Clearly it can be seen that the dominant current component is IF_1, which is not constant across frequencies regardless of the full control of the corresponding IF_1 impedance component. It is important to realise that the IF_1 current shape is almost a mirror to that of $IMD_{3\&5}$ giving a clear indication that it must be linked to the same process that is causing the variation observed in $IMD_{3\&5}$ performances. However, with regard to IF_2 current component, it can be clearly seen that it is small and frequency independent but when presented to a sufficiently high impedance (50 Ω in this case) it was capable of generating a dominant IF_2 voltage component. Consequentially, IF_2 voltage changes from 1.2V to approximately 0.57V between 1 MHz and 6 MHz.

To ensure that the output fundamental and harmonic impedance presented to the device are constant while sweeping frequency and therefore not contributing any to the changes observed in IM_3 and IM_5 they are plotted in Figure 6.23 and Figure 6.24. With respect to the fundamental output impedance (ω_1 and ω_2) their magnitudes exhibit only small change and moreover, the slope of this change is almost constant for the whole modulation frequency and not a mirror to the IMD_3 and IMD_5 behaviour. Regarding the second harmonic zone impedances ($2\omega_1$, $2\omega_2$ and $\omega_1+\omega_2$ (IF_{1H})) the measured impedance for these three components is largely constant and thus appears not to be also the cause of the IMD frequency behaviour.

The frequency variation observed below 3 MHz is not related to variation in base-band or RF impedance and thus must be associated with other memory sources; i.e. thermal, surface trapping, package parasitics.

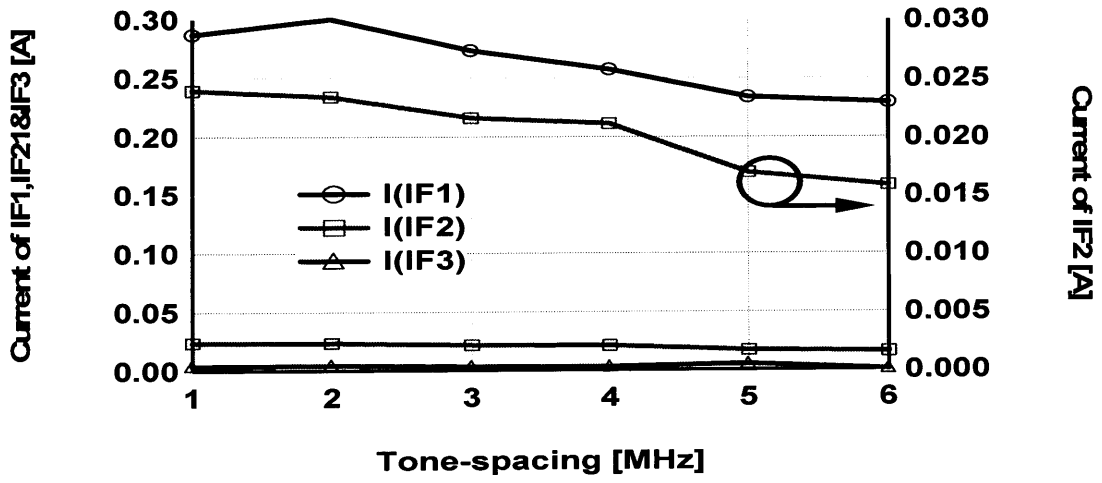

Figure 6.21 Measured output base-band current vs. Tone-spacing.

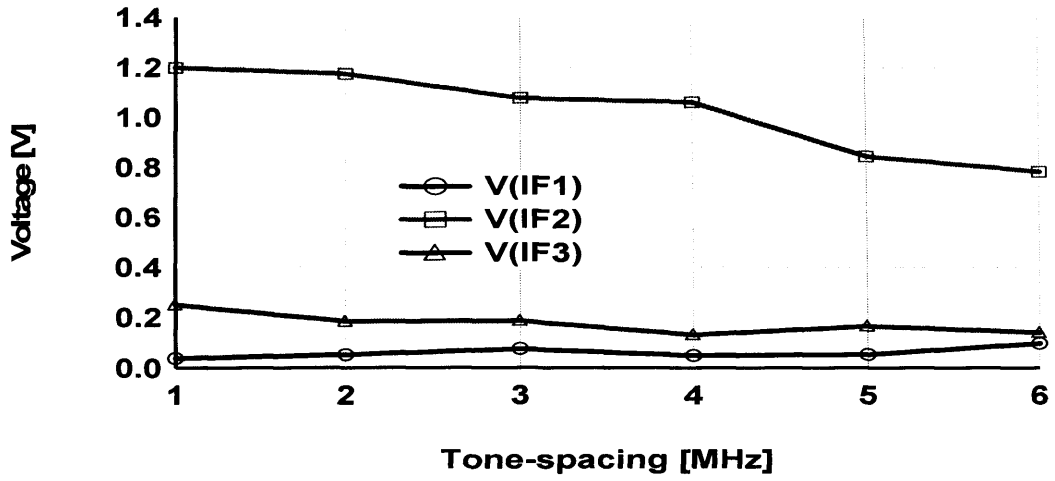

Figure 6.22 Measured output base-band voltage vs. Tone-spacing.

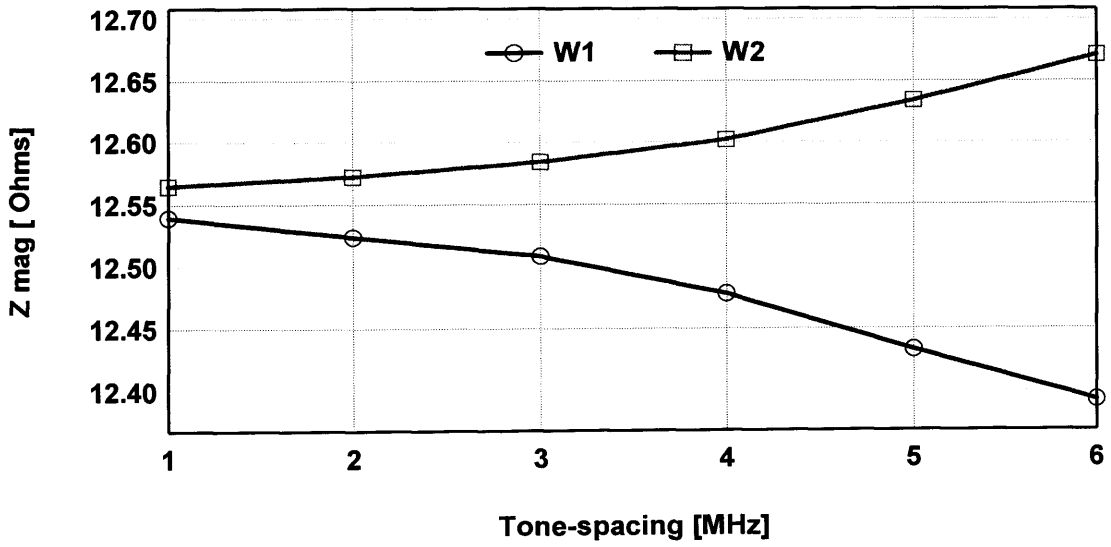

Figure 6.23 Measured fundamental output impedance vs. Tone-spacing.

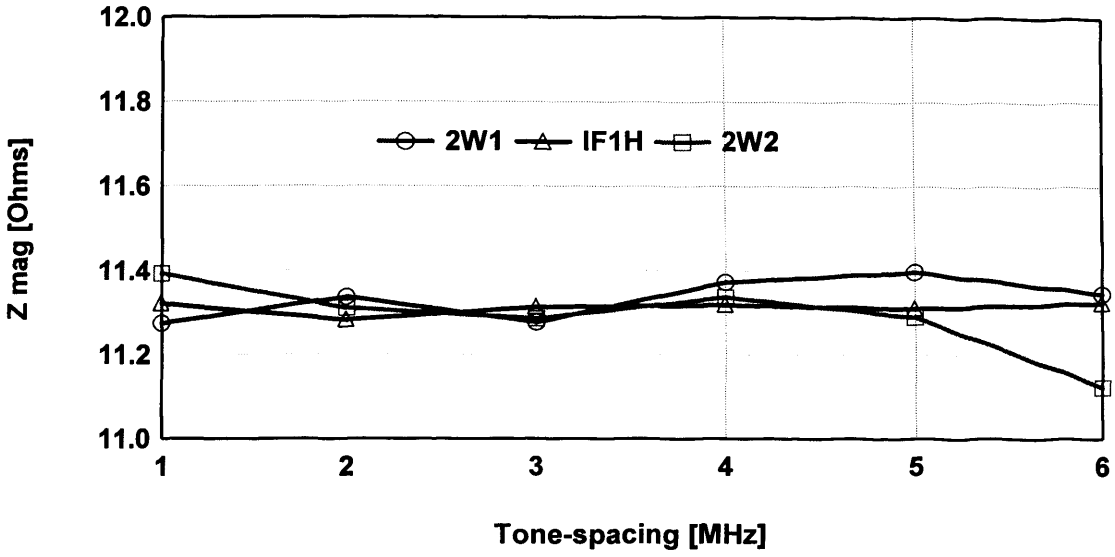

Figure 6.24 Measured second harmonic output impedance vs. Tone-spacing.

Last experiment indicates the device sensitivity to terminating the base-band component IF_1 to short. Variation of the $IMD_{3\&5}$ was observed therefore it was decided to do an extra measurement in which all dominant IF will be terminated into 50 Ω (using off-set 50Ω) while sweeping frequency from 1 to 6 MH on the same device and bias conditions.

Figure 6.25 illustrate the measured IF impedance components (IF_1, IF_2, IF_3 and IF_4).

The behaviour of the two output tones (ω_1 and ω_2) and $IMD_{3\&5}$ is clearly observed to be almost independent of two-tone frequency spacing as shown in Figure 6.26. This result indicates that if an appropriate frequency independent constant base-band termination is utilised in the Power Amplifier drain bias network no modulation frequency sensitivity in $IM_{3\&5}$ responses would be observed [7].

The observed IMD_3 response found to be higher than the one in the previous experiment (IF_1 to short and IF_2 to 50) while the observed IMD_5 response was found to be improved.

The base-band current and voltage components are shown in Figure 6.27 and Figure 6.28 respectively. Clearly it can be seen now that the all current components IF_1, IF_2 and IF_3, are observed to be very frequency invariant when terminated into 50 Ω. Also the base-band voltage VIF_2 and VIF_3 are constant. Regarding VIF_1, the magnitude of the IF_1 impedance varies slightly with two-tone spacing as shown in Table 2. This small variation in the base-band impedance causes the VIF_1 to vary as shown in Figure 6.28.

Table 6.2 Measured real part of the IF_1 impedance for all tone-spacing frequency

Tone-spacing [MHz]	1	2	3	4	5	6
Impedance (real)	57.45	57.35	53.91	50.91	50.7	50.4
Impedance (Imaginary)	-7.79	-7.85	-5.1	-3	-2.73	-2.27

It could be said that the IMD performance will remain constant with respect to two-tone frequency spacing if the base-band impedance are large and constant.

For a comparison point of view, the two cases of IF impedance, State 1, where 50Ω is presented to all IF components and State 2, where a short circuit is presented to IF_1 and 50 Ω to IF_2 are both plotted in Figure 6.29.

Suppression of memory effect has been achieved in the case of State 1 at the expense of higher IMD_3 level; however a device/PA with this behaviour would be very attractive to those dealing with linearisation technique.

Reference [15] stated that the linearisability of memory-less device is much better than the one of devices with memory. This could be the perfect application for such a scenario (50 Ω terminations). In contrast state 2 has lower values of IM_3 inter-modulation distortion. This makes it attractive for those applications that will not necessary require higher carrier to inter-modulation ratio.

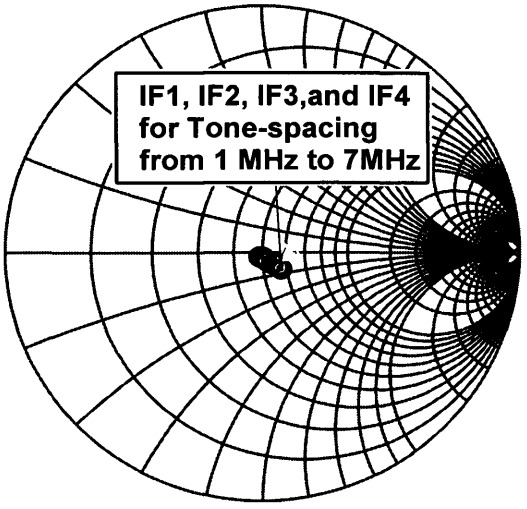

Figure 6.25 Measured IF_1, IF_2, IF_3 and IF_4 vs. Tone-spacing ranging from 1 MHz to 7 MHz.

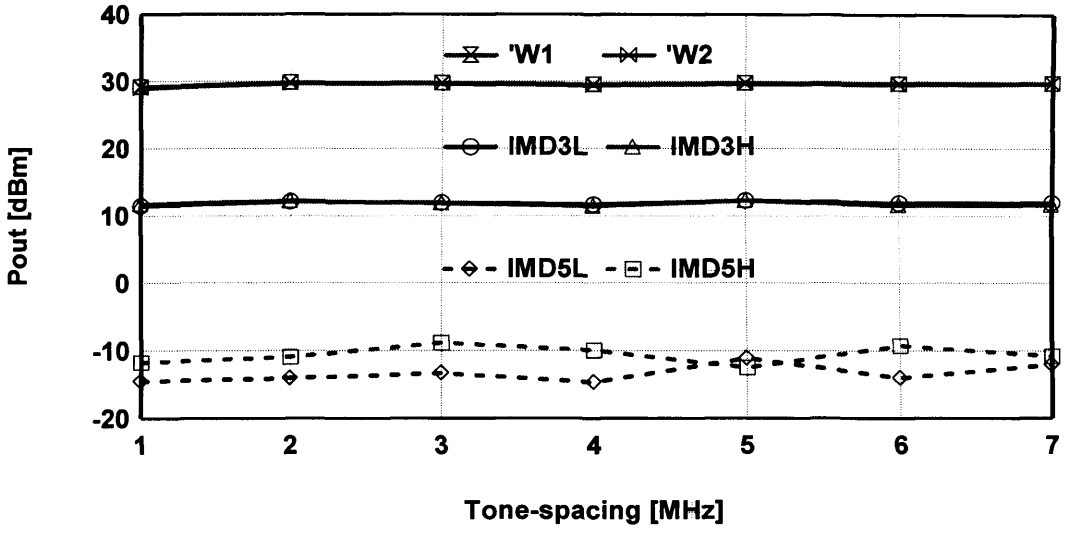

Figure 6.26 Measured fundamental and IMD power at different Tone-spacing at a constant drive level of 1dB below the 1dB compression point (see Pref in Figure 19) with IF_1, IF_2, IF_3 and IF_4 terminated to 50Ω.

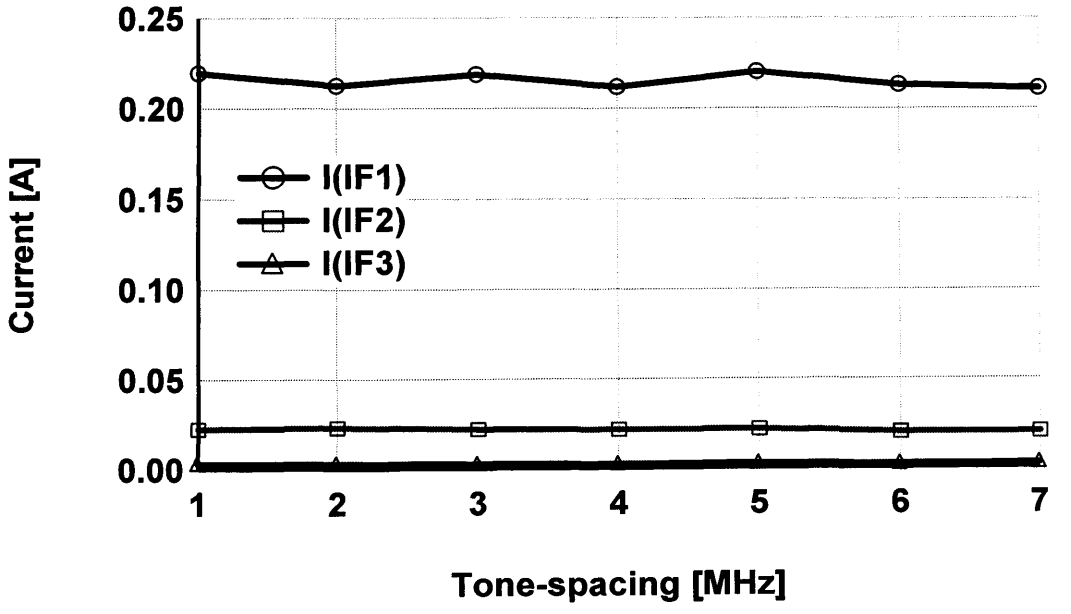

Figure 6.27 Measured output base-band current vs. Tone-spacing with IF_1, IF_2, IF_3 and IF_4 terminated to 50Ω.

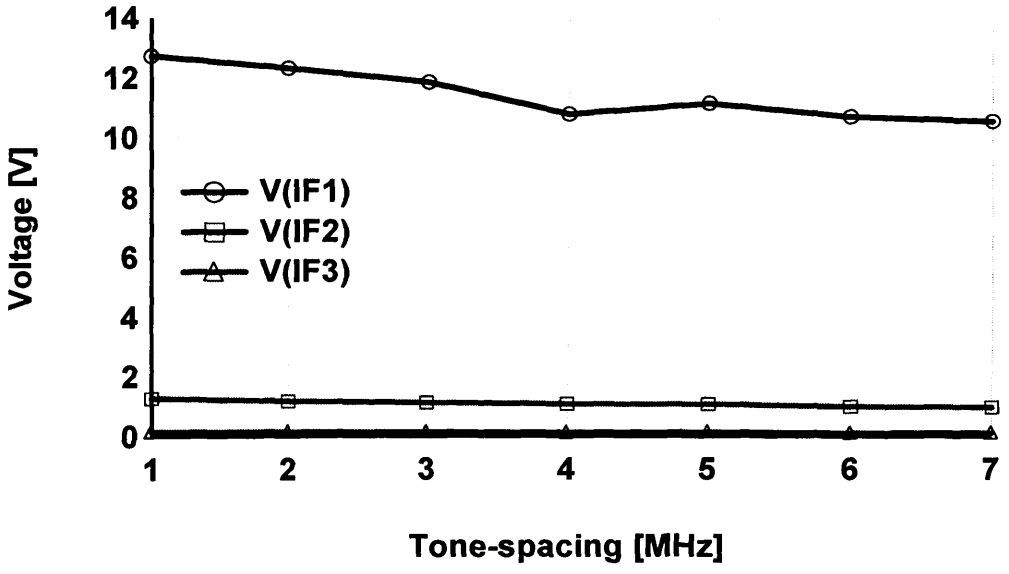

Figure 6.28 Measured output base-band voltage vs. Tone-spacing with IF_1, IF_2, IF_3 and IF_4 terminated to 50Ω.

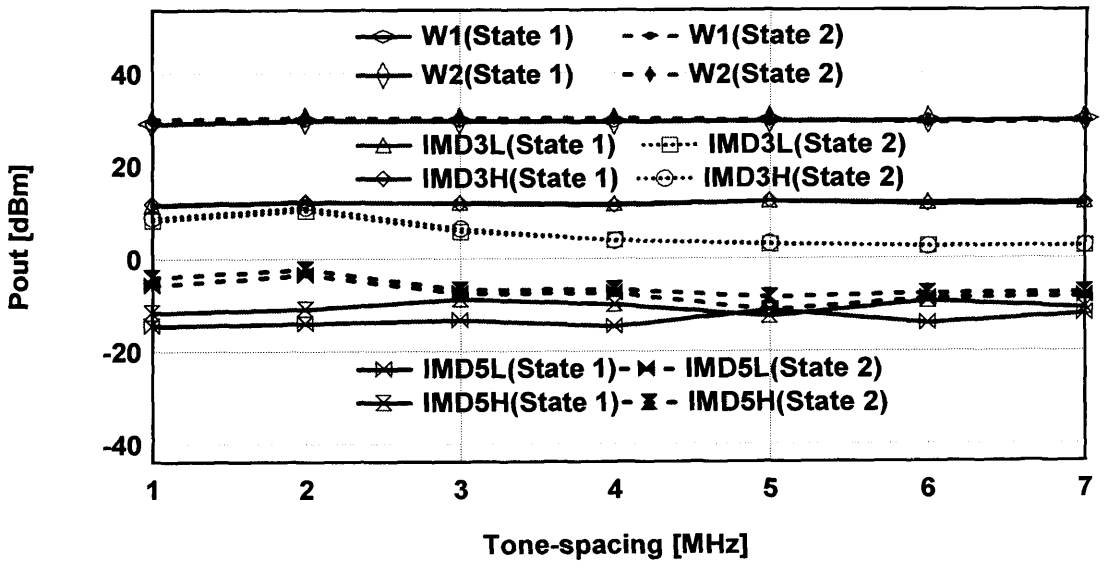

Figure 6.29 Measured fundamental and IMD power for two impedance States at different tone-spacing at a constant drive level of 1dB below the 1dB compression point.

6.4. Base-Band Memory Effect Investigation using Active Load Pull (IF_1 and IF_2 are short)

The main objective of this investigation was to present short circuit to both IF_1 and IF_2 simultaneously using a Freescale seventh generation (HV7) 12W LDMOS device. Termination of these frequency components into a short circuit would be possible, particularly for tone-spacing ranging between 0.37MHz and 7MHz. In order to have a decent comparison for the result of this experiment with the previous one (HV7 20W device) it was decided also to present a short to IF_1 and 50 Ω to IF_2. To achieve this active IF load-pull was employed to independently engineer different, frequency independent, impedance environments at the two significant IF components; IF_1 and IF_2.

Figure 6.30 illustrates just how effective the IF load-pull is in maintaining a frequency independent IF_1 and IF_2 short circuit impedance.

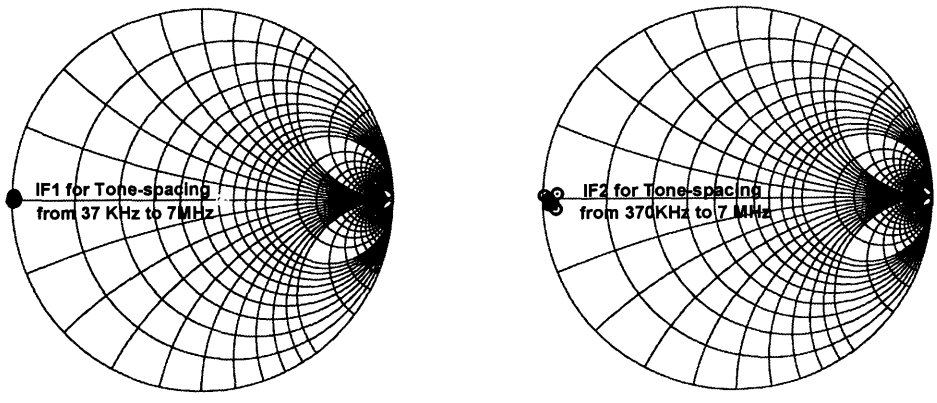

Figure 6.30 Measured IF1 and IF2 vs. tone spacing.

The measured RF two-tone spectral power performance for the two cases of IF impedance, state 1, where a short circuit is presented to IF_1 and 50Ω to IF_2 and state 2, where a short circuit is presented to both IF_1 and IF_2 is shown in Figure 6.31. A typical behaviour, 1:1 slope for the two tones and approximately 1:2.4 for the IM3 inter-modulation components, is observed over a power sweep of some 30 dB. The slope of IM_3 will not however be 1:3 unless IM_5 inter-modulation components are set to zero. In this case the two-tone spacing is 5 MHz. The variation of measured IM_3 response as a function of IF impedance is clearly seen.

Figure 6.32 summarises the $IM_{3\&5}$ behaviour at these two different IF impedance states for different values of tone spacing ranging between 0.37MHz and 7 MHz, at a single drive level (Pref 1), this power level corresponds to a point 1dB below the 1dB compression point.

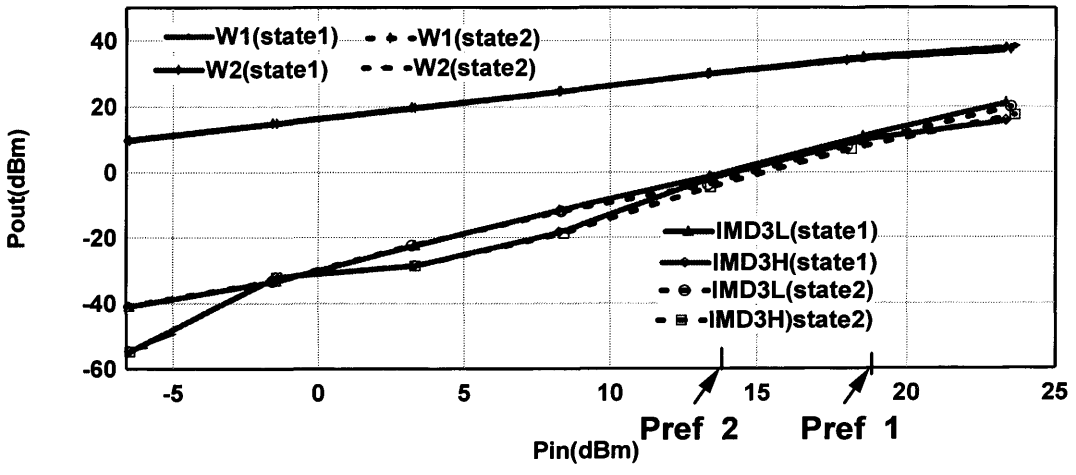

Figure 6.31 Measured two-tone power sweeps for 5MHz frequency separation for both impedance states.

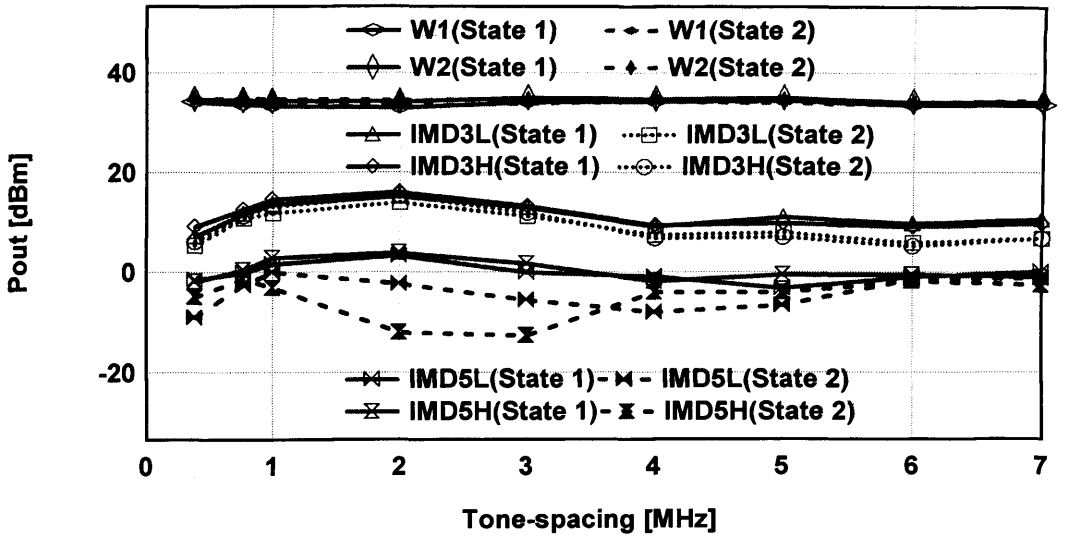

Figure 6.32 Measured fundamental and IMD power for two impedance states (State 1: IF_1=0 Ω, IF_2=50 and State 2 IF_1=IF_2=0Ω) at different two-tone frequency separations at a constant drive level of 1dB below the 1dB compression point (see Pref 1 in Figure 31).

The behaviour of the two output tones (ω_1 and ω_2) is clearly observed to be almost independent of both the tone spacing frequency and IF termination. In the IF impedance state 1 the observed IMD_3 response is higher than the reference state 2. However, in both cases of state 1 and 2 modulation frequency independence was only observed between 4 and 7 MHz.

The frequency variation observed below 4 MHz is not related to variation in base-band impedance and thus must be associated with other memory sources; i.e. thermal, surface trapping, package parasites. This conclusion is consistent with observations made in the previous measurement with the 20W HV7 device.

To examine the device (12W) sensitivity toward 50Ω termination and to compare its behaviour with the 20W device, it was decided to plot the measured results for the two cases of IF impedance, state 1, where a 50Ω is presented to IF_1 and IF_2 and state 2, where a short circuit is presented to both IF_1 and IF_2 is shown in Figure 6.33. The overall performance of 12W device is similar to that of the 20W device.

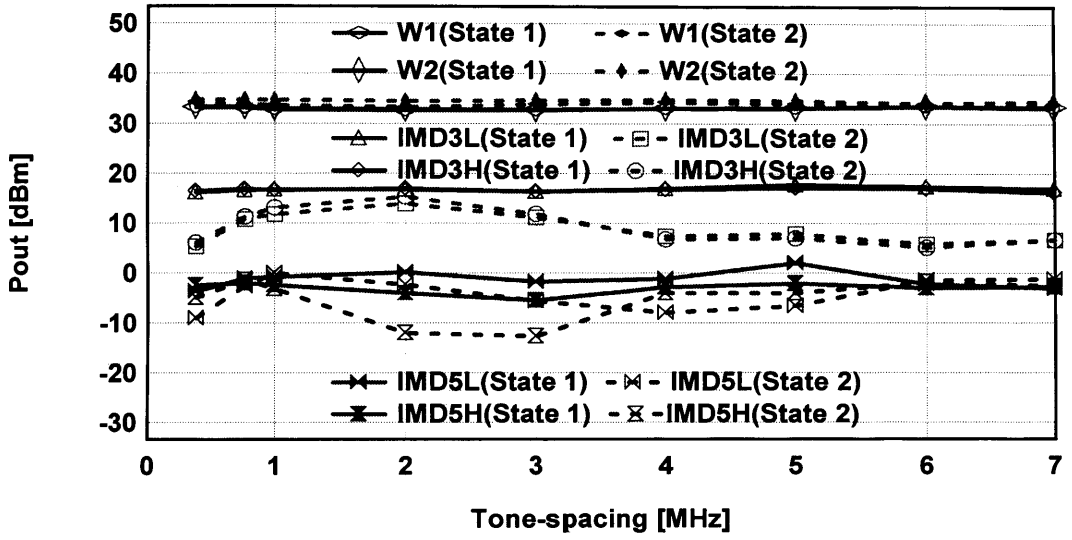

Figure 6.33 Measured fundamental and IMD power for two impedance states (State 1: IF_1=IF_2=50Ω, and State 2 IF_1=IF_2=0Ω at different two-tone frequency separations at a constant drive level of 1dB below the 1dB compression point (Pref).

In order to investigate the repeatability of the previous device measurements, especially the inter-modulation distortion ($IMD_{3\&5}$) behaviour in state 2 when both IF_1 and IF_2 were terminated to short, the output power of the fundamental (ω_1 and ω_2) and $IMD_{3\&5}$ were measured at different input drive levels of 6 dB below the 1 dB compression point (identified as Pref 2 in Figure 6.31) with a short circuit presented to IF_1 and IF_2. As can be seen from Figure 6.34, the

similarity between the $IMD_{3\&5}$ behaviour in either case of an input power of 1dB or an input power of 6 dB below the compression point is observed.

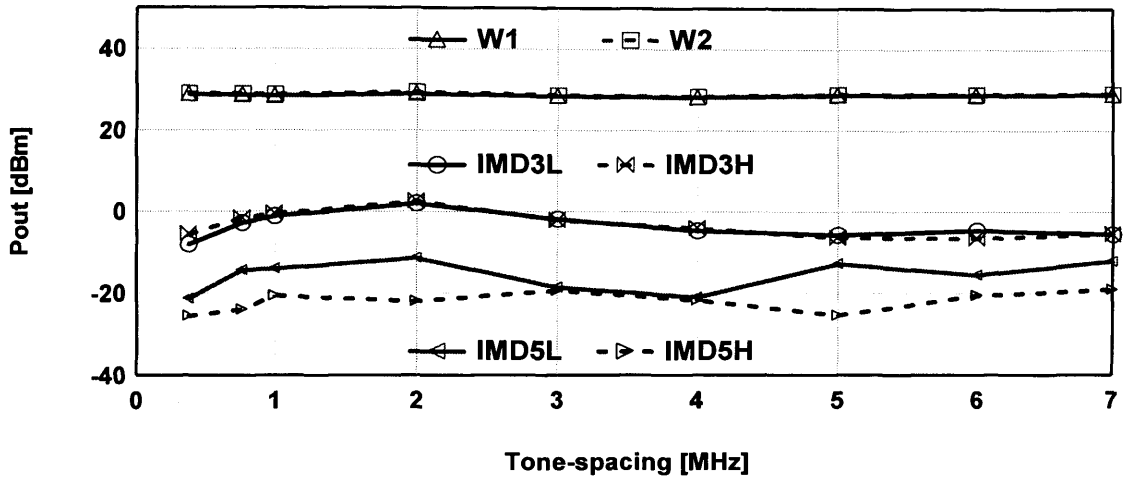

Figure 6.34 Measured fundamental and IMD power vs. Tone-spacing at a constant input drive level of 6dB below the 1 dB compression point.

So far all devices discussed in this thesis have been characterised by the magnitude of their IMD only in order to describe their behaviour as a memory-less devices. However, this is only true if their phases are also memory-less (frequency independent). Because all devices used in this thesis are packaged devices, therefore in order to measure their absolute phase they must be first de-embedded and this is beyond the scope of this work. However, relative phase investigations are possible. The absence of this package de-embedding step makes it impossible to look at the terminal voltage and currents for the RF frequency components as was done previously at IF. Phase investigation will be restricted only to 12 W devices used in section 5 .4 since the trend observed is the same.

Figure 6.35 plots the measured values of the relative inter-modulation $IMD_{3L\&H}$ phase when both IF_1 and IF_2 were terminated to short as a function of tone-spacing at a fixed input power level corresponding to a point 6 dB below the 1 dB compression point (defined as Pref 2 in Figure 6.31). The slope of the two output tones (ω_1 and ω_2) and $IMD_{3L\&H}$ is approximately constant for all two-tone frequency spacing. Therefore, this device can be classified as a memory-less device and only exhibits a constant group delay.

The phase behaviour when both IF_1 and IF_2 were terminated to 50Ω is illustrated in Figure 6.36. Again the slope of the fundamental and IMD power is constant thus, this device does not exhibit memory, only again a constant group delay, for frequency ranging from 0.37 MHz to 7 MHz.

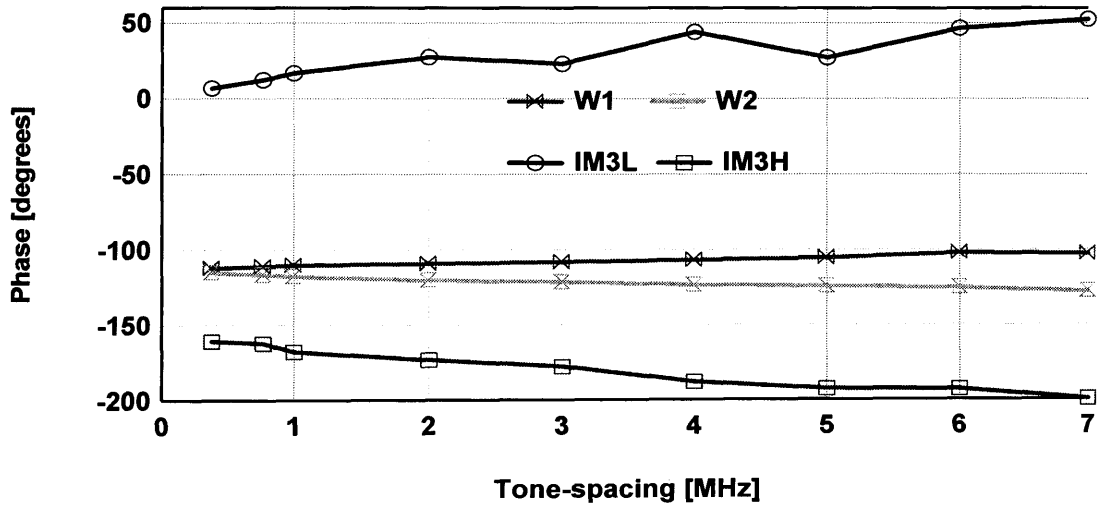

Figure 6.35 Measured fundamental and IMD phase when terminating IF_1 and IF_2 to short at different tone-spacing frequency at a constant input drive level of 6 dB below the 1 dB compression point (defined as Pref 2 in Figure 31).

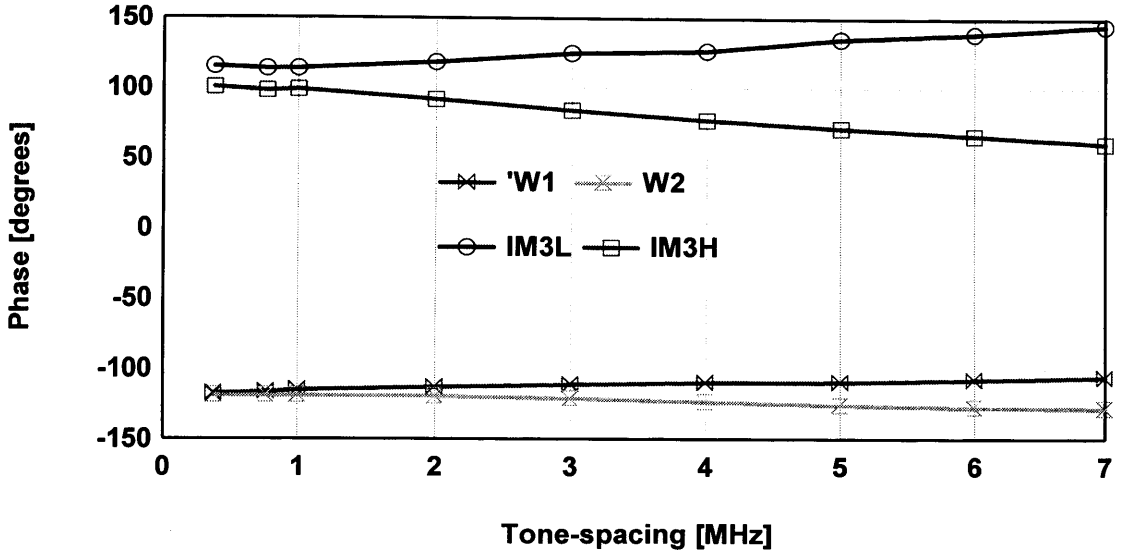

Figure 6.36 Measured fundamental and IMD phase when terminating IF_1 and IF_2 to 50Ω at different tone-spacing frequency at a constant input drive level of 6 dB below the 1 dB compression point (defined as Pref 2 in Figure 31).

6.5. Phase Sweep of Base-Band Impedance

So far analysis of the base-band impedance magnitude shows that IF impedance can considerably influence the device performance and more importantly its linearity. In this section investigation into the influence of the phase of IF reflection coefficient at a magnitude of unity (at the edge of the Smith chart) will be examined.

Based on the results of the previous measurements, an investigation of the effect of the IF base-band impedance, (particularly the most significant components IF_1 and IF_2), on the output power and linearity is performed there is a need to optimise the base-band impedance environment, rather than to just present short circuits [8] [10] as is usually assumed. Such an investigation would examine and support the observation made in the previous passive and

active load pull measurement, that IF_2 impedance was considered to be the primary cause of the observed variation in IMD response.

To do this investigation the value of the IF_2 impedance was varied while fixing the IF_1 at a short circuit for two different devices. The variation of $IMD_{3\&5}$ responses versus IF_2 impedance for 12W LDMOS at 5MHz tone spacing is shown in Figure 6.37, and the 20W LDMOS at 2MHz tone spacing is shown in Figure 6.38. These results clearly show that variations in IF_2 impedance, which is four times the modulation frequency, modify the levels of $IM_{3\&5}$ inter-modulation components. The results also indicated that there is an optimum IF_2 impedance that minimises the $IM_{3\&5}$ terms. The optimum IF_2 impedance for the 12W device is 135° while phase of 90° found to optimum for the 20W device [16].

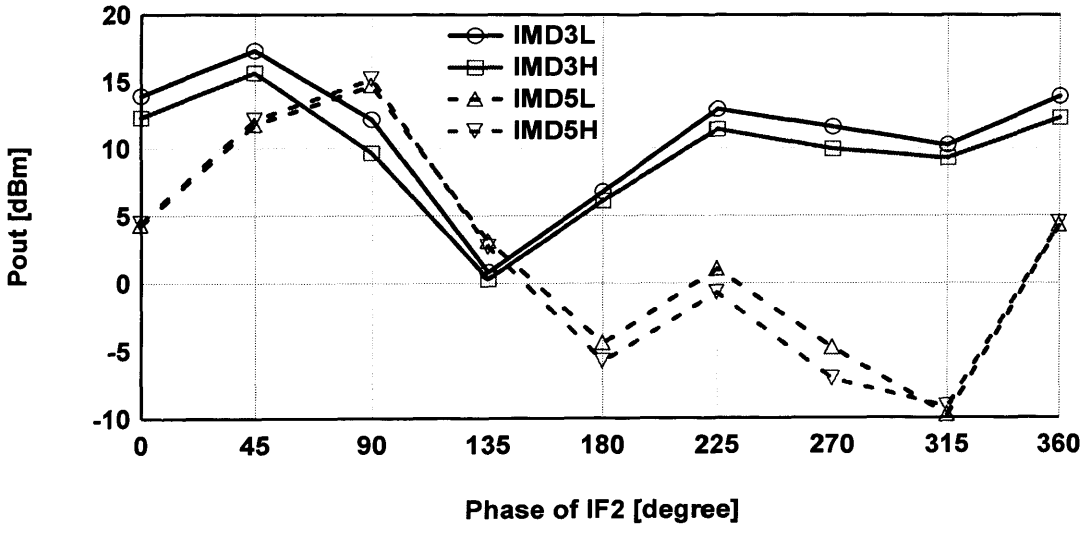

Figure 6.37 Measured IMD magnitude vs. phase of IF_2 for 5MHz frequency separation with IF_1 held a constant short for 12W device.

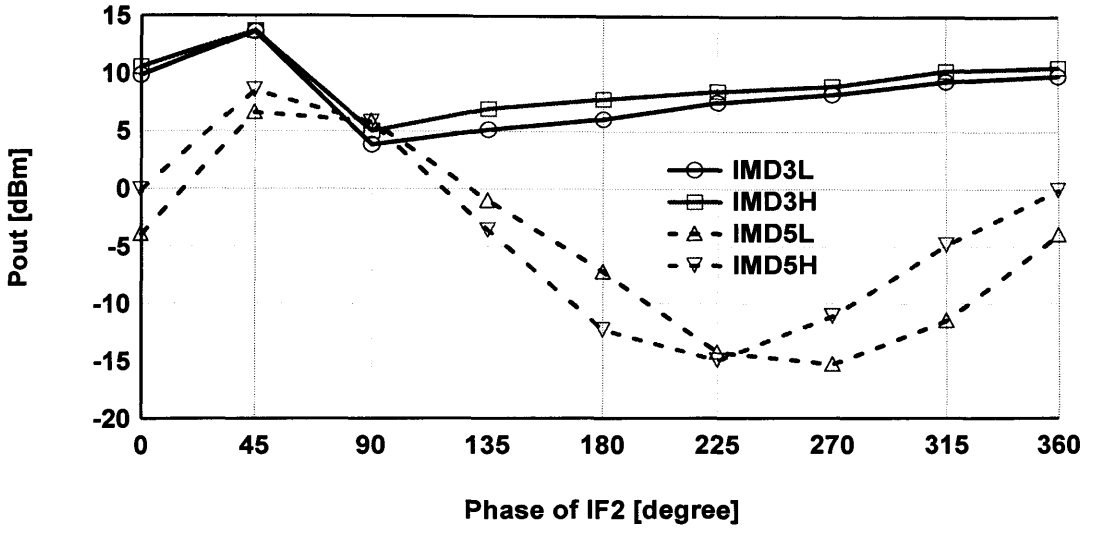

Figure 6.38 Measured IMD magnitude vs. phase of IF_2 for 2MHz frequency separation with IF_1 held a constant short for 20W device.

A similar response is obtained if the IF_1 impedance is varied while the IF_2 impedance is held constant. The variation of $IMD_{3\&5}$ responses versus IF_1 impedance for 12W LDMOS at 5MHz tone spacing is shown in Figure 6.39, and the 20W LDMOS at 2MHz tone spacing is shown in Figure 6.40. The optimum IF_1 impedance is not necessary short circuit (0°) but found to be 225° for the 12W device and approximately 270° for the 20W device.

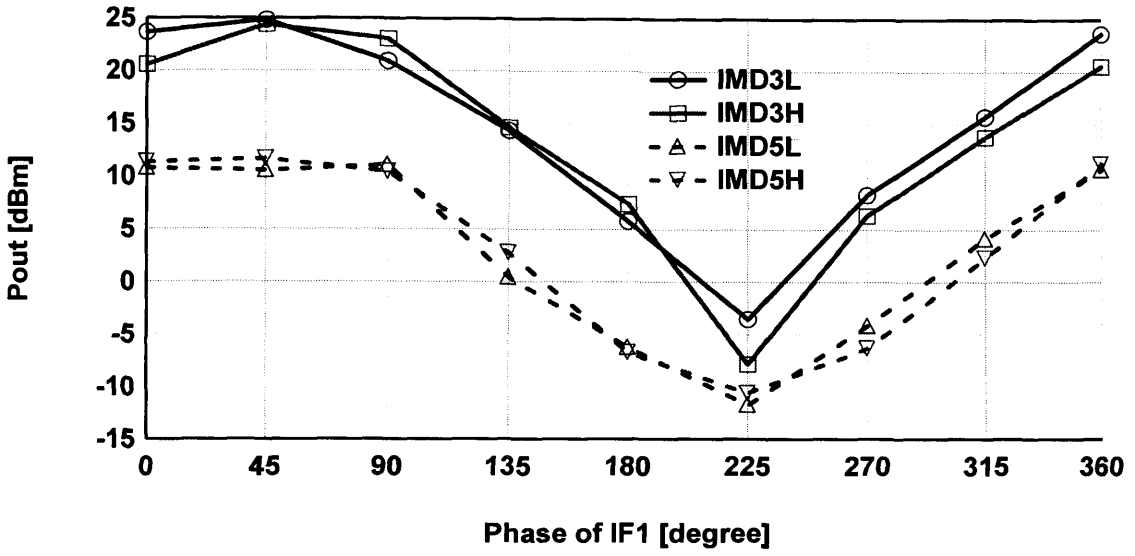

Figure 6.39 Measured IMD magnitude vs. phase of IF_1 for 5MHz frequency separation with IF_2 held a constant 50Ω for 12W device.

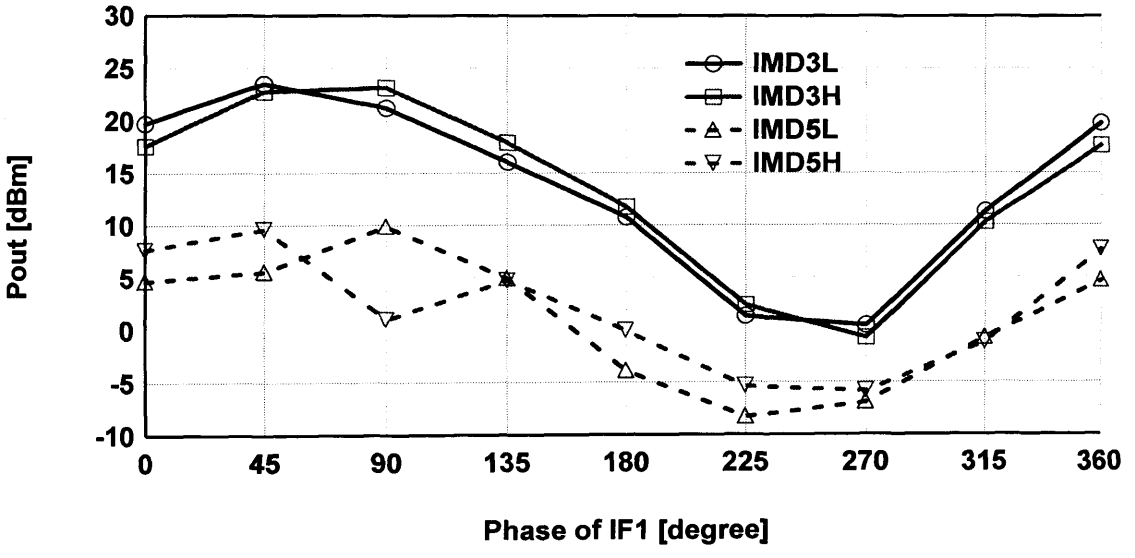

Figure 6.40 Measured IMD magnitude vs. phase of IF_1 for 2MHz frequency separation with IF_2 held a constant 50Ω for 20W device.

The results show that not only IF_1 but also IF_2 can modify the value of the inter-modulation distortion components. Thus to achieve modulation

frequency independent response the base-band impedance must be engineered to be frequency independent over a bandwidth that must be at least four times that of the modulation frequency. The results also indicate that there are separate, optimum IF_1 and IF_2 impedances that can minimise IM_3 and IM_5 terms simultaneously.

The measurement results also show optimum base-band impedance is not necessarily zero but could probably be a complex impedance instead. This important observation has large implications for modern PA linearisation techniques, as well as requiring careful consideration when designing PA bias networks. For applications utilising wide modulation bandwidths this will become a serious design constraint.

6.6. Location of Optimum IF Impedance Termination

Initial measurement results clearly indicated that there is an optimum IF impedance that is effective in minimising $IMD_{3\&5}$ distortion term, and suggests that there is a need to optimise the base-band impedance environment. These investigations are performed using the previous 20W LDMOS device characterised at 2.1 GHz. From the results of the previous measurement shown in Figure 6.38 it is clear that an optimum IF_1 impedance resided in a region between 225° and 270°. Further 'probing' measurements suggested that the optimum load was not actually located at the edge of the Smith chart but it was found to be in the region identified as 'Zone-1' in Figure 6.41. In an attempt to further investigate this, the next investigation involved a similar approach where this time the IF_2 impedance was fixed at the earlier identified optimum, see Figure 6.36, of $\Gamma_{L_{IF2}}=1\angle 90^0$, also shown in Figure 6.41.

A reduction of approximately 10 dB in IMD_3 was observed within this region, albeit at the expense of a significant increase in IMD_5 of approximately 12 dB,

which was not observed in all the previous IF_1 and IF_2 sweeps. It should be noted, with regard to Figure 6.38, that there is a weak dependence of IM_3 on phase variation but an extremely strong dependence of IM_5. The optimum value of IM3 is at IF_2 phase of 90 degrees, however, the IM3 degradation is only around 3 dBm at IF_2 of 225 degrees. But from IM_5 point of view, the optimum phase would approximately be between 225 and 270 degrees where its value has improved by almost 20 dBm. Therefore, it would be logical alternative approach to move IF_2 toward 225°. Further analysis showed that by moving and then maintaining IF_1 load constant within an experimentally determined different zone of the Smith chart (Zone-2) and keeping IF_2 close enough to that Zone (225°), IMD_3 and IMD_5 distortion products could be simultaneously reduced by more than 10 dB. Again, this is in comparison to the previous case where the IF_1 load was maintained at $\Gamma_{L_{IF1}}=1\angle 270^0$ and IF_2 to $\Gamma_{L_{IF2}}=1\angle 90^0$.

To confirm that Zone-2 was indeed the optimum termination for IF_1, for the high power 20W LDMOS used, regardless of the modulation frequency and the power level, it was decided to perform an extra measurement in which the input power was swept for two different tone separations, of 1 and 2 MHz.

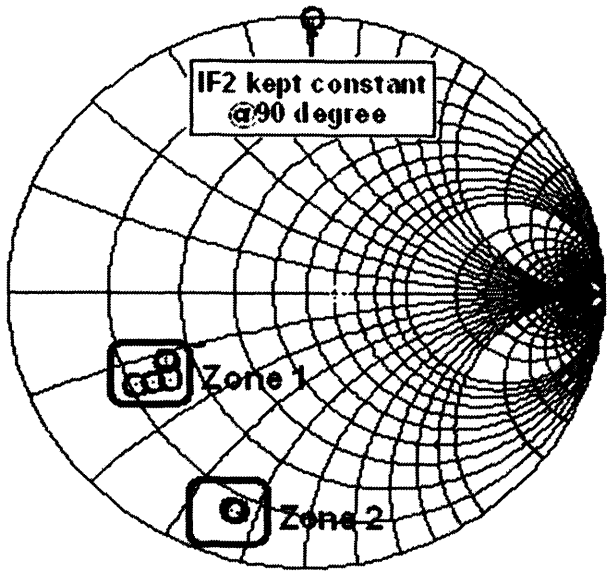

Figure 6.41 Phase sweep of IF_1 while IF_2 kept constant at 90° degree.

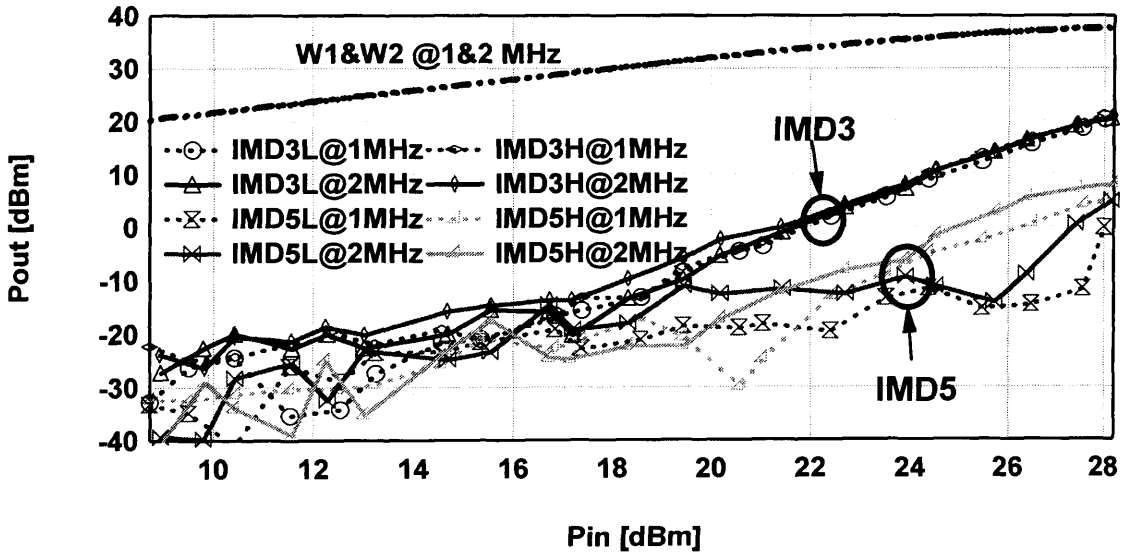

Figure 6.42 Measured two-tone power sweeps for 1 and 2MHz frequency separation inside zone 2.

The measured spectral power performance for the case where the IF_1 load resides within Zone-2 and IF_2 load is fixed at a constant $\Gamma_{L_{IF1}}=1\angle 90^0$ is shown in Figure 6.42. Once again, a typical behaviour of 1:1 slope for the two tones and 1:3 for the IM3 inter-modulation components is observed over a power sweep of some 10 dB. The behaviour of the two fundamental output tones (ω_1 and ω_2) and IMD_3 is clearly almost independent of the tone-separation frequency at input power equal or greater than the compression point. With regards to the magnitude of inter-modulation products IMD_{5L} and IMD_{5H}, they are found to be very close to the lower dynamic range of the measurement system, resulting in noisy measurements at low drive levels.

Conclusively, terminating the IF_1 component into Zone-2 impedance provided the best overall linearity, where both IMD_3 and IMD_5 were found to improve by approximately 10 dB. It is worth noting that when comparing IMD for terminations of IF_1-Zone-2 and IF_1-short-circuit (see Figure 6.32), at an equal input drive level of 18dBm (Pref 1 in Figure 6.31), an improvement of more than 20dB is achieved for IMD_{3L} and IMD_{3H}, and more than 12 dB in the case of IMD_{5L}.and IMD_{5H}.

This observation is confirmed by the mathematical analysis in [17] which indicates that short circuiting base-band impedance does not minimise IM3, but alternatively there may exist some base-band complex impedance which could minimise IM3 components [16].

6.7. Effect of Base-Band Impedance on Gain

In addition to linearity gain and efficiency are needed. To achieve linear behaviour, the operating transmit power is reduced, typically by around 6 dB, from the power amplifier's compression point. There is, however, the drawback of lowered efficiency. However, there is usually a trade-off between linearity and gain, because power amplifiers generate large

distortion when operated in gain compression. In this particular investigation, this is not what is happening where the optimum impedance for linearity is also optimum for gain (gain expansion) hence; Inter-modulation distortion and gain are coupled. Constant gain requires the use of a highly linear amplifier, where the inter-modulation products of the third and higher order do not compress the device.

Figure 6.43 shows the result of the phase sweep of IF_1 from 0 to 360 degrees at the edge of the Smith chart, with IF_2 held as a constant at 50Ω with a two-tone spacing of 2 MHz for a 20W LDMOS device. It has been possible to achieve an extra gain of approximately 6 dB at the optimum impedance (found to be between 225° and 270°). The optimum impedance for linearity however is in this case the same as for gain. The relation between the IMD and gain is generally unrelated. Similar responses were obtained when IF_1 impedance was kept constant at short while the IF_2 impedance was variable. The gain achieved is smaller in this case, when sweeping IF_2, compared to the previous case when IF_1 was swept (See Figure 6.44). This is to be expected since the magnitude of IF_1 is usually bigger than the magnitude of the IF_2 component.

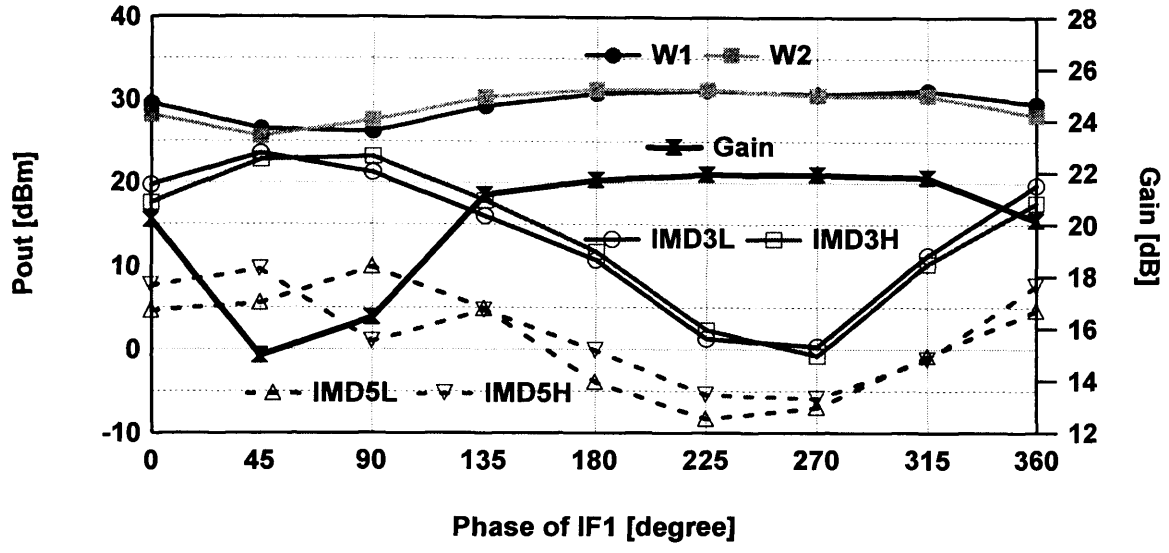

Figure 6.43 Measured gain, fundamental and IMD power vs. phase of IF_1 for 2MHz frequency separation with IF_2 held a constant 50Ω for 20W device.

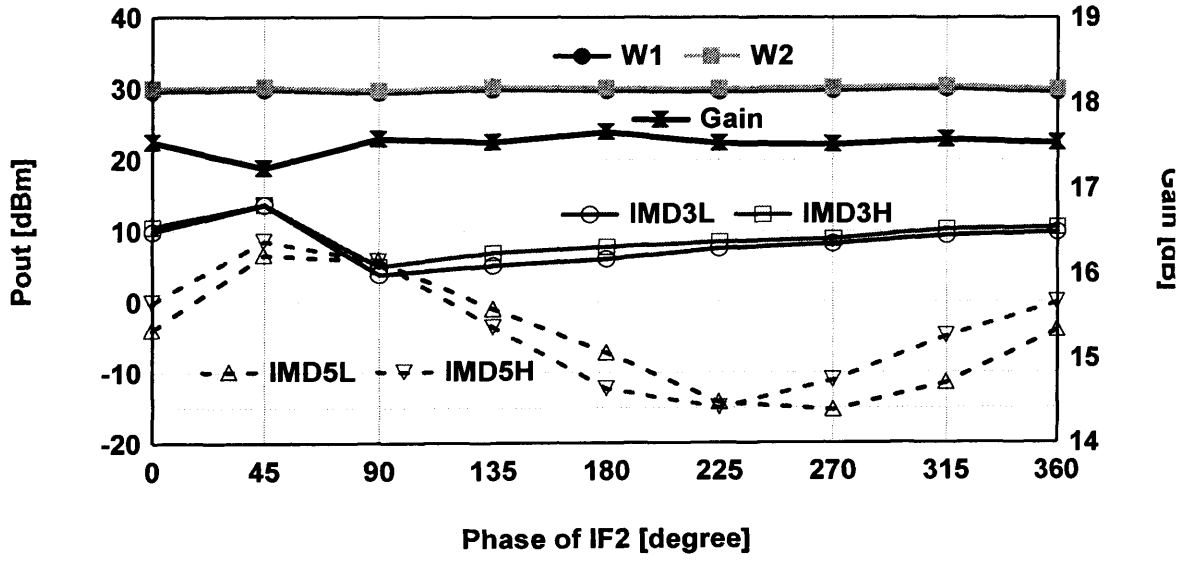

Figure 6.44 Measured gain, fundamental and IMD power vs. phase of IF_2 for 2MHz frequency separation with IF_1 held a constant short for 20W device.

Another example of finding optimum impedance for maximum linearity and gain is shown below. In this case, the impedance of IF_1 was varied as shown in Figure 6.45. The location of the Z_1 impedance found to be the one that minimise the IMD_3 hence increases the output third-order intercept point (IP3). Z_1 is conveniently the optimum impedance to maximise gain and minimise inter-modulation, while Z_9 deteriorates both gain and distortion.

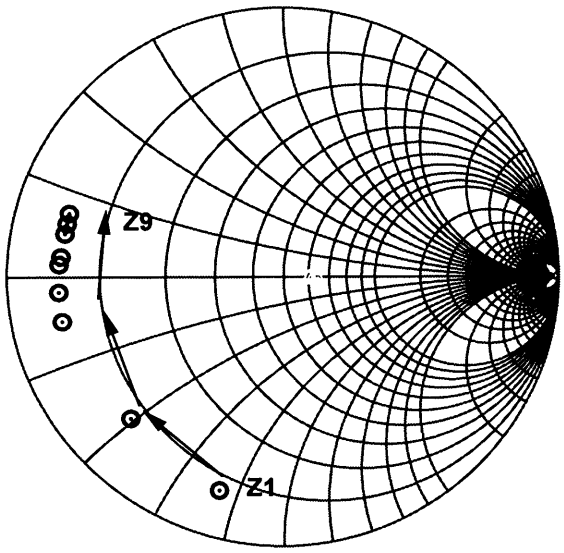

Figure 6.45 Various base-band impedances presented to the device for optimum gain.

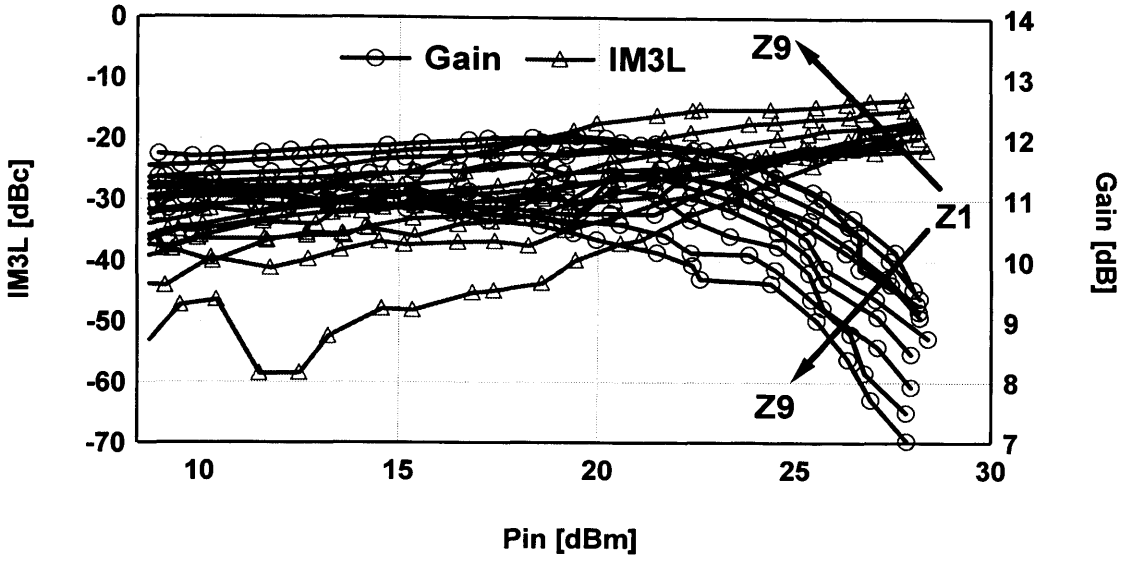

Figure 6.46 Measured Gain and IM3L for all different impedances shown in Figure 6.45.

6.8. Effect of Base-Band Impedance on Second Harmonic Band

Injection of base-band signals to suppress inter-modulation distortion is desirable. Experimental measurement using a-12W LDMOS device characterised at 2.1 GHz for two-tone spacing of 5MHz and biased as Class AB using two-tone technique have been selected to compare two cases of IF impedance. State 1, where 50 is presented to IF_1 and IF_2 and State 2, where a short circuit is presented to IF_1 and IF_2.

The measured RF two-tone second harmonic spectral power for the two cases of IF impedance is shown in Figure 6.47. It was observed that for State 2, the in-band distortions are suppressed while it results in an increase in the out-of-band second harmonic distortions. In contrast State 1 is a complete contrast to State 2 resulting in an increase in the in-band distortion and a decrease for the out-of-band components. These results, therefore, indicates that there is a very

strong link between the injected base-band signal and the second harmonic components.

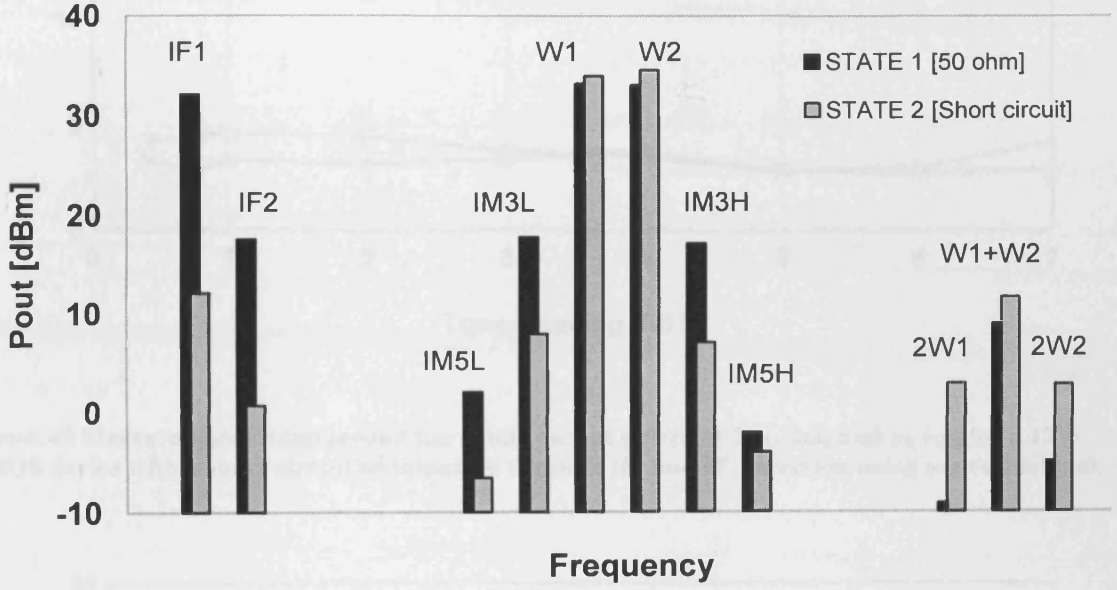

Figure 6.47 Measured spectrum output power for State 1 (50Ω presented to IF_1&IF_2) and State 2(short circuit presented to IF_1&IF_2).

To investigate whether the above observation is valid for the whole bandwidth of interest, it was necessary to sweep the frequency from 0.385 MHz to 7 MHz at a constant input power of approximately 18 dBm corresponding to a point of 1 dB below the compression point (see Figure 6.31). Plots of all second harmonic components for both States are shown in Figure 6.48 and Figure 6.49. With regard to output second harmonic IF_{1H} ($\omega_1+\omega_2$), an increase of approximately 3 dB, which equals to double the power, is observed for State 2 over state 1 for all tone-spacing frequency. Also the second harmonic output power of $2\omega_1$ and $2\omega_2$ were amplified by a rapid increase of approximately 9 dB.

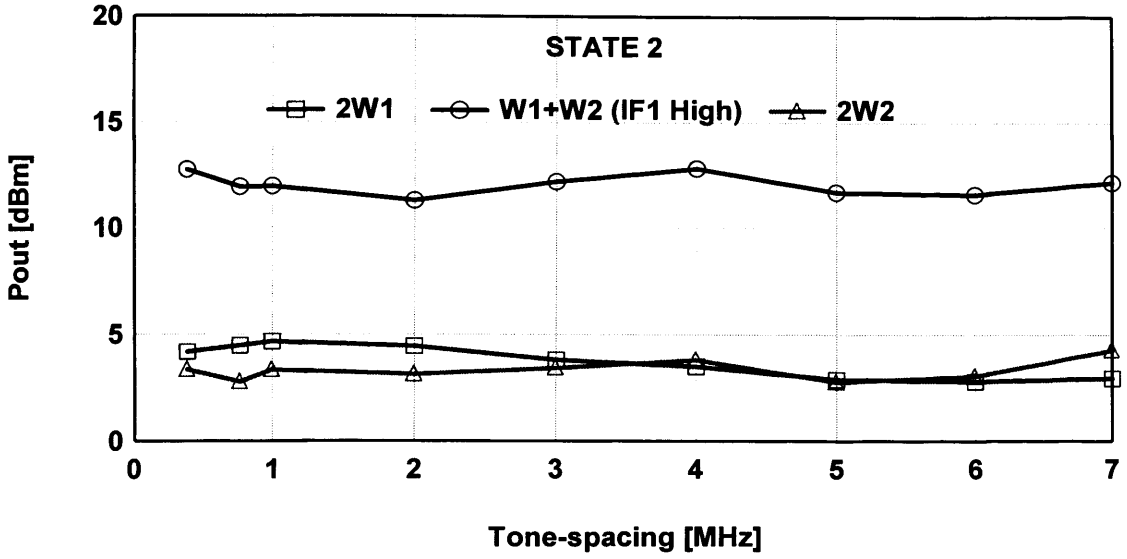

Figure 6.48 Measured generated second harmonic output power of $2\omega_1$, $2\omega_2$ and $\omega_1+\omega_2$ for a 12W LDMOS device with a short circuit termination through IF_1 and IF_2 injection using active load pull.

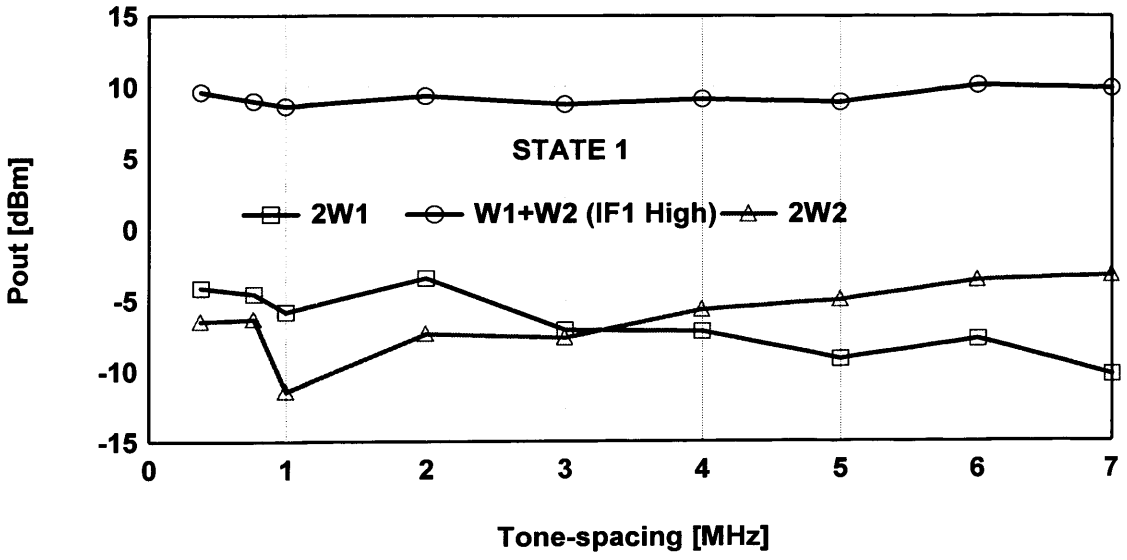

Figure 6.49 Measured generated second harmonic output power of $2\omega_1$, $2\omega_2$ and $\omega_1+\omega_2$ for a 12W LDMOS device with a 50Ω offset termination at IF_1 and IF_2.

Unlike base-band voltages and currents, second harmonic voltages and currents cannot be analysed in the same way due to the fact that all the devices that have been used so far in this work are package devices. Therefore, unless package de-embedding was performed, their contribution to the shape of the waveform is unknown. However, the second harmonic voltages and current are plotted to show the impact of base-band impedance termination on the second harmonic voltages and currents. Figures 6.50 and 6.51, State 2, with Figures 6.52 and 6.53, State 1, show the corresponding measured second harmonic output current components generated by the non-linear behaviour of the transistor, as well as the resulting second harmonic output voltage components developed by their corresponding load impedances. Clearly it can be seen that the dominant current component, in the second harmonic zone, is IF_{1H} $(\omega_1+\omega_2)$. However, there are also significant $2\omega_1$ and $2\omega_2$ current components, which when presented with a high enough impedance are capable of generating dominant $2\omega_1$ and $2\omega_2$ voltage components. Clearly it can be seen that the measured second harmonic output voltages and currents for State 2 are always greater than the measured second harmonic output voltages and currents for State 1, resulting in a second harmonic output power increase in the case of State 2.

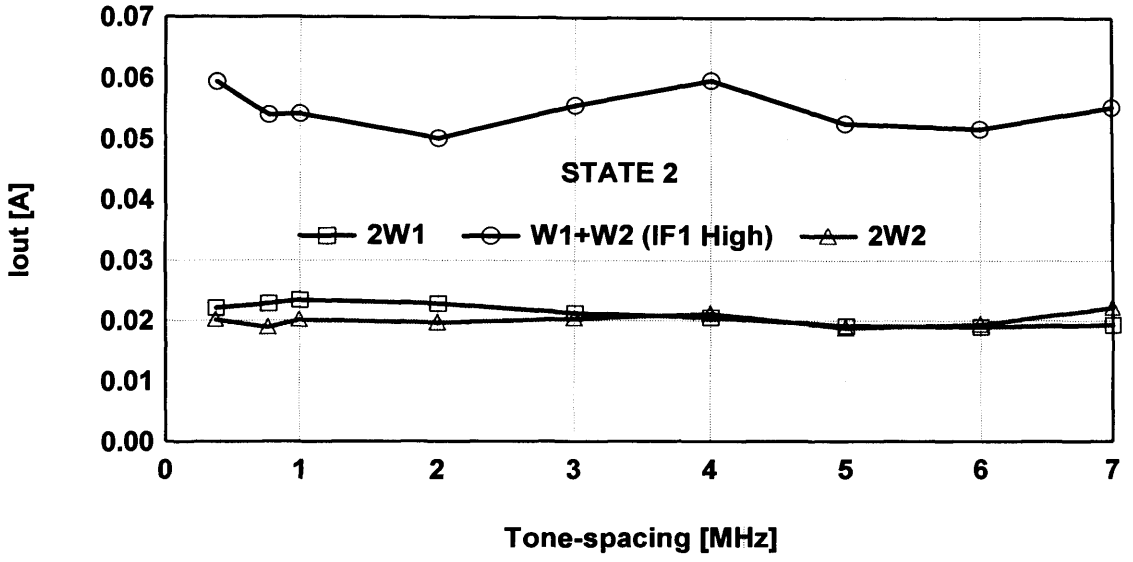

Figure 6.50 Measured generated second harmonic output current of $2\omega_1$, $2\omega_2$ and $\omega_1+\omega_2$ for a 12W LDMOS device with a short circuit termination at IF_1 and IF_2.

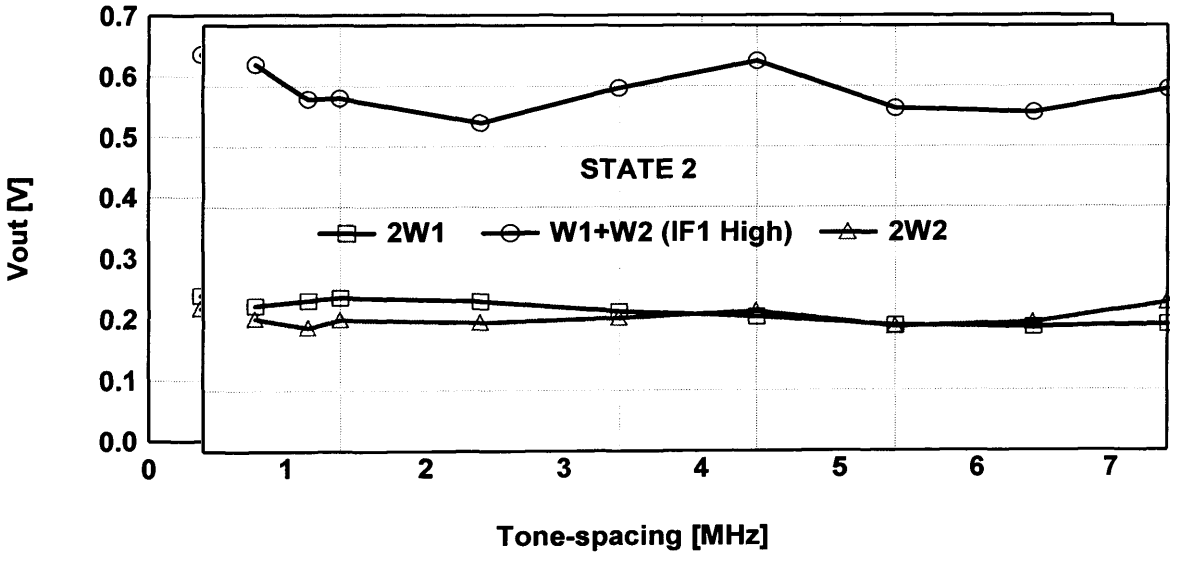

Figure 6.51 Measured generated second harmonic output voltage of $2\omega_1$, $2\omega_2$ and $\omega_1+\omega_2$ for a 12W LDMOS device with a short circuit termination at IF_1 and IF_2.

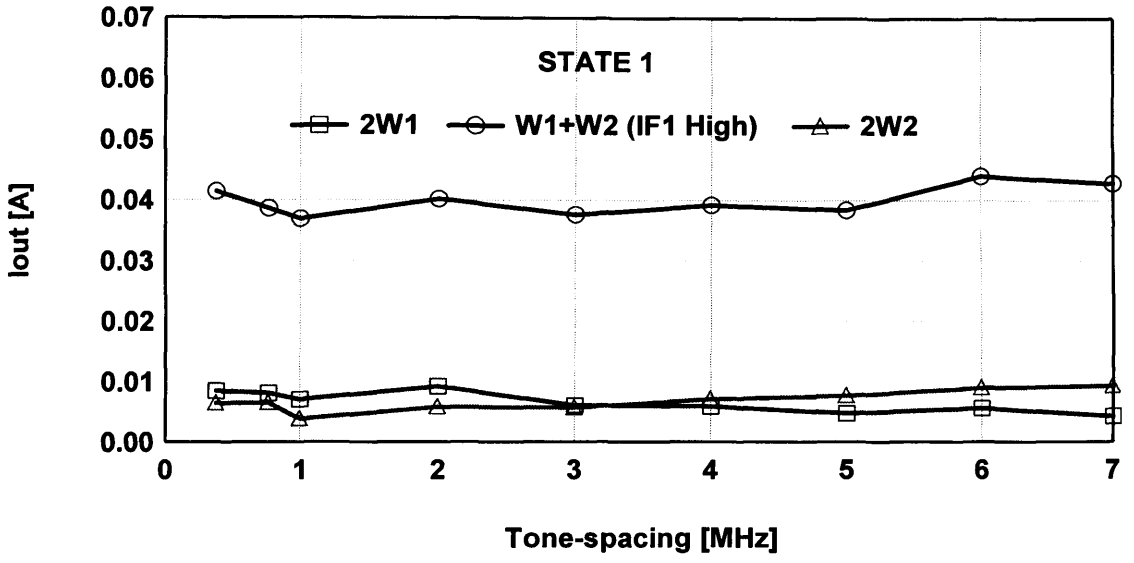

Figure 6.52 Measured generated second harmonic output current of $2\omega_1$, $2\omega_2$ and $\omega_1+\omega_2$ for a 12W LDMOS device with a 50Ω offset termination at IF_1 and IF_2.

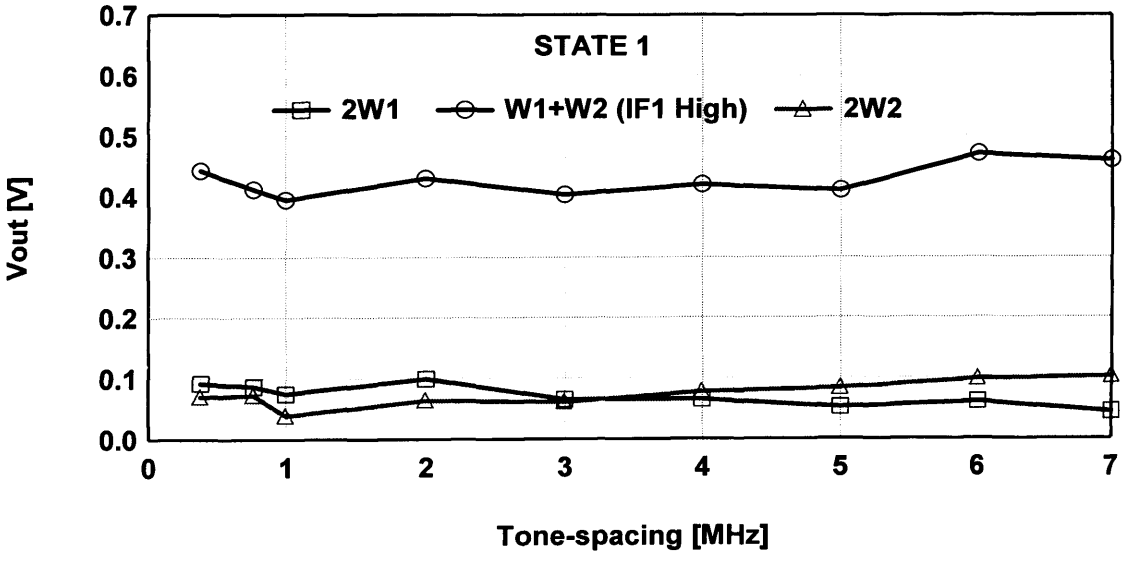

Figure 6.53 Measured generated second harmonic output voltage of $2\omega_1$, $2\omega_2$ and $\omega_1+\omega_2$ for a 12W LDMOS device with a 50Ω offset termination at IF_1 and IF_2.

Further research on the impact of base-band impedance on the second harmonic components was carried out, where the IF_1 impedance was varied, around the perimeter of the Smith chart. The results of this measurement are shown in Figure 6.54, where it is clear that variations in IF_1 impedance significantly modify the levels of both IM_3 inter-modulation components and second harmonic components. Again the output voltages e.g. $IM_{3L\&H}$, $2\omega_1$, $2\omega_2$ and $\omega_1+\omega_2$ are plotted in Figure 6.55, as a function of IF_1.

The magnitude of the second harmonic components reacts to the IF_1 variations in inverse proportion to that of the IM_3 inter-modulation components (see Figure 6.54 and 55). It could therefore be concluded on the basis of this data that this behaviour is due to the mixing process between output components. To be more precise, when the output fundamental signals mix with IF_1 signals, there is a possibility that they generate products which are out of phase with IMD_3 (reduction in IMD_3) and in phase with second harmonic components (increment in $2\omega_1$, $2\omega_2$ and $\omega_1+\omega_2$).

Consequentially, base-band impedance modifies not only the level of in-band distortion components but also modifies the level of out-of-band distortion components especially those around the second harmonic of the carrier. This result again shows the strong link between base-band and second harmonic components. These results also show that optimum base-band impedance for the in-band distortion (IMD) is the one that maximises the second harmonic components.

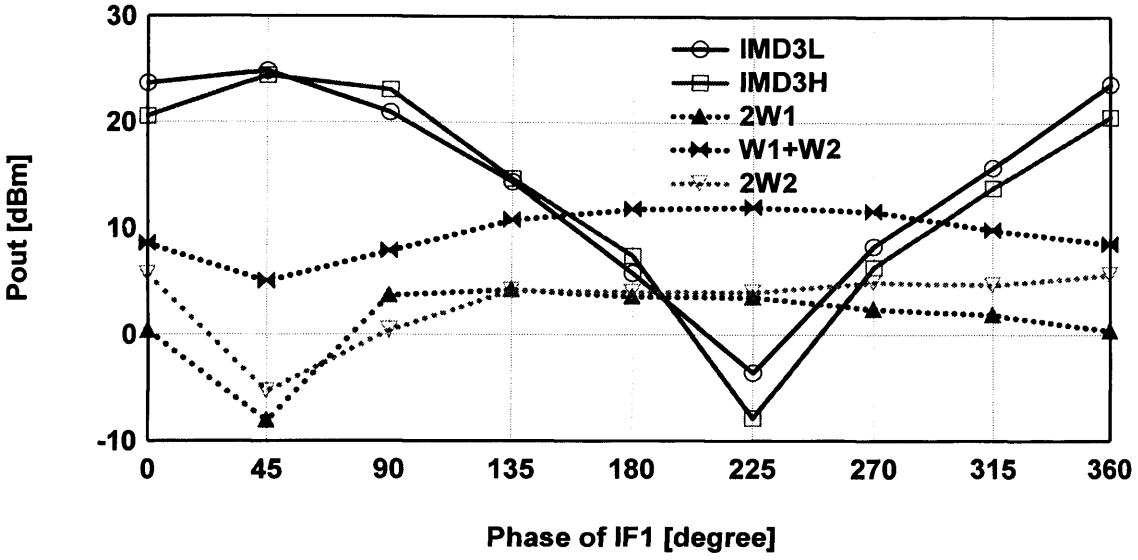

Figure 6.54 Measured output power of 12W LDMOS device for IMD_3 and 2nd harmonic components.

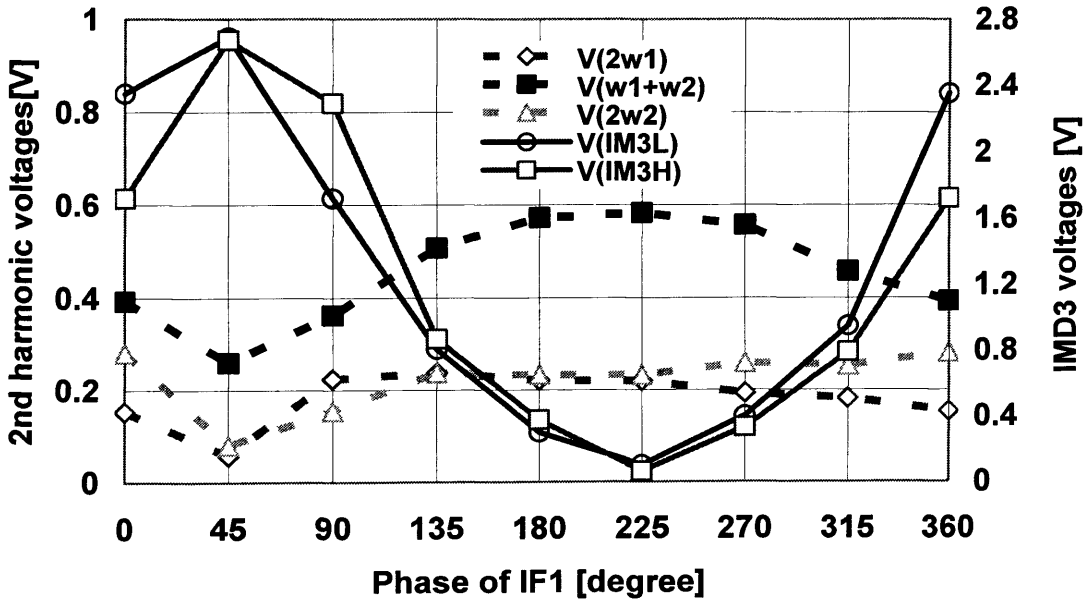

Figure 6.55 Measured output voltage of 12W LDMOS device for IMD_3 and 2nd harmonic components.

6.9. Effect of Bias Voltage on LDMOS Inter-Modulation

The bias voltage can cause a variation in the inter-modulation distortion level and may cause asymmetry between lower and higher IM components. This can be explained using equations (2.18) and (2.19) which show that the valued nonlinearity coefficients $a_0, a_1, a_2, \ldots a_n$ are function of the DC bias voltage. An investigation of the effect of the bias voltage is made possible by using the high power measurement system with two-tone stimulus frequency of 2099 MHz and 2101 MHz, at different input power using a 20W LDMOS device. The gate bias voltage was varied from -2.45V to 3.1V in steps of 0.05V at a constant drain voltage of 28V over a power sweep of some 30 dB. Figure 6.56 shows that the terminating impedance for the most significant IF components (IF_1 and IF_2) has been successfully held constant for all bias voltage. Figure 6.57 shows the output power of the inter-modulation distortion IMD_3 as a function of input drive level for all bias voltages. The maximum symmetry is different from one input power to another. For instance, the maximum symmetry at input drive level of 14dBm is found to be at bias voltage of 2.78V while maximum symmetry at input drive level of 18dBm is found to be at bias voltage of 2.94V. Figure 6.58 summarise the device performance at the input drive level of 14 dBm where minimum IM_3 terms were observed to be at gate voltage of 2.8V while the maximum symmetry (minimum delta) is observed to be at 2.78V. Moreover, it should be noted that at 22dBm input drive level, where the device is saturated, an asymmetry of about 2.5 dB exists for the whole gate voltage sweep. This plot also illustrates a reduction of IM_3 term at low input drive level of approximately 3 dB at bias voltage of around 2.8V.

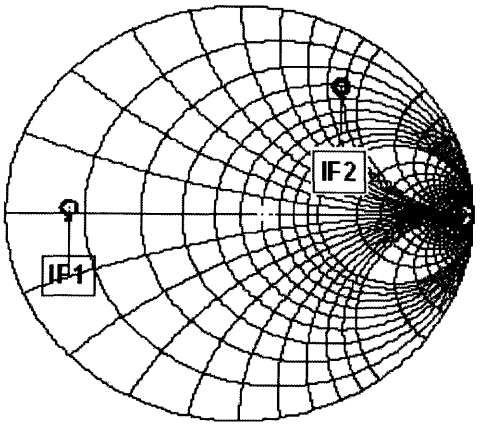

Figure 6.56 Measured IF_1 and IF_2 impedance for all gate bias voltages with tone-spacing of 2MHz.

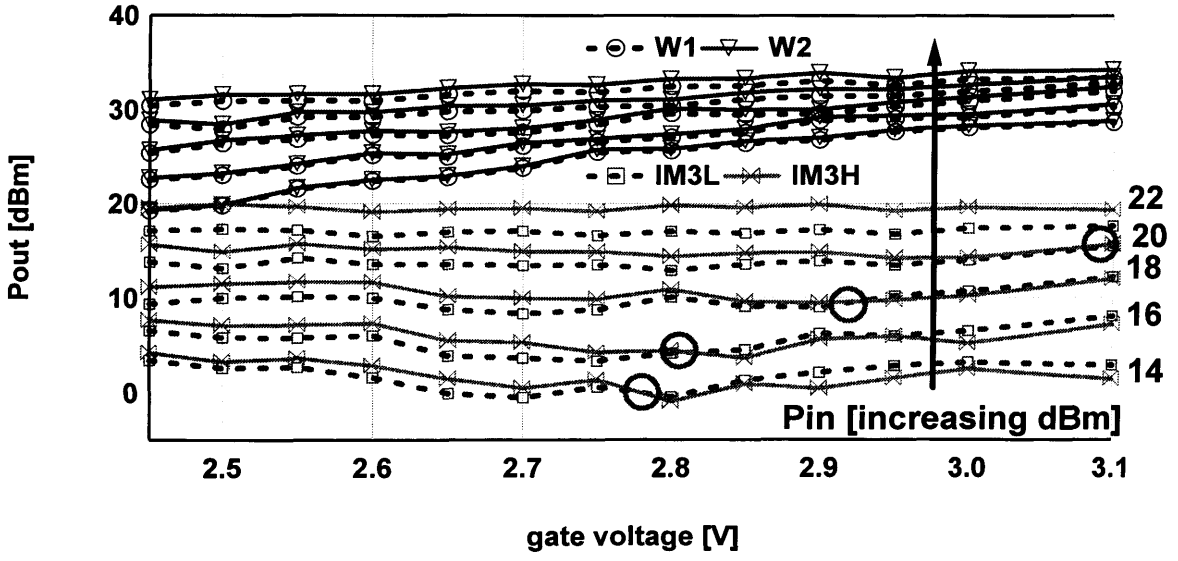

Figure 6.57 Measured fundamental and IMD power vs. gate voltage for different input drive level at tone-spacing frequency of 2MHz for the IF_1 and IF_2 impedances shown in Figure 6.56.

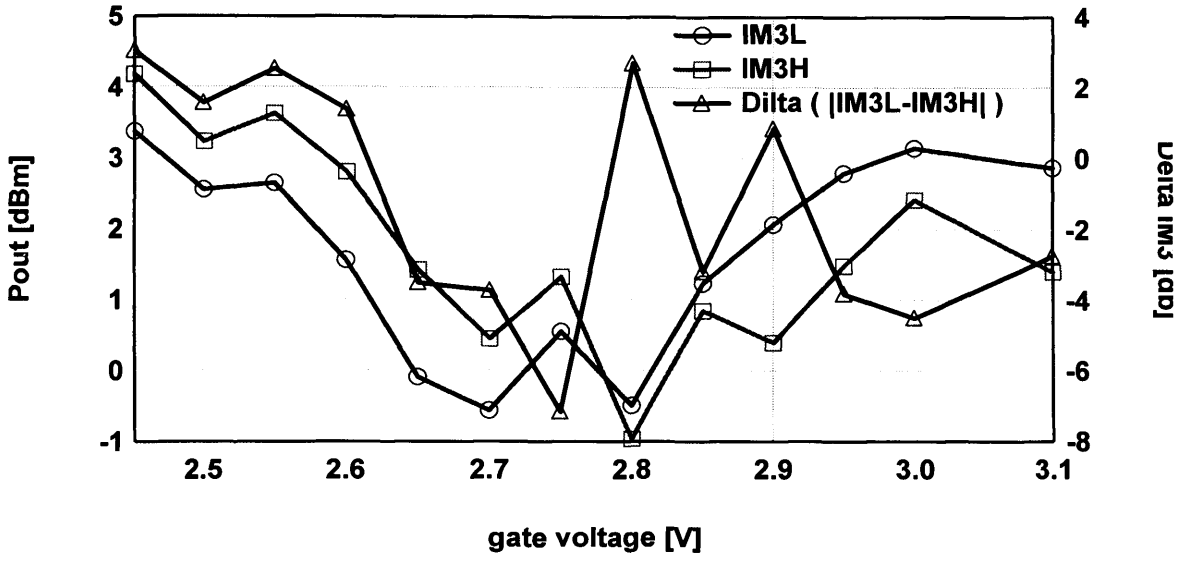

Figure 6.58 Measured IMD_3 at a constant input power level of 14 dBm and delta IM3 ($\Delta IM_3 = | IM_{3L} - IM_{3H} |$) as extracted from Figure 6.57.

6.10. Summary

In this chapter it has been demonstrated how the developed measurement system is capable of allowing detailed investigations of the linearity and related memory behaviour of high power transistors to be undertaken now. The results achieved provide new insight into the both intermodulation distortion produced by these high power transistors and its sensitivity to the terminating impedance environment. The investigation undertaken in this case have mainly focused on the sensitivity to the terminating IF impedance at the transistor output.

6.11. References

1. Le Gallou, N., et al. *Analysis of low frequency memory and influence on solid state HPA intermodulation characteristics*. 2001.

2. Vuolevi, J., J. Manninen, and T. Rahkonen. *Cancelling the memory effects in RF power amplifiers*. in *Circuits and Systems, 2001. ISCAS 2001. The 2001 IEEE International Symposium on*. 2001.

3. Tornblad, O., et al. *Modeling and Measurements of Electrical and Thermal Memory Effects for RF power LDMOS*. in *Microwave Symposium, 2007. IEEE/MTT-S International*. 2007.

4. Vuolevi, J.H.K., T. Rahkonen, and J.P.A. Manninen, *Measurement technique for characterizing memory effects in RF power amplifiers*. Microwave Theory and Techniques, IEEE Transactions on, 2001. **49**(8): p. 1383-1389.

5. Parker, A.E. and J.G. Rathmell, *Bias and frequency dependence of FET characteristics*. Microwave Theory and Techniques, IEEE Transactions on, 2003. **51**(2): p. 588.

6. Alghanim, A.L., J.; Williams, T.; Benedikt, J.; Tasker, P. *Investigation of electrical base-band memory effects in high-power 20W LDMOS Power Amplifiers*. in *EUMC*. 2007. Munich.

7. Alghanim, A.L., J.; Williams, T.; Benedikt, J.; Tasker, P. *Using active IF load-pull to investigate electrical base-band induced memory effects in high-power LDMOS transistors*. in *APMC*. 2007. Bangkok.

8. Williams, D.J., J. Leckey, and P.J. Tasker. *A study of the effect of envelope impedance on intermodulation asymmetry using a two-tone time domain measurement system*. 2002.

9. Carvalho, N.B. and J.C. Pedro. *Two-tone IMD asymmetry in microwave power amplifiers*. 2000.

10. Carvalho, N.B. and J.C. Pedro. *Two-tone IMD asymmetry in microwave power amplifiers*. in *Microwave Symposium Digest., 2000 IEEE MTT-S International*. 2000.

11. Abdulrahman Alghanim, J.B., and P. J. Tasker. *Investigation of electrical base-band memory effects in high-power 20W LDMOS transistors using IF passive load pull*. in *Information and Communication Technologies, 2008. ICTTA '08. 3rd*. 2008. Damascus.

12. Wakejima, A., et al. *370-W output power GaN-FET amplifier with low distortion for W-CDMA base stations*. 2006. San Francisco, CA, United States: Institute of Electrical and Electronics Engineers Inc., Piscataway, NJ 08855-1331, United States.

13. Franco, M., et al. *Minimization of bias-induced memory effects in UHF radio frequency high power amplifiers with broadband signals*. 2007. Long Beach, CA, United States: Institute of Electrical and Electronics Engineers Computer Society, Piscataway, NJ 08855-1331, United States.

14. A Alghanim, J.L., T. Williams, J. Benedikt and P. J. Tasker, *Investigation into the sensitivity of Electrical Base-Band Memory Effects to higher order IF components for High-Power LDMOS Power Amplifiers*. Electronics Letters, 2008. **44**(5): p. 358-359.

15. Martins, J.P., et al., *A Metric for the Quantification of Memory Effects in Power Amplifiers*. Microwave Theory and Techniques, IEEE Transactions on, 2006. **54**(12): p. 4432.

16. Abdulrahman Alghanim, J.L., Tudor Williams, J. Benedikt, and P. J. Tasker. *Reduction of Electrical Baseband Memory Effect in High-Power LDMOS Devices using Optimum Termination for IMD3 and IMD5 using Active Load-Pull*. in *IMS*. 2008. Atlanta.

17. Sevic, J.F., K.L. Burger, and M.B. Steer. *A novel envelope-termination load-pull method for ACPR optimization of*

RF/microwave power amplifiers. in *Microwave Symposium Digest, 1998 IEEE MTT-S International*. 1998.

CHAPTER 7

Conclusion and Future Work

7.1. Conclusion

A key aim of this work was to investigate how to further develop the Cardiff waveform measurement and engineering systems and render them suitable for characterising the high power RF power amplifier under multi-tone rather than single-tone (CW) excitations. It was identified that a key advancement of the measurement system over the previous one was the requirement to be able to handle IF power of approximately 100W, hence the need for a new IF measurement solution. This new IF measurement solution, when combined with the existing 100W RF measurement system, should then be able to actively provide source and/or load pull functionality over an approximate bandwidth of 10 kHz to 12 GHz with dynamic range of about 50 dB. Since, no active IF load and source pull measurement solutions existed with this same capacity for power they also had to be established. This was successfully achieved delivering a high

power waveform measurement and engineering system with the following capabilities;

	IF SYSTEM	RF SYSTEM
Bandwidth	50 kHz – 50 MHz	1 GHz – 12 GHz
Current	10A	10A
Voltage	1000V	100V
Power	> 50W	> 100W

The new high power multi-tone waveform measurement and engineering system, integrating high power RF and IF measurement capability has been used to investigate nonlinear behaviour, including the base-band memory effect, of high power (>10W) LDMOS RF power amplifiers. A key feature of this measurement system is the ability to measure voltage and current waveforms at all relevant frequencies. This feature provides a clear picture and inspection of the cause of nonlinearity and memory effect. This is particularly seen in Section 5.2 leading to the discovery of the importance of IF_2 components. Moreover, the capability of load- pulling low frequency components at high power provides an insight into the effect of the bias network on the overall device performance. For example, it has been possible, through using IF load pull, to suppress electrical base-band memory effect and measure and analyze any residual effects due to other sources.

A comparison between passive and active IF load pull for a high power RF power amplifier has been presented for the first time. This comparison has

led to the conclusion that it is very impracticable to passively load pull very low frequency components. To my knowledge, this comparison has never been reported before. Therefore, the alternative more realistic solution for such a problem is active load pull.

The results confirmed that electrical memory introduced by frequency variation of the terminating IF impedances, typically associated with the bias network, tend to be dominant. In fact it was shown that base-band impedance must be engineered to be frequency independent over a bandwidth of at least four times, not twice as commonly believed, that of the modulation frequency, in order to achieve a response independent of modulation frequency.

The measurement system's capability in capturing and providing phase information allows optimum base-band impedance to be located and minimises the in-band distortion by more than 20dB, in contrast to conventional IF short termination.

It was also observed that the base-band impedance modifies not only the level of in-band, but also modifies the level of out-of-band distortion components, especially those around the second harmonic of the carrier. These results show the strong link between the injected-base-band signal and the second harmonic components.

7.2. Future Work

The measurement system hardware developed is capable of characterising IF signals down to 50 kHz, hence modulation rates as low as 25 kHz. However, due to limitation in the multi-tone sampler configuration utilised during the course of this thesis work it was not possible to go below a modulation frequency of 185 kHz (370 kHz of tone-spacing). This limitation has now been resolved and it is currently possible, therefore, to use the measurement system to investigate thermal memory effect occurring at low frequencies (< 100 kHz). This is clear of topic of major interest that can now be undertaken.

The conclusions drawn from this thesis indicate that, for high power transistors, the first two IF components are a major contributor in modifying the performance of inter-modulation distortion terms. It would may be possible therefore, that for even higher power devices than the ones used in this work, for example 100W, that the higher IF components such as IF_3 and IF_4 may influence the behaviour of IMD in a way which ensures they can no longer be ignored. This problem will be compounded in the case of Wimax PA's, which uses a channel bandwidth of 23 MHz. It means that, if the first four base-band components (IF_1, IF_2, IF_3 and IF_4) are a cause for concern, an IF test-set with a bandwidth of at least 92 MHz (4*23=92) is needed. The present IF high power test-set is scaleable and can be easily scaled to 1 GHz provided that there is a bias tee with a bandwidth of 1 GHz. The research work made this possible through the on-site design of a 2A bias tee with a wide bandwidth of 50 kHz to

approximately 1 GHz. The performance of this wide bandwidth bias tee is shown in Figure 7.1.

It would be also possible to move from a simple two-tone stimulus to more complex stimulation such as three-tone, four-tone...etc since the measurement system hardware allows for such investigations.

It is important to note that it was not possible during this work to load pull IF components for modulation frequencies greater than approximately 12 MHz due to the bandwidth limitations of the IF PA used. To further investigate base-band memory effect at wider bandwidth, it is necessary to purchase a suitable IF power amplifier. This could be, for example, the ENI 50L 1 MHz to 240 MHz, 50W linear power amplifier retailing at $4,295 from BEEL ELECTRONICS.

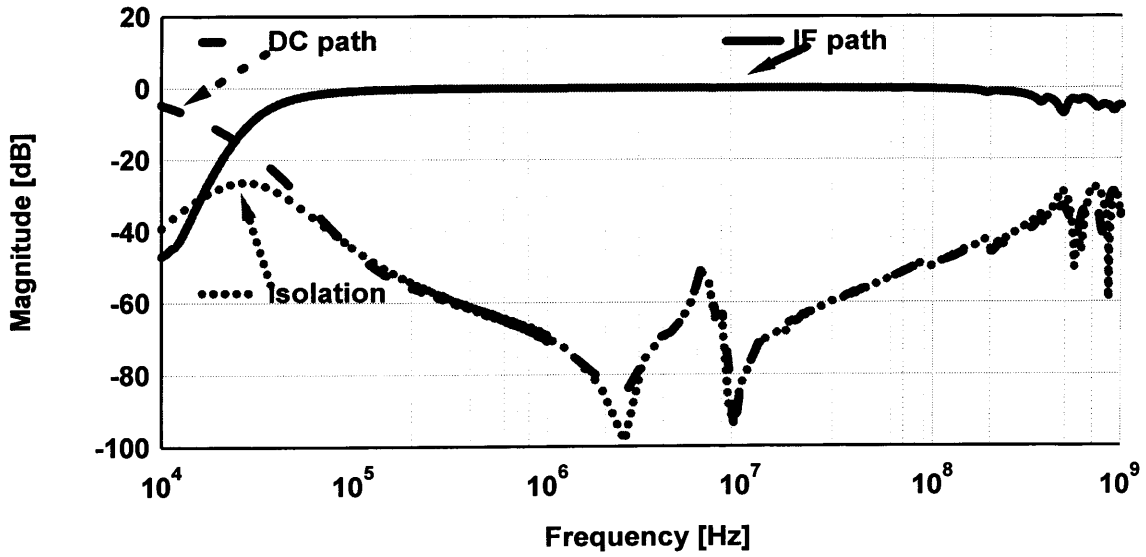

Figure 7.1 Measured amplitude frequency response of the 1 GHz bandwidth IF bias.

The other obvious future work is to control the RF impedance as well as the IF impedance. Equation (2.19) indicates that it would be possible to linearise the DUT via second harmonic impedance variation using RF load pull. It is not yet clear how much the variation in in-band distortion is related to the variation in the second harmonic impedance (not controlled in this work but terminated to a 10Ω). It would be important to investigate in more detail the impact of second harmonic termination on in-band distortion and possibly find a figure of merit for the one that has the greater impact on it. Is it base-band or second harmonic impedance? It was therefore decided to design a high power RF amplifier on site to allow second harmonic components ($2\omega_1$, $2\omega_2$ and ω_{1+} ω_2) to be load-pulled. The performance of this power amplifier is shown below. Figure 7.2 shows the measured output power as a function of both input power and bandwidth. This power amplifier is capable of delivering approximately 60W that is relevant to the investigation of high power devices. Figure 7.3 demonstrates that the minimum gain of this power amplifier is approximately 35 dB.

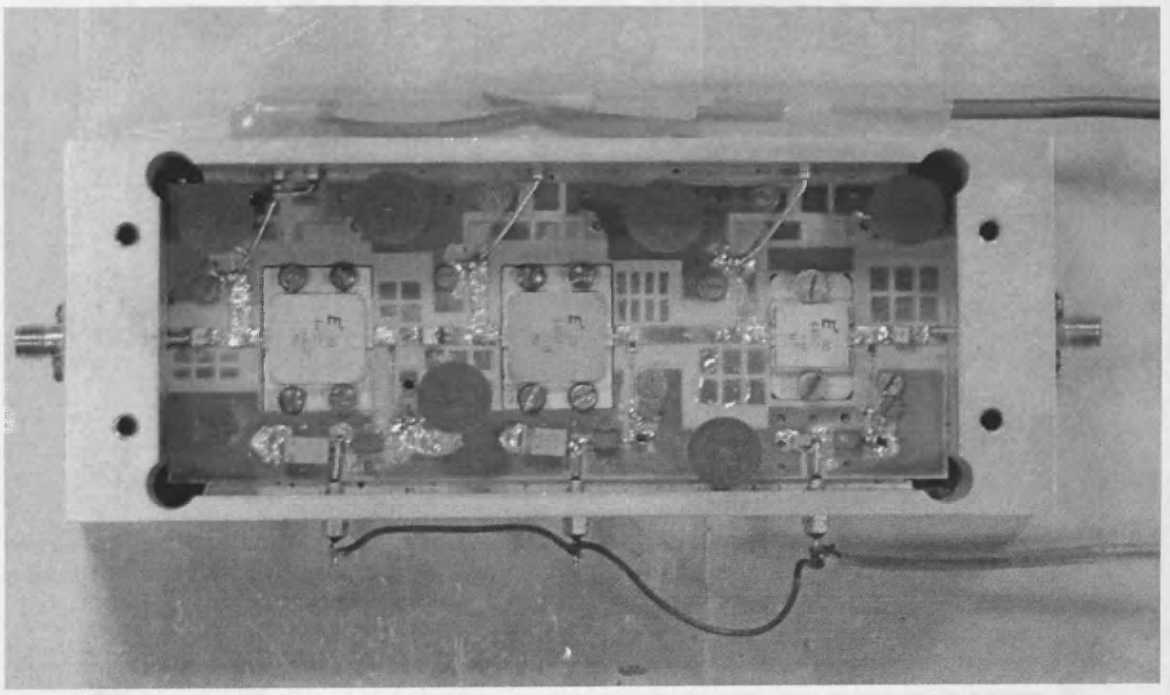

Figure 7.2 Designed 50W RF power amplifier for second-harmonic load pull.

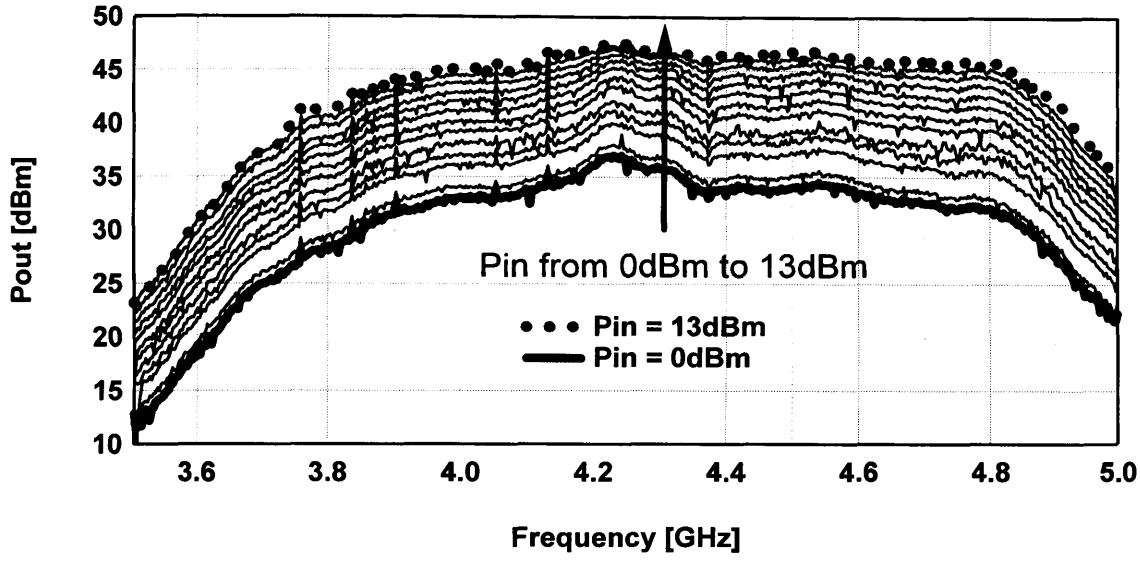

Figure 7.3 Measured output power over bandwidth at different input power ranging from 0 dBm (solid curve) to 13 dBm (dotted curve).

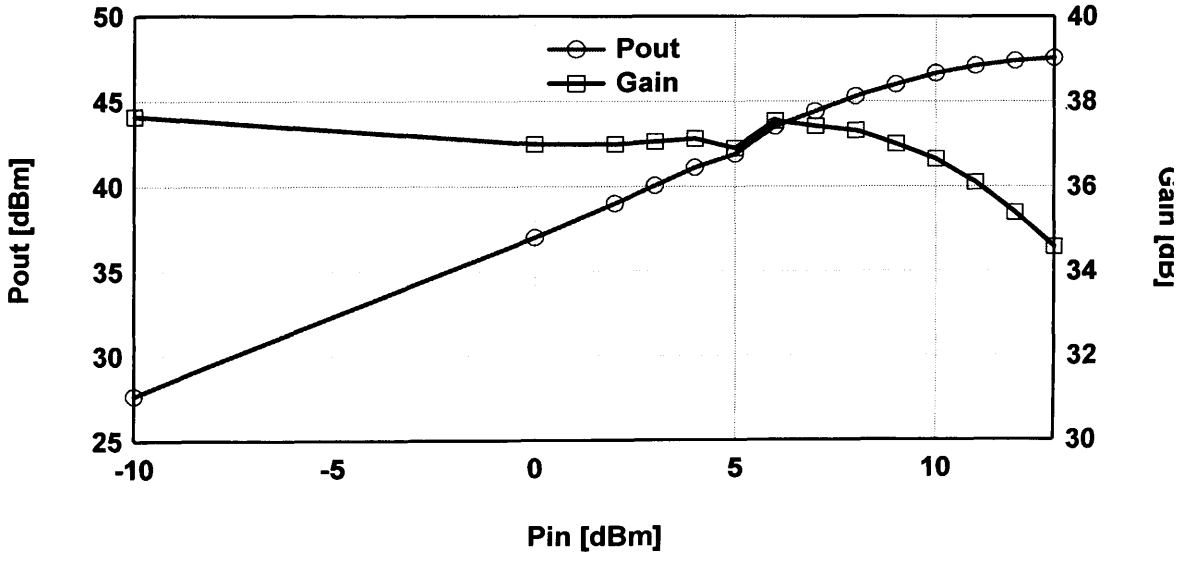

Figure 7.4 Measured output power (left axis) and gain (right axis) at center of bandwidth.

With this PA it is possible to use the envelope load pull (see Figure 7.5 and Figure 7.6) in order to load pull the second harmonic impedance and observe the performance of the device under test. The obvious advantage of using the second harmonic load pull over the base-band is that it can exploit the integrated broadband RF impedance transformer (see Figure 5.11) to lower the power, in comparison to IF load pull, required for load pulling high power components.

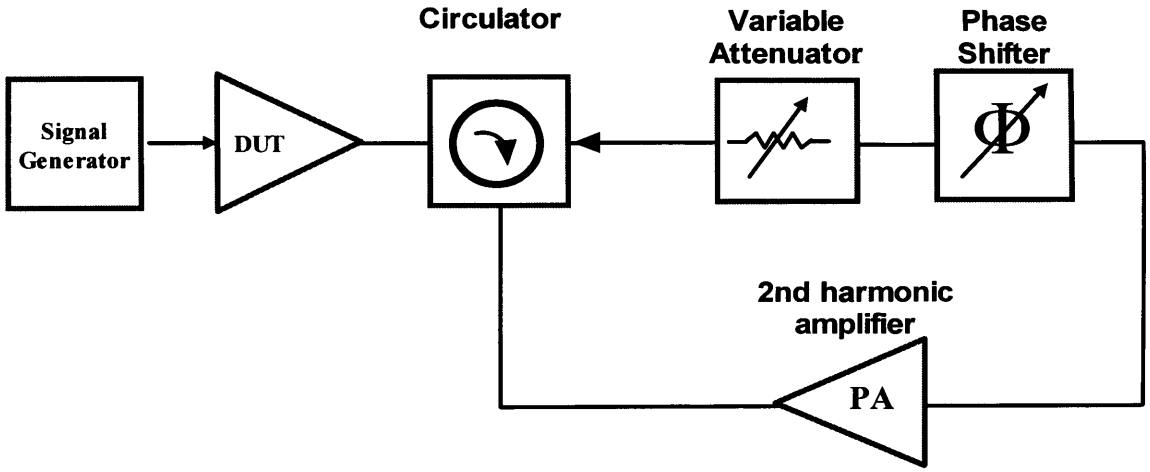

Figure 7. 5 Typical closed envelope load pull system.

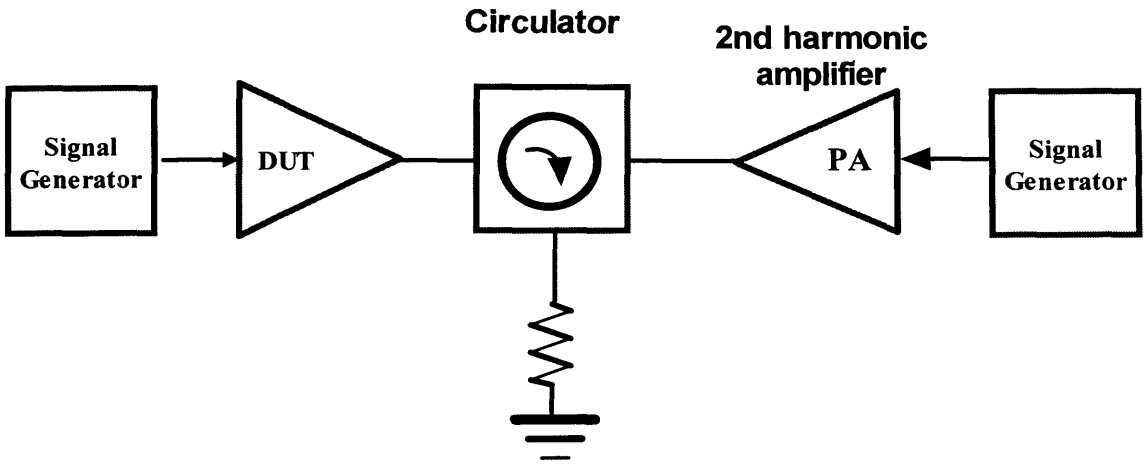

Figure 7. 6 Typical open envelope load pull system.

It would be possible now to investigate high frequency electrical memory effect in addition to low frequency. It would be interesting to use the combined RF and IF measurement system to find a figure of merit for both the optimum IF and F_{2nd} (second harmonic) frequency components at the same time.

Appendix A Publications

A measurement test-set for characterisation of high power LDMOS transistors including memory effects

Abdurrahman Alghanim, Johannes Benedikt and Paul Tasker
Cardiff University, School of Engineering, Cardiff CF24 3TF
e-mail – ALGHANIMA@cf.ac.uk

Abstract –The paper presents a test-set enabling precise measurement of all signal components generated by a modulated stimulus, hence allowing for device characterisations relevant for communication systems. The presented test-set utilises two different types of coupler networks to detect the fundamental and harmonic signal components, and the IF signal components, respectively. Furthermore, the test-set is capable of handling power levels above 100W making it applicable to devices relevant for the basestation market.

1. INTRODUCTION

Traditionally, high-frequency measurement systems employ CW signals for investigations of device characteristics. Device characterisations at CW frequencies only do not allow for the measurement and investigation of important device characteristics, e.g. memory effects [1]. Spectrum analyser based systems allow for the use of modulated signals, however, due to their limitations, allow only for the measurement of the spectrum magnitudes. Consequently, it is rather difficult to utilise such systems for accurate and unambiguous analysis of non-linear circuits as a limited set of magnitudes can generate an infinite amount of current and voltage waveforms.

Interestingly, new generation of non-linear instruments is capable of detecting modulated signals. However, test-sets utilised within such systems are not suitable for modulated signals. For instance, the directional couplers exhibit large bandwidth yet have lower cut-off frequencies in the range of several hundred megahertz making them unsuitable for the detection of low-frequency IF signal components. The problems are further compounded when high-power devices are to be characterised as there are no bias tees capable of handling the high-powers at DC, IF and RF with sufficient bandwidth.

2. TEST-SET FOR MODULATED SIGNALS

The proposed test-set is shown in Figure 1 and consists of two main parts: the RF part (upper level) and the IF part (lower level) which is identical in both components architecture and principle of operation. The two parts are separated by the RF bias tee which should have an IF bandwidth at least an order of magnitude larger than the modulation frequencies used for device characterisation to allow for the detection of the fundamental and harmonic signal components of the IF signal.

The RF test- set consists of two directional couplers used to measure the incident and reflected waveforms with a bandwidth of 1GHz-12GHz and two bias tees [2] with the same bandwdith and a maximum current and voltage handling of 10A and 100V respectively. Both components the RF couplers and bias tees are capable of handling up to 100W CW.

To overcome the problem of detecting the low-frequency signal components in the IF set, the RF coupler were replaced with commercially available directional couplers providing the IF test set with a bandwidth of 100KHz-1000MHz with a maximum power

of 100W CW. The resulting eight separate waves are combined through diplexers, hence avoiding the use of two separate samplers as in [3]. Due to the limited DC handling of the IF couplers it was decided to place the IF bias tee in front. However, despite substantial efforts it was not possible to source any suitable IF bias tee capable of handling high DC and RF voltage and currents over a large bandwidth. Therefore, it was decided to design suitable IF bias tees on site to complete the architecture of the IF set.

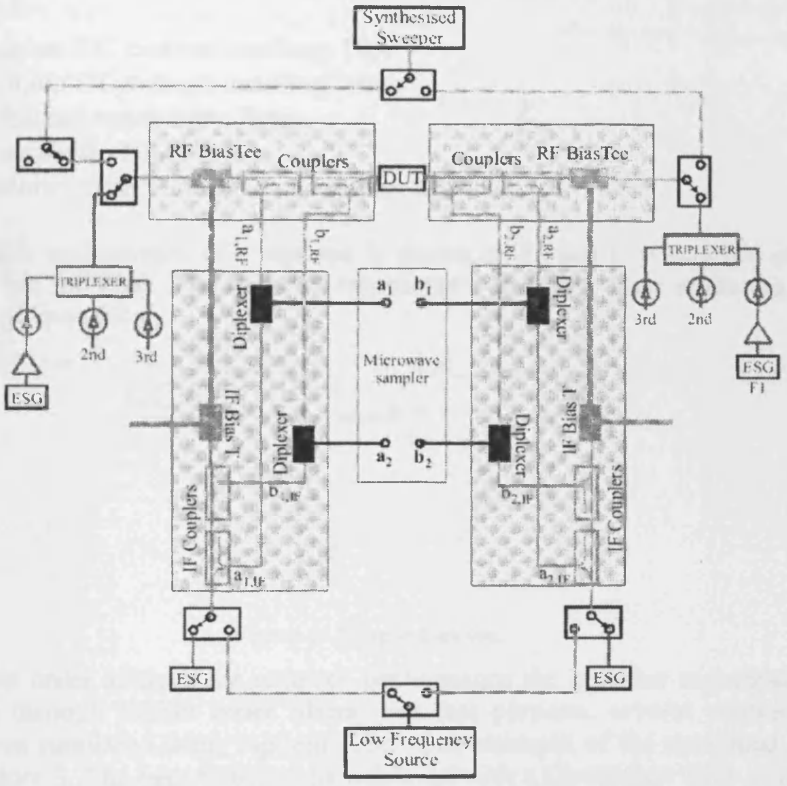

Figure 1: Schematic of the measurement System

3. IF BIAS TEE REALISATION

A major driver for the test-set development was the requirement to test high-power devices under modulated signal conditions, hence allowing device investigations which are relevant for the basestation market. Currently, the dominant device technology is LDMOS with commercially available devices delivering maximum output power levels of up to 180W at CW conditions. However, it was thought that an immediate step to such high powers poses to high of a risk, bearing in mind that the typical power handling of broadband RF test-sets is approximately 20W, and it was decided to set the maximum power handling of the test-set under development to 100W CW. The range up to 100W CW represents also the largest part of the high-power device market.

Consequently, the DC and IF requirements for the IF bias tee have been derived for the characterisations of LDMOS devices with a maximum output power of 100W. Currently, the typical quiescent bias condition for LDMOS devices is Vd=26-28V while

the quiescent current can reach 10A, assuming a 40% drain efficiency at the maximum output power. The CW power at IF frequencies is expected to be 10dB below the RF fundamental power resulting in a maximum power handling requirement for the IF bias tee of 10W. The IF bandwidth requirement was set to 50MHz which is an order of magnitude larger than the modulation bandwidth of W-CDMA systems. The resulting specification for the IF bias tee are summarised below:

- Maximum DC current handling: 10A
- Maximum DC voltage handling: 100V
- DC channel bandwidth: 7kHz
- IF bandwidth: 50MHz
- IF channel maximum power handling: 10W

The principle architecture of a bias tee is shown in Figure 1. It consists of just one capacitor and one inductor. The inductor represents a low pass filter while the capacitor represents a high pass filter.

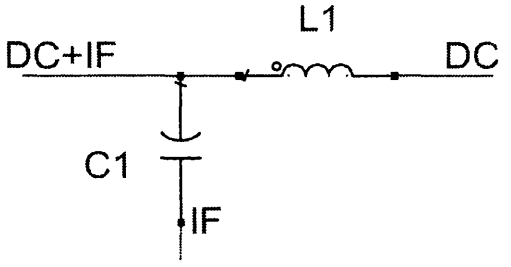

Figure 2: Simple bias tee.

However, in order achieve the required performance the inductor and capacitor have been replaced through higher order filters. For this purpose, several combinations of filters have been simulated using Agilent ADS. One example of the simulated circuits is depicted in Figure 3. The best results were achieved with a Chebyshev filter with 0.01 dB ripple for the low pass filter and a Butterworth filter for the high pass filter. The obtained optimum circuit has been realized using off-the-shelf inductors and capacitors.

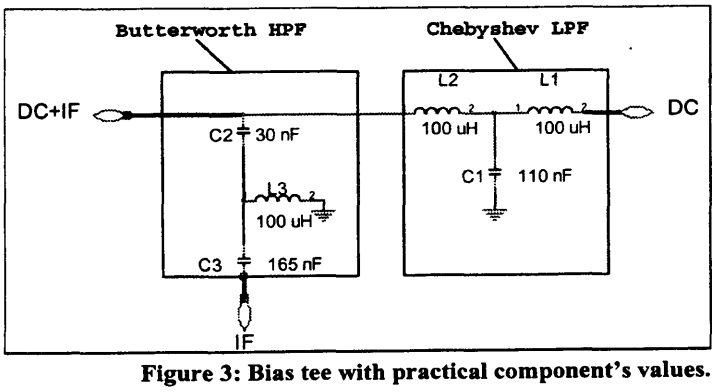

Figure 3: Bias tee with practical component's values.

3 BIAS TEE MEASUREMENTS

The realised IF bias tee has been tested using the 8753E VNA and the results are shown in Figure 4. The transmission loss of the IF port is better than -3dB for the entire frequency range from 30 KHz to 50 MHz and the isolation between DC &IF is 37 dB minimum. Unfortunately, the available bandwidth of the VNA is only 30 KHz-6 GHz, hence is was not possible to measure accurately the bandwidth of the DC channel. Nevertheless, a DC test was applied on the IF bias tee showed a dc resistance of 0.8Ω.

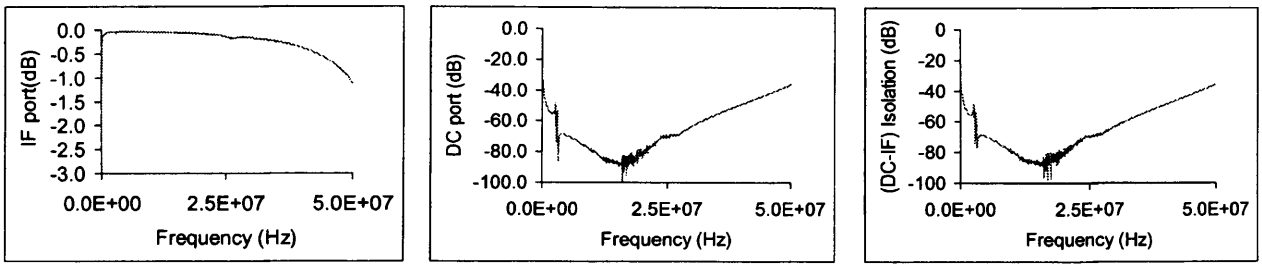

a) b) c)

Figure 4: a) Measured transmission of IF port b) return loss of DC port and c) Isolation between DC & IF.

4. CONCLUSIONS

A new high power measurement system has been developed to handle RF power of more than 100W and to combine two systems namely RF and IF system to study the effects of IF and RF impedance terminations and electrical memory effects on the linearity and efficiency of high- power transistors.

References

[1] Vuolevi, J.H.K.; Rahkonen, T.; Manninen, J.P.A, "Measurement technique for characterizing memory effects in RF power amplifiers" Microwave Theory and Techniques, IEEE Transactions on Volume 49, Issue 8, Aug. 2001 Page(s):1383 - 1389

[2] J. Benedikt, and P. Tasker, "High power time-domain measurement bench for power amplifier development," ARFTG Conference Digest, Fall 2002. 60th , 5-6 Dec. 2002, pp.107-110.

[3] David J. Williams, Jonathan Leckey and Paul J. Tasker, "A study of the Effect of Envelope Impedance on Intermodulation Asymmetry Using a Two-Tone Time Domain Measurement System" Microwave Symposium Digest, 2002 IEEE MTT-S International Volume 3, 2-7 June 2002 Page(s):1841 – 1844

Investigation of electrical base-band memory effects in high-power 20W LDMOS transistors using IF passive load pull

Abdulrahman Alghanim, J. Benedikt, and P. J. Tasker

Dept of Electrical and Electronic Engineering, Cardiff School of Engineering,
Cardiff University, The Parade, Cardiff, CF24 3TF, Wales, UK
E-mail: alghanima@Cardiff.ac.uk Tel: +44 2920 876349

Abstract— **Memory effects are complex phenomena that present major problems in modern high-power linear microwave PA design. Specifically, these effects have a profound influence on spectral symmetry and modulation frequency sensitivity, consequently impacting overall linearity and most importantly, the suitability of a Power Amplifier (PA) to linearisation through pre-distortion. This paper presents detailed, two-tone modulated measurements that clearly show how electrical memory, introduced by non-ideal low-frequency base-band impedances, represents the most significant contributor to overall observed memory effects in high-power LDMOS PA design. The analysis is achieved through the characterisation of a 20W LDMOS device at 2.1 GHz using two-tone excitation and a purpose- built, high-power measurement system, which enables the collection of both RF and IF voltage and current waveforms, together with all associated impedances.**

I. INTRODUCTION

The evolution of 3rd and 4th generation (3G, 4G) mobile communication services has generated more concern about the development of the communication system. The 3G system is based under the International Mobile Telecommunications programme (IMT-2000), which employs wideband code division multiple access (W-CDMA) and achieves a transmission rate of 2 Mbit/s with a 5-MHz frequency bandwidth. The 3rd generation of mobile communication systems is designed for applications such as Internet services, e-mail, database retrieval, video telephony, interactive video and sound (music and TV).

Despite the enhanced features of 3G systems, it is still evident that a broader bandwidth is required - particularly when dealing with full-motion video applications. New mobile communication services and applications require a higher data bit- rate which demands a greater bandwidth. The 4th generation (4G) communication system will be capable of delivering speeds of 100 Mbit/s and 1 Gbit/s using channel bandwidths of 1.25 to 23 MHz, therefore offering enhanced quality (e.g. in multimedia, video and sound).

The radio frequency (RF) power amplifier (PA) in base station systems is typically the most costly component. The increasing number of mobile users, combined with growing demands for a higher data rate, has pushed the RF designer to try and exploit allocated bandwidth to its full potential. This requires the design of a linear power amplifier capable of producing a linear response over a wide bandwidth. Intensive research on the linearity of RF power amplifiers in wireless communication has become a global concern.

II. LINEARITY AND MEMORY EFFECTS

Linearization techniques can be used to achieve high linearities (carrier to intermodulation (C/I) ratio). Memory effects, however, which can be defined as changes in the amplitude or phase of distortion components (IMD) caused by changes in modulation frequency ($\Delta\omega$), restrict the linearization techniques for devices exhibiting memory [1] [2].

In order to use the entire bandwidth at maximum efficiency, RF power amplifiers with a higher carrier to intermodulation ratio level and memory-less device performance is necessary. For example, the maximum permissible adjacent channel leakage ratios (ACLR) for mobile terminals are -33dBc and -43dBc for 5 MHz and 10 MHz respectively [3] [4], otherwise distortion into adjacent channels and error in detection of the desired signal may occur. A typical value of carrier to intermodulation (C/I) ratio for a linear power amplifier is 30 dB or more [5] [6].

To meet these challenging standards, circuit designers have two major approaches aimed at gaining a higher C/I ratio. They may terminate the DUT with an appropriate impedance or use one of the available linearization techniques.

In this paper the linearity and memory are studied and examined via the behavior of the in-band intermodulation distortion (IMD). The main source of the in-band distortion is the out-of-band distortion related to impedances presented at either the input or the output of the device, especially those of low frequency impedance (baseband impedance). In order to regulate the in-band distortion, the out of-band distortion must be controllable (engineered).

Memory effects in microwave PAs are generally attributable to a number of physical processes that involve thermal [7], electrical [8] and surface effects [9]. Electrical base-band memory effect is generally considered to be the

major contributor and therefore, one obvious way to develop a more complete understanding is to attempt to eliminate the most likely contributing factor, and to measure and analyse any residual effects due to the others.

Full investigation of electrical memory effect requires a thorough examination of all impedances presented across the complete frequency spectral (preferably from DC to some of nRF). Unfortunately current commercial measurement systems do not accommodate low frequency impedance due to limitations in technology at these frequencies [10] [11] [12].

The difficulty in investigating low frequencies is compounded by the fact that the biasing network should have constant, and ideally, zero impedance at all low frequency (IF) ranges. Otherwise, AC voltages may be generated and added to the power supply voltage, causing amplitude and/or phase modulation, and resulting in asymmetry in the IMD [5] [8]. In the case of a 5 MHz W-CDMA signal, for example, such a bias network needs to be constant and ideally at zero for at least eight decades of bandwidth. In contrast, designing a matching network with consistent impedance for the RF frequency and its first 10 harmonics requires only one decade of bandwidth. This highlights the complexity of bias network design.

In this work, the measurement of inter-modulation products resulting from two-tone excitation, performed as a function of varying tone-spacing is used as a reliable indicator of the presence of memory effects [13] [14]. The objective of this approach is to eliminate the sources of electrical memory and thus establish whether the measured 3rd order intermodulation distortion (IMD3) levels and symmetry become frequency independent over a wide range of stimulus tone-spacing. This is achieved by presenting a low baseband impedance environment across a wide modulation bandwidth. Such measurements has been made possible by the development and fabrication of a pioneering new modulated waveform measurement system which permits the gauging and engineering of all relevant frequency components, i.e. RF, baseband and DC [13] [10].

III. Measurements and Results

A. *Measurement and Result using a Simple Bias Network*

Passive load-pull has been employed as a means of engineering the most significant baseband component (IF1=w2-w1) resulting from 2-tone excitation with a tone-separation between 0.385 and 10 MHz.

The fundamental and harmonics of the measurement system were terminated with the nominal impedance of 10Ω, while the IF measurement system was used to emulate a simple practical resonant bias network. To achieve this (see Fig. 1) the IF measurement system was used to present short impedance to the output IF_1 component ($IF_1=w_2-w_1$) at frequencies 1 and 2 MHz(default optimum) with a view to obtaining symmetrical IMD terms as common practice for envelope termination [13] [15] and variation at other frequencies, as in the case of a practical bias network.

This measurement is performed on a Freescale 4th generation (HV4) 20W LDMOS device characterized at 2.1 GHz. The two-tone measurement was used with the device biased as Class AB at a drain voltage of 28V and a gate voltage of 3.6V. resulting to a quiescent current of 161 mA.

Fig. 2 shows the variations in the IF_1 load impedance, within a practical bias network, and therefore the IF load reflection coefficient (ΓL) as a function of the modulation frequency. The magnitude of the reflection coefficient could not be brought precisely to short because of the losses and the delay introduced by the system itself.

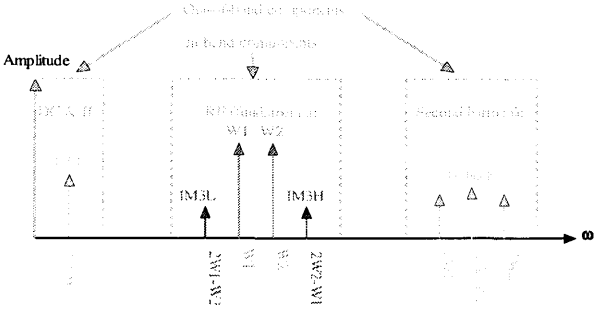

Figure. 1 simplified two-tone spectrum.

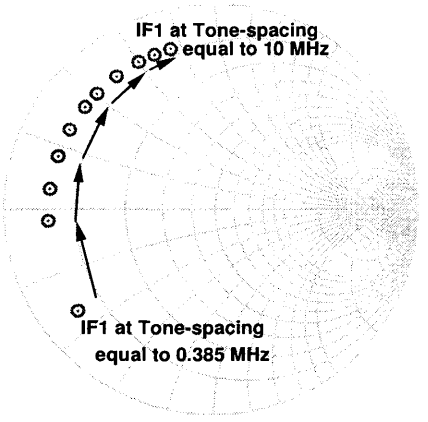

Figure. 2 Measured IF_1 impedance vs. Tone-spacing with a simple (practical) bias network.

Fig. 3 shows the measured RF two-tone power performance as a function of both the input drive level and the base-band impedance presented to the drain of the device for all tone-spacing. The measured output inter-modulation products, IM_{3L} and IM_{3H}, are frequency dependent and demonstrate all the

characteristics of memory. The variation in the intermodulation distortion IM_{3L} and IM_{3H}, for example, is greater then 10 dB at an input drive level of 29 dBm: a point at which the device starts to compress. This is clearly summarized in Fig. 4, where measured values are plotted, illustrating both fundamental output power and inter-modulation distortion IMD_3 as a function of tone-spacing, at a fixed input power level of 29 dBm. With regard to the intermodulation distortion IM_{3L} and IM_{3H}, it is clear that the carrier to intermodulation ratio of IMD_3 degrades at a higher tone-spacing frequency. For example, the magnitude of $IMD_{3L\&H}$ at a tone-spacing of 1 MHz is approximately 0 dBm while it is approximately 10 dBm at a tone-spacing of 10 MHz. This highlights the shortcomings of the simple bias network and the complexity of bias network design. However, Fig. 4 also indicates that it would be possible to have approximately frequency independent inter-modulation distortion (IMD_3) for modulation frequency ranging from 1 to 7 MHz regardless of the variation in the baseband impedance (see Fig. 2). This baseband impedance variation is the tolerance that the bias network designer could have.

As far as fundamental output power is concerned, ω_1 and ω_2, maximum symmetry was observed at low tone-spacing frequencies, while a difference of approximately 2 dBm is observed at a tone-spacing of 10 MHz (see Fig. 4). It is important to mention that the difference between the fundamental output power, ω_1 and ω_2 demonstrated in Fig. 4 is correlative and found to be proportional to the variation observed in the input power (ω_{1in} and ω_{2in}) illustrated in Fig. 5. Since these two signals vary at the device reference plane (adjusted to have the same magnitude from the ESG but they varied as they hit the device input) and are applied at the input of a power amplifier, it could therefore be expected that the power amplifier would amplify these two signals as well as the difference between them. Consequently, the asymmetry in the output signals, ω_1 and ω_2, is attributed to the asymmetry in the input signals.

However, it is still difficult to distinguish whether the change in IMD magnitude, at constant input drive level, is a result of the variation of the base-band impedance or associated with other sources of memory effect such as thermal or trapping memory.

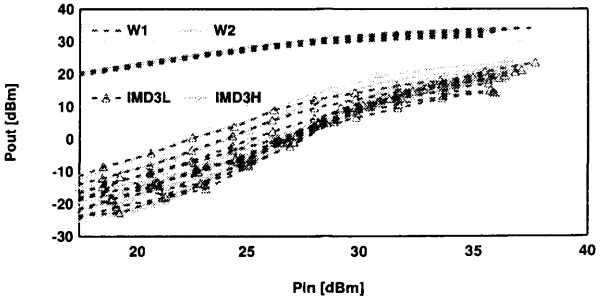

Figure 3 Measured two-tone power sweeps (w_1 and w_2) for all tone-spacing frequency, ranging from 0.37MHz to 10 MHz.

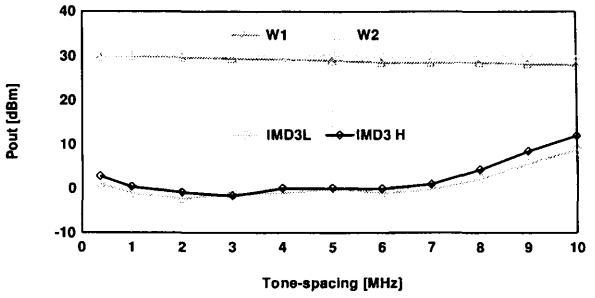

Figure. 4 Measured fundamental and IMD power vs. Tone-spacing at 27dBm drive level for simple bias network.

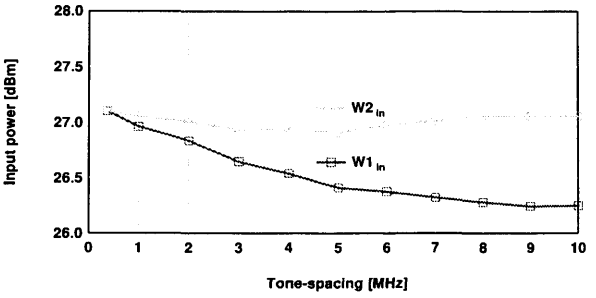

Figure. 5 Measured fundamental input power (W1 and W2) vs. Tone-spacing.

B. Measurement and Results using an Ideal Bias Network

In the second experiment, the passive IF load pull system was used to emulate an ideal bias network, predicted to have short circuit impedance for all tone-spacing ranging from 037MHz and 10MHz.

Fig. 6 illustrates the ideal bias network performance, which is almost constant and almost short impedance, regardless of frequency variations.

The two-tone output fundamentals (ω_1 and ω_2) as well as the output inter-modulation IMD are shown in Fig. 7. The maximum asymmetry between IM_{3L} and IM_{3H} at an input power of 29 dBm, corresponding to a 1dB compression point, is less than 3 dB as opposed to an asymmetry of 10dB (for the simple bias network) before an ideal bias network was emulated. It was initially evident, that due to the lack of output fundamentals (ω_1 and ω_2) and IMD variations regarding tone-spacing frequency, the memory can be suppressed by designing ideal bias networks[13] [16] [17]. This is clearly summarized again in Fig. 8 which plots the measured values of both fundamental output power and inter-modulation distortion

IMD_3 as a function of tone-spacing, at a fixed input power level of 29 dBm for both bias networks. The fundamental of the output ω_1 and ω_2 as well as the intermodulation distortion IM_{3L} and IM_{3H} remain constant and independent of the modulation frequency for the ideal bias network. Fig. 8 also indicates the improvement achieved when designing an ideal bias network with constant impedance at all modulation frequencies. For example, $IMD_{3L\&H,}$ in the case of ideal bias network, have been improved by approximately 10 dBm at 10 MHz in contrast with the simple bias network.

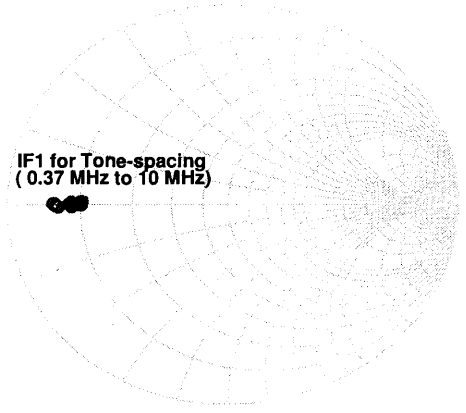

Figure. 6 Measured IF_1 impedance vs. Tone-spacing with ideal bias network.

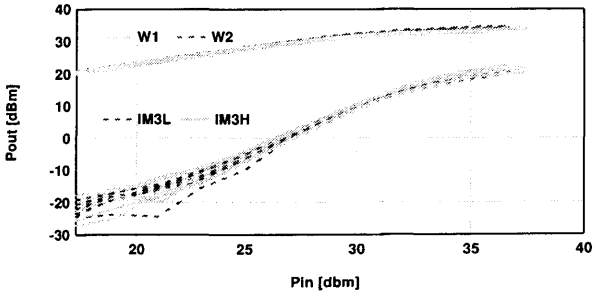

Figure. 7 Measured two-tone power sweeps (w_1 and w_2) for all two-tone frequency separations.

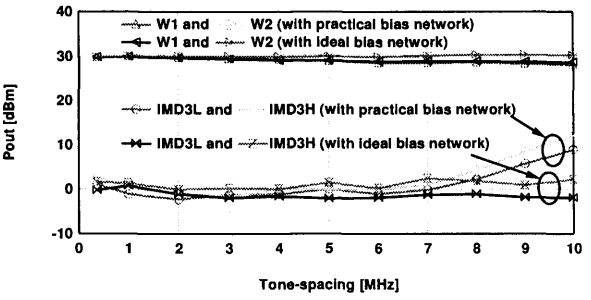

Figure. 8 Measured fundamental and IMD power vs. Tone-spacing at 30dBm drive level for both practical and ideal bias networks.

IV. CONCLUSIONS

This paper presents detailed two-tone modulated measurements. These measurements clearly demonstrate how electrical memory, introduced by non-ideal low-frequency base-band impedances, represent the most significant factors in overall observed memory effects related to high-power LDMOS PA design. Suppression of electrical memory has been achieved through the use of passive IF load-pull to emulate an ideal bias network, and the synthesis and presentation of frequency invariant IF impedances. Using this approach, a constant spectral symmetry has been demonstrated over a wide modulation bandwidth.

ACKNOWLEDGMENTS

The authors would like to thank Freescale for supplying the LDMOS devices used in these measurements.

REFERENCES

[1] Carvalho, J.C.P.a.N.B., *Intermodulation Distortion in microwave and Wireless Circuits.* 2003, Norwood MA: Artech House.

[2] Jeonghyeon, C., et al., *Optimum design of a predistortion RF power amplifier for multicarrier WCDMA applications.* IEEE Transactions on Microwave Theory and Techniques, 2004. **52**(2): p. 655.

[3] A.Toskala, H.H.a., *WCDMA for UMTS: Radio Access For Third generation Mobile Communications.* 2nd ed. 2002, West Sussex: john Wiley & Sons, Ltd.

[4] Leung, V.W., et al., *Analysis of envelope signal injection for improvement of RF amplifier intermodulation distortion*

[5] *Analysis of envelope signal injection for improvement of RF amplifier intermodulation distortion.* Solid-State Circuits, IEEE Journal of, 2005. **40**(9): p. 1888.

[6] Cripps, S.C., *RF Power Amplifiers for Wireless Communication.* 2006, Norwood,MA: Artech house.

[7] Frederick H. Raab, P.A., Steve Cripps, Peter B. Kenington, and N.P. Zoya B. Popovich, John F. Sevic and Nathan O. Sokal, *"RF and Microwave Power Amplifier and Transmitter Technologies".*

IEEE Transactions on Microwave Theory and Techniques, March 2003. **50**(1).

[8] Vuolevi, J.H.K., T. Rahkonen, and J.P.A. Manninen, *Measurement technique for characterizing memory effects in RF power amplifiers.* Microwave Theory and Techniques, IEEE Transactions on, 2001. **49**(8): p. 1383-1389.

[9] Bosch, W. and G. Gatti, *Measurement and simulation of memory effects in predistortion linearizers.* Microwave Theory and Techniques, IEEE Transactions on, 1989. **37**(12): p. 1885-1890.

[10] Parker, A.E. and J.G. Rathmell, *Bias and frequency dependence of FET characteristics.* Microwave Theory and Techniques, IEEE Transactions on, 2003. **51**(2): p. 588.

[11] Alghanim, A., J. Benedikt, and P. Tasker. *A measurement test-set for characterisation of high power LDMOS transistors including memory effects.* in *High Frequency Postgraduate Student Colloquium, 2005.* 2005.

[12] Spirito, M., et al., *Active harmonic load-pull for on-wafer out-of-band device linearity optimization.* IEEE Transactions on Microwave Theory and Techniques, 2006. **54**(12): p. 4225.

[13] FocusMicrowave. *Active Load Pull Systems: Strengths-Weaknesses-Alternatives [Online].* [cited; Available from: http://www.focus-microwaves.com//template.php?unique=232.

[14] Williams, D.J., J. Leckey, and P.J. Tasker. *A study of the effect of envelope impedance on intermodulation asymmetry using a two-tone time domain measurement system.* 2002.

[15] Carvalho, N.B. and J.C. Pedro. *Two-tone IMD asymmetry in microwave power amplifiers.* 2000.

[16] Carvalho, N.B. and J.C. Pedro. *Two-tone IMD asymmetry in microwave power amplifiers.* in *Microwave Symposium Digest., 2000 IEEE MTT-S International.* 2000.

[17] Wakejima, A., et al. *370-W output power GaN-FET amplifier with low distortion for W-CDMA base stations.* 2006. San Francisco, CA, United States: Institute of Electrical and Electronics Engineers Inc., Piscataway, NJ 08855-1331, United States.

[18] Franco, M., et al. *Minimization of bias-induced memory effects in UHF radio frequency high power amplifiers with broadband signals.* 2007. Long Beach, CA, United States: Institute of Electrical and Electronics Engineers Computer Society, Piscataway, NJ 08855-1331, United States.

Investigation of Electrical Base-Band Memory Effects in High-Power 20W LDMOS Power Amplifiers

Abdulrahman Alghanim, Jonathan Lees, Tudor Williams, Johannes Benedikt, and Paul Tasker

Dept of Electrical and Electronic Engineering, Cardiff School of Engineering, Cardiff University
The Parade, Cardiff, CF24 3TF, Wales, UK

alghanima@Cardiff.ac.uk

***Abstract*— Memory effects are complex phenomena that present major problems in modern high-power linear microwave PA design. Specifically, these effects have a large influence on spectral symmetry and modulation frequency sensitivity which in turn impacts overall linearity and importantly the suitability of a Power Amplifier (PA) to linearisation through pre-distortion. This paper presents detailed two-tone modulated measurements that clearly show how electrical memory introduced by non-ideal low-frequency base-band impedances represent the most significant contributor to overall observed memory effects in high-power LDMOS PA design.**

The analysis is achieved through the characterisation of a 20W LDMOS device at 2.1 GHz using two-tone excitation and a purpose built high-power measurement system that allows the collection of both RF and IF voltage and current waveforms along with all associated impedances.

I. Introduction

Memory effects in microwave PAs are generally attributable to a number of physical processes that involve thermal [1], electrical [2] and surface effects [3]. Although electrical memory is generally considered as the major contributor, the relative significance of the different effects is however still not clearly understood. One obvious way to develop a more complete understanding is to attempt to remove the most likely contributing factor, and to measure and analyse any residual effects due to the others.

In this work, and for the first time at high power levels, simple two-tone modulation and inter-modulation product symmetry as a function of varying excitation tone-spacing is used as reliable indicator of the presence of memory effects [4, 5]. Using this approach, it can be shown that by controlling the sources of base-band electrical memory and specifically by using passive IF load-pull to maintain a constant IF impedance environment for a wide range of two-tone stimulus frequency separations, the measured IM3 terms remain largely symmetrical and tone spacing invariant.

II. Measurement System

This investigation has been made possible by the development of a novel high-power modulated waveform measurement system that allows the observation and control of all relevant frequency components (RF, IF and DC) [4, 6]. The developed measurement system is capable of handling IF and RF power levels in excess of 100W which makes it particularly relevant to the characterisation of devices used in mobile communications system base-station applications.

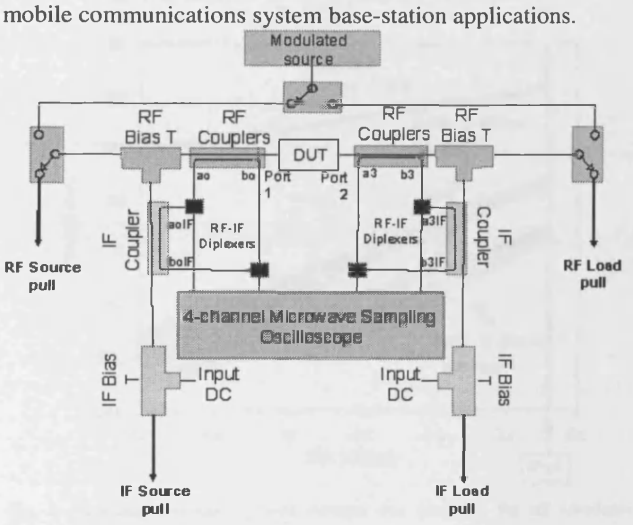

Fig 1 Schematic of the high power measurement system

The measurement system itself is shown in Figure 1 and consists of two main entities: the RF test-set (upper level) and the IF test-set (lower level) which are identical in terms of both component architecture and principle of operation.

The architecture incorporates combined IF and RF capabilities allowing the collection of all four travelling waves at both IF and RF frequencies. Diplexing the coupled RF and IF components of the signal prior to measurement is a key feature, and ensures phase coherence between measured IF and RF components. The system is fully vector-error corrected, and can therefore account for any errors introduced due to losses, mismatches and imperfect directivities in the system, thus allowing for the measurement of the complete modulated voltage and current waveforms and impedances that exist at the DUT plane.

Whereas the RF test-set is made up of off-the-shelf components, it was not possible to source an IF bias-tee possessing the combined DC current, RF power and bandwidth capabilities required. It was necessary therefore to design and manufacture suitable bias networks in-house to meet the required criteria and to allow the measurements discussed in this paper. This completed the measurement

architecture and provides the ability to present specific impedances to the significant IF frequency components, allowing for instance a near constant IF impedance environment to be maintained across a wide IF bandwidth during two-tone excitation.

III. MEASUREMENT RESULTS

Active harmonic load-pull is a relatively simple concept and is effective in allowing the presentation of specific loads to specific frequency components generated by a device [7]. Presenting constant IF and RF loads actively across wide modulation bandwidths is however extremely difficult in comparison, and fraught with complexity. For the measurements presented in this paper, input and output RF impedances were established at 10 Ohms using broad-band 5:1 impedance transformers [8].

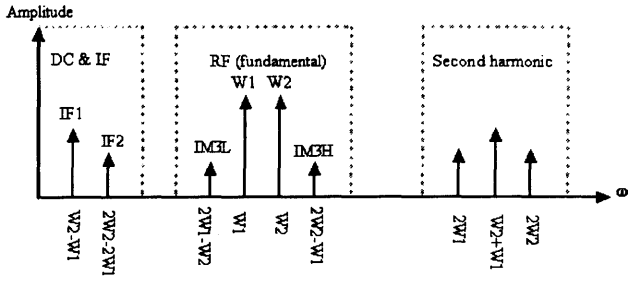

Fig 2 simplified two-tone spectrum

In terms of IF, and with reference to fig-2, passive load-pull was employed as a means of presenting a near short to IF_1 - the most significant IF component, for tone-spacing ranging between 1MHz and 9MHz. In order to minimise the physical length of the passive delay elements required at IF_1, an offset-short termination was used for values of tone-spacing between 1MHz and 3MHz (range-1), whereas an offset-open termination was used for values of tone-spacing between 4MHz and 9MHz (range-2). It is important and interesting to note however that this approach, although very effective in presenting near constant impedances to IF_1 is ineffective in stabilising the impedance presented to IF_2 and other, higher IF components that are generally ignored during memory investigations and discussions. For example, figure 3 shows how the impedance presented to IF_2 varies significantly, moving around the Smith chart for the two termination cases and values of tone spacing.

It is important to note however that when the offset-short termination is used (range-1), the IF2 load presented to the device is low impedance, whereas when the offset-open termination is used (range-2), the IF2 load presented to the device is relatively high impedance.

Fig. 4 shows the measured RF two-tone power performance as a function of input drive level for all tone spacing. The behaviour of the two output tones (w_1 and w_2) is clearly almost independent of the tone spacing frequency.

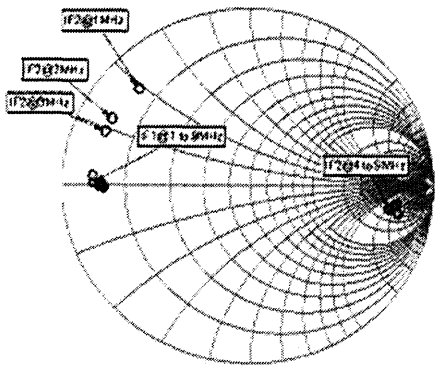

Fig 3 Measured IF_1 and IF_2 impedance vs. tone spacing

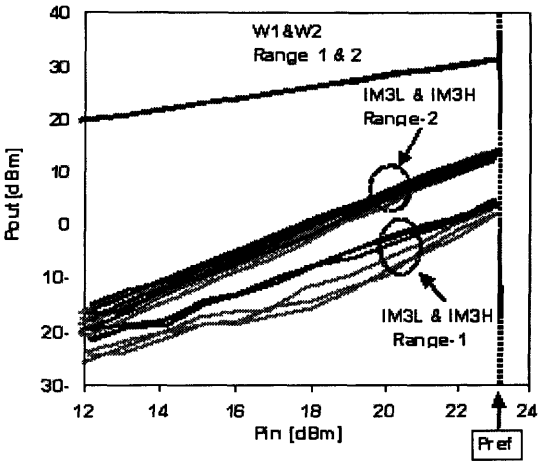

Fig 4 Measured two-tone power sweeps (w_1 and w_2) for all two-tone frequency separations

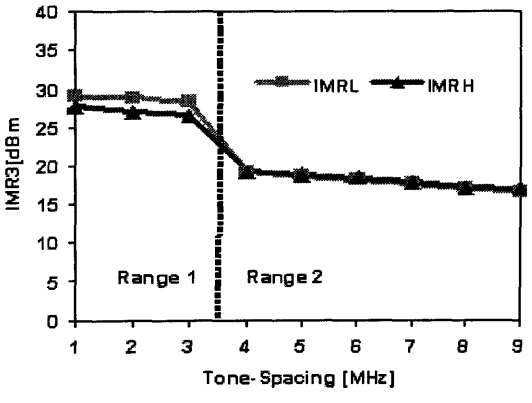

Fig 5 Measured IMR3L and IMR3H vs. Tone-Spacing

With regards to the inter-modulation products, IM3L and IM3H, two distinct responses are observed. This is clearly summarized in fig. 5 which plots the measured value of inter-modulation distortion ratio IMR3 as a function of tone-spacing, at a fixed input power level of about 23.2 dBm which

is 5dB below the 1 dB compression point and identified as Pref (see fig4). As can be seen from this graph, two distinct regions are observed correlating directly to the two different passive load-pull regions. IMR3 is approximately 26 dB over range-1 and approximately 17 dB over range-2. This symmetry and a lack of any variation with tone separation frequency is a clear indication of the absence of memory effect in an environment where IF impedances are frequency invariant. The results show clearly that the variation of the impedance of the higher orders IF terms, which in this passive load-pull case are not deliberately controlled, contribute significantly to the observed variation over frequency.

To help understand this, figures 6 and 7 show the corresponding measured IF current components generated by the non-linear behavior of the transistor along with the resulting IF voltage components developed by the IF load impedances. Clearly it can be seen that the dominant current component is IF_1, again seen to be very frequency invariant due to the control of the corresponding IF impedance component. However, there is also a significant IF_2 current component, which when presented with a high enough impedance is capable of generating a dominant IF_2 voltage component. Consequentially, IF_2 voltage changes rapidly from 0.73V to about 5.5V between range 1 and range 2, resulting in a different IM3 distortion in the two regions. This result suggests that all significant IF impedance components must be controlled and correctly terminated in order to remove the electrical memory.

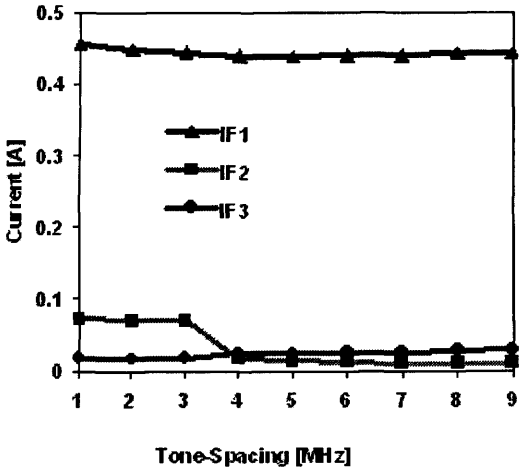

Fig 6 Measured IF current vs. Tone-Spacing

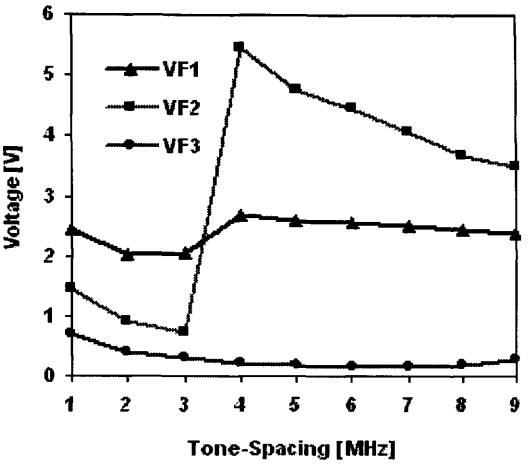

Fig 7 Measured IF voltage vs. Tone-Spacing.

IV. CONCLUSIONS

This paper presents detailed two-tone modulated measurements using a combined RF-IF measurement system. These measurements clearly demonstrates how electrical memory introduced by non-ideal low-frequency base-band impedances represent the most significant contributor to overall observed memory effects in high-power LDMOS PA design. Suppression of electrical memory has been achieved through the use of passive IF load-pull, and the synthesis and presentation of frequency invariant IF impedances. Using this approach, a constant spectral symmetry has been demonstrated over a wide modulation bandwidth.

Measurements show that third order inter-modulation behaviour is not only dependent on the most significant IF component (IF_1), but is also very sensitive to higher order IF components. This important observation has large implications for modern PA linearisation techniques, as well as requiring careful consideration when designing PA bias networks.

ACKNOWLEDGMENT

The authors would like to thank Freescale for supplying the LDMOS devices used in these measurements.

REFERENCES

[1] Joel H. K. Vuolevi, Timo Rahkonen, Jani P. Manninen, "Measurement technique for characterizing memory effects in RF power amplifiers," in IEEE Trans. MTT, vol. 49, no.9, pp. 1383-1389, Aug. 2001.

[2] W. Bosch and G. Gatti, "Measurement and simulation of memory effects in predistortion linearizers," *IEEE Trans. Microwave Theory Tech.*, vol. 37, pp. 1885–1890, Dec. 1989

[3] A. E. Parker and J. G. Rathmell, "Bias and frequency dependence of FET characteristics," in *IEEE Trans. Microwave Theory Tech.*, vol. 51, pp. 588–592, Feb. 2003

[4] D.J. WilLiams, 1. Lakey, P.J. Tasker "A Study of the Effect of Envelope Impedance on intermodulation asymrnetry using a two-tone Time Domain Measurement System" IEEE MTT-S Int. Microwave S p p . Dig., Vol. 3, 2002 pp. 1841-1844,

[5] N.B. Carvalho, J.C. Pedro, "Two-Tone IMD Asymmetry in Microwave Power Amplifiers" IEEE MTT-S Int. Microwave Symp. Dig., Vol. 1, 2000 pp. 445-448

[6] Alghanim, A.; Benedikt, J.; Tasker, P., "A measurement test-set for characterisation of high power LDMOS transistors including memory effects," High Frequency Postgraduate Student Colloquium, 2005, vol., no.pp. 29- 32, 5-6 Sept. 2005.

[7] Benedikt, J.; Gaddi,R.; Tasker, P.J.; Goss, M.; "High-power time-domain measurement system with active harmonic load-pull for high-efficiency base-station amplifier design", IEEE Transactions on Microwave Theory and Techniques, Vol. 48, Issue 12, Dec. 2000, pp. 2617-2624.

[8] Z. Aboush, C. Jones, G. Knight, A. Sheikh, H. Lee, J. Lees, J. Benedikt, and P. J. Tasker, "High Power Active Harmonic Load-Pull System for Characterization of High Power 100Watt Transistors," IEEE MTT-S Int. Microwave Symposium, 2005 .

Sensitivity of electrical baseband memory effects to higher-order IF components for high-power LDMOS power amplifiers

A. Alghanim, J. Lees, T. Williams, J. Benedikt and P.J. Tasker

Memory effects are complex phenomena that present major design problems in modern high-power microwave power amplifier (PA) design, having a large influence on the suitability of a PA to linearisation through pre-distortion. Presented are detailed modulated measurements that clearly show how baseband electrical memory, introduced by the baseband impedance presented to the device, is by far the most significant contributor to overall observed memory effects in a high-power LDMOS PA design. These investigations are performed on a 20W LDMOS device characterised at 2.1 GHz within a purpose-built, high-power measurement system.

Introduction: Memory effects in microwave power amplifiers (PAs) are generally attributable to a number of physical processes that involve thermal [1], electrical [2] and surface effects [3]. Although baseband electrical memory is generally considered as the major contributor, the relative significance of the various effects is however still not clearly understood. One obvious way to gain further understanding is to suppress the most likely contributor, and observe the remaining residual effects.

In this Letter, the measurement of inter-modulation products resulting from two-tone excitation, performed as a function of varying tone-separation, is used as a reliable indicator of the presence of memory effects [4, 5]. The objective of this approach is to eliminate the sources of electrical memory and thus observe if the measured third-order intermodulation distortion (IMD3) levels and symmetry become frequency independent over a wide range of stimulus tone-separation. This is achieved by presenting a low baseband impedance environment across a wide modulation bandwidth. This type of measurement has been made possible by the development and fabrication of a novel modulated waveform measurement system that allows the measurement and engineering of all relevant frequency components, i.e. RF, baseband and DC [4, 6].

Measurement and results: Passive load-pull has been employed as a means of engineering and presenting a near short to the most significant baseband component (IF1 = w2−w1) resulting from two-tone excitation with a tone-separation between 1 and 9 MHz. To minimise the physical length of the necessary passive delay elements, an offset-short termination has been used for tone-separation between 1 and 3 MHz (region-1), whereas an offset-open termination has been used for tone-separation between 4 and 9 MHz (region-2). It is important to note that this approach, although very effective in presenting constant impedance to IF1, is less effective in controlling the impedances presented to the generally overlooked higher frequency baseband components, such as the second-harmonic baseband component IF2 = 2(w2 − w1). This is illustrated in Fig. 1, where the impedance presented to IF2 is observed to differ significantly for the two cases of termination.

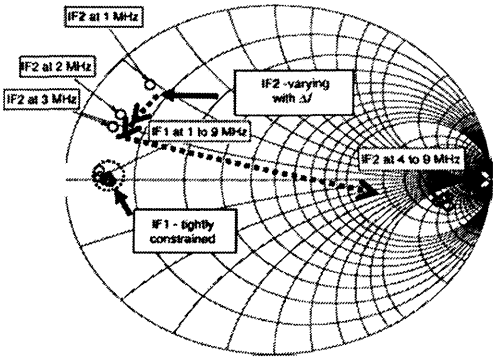

Fig. 1 *Measured IF_1 AND IF_2 impedances against tone-separation*

Fig. 2 shows measured RF two-tone power performance against tone-separation, at a fixed input power level of 5 dB below the 1 dB compression point, where it is clear that the behaviour of the two output tones (w1 and w2) is almost independent of the tone separation. Moreover, Fig. 2 presents the measured third-order intermodulation distortion products IMD3L and IMD3H, where two distinct regions are observed correlating directly to the two different passive load-pull regions. The measured IMD3 products are approximately 3 dBm in region-1 and 12 dBm in region-2.

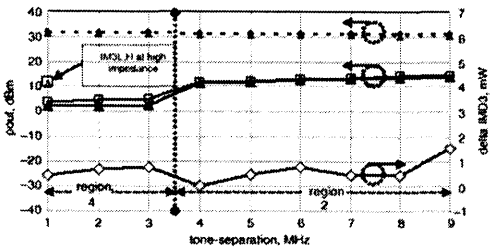

Fig. 2 *Measured fundamental, IMD power and asymmetry for two impedance regions, at different two-tone frequency separations and at constant drive level*

- W1
- W2
- IMD3L
- IMD3H
- Delta IMD3

The measured asymmetry (Delta IMD3), which is defined as the difference in mW between IMD3H and IMD3L remains largely constant for all values of tone separation, regardless of the existence of the two impedance regions.

This result clearly shows that it is variation of the impedance at the second-harmonic baseband component, which was not controlled, that accounts for the observed variation, i.e. electrical memory, in IMD3 response with tone-separation used. To help understand this, Figs. 3 and 4 show the corresponding measured IF current components generated by the nonlinear behaviour of the transistor along with the resulting IF voltage components developed by the IF load impedances. It can be seen that the dominant current component IF1 is clearly frequency invariant due to the control of the corresponding IF impedance component. However, there is also a significant IF2 current component, which when presented with a high enough impedance, is capable of generating the dominant IF2 voltage component shown in Fig. 4.

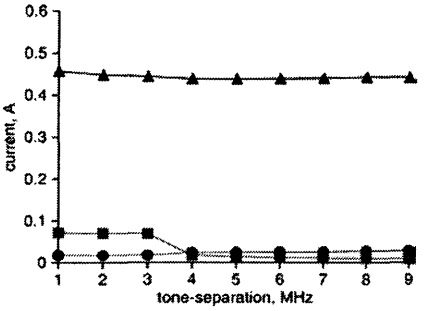

Fig. 3 *Measured IF current against tone-separation (MHz)*

- I(IF1)
- I(IF2)
- I(IF3)

To confirm this interpretation, it was necessary to design and manufacture a suitable diplexer to separate the two IF harmonic components. The achieved isolation between IF1 and IF2 was 20 dB. Using this approach, the magnitude of the IF2 reflection coefficient at 1 MHz tone-separation shown in Fig. 1 was now independently load-pulled towards an open circuit (region-2), while maintaining a constant IF1 load. The achieved variation in IF2 impedance at 1 MHz results in a shift in the IM3L and H value, identified in Fig. 2 as IM3L&H at high impedance, to that consistent with the region 2 values achieved at higher tone-separation. This highly controlled elimination of the IMD3 variation with tone-separation used is solid evidence of the preceding interpretation.

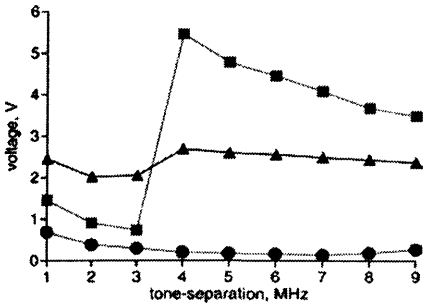

Fig. 4 *Measured IF voltage against tone-separation (MHz)*

This result clearly shows that variations in IF2 as well as IF1 load impedance can significantly modify the levels of IMD3 components. Thus, to achieve a modulation frequency independent response, the baseband impedance must be engineered to be frequency independent over a bandwidth that must be not twice, as previously assumed, but at least four times that of the modulation frequency, i.e. twice the tone separation.

Conclusions: In this Letter, it is shown how it is possible to experimentally validate and demonstrate the dependence of electrical memory effects on baseband impedance. It has been shown that the power levels and therefore the frequency dependence of inter-modulation distortion is not only dependent on the impedance presented to the most significant baseband component IF1 but also higher baseband frequency components. Hence, suppression of the electrical memory effects, i.e. elimination of the frequency dependence of IMD components, requires control of baseband impedance over a much larger bandwidth than previously considered. The implication of this is significant, especially when designing PA bias networks for applications utilising wide modulation bandwidths such as WiMAX.

19 November 2007
Electronics Letters online no: 20083348
doi: 10.1049/el:20083348

A. Alghanim, J. Lees, T. Williams, J. Benedikt and P.J. Tasker (*Department of Electrical and Electronic Engineering, Cardiff School of Engineering, Cardiff University, The Parade, Cardiff CF24 3TF, Wales, United Kingdom*)

E-mail: alghanima@cf.ac.uk

References

1 Vuolevi, J.H.K., Rahkonen, T., and Manninen, J.P.: 'Measurement technique for characterizing memory effects in RF power amplifiers', *IEEE Trans. Microw. Theory Tech.*, 2001, **49**, (9), pp. 1383–1389
2 Bosch, W., and Gatti, G.: 'Measurement and simulation of memory effects in predistortion linearizers', *IEEE Trans. Microw. Theory Tech.*, 1989, **37**, (12), pp. 1885–1890
3 Parker, A.E., and Rathmell, J.G.: 'Bias and frequency dependence of FET characteristics', *IEEE Trans. Microw. Theory Tech.*, 2003, **51**, (2), pp. 588–592
4 Williams, D.J., Lakey, J., and Tasker, P.J.: 'A study of the effect of envelope impedance on intermodulation asymmetry using a twotone time domain measurement system', *IEEE MV-S Int. Microwave Symp. Dig.*, 2002, **3**, pp. 1841–1844
5 Carvalho, N.B., and Pedro, J.C.: 'Two-tone IMD asymmetry in microwave power amplifiers', *IEEE MTT-S Int. Microw. Symp. Dig.*, 2000, **1**, pp. 445–448
6 Alghanim, A., Benedikt, J., and Tasker, P.: 'A measurement test-set for characterisation of high power LDMOS transistors including memory effects'. High Frequency Postgraduate Student Colloquium, Leeds, UK, September 2005, pp. 29–32

Using active IF load-pull to investigate electrical base-band induced memory effects in high-power LDMOS transistors

Abdulrahman Alghanim , Jonathan Lees, Tudor Williams, Johannes Benedikt, and Paul Tasker

Dept of Electrical and Electronic Engineering, Cardiff School of Engineering, Cardiff University, The Parade, Cardiff, CF24 3TF, Wales, UK

E-mail: alghanima@Cardiff.ac.uk Tel: +44 2920 876349,

Abstract— **Memory effects are generally attributable to thermal, electrical, packaging and/ or surface effects. This behaviour in turn impacts overall linearity and importantly the suitability of a Power Amplifier (PA) to linearisation through pre-distortion. It is assumed that electrical memory introduced by the low-frequency baseband impedance environments associated with the power amplifier bias insertion networks being frequency dependent represents a significant contributor to overall observed memory effects in high-power LDMOS PA design. In this work, baseband or IF active load-pull is used to provide an effective way to engineer all the significant IF components generated as a result of multi-tone excitation, independent of modulation frequency. Specific IF impedance environments are presented to a device with this approach in order to probe the sensitivity to IF impedance variations. These investigations are performed on a 12W LDMOS device characterised at 2.1 GHz within a purpose built, high-power measurement system, that allows the collection of both RF and IF voltage and current waveforms along with all associated impedances.**

I. INTRODUCTION

One approach in developing understanding of memory effects in microwave PAs is to analyze and control the most likely contributing factors, frequency varying IF impedance. Previous work[1] employed passive IF load-pull in order to control the low-frequency impedances presented to the most significant IF components generated by a device. This approach however is restricted by a number of factors: firstly the realisable reflection coefficients are limited by the presence of significant losses associated with both the IF test-set and the physically long delay-lines necessary to realize the required necessary offset short terminations. As a consequence, the minimum IF impedance realizable using this system was approximately 7Ω, which is some way from a short circuit. This is especially true considering the relatively low optimum output impedance of the high-power LDMOS device employed. Secondly, only one IF frequency component could be controlled at any one time. As a consequence, while controlling of the most significant IF frequency component, the other IF components are terminated in arbitrary impedances, making results difficult to interpret.

In this work, and for the first time at power levels relevant to base-station PA design, active IF load-pull has been used to offer fully independent control of the impedance presented to all the significant IF components generated by a 12W LDMOS device, overcoming all of the problems associated with the previously described passive approach. Using two-tone modulation, the IM3 inter-modulation products are measured as a function of varying excitation tone-spacing and IF impedance. By using active IF load-pull to control IF drain impedance, it can be shown that the measured IM3 terms are a strong function of the IF impedance over bandwidths that are at leased four times that of the modulation frequency.

II. MEASUREMENT SYSTEM

This investigation has been made possible by the development of a novel high-power modulated waveform measurement system that allows the observation and control of all relevant frequency components (RF, IF and DC) [2, 3]. The developed measurement system is capable of handling IF and RF power levels in excess of 100W which makes it particularly relevant to the characterization of devices used in mobile communications system base-station applications.

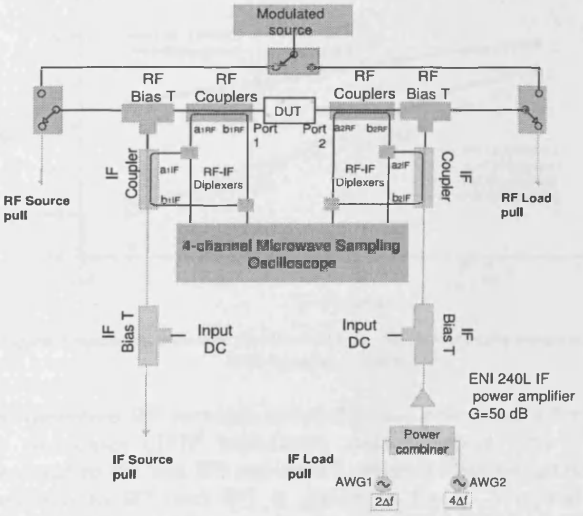

Figure 1 Schematic of the high power measurement system

The measurement system itself is shown in fig 1 and consists of two main entities: the RF test-set (upper level) and the IF test-set (upper level) and (lower level) which are identical both in terms of component architecture and principle of operation.

The architecture incorporates combined IF and RF capabilities allowing the collection of all four traveling waves at both IF and RF frequencies. Diplexing the coupled RF and IF components of the signal prior to measurement is a key feature, and ensures phase coherence between measured IF and RF components. The system is fully vector-error corrected, and can therefore account for any errors introduced due to losses, mismatches and imperfect directivities in the system, thus allowing for the measurement of the complete modulated voltage and current waveforms and impedances that exist at the DUT plane.
Whereas the RF test-set is made up of off-the-shelf components, it was not possible to source an IF bias-tee possessing the combined DC current, RF power and bandwidth capabilities required. It was necessary therefore to design and manufacture suitable bias networks in-house to meet the required criteria and to allow the measurements discussed in this paper. In addition, for a high power device, such as the 12W LDMOS used in this measurement, the IF components generated are large. This is especially true of IF1 (twice the modulation frequency) and IF2 (four times the modulation frequency), the most significant base-band components. In order to actively load-pull these components; an ENI 240L 20 KHz to 10 MHz, 40W linear power amplifier was used to amplify the signal from the arbitrary wave generators (AWG) as seen in fig 1. This integrated measurement architecture provides the ability to present, independently, specific impedances to the two significant IF frequency components, allowing for instance a constant IF impedance environment to be maintained across a wide IF bandwidth during two-tone excitation.

III. MEASUREMENT RESULTS

Active harmonic load-pull is a relatively simple concept and is effective in allowing the presentation of specific loads to specific frequency components generated by a device [4]. Presenting constant RF loads actively across wide modulation bandwidths is however extremely difficult in comparison, and fraught with complexity. For the measurements presented in this paper, input and output RF system impedances were established at 10 Ohms using broad-band 5:1 impedance transformers [5], while IF system impedances remained at 50 Ohms. To achieve IF impedances other than 50 Ohms active IF load-pull was employed to independently engineer different, frequency independent, impedance environments at the two significant IF components; IF1 and IF2, defined in fig 2. Termination of these frequency components into a short circuit would be desirable, particularly for tone-spacing ranging between 1MHz and 10MHz. Fig 3 illustrates just how effective the IF load-pull is in maintaining a frequency independent IF1 short circuit impedance. The observed variation is very small and can be seen to be less than 0.07 magnitude and 1.5 degrees in phase over the entire IF bandwidth. It is important to note that IF2 is not successfully load-pulled for modulation frequencies greater then 7MHz due to bandwidth limitations of the IF PA. This is highlighted in fig 3, which shows the significant variation in IF2 impedance from the desired short circuit for frequencies from 8 MHz to 10 MHz.

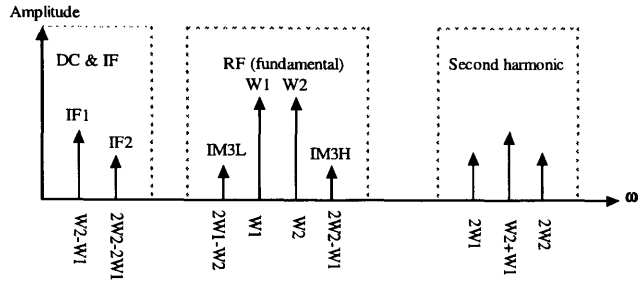

Figure 2 simplified two-tone spectrum

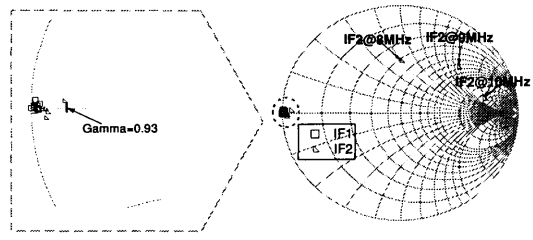

Figure 3 Measured IF1 vs. tone spacing at Z_0=50Ω

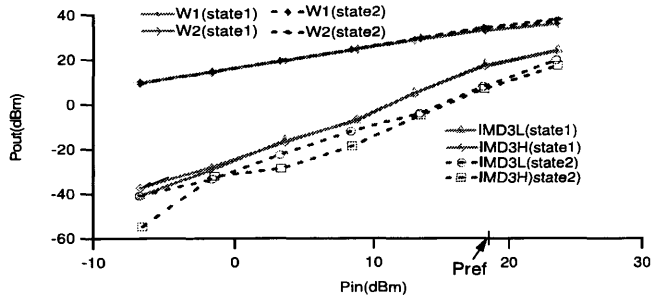

Figure 4 measured two-tone power sweeps for 5MHz frequency separation for both impedance states.

The measured RF two-tone spectral power performance for the two cases of IF impedance, state 1, where 50Ω is presented to IF1 and IF2 and state 2, where a short circuit is presented to IF1 and IF2 is shown in fig 4. A typical behavior, 1:1 slope for the two tones and 1:3 for the IM3 inter-modulation components, is observed over a power sweep of some 30 dB. In this case the tone-spacing is 5

MHz. The variation of measured IM3 response as a function of IF impedance is clearly seen.

Fig 5 summarizes the IM3 behavior at these two different IF impedance states for different values of tone spacing ranging between 1 and 10 MHz, at a single drive level (Pref), this power level corresponds to a point 1dB below the 1dB compression point.

The behavior of the two output tones (w_1 and w_2) is clearly observed to be almost independent of both the tone spacing frequency and IF termination. In the IF impedance state 1 the observed IMD_3 response, while higher than the reference state 2, is found to be independent of tone-spacing. This result indicates that if a frequency independent constant base-band termination is utilized in the Power Amplifier drain bias network no modulation frequency sensitivity in IM3 response would be observed. However, in the case of state 2, short circuit base-band terminations, modulation frequency independence was only observed between 4 and 7 MHz.

It is important to note that IF2 is not load-pulled for modulation frequencies greater then 7MHz due to bandwidth limitations of the IF PA. This variation in IF2 impedance is considered to be the primary cause of the observed variation in IMD_3 response above 7 MHz. This conclusion is consistent with observations made in previous work [1]. To confirm this interpretation the value of the IF2 impedance was varied while fixing the IF1 at a short circuit. The variation of IMD_3 response versus IF2 impedance at 5MHz tone spacing is shown in fig 6. This result clearly shows that variations in IF2 impedance, which is four times the modulation frequency, modify the levels of IM3 inter-modulation components. Thus to achieve modulation frequency independent response the base-band impedance must be engineered to be frequency independent over a bandwidth that must be at least four times that of the modulation frequency. The results also indicated that there is an optimum IF2 impedance that minimizes the IM3 terms. A similar response is obtained if the IF1 impedance is varied while the IF2 impedance is held constant see fig 7. The frequency variation observed below 4 MHz is not related to variation in base-band impedance and thus must be associated with other memory sources; i.e. thermal, surface trapping, package parasitics.

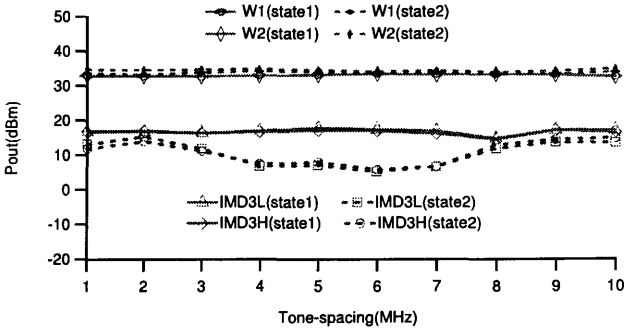

Figure 5 Measured fundamental and IMD power for two impedance states at different two-tone frequency separations at a constant drive level.

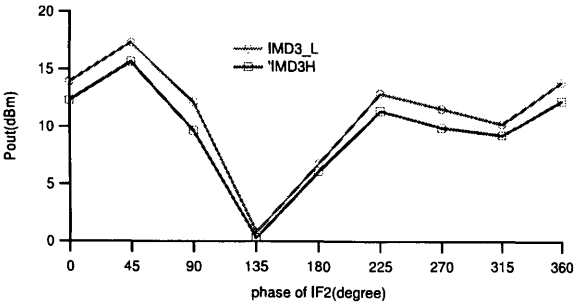

Figure 6 Measured IMD magnitude vs. phase of IF2 for 5MHz frequency separation with IF1 held a constant short

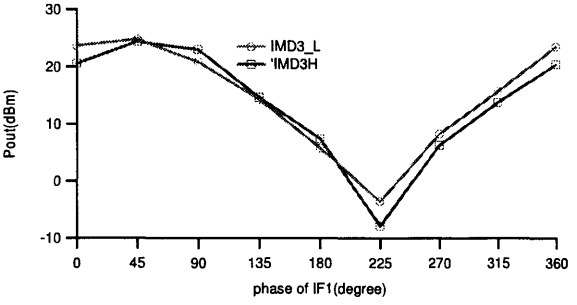

Figure 7 Measured IMD magnitude vs. phase of IF1 for 5MHz frequency separation with IF2 held a constant short.

IV. CONCLUSIONS

This paper presents detailed two-tone modulated measurements using a combined RF-IF measurement system. These measurements clearly demonstrate how non-ideal, frequency dependent, low-frequency base-band impedances will induce significant memory effects in high-power LDMOS Power Amplifiers. The results show that the bandwidth over which the base-band impedances must be controlled must be extended to at least four times the modulated bandwidth.

This important observation has large implications for modern PA linearisation techniques, as well as requiring careful consideration when designing PA bias networks. For applications utilizing wide modulation bandwidths this will become a serious design constraint.

ACKNOWLEDGMENT

The authors would like to thank Freescale for supplying the LDMOS devices used in these measurements.

REFERENCES

[1] Alghanim, A.L., J.; Williams, T.; Benedikt, J.; Tasker, P. Investigation of electrical base-band memory effects in high-power 20W LDMOS Power Amplifiers. in EUMC. 2007. Munich., in press.

[2] D.J. WilLiams, 1. Leckey, P.J. Tasker "A Study of the Effect of Envelope Impedance on intermodulation asymmetry using a two-tone Time Domain Measurement System" IEEE MTT-S Int. Microwave S p p . Dig., Vol. 3, 2002 pp. 1841-1844,

[3] Alghanim, A.; Benedikt, J.; Tasker, P., "A measurement test-set for characterisation of high power LDMOS transistors including memory effects," *High Frequency Postgraduate Student Colloquium, 2005* , vol., no.pp. 29- 32, 5-6 Sept. 2005.

[4] Benedikt, J; Gaddi, R; Tasker,P.J.; Goss,M; "High-Power time domain measurement systems with active harmonic load-pull for high-efficiency base-station amplifier design", IEEE Transactions on Microwave Theory and Techniques, Vol.48, Issue 12, Dec 2000, pp.2617-2624.

[5] Z. Aboush, C. Jones, G. Knight, A. Sheikh, H. Lee, J. Lees, J. Benedikt, and P. J. Tasker, "High Power Active Harmonic Load-Pull.System for Characterization of High Power 100Watt Transistors," IEEE MTT-S Int. Microwave Symposium, 2005.

Reduction of Electrical Baseband Memory Effect in High-Power LDMOS Devices using Optimum Termination for IMD_3 and IMD_5 using Active Load-Pull

Abdulrahman Alghanim, Jonathan Lees, Tudor Williams, J. Benedikt, and P. J. Tasker

Dept of Electrical and Electronic Engineering, Cardiff School of Engineering,
Cardiff University, The Parade, Cardiff, CF24 3TF, Wales, UK
E-mail: alghanima@Cardiff.ac.uk Tel: +44 2920 876349

Abstract— **The usual approach in minimizing electrical memory in PA design is to terminate base-band impedances into a broadband short circuit, usually provided in the form of an array of bypass capacitors attached close to the output terminal of the device. This paper investigates the validity of this approach and compares linearity performance under different IF impedance terminations. Active IF load-pull is used as a modulation-frequency independent means of engineering the significant low-frequency IF voltage components generated as a result of two-tone excitation. Selective IF loads are presented in order to probe device linearity as a function of IF impedance. One significant observation is the existence of specific IF loads that result in the suppression of both IM_3 and IM_5 intermodulation components by more than 16dB and 10dB respectively, in comparison to the case of a conventional IF short termination. These investigations are performed using a 20W LDMOS device characterised at 2.1 GHz within a purpose built, high-power measurement system.**

I. Introduction

One approach in developing understanding of memory effects in microwave PAs is to analyze and control the most likely contributing factor: frequency-varying IF impedance. Previous work [1] employed passive IF load-pull in order to control the low-frequency impedances presented to the most significant IF components generated by a device. This approach however is restricted by a number of factors: firstly the realizable reflection coefficients are limited by the presence of significant losses associated with both the IF test-set and the physically long delay-lines necessary in realizing the required offset-short terminations. As a consequence, the minimum IF impedance realizable using this system at frequencies between 1MHz and 10MHz was approximately 7Ω, which represents a rather poor short circuit. This is especially true when considering the relatively low optimum output impedance of the high-power LDMOS device employed. Secondly, only one IF frequency component could be controlled at any one time. As a consequence, while engineering the most significant IF frequency component, the other IF components are terminated into arbitrary impedances, making results difficult to interpret. In this work, and for the first time at power levels relevant to base-station PA design, active IF load-pull has been used to offer fully independent control of the impedances presented to all the significant IF components generated by a 20W LDMOS device, thus overcoming all of the problems associated with the previously described passive approach. Using simple two-tone modulation, the IM_3 and IM_5 distortion products are measured as a function of tone-separation and IF impedance. By using active IF load-pull to control IF output impedance, it can be shown that the measured IM_3 and IM_5 distortion terms are a strong function of the IF impedance over bandwidths that are in excess of four times the modulation frequency.

II. Measurement System

At the heart of this investigation lies a novel, high-power modulated waveform measurement system that allows the observation and control of all relevant frequency components (RF, IF and DC) [2] [3]. The developed measurement system is capable of handling IF and RF power levels in excess of 100W which makes it particularly relevant in the characterization of devices used in mobile communications system base-station applications.

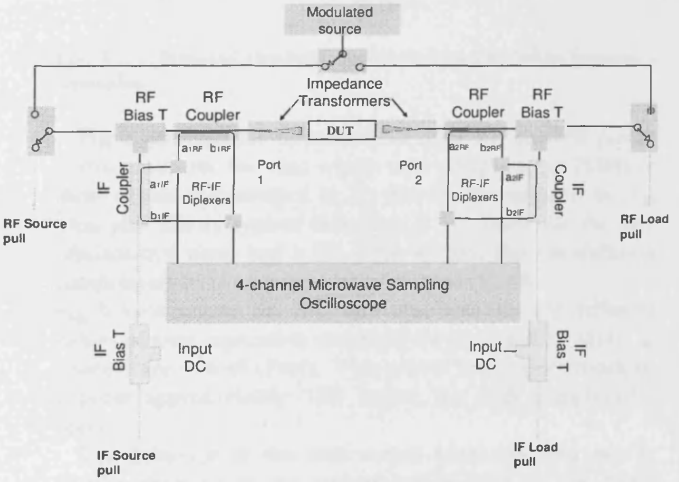

Fig. 1. Schematic of the high power measurement system.

The measurement system itself is shown in fig 1 and consists of two main entities: the RF test-set (upper level) and the IF test-set (lower level) which are identical both in terms of component architecture and principle of operation. The architecture incorporates combined IF and RF capabilities allowing the collection of all four traveling waves at both IF and RF frequencies. Recombination of the coupled RF and IF components of the signal prior to measurement is a key feature, and ensures phase coherence between measured IF and RF components. The system is fully vector-error corrected, and can therefore account for any errors introduced due to losses, mismatches and imperfect directivities in the system. This allows for the measurement of the complete modulated voltage and current waveforms and impedances that exist at the DUT plane.

Whereas the RF test-set is made up of off-the-shelf components, it was not possible to source an IF bias insertion network that possessed the combined DC current, RF power and bandwidth capabilities required. It was necessary therefore to design and manufacture suitable bias networks 'in-house' to meet the required criteria, and to allow the measurements discussed in this paper. In addition, for a high-power device such as the 20W LDMOS devices used in this measurement, the IF components generated are large. This is especially true of IF_1 (*twice the modulation frequency*) and IF_2 (*four times the modulation frequency*), the most significant base-band components. In order to actively load-pull these components; an ENI240L20 0.02-10MHz, 40W linear instrumentation PA was used to amplify the IF load-pull signal generated by the Arbitrary Waveform Generator (AWG). This integrated measurement architecture provides the ability to independently present specific impedances to the most significant IF frequency components, allowing for instance a constant IF impedance environment to be maintained across a wide IF bandwidth during two-tone excitation.

III. MEASUREMENT RESULTS

Active harmonic load-pull is effective in allowing the presentation of specific loads to specific frequency components generated by a device [4]. Presenting constant RF loads actively across wide modulation bandwidths is however extremely difficult in comparison, and fraught with complexity. For the measurements presented in this paper, input and output RF system impedances were established at 10 Ohms using broadband 5:1 impedance transformers [5], while IF system impedances remained at 50Ω. For the first investigation, IF_1 was terminated into a short circuit while IF_2 was terminated into 50Ω and the tone-separation varied between 1MHz and 10MHz. Fig 2 illustrates just how effective IF load-pull is in presenting and maintaining a frequency independent IF_1 short circuit impedance across the entire modulation bandwidth. The observed variation in load is very small and less than 0.03 magnitude and 1 degree in phase. It is important to note that IF_2 cannot be successfully load-pulled for tone-separations greater than 6MHz, due to bandwidth limitations of the IF PA. This is highlighted in fig 2, which shows a significant 'outwardly spiraling' variation in IF_2 impedance from the desired 50Ω, observed for frequencies from 7 MHz to 10 MHz.

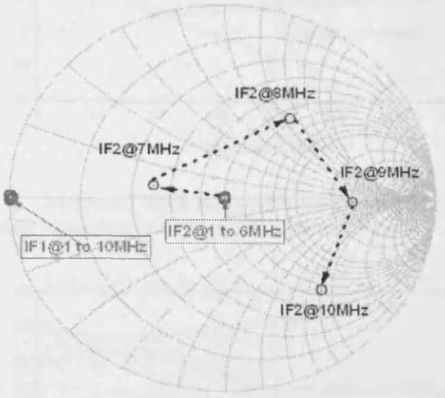

Fig. 2. Measured IF_1 and IF_2 vs. tone-separation at Z0=50Ω.

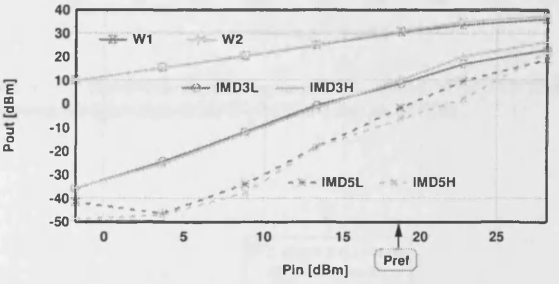

Fig. 3. Measured two-tone power sweeps for 2MHz frequency separation.

Fig 3. presents the measured two-tone RF spectral power performance for the case where tone separation is 2MHz, a short circuit is presented to IF_1 and 50 Ω presented to IF_2. This plot shows typical behavior: a 1:1 slope for the two fundamental tones and a 1:3 slope for IM_3 inter-modulation components over a power sweep of some 30 dB.

Fig 4 summarizes the IM_3 and IM_5 behavior for different values of tone-separation ranging between 1 and 10 MHz, at a single drive level (Pref). This power level corresponds to a point approximately 1dB below the 1dB compression point.

The behavior of the two output tones (ω_1 and ω_2) is clearly observed to be almost independent of the tone-separation frequency. The observed IMD_3 and IMD_5 responses are found to be modulation frequency independent only between 4 and 7 MHz.

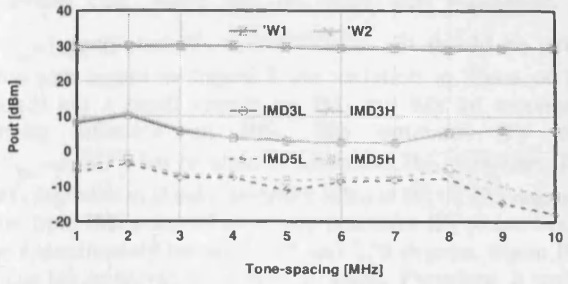

Fig. 4. Measured fundamental and IMD power at different tone separations at a constant drive level.

Firstly, it is important to note that the observed variation in IM_3 component magnitude observed below 3 MHz is considered not to be related to variations in base-band impedance, but more likely due to other sources of memory such as thermal or surface effects. It is also important to remember that the IF_2 impedance cannot be accurately controlled for modulation frequencies greater then 7MHz due to bandwidth limitations of the IF PA. The variation in IF_2 impedance is considered to be the primary cause of the observed variation in IMD_3 and IMD_5 responses above 7 MHz, and this conclusion is consistent with observations made in previous work [1,6].

To further confirm and investigate this interpretation, the magnitude of IF_2 reflection coefficient was maintained at unity and its phase varied while fixing the IF_1 impedance at a short circuit. Some indication of the variation of IMD_3 and IMD_5 response as a function of IF_2 load is shown in fig 5. In this case, a tone separation of 2MHz was used, and the results clearly show that variations in IF_2 impedance significantly modify the levels of both IM_3 and IM_5 inter-modulation components. Thus, to achieve a modulation frequency independent response, the base-band impedance must be controlled over a bandwidth of at least four times the modulation frequency.

IV. Location of Optimum IF Impedance Termination

Initial measurement results clearly indicated that that there is an optimum IF_2 impedance that is effective in minimizing IMD_3 and IMD_5 distortion terms, and suggests that there is a need to optimize the baseband impedance environment, rather than to just present short circuits [2] as is usually the case. In an attempt to further investigate this, the next investigation involved a similar approach where this time the IF_2 impedance was fixed at a static 50Ω, whilst the IF_1 impedance was varied, around the perimeter of the Smith chart. The results of this measurement are shown in fig 6. where it is clear that an optimum IF_1 impedance resided in a region between 225° and 270°. Further 'probing' measurements suggested that the optimum load was not actually located at the edge of the Smith chart however, it was found to be in a region identified as 'Zone-1' in fig. 7.

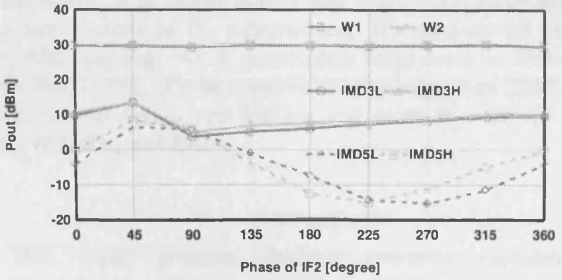

Fig. 5. Measured IMD magnitude vs. phase of IF_2 for 2MHz frequency separation with IF_1 held a constant short.

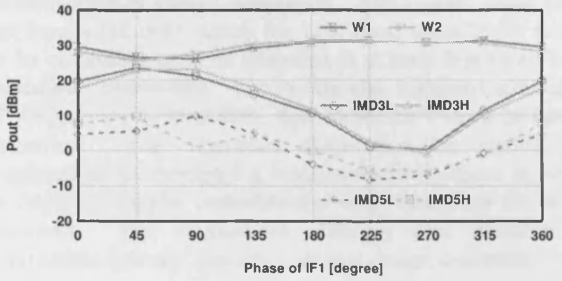

Fig. 6. Measured IMD magnitude vs. phase of IF_1 for 2MHz frequency separation with IF_2 held a constant at 50Ω.

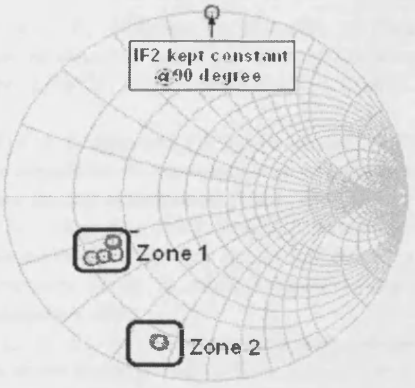

Fig. 7. Phase sweep of IF_1 while IF_2 kept constant at 90° degree.

The investigations in Zone-1 were done whilst keeping the IF_2 load fixed at the earlier identified optimum, see fig. 5, of $\Gamma_{L_{IF2}}=1\angle 90^0$, also shown in fig 7. A reduction of approximately 13 dB in IMD_3 was observed within this region, albeit at the expense of significant increase in IMD_5 of approximately 12 dB. This is in comparison to the

previous case where the IF_1 load was maintained at $\Gamma_{L_{IF1}}=1\angle 270^0$ and IF_2 to $\Gamma_{L_{IF2}}=1\angle 90^0$. It should be noted that with regard to Figure 5 the variation in Phase of IF_2 (load) has a small impact on IM_3 but has an extremely strong influence on IM_5. The optimum IF_2 load ($\Gamma_{L_{IF2}}=1\angle 90^0$) has resulted in minimum IM_3, however, The IM_3 degradation is only around 3 dBm at IF_2 of 225 degrees. But from IM_5 point of view, the optimum IF_2 phase would be approximately between 225 and 270 degrees where IM_5 value has improved by almost 20 dBm. Therefore, it would be logical to move IF_2 phase toward 225°. Further analysis showed that by moving and then maintaining IF_1 load constant within an experimentally determined different zone of the Smith chart (Zone-2) and keeping IF_2 phase close enough to that Zone (≈225°), IMD_3 and IMD_5 distortion products could be simultaneously reduced by more than 10 dB. Again, this is in comparison to the previous case where the IF_1 load was maintained at $\Gamma_{L_{IF1}}=1\angle 270^0$ and IF_2 to $\Gamma_{L_{IF2}}=1\angle 90^0$.

To confirm that Zone-2 was indeed the optimum termination for IF_1, for the high power 20W LDMOS used, regardless of the modulation frequency and the power level, it was decided to perform an extra measurement in which the input power was swept for two different tone separations, of 1 and 2 MHz.

The measured spectral power performance for the case where the IF_1 load resides within Zone-2 and IF_2 load is brought close to Zone-2 as well is shown in fig 8. Once again, a typical behaviour of 1:1 slope for the two tones and 1:3 for the IM_3 inter-modulation components is observed over a power sweep of some 10 dB. The behaviour of the two fundamental output tones (ω_1 and ω_2) and IMD_3 is clearly almost independent of the tone-separation frequency at input power equal or grater than the compression point. With regards to the magnitude of inter-modulation products IMD_{5L} and IMD_{5H}, they are found to be very close to the lower dynamic range of the measurement system, resulting in noisy measurements at low drive levels.

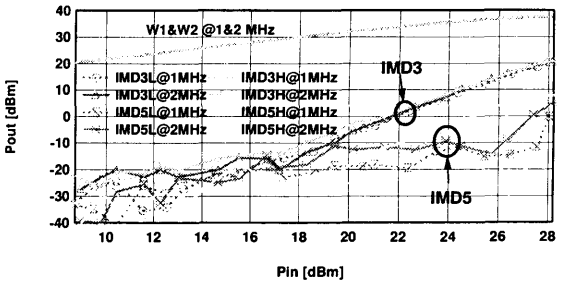

Fig. 8. Measured two-tone power sweeps for 1 and 2MHz frequency separation inside zone 2.

Conclusively, terminating the IF_1 and IF_2 component into Zone-2 impedance provided the best overall linearity, where both IMD_3 and IMD_5 were found to improve by approximately more than 16 dB and 10 dB respectively in comparison to the case of a conventional IF short termination. It is worth noting that when comparing IMD for terminations of $IF_{1,2}$-Zone-2 and IF_1-short-circuit with IF_2 50Ω (see Fig. 4), at equal input drive level of 18dBm (see Pref in Fig. 3), an improvement of more than 20dB is achieved for IMD_{3L} and IMD_{3H}, and more than 16 dB in case of IMD_{5L} and IMD_{5H}.

V. CONCLUSIONS

This paper presents detailed two-tone modulated measurements using a combined RF-IF measurement system. These measurements clearly demonstrate how non-ideal, frequency dependent, low-frequency base-band impedances will induce significant memory effects in high-power LDMOS Power Amplifiers. The results show that the bandwidth over which the base-band impedances need to be controlled must be extended to at least four times the modulated bandwidth. The results also highlight optimum IF impedance terminations that minimize overall in-band distortion. This important observation has significant implications for modern PA linearisation techniques, as well as requiring careful consideration when designing PA bias networks. For applications utilizing wide modulation bandwidths this will become a serious design constraint.

ACKNOWLEDGMENT

The authors would like to thank Freescale for supplying the LDMOS devices used in these measurements.

REFERENCES

[1] Alghanim, A.L., J.; Williams, T.; Benedikt, J.; Tasker, P. *Investigation of electrical base-band memory effects in high-power 20W LDMOS Power Amplifiers.* in *EUMC.* 2007. Munich.

[2] Williams, D.J., J. Leckey, and P.J. Tasker. *A study of the effect of envelope impedance on intermodulation asymmetry using a two-tone time domain measurement system.* 2002.

[3] Alghanim, A., J. Benedikt, and P. Tasker. *A measurement test-set for characterisation of high power LDMOS transistors including memory effects.* in *High Frequency Postgraduate Student Colloquium, 2005.*

[4] Benedikt, J., et al., *High-power time-domain measurement system with active harmonic load-pull for high-efficiency base-station amplifier design.* Microwave Theory and Techniques, IEEE Transactions on, 2000. **48**(12): p. 2617.

[5] Aboush, Z., et al. *High power active harmonic load-pull system for characterization of high power 100-watt transistors.* in *Microwave Conference, 2005 European.* 2005.

[6] Alghanim, A.L., J.; Williams, T.; Benedikt, J.; Tasker, P. *Using active IF load-pull to investigate electrical base-band induced memory effects in high-power LDMOS transistors.* in *APMC.* 2007. Bangkok.